STOCHASTIC PREDICTION OF COLLAPSE OF BUILDING STRUCTURES UNDER SEISMIC EXCITATIONS

BY

DERYA DENIZ

DISSERTATION

Submitted in partial fulfillment of the requirements
for the degree of Doctor of Philosophy in Civil Engineering
in the Graduate College of the
University of Illinois at Urbana-Champaign, 2014

Urbana, Illinois

Doctoral Committee:

Associate Professor Junho Song, Chair and Director of Research
Professor Jerome F. Hajjar, Northeastern University, Co-Director of Research
Associate Professor Bassem Andrawes
Associate Professor Larry A. Fahnestock

ABSTRACT

Modern seismic design provisions help enhance life safety of building occupants during a strong earthquake-shaking event by ensuring acceptably small likelihood of structural collapse. Therefore, accurate estimate of collapse likelihood of buildings under seismic excitations has recently become critical in efforts to promote hazard-resilience of the society, especially in developing national building codes, regional emergency response plans, and risk management strategies. Despite recent advances in static and dynamic nonlinear constitutive modeling of such structures, accurate prediction of structural collapse with systematic incorporation of uncertainty still remains a question, especially for structural evaluation and design of actual structures.

The most commonly used approach to assess the collapse capacity of structures under extreme earthquakes is based on the concept of incremental dynamic analysis (IDA; Vamvatsikos and Cornell, 2002). Uncertainties in structural properties and applied ground motions can be integrated into probabilistic description of structural collapse performance by adopting the probabilistic basis of performance–based earthquake engineering (PBEE) framework together with IDA. The maximum inter-storey drift ratio (IDR) is often selected as the measure to represent the global behavior of structural system in the PBEE framework (Cornell et al., 2002). Likewise, assumed threshold values based on IDR or on slope of IDA curve between IDR and elastic spectral acceleration are most commonly used limit-states to identify structural collapse capacity. However, collapse assessment approaches based on IDR may not accurately represent the overall collapse behavior of structural systems due to redistribution and variation of damage within the structure. Moreover, collapse prediction is found to be sensitive to such subjective collapse limit-states based on the assumed threshold values.

Characterization of overall cumulative (i.e., load-path dependent) collapse performance of structures considering aforementioned uncertainties is needed for accurate and reliable collapse risk assessment. Since energy parameters at system-level are aggregated quantities considering redistribution and variation of each individual component-damage within the structural system, they can be excellent indicators to represent total severe structural damage history due to cyclic-loading just before collapse. This paper therefore focuses on energy-based collapse analysis of structures to assess seismic collapse risk of structures. A new energy-based collapse limit-state is

first defined to predict collapse in terms of dynamic instability due to loss of structural resistance against the gravity loads, instead of the behavior of the IDA curves. Using the new collapse limit-state, key descriptors that govern collapse capacity are identified for more effective risk assessment. Moreover, a probabilistic approach in collapse assessment is presented for systematic treatment of uncertainties in the ground motion time histories and integration with performance-based earthquake engineering (PBEE) framework.

First, nonlinear dynamic analyses are performed for experimental case studies reported in the literature (Kanvinde, 2003; Rodgers and Mahin, 2004; Lignos et al., 2008) by use of OpenSees, an object-oriented software framework developed by Pacific Earthquake Engineering Center (PEER). Using OpenSees computational models validated by corresponding experimental results, new dynamic-instability-based collapse limit-state is developed in terms of energy from the input ground motions and the gravity loads. The selected case studies are then used to test the new collapse limit-state and to identify key parameters that govern the collapse of a structural system. Next, the most effective collapse descriptor representative of structural global behavior history is developed as an equivalent velocity ratio of the system's dissipated energy to input seismic energy. Using the developed collapse limit-state and new velocity-ratio collapse descriptor, a new method is established to construct collapse fragility models for reliable probabilistic evaluation of structural collapse, considering the uncertainties in both global demand and capacity of the structural system. Finally, the effect of earthquake characteristics and structural parameters on the collapse capacity is investigated for the purpose of estimating and improving structural reliability against collapse.

ACKNOWLEDGEMENTS

I am very prideful to be a member of one of the best universities and it has been a great honor for me to learn from the most valuable professors at UIUC. I am very thankful to my advisors Dr. Junho Song and Dr. Jerome F. Hajjar for always supporting me and guiding me to pursue my Ph.D. degree. Special thanks to Dr. Bassem Andrawes and Dr. Larry A. Fahnestock for serving on my Ph.D. committee. Finally, I would like to thank my family for always being there for me and supporting me throughout my life. Without their support and faith in me, I would not be the person I am today.

This study is part of a multi-institution research project performed by the University of Illinois at Urbana-Champaign (UIUC) and Northeastern University (NEU), funded by the National Science Foundation (NSF; under grant number CMMI 1000666). Any opinions, findings and conclusions or recommendations expressed in this material are those of the authors and do not necessarily reflect the views of NSF.

The component of the NSF research project described in this dissertation, i.e., development of stochastic framework of structural collapse assessment, is the focus of my research at UIUC under the guidance of my adviser Dr. Junho Song (Director of Research) and my co-adviser Dr. Jerome F. Hajjar (Co-Director of Research). The other component of the research project that is not included in this dissertation explores the use of advanced modeling for simulating plasticity, fracture and subsequent fragmentation, and for collapse of structures made from ductile metal materials such as steel. This is conducted by Dr. Tam Nguyen and Vitality Saykin at NEU. In the final phase of the project, the research outcomes described in this dissertation and the computational simulation results of the advanced modeling strategy are incorporated into an integrated platform for validated prediction of structural collapse.

TABLE OF CONTENTS

1. INTRODUCTION

1.1 Background and Motivation

In past earthquakes, several collapses of modern building structures have been observed even though these structures were built in accordance with modern seismic design codes and construction standards. A recent example is the global collapse of the 15-story reinforced concrete residential Alto-Rio building during the 2010 Maule, Chile earthquake, which had been constructed following Chilean building codes (Song *et al*., 2012). Such observations raise important questions regarding the capability of the current seismic provisions to provide safety against structural collapse under extreme seismic forces (Villaverde, 2007). Therefore, it has become crucial to understand the causes and effects of collapse of structures in order to develop key documents such as national building codes, regional emergency response plans, and risk management strategies.

There is a recent growing interest in the prediction of accurate collapse assessment for both existing and new structures. Many researches have attempted to predict structural collapse by developing and validating advanced static and dynamic nonlinear constitutive models (Villaverde, 2007). Such models incorporate critical factors such as complex material degradation due to localized fractures; multi-axial yielding; local and system-level buckling; large deformations and significant second-order effects; and energy-dissipating damping or fuse systems. Although there are several efforts to simulate collapse by advanced analytical models, few experimental tests exist that would validate computational results at collapse or near-collapse level. Recent research on seismic loading, for example at E-Defense in Japan (Suita et al., 2008) and on selected projects in the U.S. (Rodgers and Mahin, 2004, 2006, 2009; Krawinkler et al., 2008; Lignos et al., 2008) has started to rectify this.

While numerous research efforts are reported in the literature to estimate collapse capacity of structures, an accurate probabilistic assessment of structural collapse with incorporation of "systematic uncertainty" still remains elusive. Due to significant uncertainties in loads and the chaotic nature of the dynamic instability of a structure, few researchers have considered the stochastic aspects in developing and validating collapse models. The incremental dynamic

analysis (IDA) approach (Vamvatsikos and Cornell, 2002, 2004; Zareian and Krawinkler, 2007; Liel et al., 2009), and a similar approach adopted by a recent project of the Applied Technology Council (ATC-63, 2009) are considered innovative attempts to account for the uncertainty in nonlinear dynamic response, including collapse prediction. However, the impacts of a structural model selection and the selected set of the ground motions on the developed probabilistic collapse model, and potential contributions of various performance measures or predictive parameters to accurate prediction of collapse, have not yet been investigated thoroughly by stochastic analyses of experimental and computational simulations.

1.2 Objectives, Framework and Importance of the Study

The objectives of the study are summarized as follows:

- Establish a new effective procedure to identify collapse criteria of frame structures from their dynamic instability, i.e., the loss of the ability to sustain the gravity loads.
- Identify key parameters governing collapse capacity based on the new collapse criteria for more effective risk assessment using existing approaches.
- Investigate the impact of considering multiple performance measures on the accuracy of collapse predictions of structures and propose new collapse limit-state functions using the identified significant performance measures.
- Develop a probabilistic approach of collapse assessment based on new collapse-limit-state to promote reliable probabilistic evaluation of structural collapse.
- Provide collapse fragility models through systematic treatment of uncertainties in seismic capacity, demand, and structural models for integration with performance-based earthquake engineering (PBEE) framework.

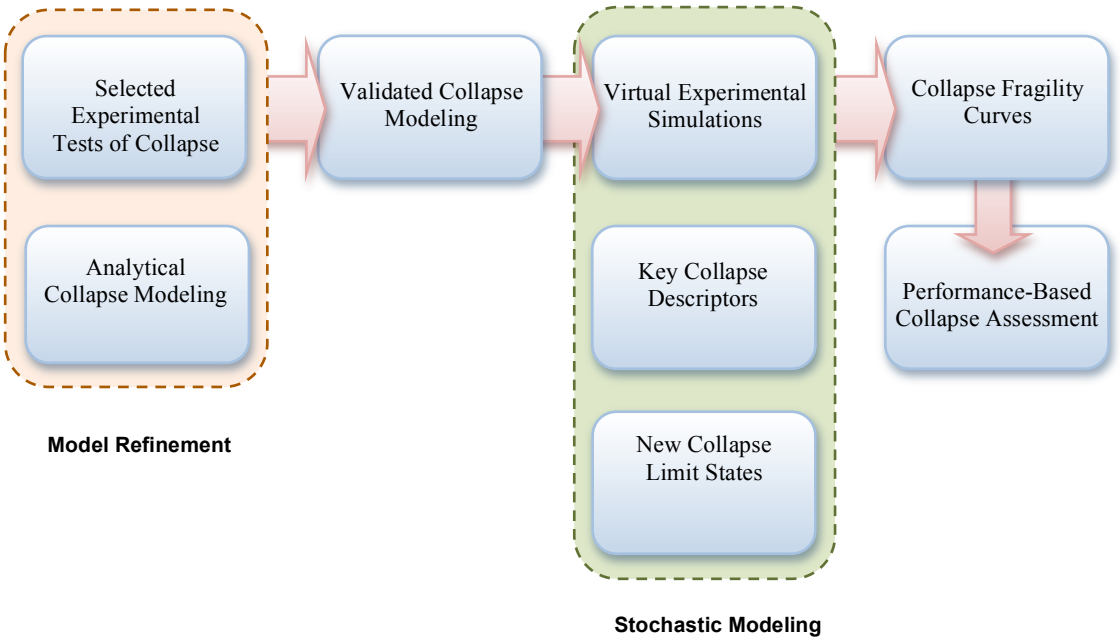

Figure 1.1 Framework for probabilistic assessment of collapse of structures.

Figure 1.1 illustrates the integration between main components of the framework of the study: development of analytical models for the selected experimental case studies of structural collapse, computational simulations of collapse behavior using refined coarse macro-models, and performance-based design and collapse assessment. First, an analytical model simplifying the structural response through the use of phenomological moment-thrust-rotation relations or similar, is developed to predict the collapse behavior and validated through comparison with available experimental test results. Second, using the analytical model validated by the test results, "virtual experimental simulations" are performed for a wide array of geometric, material, and seismic loading parameters. Third, new collapse limit-states are developed from dynamic instability of frame structures using critical collapse measures and tested with virtual experimental simulations. Fourth, collapse fragility models are derived from collapse predictions of virtual experimental simulations based on the developed collapse limit-states. Finally, uncertainties in collapse capacity and demand and structural models are quantified to form the fragility curves for use in performance-based design and collapse assessment.

Advanced high-fidelity analytical models that account for many factors to accurately simulate structural collapse process are more reliable methods but computationally demanding. These models may be highly affected by convergence problems that are likely to occur due to the complexity of the modeling details while performing several nonlinear dynamic analyses to assess collapse potential of structures. These advanced models may be impractical in developing such a stochastic framework described above. Therefore, macro-models that correlate well with experiment results of selected case studies of collapse are considered in this research to perform large-scale parametric studies in collapse assessment of structures and assessment of safety margin against collapse.

The study described here aims to advance understanding of structural behavior near collapse, to develop techniques for accurate evaluation of collapse capacity, to measure the adequacy of current collapse assessment methods, and to provide suggestions to enhance these existing methods. Therefore, this study is expected to have potential impact across several structural engineering research and practice constituencies seeking to improve building code provisions that intends to prevent disproportionate collapse; regional emergency response plans and risk management strategies that rely on accurate assessment of collapse within fragility analysis; and collapse assessment of new structural systems. In addition, through this work, life safety will be enhanced, as avoiding structural collapse due to extreme loads is a critical component to ensuring a safe infrastructure.

1.3 Organization of the Report

The chapters in this report are outlined below:

- Chapter 2 defines global collapse of structures, provides a comprehensive review of current available analytical methods to assess the collapse capacity of building structures subjected to extreme earthquakes, points out the limitations of these methods, and identifies what is required for an accurate estimate of the structural collapse capacity under seismic excitations. The chapter also summarizes recent analytical studies and past experimental work on structural collapse.
- Chapter 3 introduces the computational simulation tool used in the development of analytical models. The chapter describes the selected experimental case studies of

collapse (Kanvinde, 2003; Rodgers and Mahin, 2004; Lignos et al., 2008) and provides the development of computational models validated by corresponding experimental results. Then, the chapter explains the development of virtual experimental simulations based on validated analytical models.

- Chapter 4 gives a review of collapse limits states used in the literature. Then, using the validated computational models, new dynamic-instability-based collapse criteria are developed in terms of energy from the input seismic and gravity loads. Next, the chapter describes the improvement of conventional existing collapse limit states based on new collapse criteria.
- Chapter 5 presents critical descriptors that govern structural collapse capacity. Using statistical tools, several existing performance measure are investigated to reduce the variability in collapse capacity for more effective risk assessment using existing approaches.
- Chapter 6 introduces new structural collapse capacity and demand models to use in probabilistic assessment of structural collapse. Using safety margin approach, collapse fragility models are constructed based on the developed collapse capacity and demand models for a more reliable probabilistic evaluation of structural collapse. Then, these fragility models are enhanced using available information about applied ground motions.
- Chapter 7 investigates the sensitivity of collapse capacity to uncertainties existed in structural parameters and ground motion characteristics. Collapse fragility models are then developed to investigate effect of these uncertainties on seismic collapse performance of structures.
- Chapter 8 gives a summary of the study and the main findings, provides the limitations of the study, and lists the potential topics for future work.

2. LITERATURE REVIEW: ASSESSMENT OF STRUCTURAL COLLAPSE

The objectives of this chapter are to: (1) review existing analysis and modeling methods used for assessment of structural collapse capacity under seismic forces, (2) summarize limitations of the existing methods, and (3) describe experimental and analytical work on structural collapse reported in the literature. The chapter also points out challenges in computational simulation of dynamic instability, and identifies needs for accurate prediction of structural capacity to determine a proper level of structural reliability against dynamic collapse.

2.1. Structural Collapses under Earthquake Excitations

2.1.1. Definition of Dynamic Global Collapse

The definition of global collapse of a frame structure under seismic excitation in this study is the condition of dynamic instability, that is, the structure, or any significant part of it, is not able to find a new equilibrium configuration, therefore loses the ability to sustain the gravity loads.

One or several structural components of a building may fail due to an earthquake excitation but the structure may still be able to maintain its integrity and prevent such local failures from triggering the global instability of the structure. For example, a gravity column may fail in compression, or shear transfer may be lost between a beam and a column, or plastic hinges may form at the beam-ends. Under such conditions, the failed members are unable to resist the applied loads and look for alternative load paths to redistribute the applied forces. If the structural system achieves an alternative equilibrium configuration, then the system survives. If the damaged system is unable to find alternative load paths and equilibrium condition, global collapse or at least story collapse can occur. “Sidesway collapse” may occur if lateral drifts of a story or a number of stories increase significantly as a consequence of progressive reduction in lateral load carrying capacity. The lateral drifts keep increasing until the building losses gravity load resistance against the P-delta effects accelerated by component deterioration in strength and stiffness. On the other hand, “vertical collapse” may occur when one or several structural members directly lose gravity load carrying capacity under a seismic excitation (Krawinkler et al., 2007, 2009).

Figure 2.1 shows two examples of sidesway collapse occurred in past earthquakes: a four-story apartment building that failed at the first story during 1995 Kobe earthquake (Figure 2.1a); and a three-story parking structure, which is a moment-resisting frame structure with a mix of precast and cast-in-place, partially collapsed due to extensive bending of the first story-reinforced concrete columns during 1994 Northridge earthquake (Figure 2.1b). As seen in the figures, the first-story columns in both buildings were severely damaged resulting in global failure of the structure due to dynamic instability.

(a)

(b)

Figure 2.1 a) An apartment building failed at the first story during 1995 Kobe, Japan earthquake, and b) bending of columns and partial collapse of a parking structure in 1994 Northridge earthquake (Photo credit: National Information Service for Earthquake Engineering, University of California, Berkeley; National Geophysical Data Center (NGDC) /NOAA).

(a)

(b)

Figure 2.2. a) Story collapse of a metal frame at 5th floor in 1995 Kobe earthquake, and b) collapse of upper levels of a steel building observed in 1985 Mexico City earthquake (Photo credit: National Geophysical Data Center (NGDC) /NOAA, Dr. Roger Hutchison; H. Martin).

Failure of the first story of a building is the most common shape of sidesway collapse mechanism observed in past earthquakes since seismic forces usually impose largest maximum shear forces on the lowest stories of buildings leading to failure in story shear resistance at the bottom levels. However, a weak story or a number of weak stories may form in the mid-level or upper levels of the building that may be due to discontinuities of stiffness through the structure, for instance, as a result of irregular placement of infill walls, or due to higher mode effects that may take place especially in tall buildings under a seismic input. Figure 2.2a shows that the fifth floor on an eight-story high-rise metal frame totally collapsed with a large lateral drift under seismic excitations of 1995 Kobe earthquake. It appears that the other stories were designed with adequate strength to overcome impulsive forces due to the failure of the fifth story, and thus, escaped story collapse. By contrast, Figure 2.2b shows that the columns of top stories of a steel concentrically braced frame failed in gravity against impulsive forces associated with initially collapsed story leading to a successive vertical collapse of upper floors (pancake collapse) during 1985 Mexico City earthquake.

2.1.2. Seismic Performance of Modern Buildings

The design philosophy of modern seismic provisions recognizes needs for sufficient strength, ductility and energy dissipation capacity to prevent global collapses of structures by strong earthquake excitations. The fundamental concepts covered in these design provisions are:

- "Strong column and weak beam" design to maintain structural integrity under gravity forces
- Design of dissipative regions concentrated at the beam ends and at the base of the columns, which ensures the nodal zones have sufficient strength and rotation capacity in order to avoid brittle failure,
- Ductile detailing design to provide structural ability of dissipating energy after yielding when subjected to a series of large inelastic deformation cycles, and
- Proper design of structure to stand within allowable story-drift limits in order to keep vertical stability of the structure.

Many structural collapses occurred in recent earthquakes have taken place in non-ductile frames such as older buildings designed with inadequate seismic design or other buildings with poor

quality of design and construction (Figure 2.1 and Figure 2.2). However, several collapses of modern structures have also been observed even when these structures were built in accordance with the requirements of seismic building code and construction practice standards (Villaverde, 2007). An example is the total collapse of the 22-story steel frame building of Pino Suarez complex during the 1985 Mexico City earthquake (see Figure 2.3). Ger et al. (1993) investigated the reasons of the collapse and performed dynamic analyses on a three-dimensional finite element model of the collapsed structure under the same ground motion. The authors have found that ductility demands in longitudinal girders exceeded the design-based ductility capacity leading the girders to redistribute the applied forces and so the nearby columns to fail in local buckling, therefore resulting in complete collapse of the building against gravity forces under amplified P-delta effects.

Figure 2.3 Wreckage of a 22- story steel-constructed building in the Pina Suarez Apartment Complex in 1985 Mexico City earthquake comparing to the identical building standing in background (Photo credit: National Geophysical Data Center, NOAA, E.V. Leyendecker, National Bureau of Standard).

Another example is the collapse of Alto Río building in the 2010 Maule, Chile earthquake. It was a 15-story reinforced concrete structure completed in 2009, following the present Chilean building codes. The building was designed with reinforced concrete structural walls occupying nearly 7% of the floor area for earthquake resistance. Failure of the structural walls at the first story under the seismic actions caused the building to overturn entirely as seen in Figure 2.4.

Based on several analytical studies on a representative three-dimensional model, Song et al. (2012) showed that the maximum structural demand of drift ratio should be around 1% for the building to keep such integrity in Figure 2.4, therefore indicating a brittle failure mechanism. They also stated that overturning of the building required tension or bond failure in more than half of the vertical reinforcement at the failure surface. They explained that this failure can be due to the fracture of vertical bars at sections with low reinforcement ratios or unbonding of unconfined lap splices.

(a) (b)

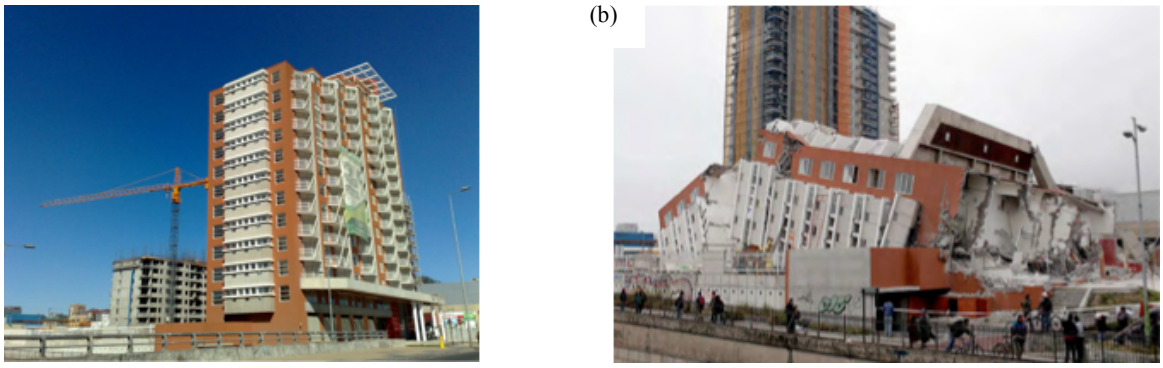

Figure 2.4 The 15-story reinforced concrete Alto Rio building a) before, and b) after 2010 Maule, Chile earthquake (Photo credit: http://www.chw.net/foro/off-topic-f16/309633-edificio-alto-rio-concepcion-antes-despues.html; Jorge Arturo Borbar Cisternas).

Moreover, unexpected extensive damage observed in the 1994 Northridge earthquake as well as in the 1995 Kobe earthquake (Bertero et al. 1994; FEMA-355E, 2000; Nakashima et al. 2000; Engelhardt, 2001). Many modern steel frames experienced fractures in their welded beam-column connections although these frames had been considered ductile enough to be able to resist large inelastic cyclic deformations (see Figure 2.5). Moment resisting frame (MRF) buildings with fractures in connections are extremely vulnerable to dynamic instability in brittle failure mode because of lack of redundancy in connection design that can cause a sudden collapse without warning signs. Once fracture is initiated in connections, such structures are not able to show significant deterioration of strength and stiffness therefore has very limited capacity to absorb and dissipate the destructive energy of strong ground shaking, resulting in the collapse mode of the steel building shown in Figure 2.3.

Although modern seismic provisions for collapse protection have been used for many years, observations of unsatisfactory performance under dynamic earthquake loadings have raised questions about accuracy of these provisions. As a result, several studies have been conducted to improve current building codes to prevent collapse of structures. Following sections summarize current collapse assessment methods reported in the literature and needs for further research on understanding structural collapse and regional seismic hazard.

(a) (b)

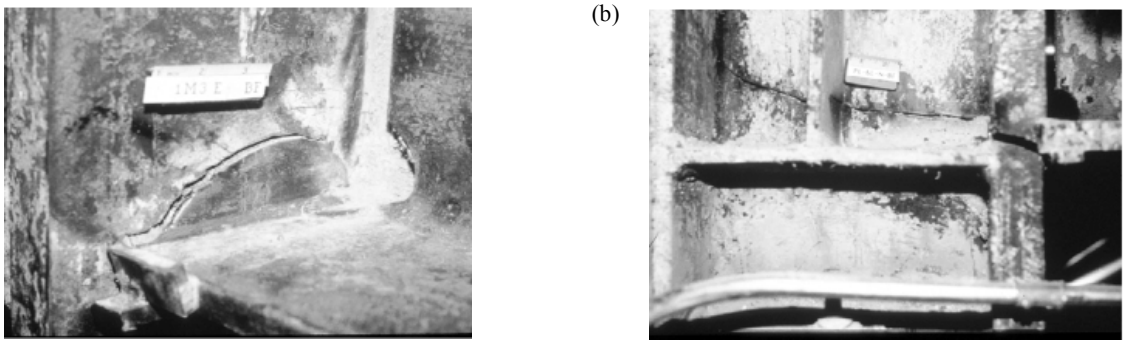

Figure 2.5 a) Fractured column flange, and b) fracture through a column flange and web at a moment connection immediately found after the Northridge Earthquake (Photo credit: Engelhardt, 2001).

2.2. Methods to Assess Collapse Capacity

Assessment of collapse capacity of structures under earthquakes requires: (1) analytical modeling of structures considering collapse triggering factors such as P-delta effects and component degradation, (2) selection of seismic ground motions, (3) performing nonlinear dynamic analyses to get the structural behavior up to collapse, and (4) prediction of the structural collapse with integration of uncertainties in ground motions and analytical models (Krawinkler, 2007).

Selection of a representative set of seismic inputs used in collapse prediction and assessment of collapse fragility curves with incorporation of uncertainties in models and ground motions are described in depth in the following chapters. The literature review described here focuses on the modeling and analysis options and recent studies to assess collapse capacity of structures.

Modern design guidelines (FEMA-350, 2000a; FEMA-351, 2000; FEMA-356, 2000b) allow for the use of nonlinear static and nonlinear dynamic methods to evaluate the collapse capacity of a building structural system. Assessment methods based on linear behavior of structures are often used in design codes but not preferred for collapse assessment because of complex nonlinear behavior of structures including ductility effects.

2.2.1. Nonlinear Static Procedure

The nonlinear static procedure, or so-called "pushover analysis" evaluates the relationship between base shear and top lateral displacement of a nonlinearly modeled structure subjected to monotonically increasing lateral forces with a prescribed distribution over the height of the structure. The analysis continues until the displacement at top reaches the target amount or until the base shear reduces to zero. The target value is set as the maximum displacement that the structure possibly experiences based on the intended seismic hazard level. Reduction of the base shear to zero after a negative slope in the pushover curve indicates the loss of lateral and so vertical resistance therefore signifies a global collapse. The performance of the structure is assessed by evaluating the force and deformation demands (e.g., plastic hinge rotations and elements shear forces) corresponding to target top displacement value against the prescribed tolerances. These tolerances are determined considering material type, member type and importance and intended structural performance level. The procedure needs to be supplemented with a linear dynamic analysis for the structures with significant higher mode effects (FEMA-273, 1997; FEMA-356, 2000b).

Pushover analysis has become a preferred standard method by practitioners for the purpose of evaluating seismic performance and safety of structures. However, comparison between findings from damaged buildings in the 1994 Northridge earthquake and the results from nonlinear time history analyses performed by several researchers, nonlinear static methods are found to underestimate story drifts and fail to detect correct locations of formed plastic hinges, especially for ductile structures that show remarkable inelastic behavior and a significant degradation in lateral capacity. Therefore, nonlinear static methods are considered not reliable enough to assess collapse capacity of structures. In particular, Villaverde (2007) noted that such methods tend to:

- Neglect ground motion characteristics such as duration and frequency content by

assuming constant equivalent lateral forces distributed over the height of the structure,

- Ignore load-path dependency of nonlinear structural behavior, and
- Assume constant structural parameters such as period by ignoring gradual changes due to dynamic forces.

To overcome these limitations, some researchers improved the pushover analysis approach by applying a time-variant distribution of the equivalent lateral forces on the structures or by considering the contribution of higher modes (Villaverde, 2007). Although these studies have improved the prediction for some cases, it is noted that the performance predicted by pushover analysis is not directly related to that at the near-collapse level because the original objective of the approach is to be able to achieve a target displacement without excessive component degradation (Krawinkler, 2007). It is now widely accepted that nonlinear dynamic analyses need to be performed to assess collapse capacity of structures accurately (Villaverde, 2007; Krawinkler, 2007).

2.2.2. Incremental Dynamic Analysis

The U.S. Federal Emergency Management Agency (FEMA) guidelines recently adopted incremental dynamic analysis (IDA; Vamvatsikos and Cornell, 2002, 2004; Zareian and Krawinkler, 2007; Liel et al., 2009; FEMA-350, 2000a; FEMA-351, 2000) as a method to determine the global collapse capacity of a structural system under earthquake excitations. This approach is based on the behavior of so-called "IDA curves," which track relationship between an "intensity measure (IM)" (e.g., spectral acceleration of an earthquake input) and a "damage measure" (DM) or "engineering decision parameter" (EDP) (e.g., maximum inter-story drift ratio) through nonlinear dynamic analyses under several ground motions at incrementally increased intensity levels. The main premises of this approach are: DM increases at constantly higher rates; and, as DM accelerates towards "infinity," i.e., the IDA curve almost flattens, which indicates the collapse of the structural system. Parametric and non-parametric statistical approaches have been proposed to describe the uncertainties in the DM-IM relationship, which is incorporated into the probabilistic framework of performance-based earthquake engineering (Cornell and Krawinkler, 2000). A similar approach has been adopted by a recent research project of the Applied Technology Council (ATC-63, 2009), *Quantification of Building Seismic*

Performance Factors. Seismic collapse fragilities – conditional probabilities of collapse given a seismic IM – have been also developed (Krawinkler and Zareian, 2007) by use of lognormal distributions fitted to the statistics of the levels of IMs causing collapse during the IDA.

Seismic collapse assessment of structures obtained through IDA curves depends on the selection of IM and DM used to construct these IDA curves as well as variability in the set of ground motions considered in the analysis (Villaverde, 2007). IDA curves usually reach a flat plateau as an indication of collapse (i.e., a large increase in the structural response corresponding to a small increase in the ground motion intensity) but this plateau may occur at several different intensity levels of ground motions. According to Krawinkler et al. (2003), the dispersion in collapse-causing intensity levels can be handled by selection of a large set of ground motions including a meaningful variability in their characteristics such as duration, frequency content, and magnitude, but it requires a significant computation effort to perform nonlinear dynamic analyses under such a large sample of ground motions therefore making IDA computationally demanding.

Moreover, occurrence of "collapse" in IDA curves may not be clear or curves may show unusual behaviors such as non-monotonic behavior and discontinuities instead of flattening of the curve (Vamvatsikos and Cornell, 2002). For example, in Figure 2.6, IDA curves of a 5-story braced steel frame under thirty ground motions show large variability in collapse capacity from ground motion to ground motion and some curves show chaotic behaviors. To overcome such challenges in the identification of collapse occurrence, some rules have been proposed by Vamvatsikos and Cornell (2002). The building's global drift capacity was assumed as the maximum story drift ratio at which the slope of the curve reduces to 20% of the initial slope (IM-based rule), but if IDA curve does not fulfill the IM-based rule, then one checks if the drift ratio exceeds an assumed global drift capacity, 10% (DM-based rule). However, these IDA-based collapse identification rules depend on assumed threshold values on IM and DM, therefore not sufficient for objective and physics-based identification of a structural collapse based on actual dynamic instability of a structure. This deficiency reveals research needs in developing collapse criteria based on dynamic instability in order to evaluate structural capacity accurately against earthquake-induced collapse.

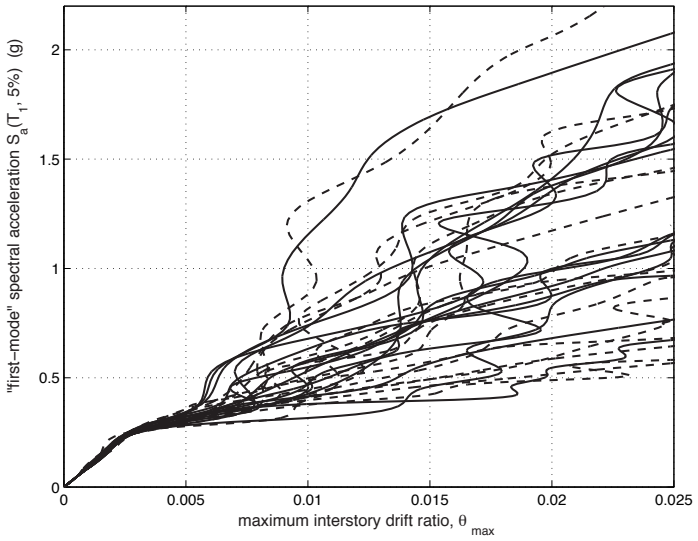

Figure 2.6. IDA curves for 30 records on a 5- storey steel braced frame (Vamvatsikos and Cornell, 2002).

Large dispersion observed in collapse-causing intensities of ground motions has initiated search for alternative intensity measures to assess collapse capacity of structures. For example, one could consider the following intensity measures in IDA analysis: Arias intensity (Arias, 1970), potential destructiveness (Araya and Saragoni, 1980), characteristic intensity (Park et al., 1985), integration of elastic spectral acceleration with epsilon (Baker and Cornell, 2005), modified earthquake power index (Housner, 1975, and Riddell, 2007), and intensity formulations as a function of inelastic spectral parameters (Tothong and Cornell, 2007, 2008). Furthermore, as noted by Vamvatsikos and Cornell (2002), one can consider alternative damage measures for IDA, such as maximum interstory drift ratio, maximum base shear, node rotations, peak story ductilities, roof drift, floor peak interstory drift angles, and damage indices including a global cumulative hysteretic energy such as Park-Ang index (Park and Ang, 1985), stability index (Mehanny and Deierlein, 2000) and others (Castiglioni and Pucinotti, 2009). It is also noted that, depending on the collapse mechanism of a particular structural system, it may be desirable to use more than one DM or IM in an IDA to predict the collapse more accurately. For example, Vamvatsikos and Papadimitriou (2005) assign a threshold value to each of selected DMs and the system is considered to reach the collapse limit-state when at least one threshold is exceeded. However, most of recent research on the IDA-based approach has selected only one DM and one IM (mostly maximum story drift ratio and elastic spectral acceleration) and lacks thorough

investigation on optimal selection/combination of multiple performance measures that describe the limit-state most effectively and on the benefit of having more than one DM or IM for collapse capacity prediction. Moreover, the aforementioned premise of the IDA approach – a flat plateau of the curve indicates collapse – has not been examined through comparison with experimental test results. Maison et al. (2008) have recently observed a significant gap between the collapse capacities observed by full-scale tests and those predicted by design guidelines employing IDA with macro-models (See Figure 2.7). Limitations of IDA mentioned herein are mainly due to the intrinsic difficulty in obtaining sufficient number of test data points that can describe the actual limit-state surface in the space of multiple performance measures.

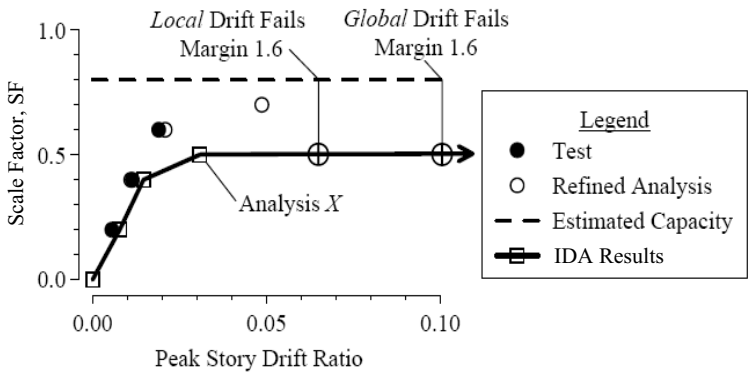

Figure 2.7 FEMA-351 collapse prevention evaluation (Masion et al., 2008).

2.3. Structural Models for Collapse Assessment

Structural collapse under dynamic loads is highly nonlinear complex phenomenon affected by several key factors that are difficult to quantify accurately. Besides the factors related to ground motions applied to the structure (e.g., intensity, duration, and frequency content) and soil-structure interaction (e.g., stiffness of foundation soil, and soil settlements), key 'structural' parameters, which should be considered in the realistic analytical modeling are listed as follows (Villaverde, 2007):

- Geometry of the structure with consideration of torsional effects due to existence of irregularities

- Dynamic properties of the structure such as damping and period
- Material properties of structural components such as stiffness, strength, and post elastic and post-buckling parameters
- Cyclic degradation of components due to spread of plasticity and fracture at connections, and local/global buckling at several elements
- Influence of applied gravity forces on lateral drifts
- Effects of nonstructural components (e.g., stairs, cladding, and infill walls) on structural behavior
- Fabrication issues such as residual stresses and initial imperfections existed in structural components

There are several efforts reported in the literature to simulate structural collapse from simplified single-degree-of-freedom (SDOF) models to complex high-fidelity models. Each assumption made in analytical models increases uncertainty in collapse predictions. Therefore, the point that should be considered in adapting a collapse model is the amount of additional dispersion tolerated in the evaluation of collapse capacities. Obviously, the more accurate model one uses, the more reliable results are obtained. However, it should be also noted that collapse analysis of such advanced and complex models can be computationally demanding and highly sensitive to numerical convergence issues in nonlinear dynamic analysis especially when the structure is near collapse.

2.3.1. SDOF Models

Numerous studies reported in the literature used simple SDOF models for collapse assessment of structural systems because of practical applicability (Takizawa and Jennings, 1980; Bernel, 1987, 1992, 1998; Williamson, 2003; Miranda and Akkar, 2003; Adam et al., 2004). Most recently, there were studies to assess collapse capacity by use of simplified SDOF models based on the properties found from a pushover analysis or based on the relationship developed between pushover and incremental dynamic analysis (Adams et al., 2004; Vamvatsikos and Cornell, 2005). For instance, Adam et al. (2004) investigated the P-Delta effects of non-deteriorating systems with an assumption that collapse mechanism can be predicted from post-yield global stiffness obtained from a pushover analysis. The results showed good accuracy between the

collapse capacities obtained from simplified SDOF models and the corresponding actual single-bay multi-degree-of-freedom (MDOF) structures through incremental dynamic analyses for 40 ground motions assuming a large increase in the structural response as an indication of dynamic instability (Adam et al., 2004).

SDOF models are practical and very efficient in terms of computation time but less reliable since these models cannot simulate the collapse mechanism (i.e., deformed shape of the structure near collapse) as in the case of MDOF models that accounts for effects of higher-order modes on the structural behavior. Bernal (1992, 1998) studied the capacity against dynamic instability of two-dimensional buildings by reducing them into elasto-plastic and stiffness-degrading SDOF models with second-order effects. Bernal assessed the minimum necessary base shear to prevent dynamic instability under a selected set of 24 earthquake records from firm ground sites. Comparing the results from simplified models to those from actual structures, Bernal found that the dynamic instability of the structures is highly sensitive to collapse mechanism. Therefore, collapse mechanism cannot be presented accurately by either simplified SDOF models or pushover analysis (Villaverde, 2007).

2.3.2. Finite-Element-Based Macro-Models

Most of recent collapse assessment by practitioners and researchers entails the use of stress-resultant macro-models, such as beam-type finite element based models. A sudden increase in structural response during such analysis is usually considered as an indicator for dynamic instability (Villaverde, 2007).

One of the collapsed buildings observed during the 1985 Mexico Earthquake was a 22-story steel building in Mexico City. This collapse case raised questions about accuracy of the modern seismic provisions. Several researchers have made investigation about the collapsed building using field observations of an adjacent building which was heavily damaged in the same earthquake and almost identical to the collapsed one (see Figure 2.3). One of the investigators, Ger et al. (1993), performed dynamic analyses using a three-dimensional finite element model of the collapsed structure under the same ground motion in three-components recorded at a station near the collapsed building site. They first considered realistic nonlinear hysteretic constitutive relationships for each member of the structure such as open-web girders, welded box columns,

and H-shape diagonal brace; and also included geometrical nonlinearity for each element. They found that ductility demands exceeded the design-based ductility capacity due to high inelastic demand occurred in longitudinal girders. This caused the applied forces on failed girders to be re-distributed to nearby elements, which then resulted in local buckling of columns of the second to fourth floors. The columns under local buckling cannot resist applied forces any more and thus allow the building to sway laterally under amplified P-delta effects. Then the building finally loses its ability to sustain gravity forces and prevent a complete collapse. A significant outcome of their study is that simplified models can be used to predict collapse capacity of structures accurately if the models can simulate realistic force-deformation behaviors (Villaverde, 2007).

In another example, Challa and Hall (1994) analyzed the collapse capacity of a 20-story moment-resisting steel frame under severe ground motions by use of fiber elements to model frame elements and shear pane zone elements to model connections. They considered geometry nonlinearity due to the P-Delta effects; and developed realistic stress-stain relationships that account for column buckling, strain-hardening, axial-flexural yield interaction, residual stresses, and spread of yielding for both the element fibers and the panel zones. During step-by-step analysis of the structure, they identified dynamic instability from unbound growing of lateral displacements. As stated by the authors, this study may lead to late occurrence of collapse since the developed models neglect significant softening due to deterioration in structural components, which has been recently found the most important modeling aspect in the collapse prediction (Krawinkler et al., 2009).

Several research efforts have been made to develop and calibrate analysis models to simulate cyclic degradation in structural components. For example, as part of the research conducted under the SAC Joint Venture, Lee and Foutch (2002, 2004) studied collapse of steel moment-resisting frames by using beam finite elements for the steel girders and columns, coupled with the use of uniaxial moment-rotation relations at the girder ends that include a steep drop in the moment strength at a calibrated value of rotation. This softening is implemented into the model to consider the effects of brittle fracture in the girder-to-column connection, as well as the subsequent response of the frame**.** Likewise, Rodgers and Mahin (2004) considered hysteretic behaviors of connections due to ductile and brittle fractures in the collapse analytical studies of steel frames by adjusting the moment-rotation response of the structural components in a similar

way. Additionally, Ibarra et al. (2005) established some simple hysteretic moment-rotation models based on cyclic energy dissipation to include deterioration in stiffness and strength of components under large cyclic inelastic displacements. The developed phenomenological models consider cyclic deterioration in four component parameters: yield strength, post-capping strength, unloading stiffness, and reloading stiffness. The developed models are calibrated with experimental data from tests of steel, plywood, and reinforced concrete components; and good correlation is obtained in general.

Many investigators including Haselton et al. (2009) and Liel at al. (2009) followed these hysteric rules developed by Ibarra et al. (2005) to incorporate cyclic deterioration due to concrete crushing and rebar buckling and fracture in assessing seismic collapse safety of reinforced concrete moment-frame buildings. In a similar study, Lignos et al. (2009) used a modified version of the Ibarra–Krawinkler deterioration model with the following changes: different rates of cyclic deterioration in the two loading directions and residual strength to consider asymmetric component hysteric behavior, and a sudden drop in strength at an ultimate deformation to simulate fracture in a component. Also, using the modified model, Lignos and Krawinkler (2010) quantified important parameters that affect the cyclic moment-rotation behavior at plastic hinge regions in beams and proposed empirical relations for beams with reduced beam section (RBS) and beams other than RBS based on a database on experimental data of steel components.

Lastly, some researchers investigated progressive collapse in buildings considering element removal in the structural model when the structure reaches the load-carrying capacity (Kaewkulchai and Williamson 2004; Talaat and Mosalam, 2007; Szyniszewski, 2009). For instance, Kaewkulchai and Williamson (2004) presented a beam element formulation and solution procedure for progressive collapse analysis of planar frame structures. The developed beam-column element utilizes a multi-linear, lumped plasticity model, and also accounts for the interaction of axial force and bending moment, focusing on removal of the complete element upon breaching specific damage criteria.

2.3.3. Sophisticated Analytical Models

There are also some sophisticated collapse models reported in the literature. For example, Meguro and Tagel-din (2001) proposed the Applied Element Method (AEM) to simulate the

structural behavior from initial loading to collapse by modeling a building as an assembly of small elements connected by pairs of normal and shear springs. Sun et al. (2003) applied this approach to a single-column pier collapse in the 1995 Kobe earthquake and found a good match between the analysis results and the field observations. Khandelwal and El-Tawil (2007) also developed finite element formulations for collapse modeling of steel structures based on the use of a moderately fine mesh of shell elements to represent the steel members and connections. Through calibration for phenomenological modeling of such effects as lateral-torsional buckling, they successfully simulated experimental results of components of steel structures subjected to extreme deformations.

According to Villaverde (2007), it is possible to predict the structural collapse with improved accuracy if the computational model of the structure can adopt equilibrium equations based on updated configuration at each time step of dynamic analysis; simulate nonlinear large deformation; and use fine-meshed members to capture accurately the spread of plasticity, local instabilities, and fracture. In order to achieve reliable results, all these points need to be considered in the modeling to simulate dynamic instability. However, due to the computational cost, these could be impractical in large-scale parametric studies on collapse investigation of structures. On the other hand, most studies employing much simpler collapse macro-models typically do not consider lack of redundancy in the connections due to fracture instability that may lead the structure to global collapse. While some researchers including Lee and Foutch (2002, 2004), Rodgers and Mahin (2004) and Lignos et al. (2009) incorporated the softening response due to fracture that occurs in steel frames, the formulation is generally limited to adjusting the moment-rotation response of the element. For this reason, the researchers at Northeastern University that have been collaborating for this study are currently exploring the use of cohesive zone modeling (CZM) for simulating plasticity, fracture, and subsequent fragmentation and collapse of structures made from ductile metal materials such as steel. In particular, they are investigating what is needed to include simple fracture models and element separation in the connection region by adapting a cohesive-zone-like element at the interface between two beam elements, and aim to develop a method that integrates the softening and nodal separation due to fracture through phenomenological modeling to enable more direct modeling of collapse due to combined axial tension and flexure.

2.4. Past Experimental and Analytical Studies on Collapse of Structures

2.4.1. Summary of Past Experimental Studies on Structural Collapse

There exist few experimental tests that aim at thorough investigation of collapse of frame structures:

- Kato et al. (1973) conducted shake-table tests of 5.9 inches high H-steel columns fixed at both ends with a concentrated mass at the top. They studied strain hardening and P-delta effects on collapse behavior of the test specimen.
- Vian and Bruneau (2003) tested several simple frames with a rigid mass at the top supported by four steel columns. They investigated the effect of stability coefficient on collapse considering a story height ranging from 3.6 inches to 21.6 inches. The shake table tests are performed until collapse occurs due to geometric nonlinearities.
- Elwood and Moehle (2003) tested two one-half scale reinforced concrete plane frames up to collapse level to study the nonductile seismic performance of such structures. The frames consisted of three columns fixed at the base and a beam connected to all columns at the top. Gravity force is applied only to the central column, which was designed to be vulnerable against shear failure. They investigated the vertical load carrying capacity of the frame due to the lack of this central column support due to failure in shear.
- Kanvinde (2003) performed shake table tests on a 10 inches high, one-story, and one-bay steel frame with a rigid mass at the top. The collapse mechanism of the specimen is due to the plastic hinges formed at the top and bottom of the four steel flat columns under nonlinear large displacements (see section 3.4.1 for more details).
- Rodgers and Mahin (2004) conducted a series of one-third-scale shake-table tests to study the effects of connection degradation and fracture on the cyclic dynamic response of steel frame structures leading to collapse. This comprehensive set of studies used idealized mechanical connections between the girders and columns to establish well-documented material inelasticity and fracture performance in the connection region (see section 3.4.2 for more details).
- Lignos et al. (2008) conducted one-eighth-scale shake-table tests on a four-story, two-bay steel moment-resisting frame structure with specially manufactured plastic-hinge

elements at the connections to carefully control the behavior in the key areas of damage. Geometric nonlinearity due to large-displacements contributed heavily to the collapse by dynamic instability (see section 3.4.3 for more details).

- Suita et al. (2008) conducted full-scale shake-table tests of a four-story one-bay steel moment-resisting frame structure. The predominant damage mode consisted of severe inelastic local buckling at the tops and bottoms of the steel box columns.

Collapse experiments are needed to assess the sufficiency of existing collapse assessment methods and to advance the understanding of real structural behavior near collapse. Comprehensive and accurate measurements of key parameters from collapse experiments are especially important to validate and calibrate the developed analysis models. These tests are different but provide a complementary set of collapse failure cases that provide an excellent data set for research in collapse assessment.

2.4.2. Summary of Analytical Studies on Structural Collapse

Numerous studies on collapse assessment of frame structures under seismic excitations proved that geometry nonlinearity effects (i.e., destabilizing effects of gravity loads) and material degrading are important factors that trigger dynamic instability of structures. When the structure is in elastic range, these factors are negligible, but especially under severe cyclic loads, these factors become significant such that building is no longer able to sustain applied gravity loads. Many research efforts have been made to quantify contribution of these factors into the structural collapse capacity. Several studies have also proposed simplified techniques to get collapse assessment of structures through equivalent SDOF models. Additionally, some researchers sought for alternative methodologies or performance measures to assess collapse capacity. Lastly, there are some studies that investigated the accuracy of modern seismic provisions. Villaverde (2007) makes a well review of these analytical studies reported in the literature. Following his notes, selected studies are summarized below in the chronological order:

- Jennings and Husid (1968) found that cyclic, inelastic and large displacements caused by the ground shaking on a one-story frame with springs at column bases may result in permanent deformations in the structures. They stated that accumulation of permanent deformations in one direction may render gravity loads as the dominant forces and lead

the frame to collapse by lateral instability.

- Takizawa and Jennings (1980) represented a ductile reinforced concrete frame structure by an equivalent SDOF model with a non-degrading trilinear force-deformation behavior. The collapse capacity of the frame was investigated under the destabilizing effect of gravity forces and ground motions by examining the ultimate capacity of the restoring force in the system. This study is one of the first efforts to consider both P-Delta effects and material degradation in collapse assessment.
- Bernal (1987) proposed amplification factors based on empirical formulas including ductility factor and stability coefficient to quantify P-Delta effects taking place in the structure. He considered a non-degrading elasto-plastic SDOF model and obtained the amplification factors as the ratio of inelastic acceleration response spectrum generated with and without P-Delta effects. Bernal compared his findings with the amplification factors recommended by seismic design provisions and found that the code provisions were inadequate to reflect the destabilizing effect of gravity loads and this inaccuracy increased in direct proportion to ductility factor considered in the design.
- Bernal (1992) also studied the instability of two-dimensional moment-resisting frames subjected to earthquakes. He performed nonlinear dynamic analyses on equivalent elasto-plastic and stiffness-degrading SDOF models including P-Delta effects and investigated the correlation relationships between minimum base shear required to prevent instability and some key structural and ground motion parameters. He obtained safety factors of the frames against dynamic instability by dividing the actual base shear capacity by the minimum base shear found from the equivalent SDOF models. He concluded that safety against dynamic instability is highly sensitive to the system's failure mechanism and cannot be guaranteed by simply limiting the maximum elastic story drifts of the structure in contrast to the philosophy stated in seismic modern provisions.
- MacRae (1994) followed the approach used in the study by Bernal (1987) considering different hysteretic parameters in the structures under P-delta effects and found out that the ratio of inelastic stiffness to elastic stiffness is the major parameter that leads the structures to accumulate uni-directional permanent deformations.
- Challa and Hall (1994) analyzed the collapse capacity of a 20-story moment-resisting steel frame under severe ground motions considering nonlinear material and geometry

effects. Based on step-by-step analysis on the developed finite element based analytical model, they observed unbound growing in lateral displacements as a result of forming of significant plastic hinges in the structure's columns. This causes the collapse of the structure although the columns are designed with larger flexural strength than of its beams at all joints according to modern seismic provisions.

- Martin and Villaverde (1996) studied seismic behavior of a two-story, two-bay frame structure that meets all the requirements of the 1992 AISC seismic provisions. They found excessive plastic hinging in the columns of the nonlinear finite element model. This leads the model to collapse under a moderately strong ground motion, therefore behaving in contrast to weak beam-strong column concept intended in seismic provisions.
- Araki and Hjelmstad (2000) performed studies on SDOF models and found that a singular stiffness matrix is not enough to cause dynamic instability of structures due to unloading that may take place following such a condition resulting in recovery of the structure from dynamic instability.
- Mehanny and Deierlein (2001) developed a methodology to evaluate the collapse capacity of composite moment frames under earthquake loads. In the developed methodology, first of all, they performed nonlinear dynamic analysis using the finite element model and measured damage in each component of the structure. Then, they modified the model based on the calculated damage measure in each component and performed a second-order static analysis on the modified model considering residual displacements and gravity loads. The ratio of maximum gravity loads that initiated global static instability of the modified structure to actual gravity forces was used as a global stability index that quantified collapse capacity under a ground motion intensity.
- Vamvatsikos and Cornell (2002, 2004, 2005) described IDA comprehensively as a valuable tool to assess global collapse capacity of structures. They examined the seismic intensity-structural response curves of MDOF steel structures under incrementally increased several ground motions and described how to interpret global instability from IDA curves. They also mentioned about some possible unusual behaviors of IDA curves such as structural resurrection as well as sensitivity of these curves to a particular selection of ground motions. In a similar study, they demonstrated step-by-step efficient IDA on a nine-story steel moment-resisting frame with fracturing connections and how to

integrate IDA results into PBEE framework (2004). Additionally, they studied collapse capacity of MDOF structures through simplified SDOF models based on the relationship developed between pushover and incremental dynamic analysis (2005).

- Lee and Foutch (2002) evaluated the performance of several steel frame buildings subjected to a large set of earthquake ground motions. These buildings satisfied the design requirements of the 1997 NEHRP provisions (FEMA 1998) and included prequalified post-Northridge beam-column connections. In the development of analytical models, they considered ductile beam-column joints and modeled these connections by use of uniaxial moment-rotation relations that include a gradual degradation in the moment strength at a calibrated value of rotation. They assessed the maximum story global demand and local drift angle demand of the beam-column joints through incremental dynamic analysis employing traditional IDA-based rules. They found that all structures studied in the research had enough capacity against seismic drift demands for the selected performance objective of collapse prevention.
- Williamson (2003) studied inelastic SDOF models under various earthquake ground motions. The models consisted of rigid columns with rigid mass at the top and degrading springs at the base. He found that damage accumulation and P-Delta effects are very important parameters that may trigger structural dynamic instability; and earthquake vertical accelerations do not significantly affect the response of structures. In agreement with the observations from Bernal (1992), he also stated that limiting the maximum elastic story drifts of the structure do not guarantee safety against dynamic instability necessarily.
- Miranda and Akkar (2003) studied the minimum lateral strength required to lead dynamic instability of degrading SDOF models compromising P-Delta effects under a large set of ground motions. They established empirical formulas that described minimum lateral strengths as a function of natural period and negative post-yield stiffness.
- Adam et al. (2004) evaluated collapse capacity of single-bay MDOF structures based on post-yield global stiffness obtained from a pushover analysis on equivalent non-degrading SDOF models including P-Delta effects. He found a good match between the results provided by the simplified technique and those obtained through incremental dynamic analyses on actual structures assuming a large increase in the structural response

as an indication of dynamic instability.

- Ayoub et al. (2004) studied effects of strength softening and cyclic degradation of strength and stiffness on collapse potential of a SDOF structure with a natural period of 1.0s considering three following material models: a bilinear model, a modified Clough model, and a pinching model. They performed the collapse evaluation assuming the building's strength is zero near collapse. After performing IDA for a large set of ground motions considering different levels of degradation, they determined that systems with low degradation or with moderate degradation showed similar probability of collapse for a selected ground motion intensity. However, they found that systems with severe degradation showed higher potential for collapse.
- Ibarra and Krawinkler (2004) investigated the global collapse capacities of deteriorating MDOF frame structures subjected to seismic forces using cyclic deteriorating hysteretic models calibrated with experimental data. They assumed that plasticity were concentrated at the beam-ends and at the base of the columns in the models. They used a relative intensity measure as a function of spectral acceleration at the fundamental period of structure and base shear coefficient. Through incremental dynamic analysis, they assessed the collapse capacity based on the relative intensity measure at which intensity measure versus maximum roof drift curve becomes flat. To find out key parameters that influenced collapse capacity of structures most, they also performed a parametric study on stiff and flexible single-bay frame structures with 3, 6, 9, 12, 15 and 18 stories considering uncertainties in the frequency content of ground motions as well as in structural deterioration parameters. They concluded that softening of the post-yield stiffness and the displacement at which this softening begins were two significant factors, and cyclic deterioration was also important but not a principal factor in collapse assessment.
- In a similar study, Ibarra et al. (2005) investigated seismic demands near collapse for structures with simple hysteretic models including stiffness and strength degradation calibrated with experimental data from tests of steel, plywood, and reinforced concrete components. They performed IDA on a SDOF system with a natural period of 0.9 s for a larger ensemble of ground motions. They found that component degradation is an important triggering factor in structural collapse.

- Medina and Krawinkler (2005) studied the seismic strength demand of several regular moment-resistant frames under different ground motions. In agreement with the findings from other investigators (Challa and Hall, 1994; Martin and Villaverde, 1996), they found that the concepts of strong column-weak beam under severe ground motions may not be guaranteed even when the structural members are designed according to recent seismic provisions.
- Rodgers and Mahin (2006, 2008, 2011) studied the effect of connection hysteretic behaviors due to ductile and brittle fractures on the collapse of steel frames. They developed analytical models to simulate the fracture in connections as a sudden or gradual drop at a calibrated rotation of the moment-rotation response. They validated the model through a series of shake table tests of a two-story steel frame. They stated that the occurrences of numerous fractures in a connection may result in two following situations: a sudden loss of the connection strength capacity or post-fracture hysteretic connection behavior with a significant deformation softening. Such situations in connections may lead the structure to collapse under large excitations.
- Deierlein et al. (2007) explored the key features of ATC-63 methodology, which is a significant recent effort funded by the Federal Emergency Management Agency to evaluate the seismic performance of new and existing structural systems. This methodology provides a rational basis to quantify building seismic performance and response parameters such as R-factor, over-strength factor and displacement amplification factors. Deierlein et al. (2007) described in detail how to apply this methodology to the collapse performance assessment of code-conforming reinforced concrete special moment frames. They performed nonlinear dynamic analysis adopting Ibara-Krawinkler model for degrading hinge-type models assumed at element ends.
- Lignos et al. (2008, 2009, 2010) developed a collapse model to assess the seismic performance of a four-story steel frame under P-Delta effects. They used the shake table-test data to calibrate their collapse model that adopt a modified version of the Ibarra–Krawinkler model to simulate cyclic deterioration in structural components. They also evaluated the reliability of the frame against collapse under seismic excitations considering the uncertainties in deterioration model parameters.
- Liel et al. (2009) adopted the Ibarra-Krawinkler model to study nonductile reinforced

concrete structures. They incorporated modeling uncertainties into the assessment of seismic collapse risk of buildings. They indicated that simplified approaches assumed in analytical modeling of structures may have a large effect on evaluated risk of structural collapse. They emphasized that neglecting effects of such uncertainties may give unconservative collapse predictions.

- Haselton et al. (2009) performed IDA to assess seismic collapse safety of reinforced concrete moment-frame buildings. They followed the hysteric rules developed by Ibarra et al. (2005) to simulate the cyclic deterioration in stiffness and strength of concrete members. They described in detail about analytical modeling tools used in their study. Also, they proposed techniques regarding ground motion selection and scaling, treatment of numerical solutions, and incorporation of uncertainties into collapse assessment of structures.
- A recent study by Liel et al. (2011) compared the collapse performance of nonductile and ductile reinforced concrete frames using archetypes structures with two to twelve stories designed according to the 1967 UBC and 2003IBC building code provisions. They performed nonlinear dynamic analysis to evaluate the collapse capacities of the frames incorporating uncertainties in ground motions and structural modeling. They found that nonductile RC structures had a higher mean annual frequency of collapse, and thus were more vulnerable to collapse under seismic excitations.

As a note, more studies about collapse limit states, alternative performance measures, and prediction of the structural collapse with integration of uncertainties in ground motions and analytical models are described in the following chapters.

2.5. Research Needs in Collapse Assessment of Structures

Collapse prevention is one of the important design objectives of PBEE that ensures a safety margin against structural collapse under the maximum earthquake loads considered in the design. Although there have been several efforts to estimate collapse capacity of structures and to evaluate such a safety margin against collapse, the literature review on currently available collapse assessment methods helped identify pressing research needs for an accurate probabilistic assessment of structural collapse with incorporation of "systematic uncertainty,"

which still remains elusive because of the following reasons:

- The main premise of IDA approach is that when a large increase occurs in the structural response despite a small increase in the ground motion intensity, i.e., the IDA curve almost flattens, the structural system loses its ability to prevent the global collapse. However, the IDA curve could flatten due to large residual DMs and may not indicate the inability to sustain gravity loads necessarily.
- The collapse capacity of a structure evaluated by the IDA-approach may be sensitive to a particular selection of ground motions as well as possible chaotic behavior of the IDA curve such as "structural resurrection." Although some deterministic rules have been proposed to handle such unusual behaviors of IDA, it appears that there is a need of developing a more rigorous procedure to identify dynamic instability of several structures under the effect of variable dynamic loads.
- Most of the recent research efforts based on the IDA-based approach have used only one DM and one IM (mostly maximum story drift ratio and elastic spectral acceleration) while one might need alternative or multiple performance measures to predict the collapse more accurately using the IDA curve.
- Few researchers have considered the stochastic aspects in developing and validating collapse models to account for the uncertainty in nonlinear dynamic response and collapse prediction. However, the impacts of a structural model selection and the selected set of the ground motions on the collapse prediction have not yet been investigated thoroughly by stochastic analyses of experimental and computational simulations.

In order to overcome these challenges, this study presents a new method to identify collapse limit states of frame structures from their dynamic instability, i.e., the loss of the ability to sustain the gravity loads, not from the behavior of the IDA curves. Using the new collapse criteria, key parameters that govern collapse capacity are identified for more effective risk assessment using IDA approaches. A probabilistic framework is also developed for systematic treatment of uncertainties in the ground motion time histories and structural models to be used in performance-based earthquake engineering (PBEE) framework.

3. CASE STUDIES ON STRUCTURAL COLLAPSE

In order to develop a new stochastic framework for identifying collapse limit-state and important parameters in the collapse assessment of structures under cyclic dynamic loadings, it is necessary to build computational simulation models of collapse, which are validated by experimental tests results. This chapter gives details about the collapse experiments considered so far in the study; and describes the OpenSees computational simulation models of these experiments developed in this study.

3.1. A Finite Element Program: OpenSees

OpenSees — The Open System for Earthquake Engineering Simulation — is an object-oriented software framework developed by Pacific Earthquake Engineering Center (PEER) to simulate the seismic behavior of structural and geotechnical systems including the reliability computation (OpenSees, 2004). OpenSees has been extensively used by many researchers (Altoontash, 2004; Haselton, 2009; Liel et al. 2009, 2011) for nonlinear earthquake engineering finite-element applications because of its advanced capabilities in constitutive models, elements and solution algorithms. Moreover, it is open-source software providing researchers with the opportunity to contribute to the framework. Therefore, this study uses OpenSees to perform nonlinear dynamic collapse analysis for selected case studies for which collapse or near-collapse level experimental results are available.

Since OpenSees was written in C++ language with an object-oriented architecture, its operation components are defined through independent objects. Figure 3.1 describes the main objects of the OpenSees framework. The “Model Builder” object is responsible for constructing the structural analysis model by creating nodes, elements, material, masses, constraints, transformation, load pattern and time series. The “Domain” object stores the inputs created by the Model Builder object and transmits this information to other objects. The Domain object also holds the state of the model at each time step. The “Analysis” object performs static or dynamic analysis of the structural model. The object contains necessary sub-objects such as algorithm, integrator, handler, constraint, and solver to build the solution method of the analysis. The object moves the state of the model to the next time step by using the created solution method. Lastly, the “Recorder” object includes allows the user to monitor the structural responses during an

analysis by accessing the Domain object and writing the outputs of interest to a data file.

An interface script using Tcl, which is a simple programming language, is needed to write OpenSees input files. This approach provides users with much more control, e.g., arranging user-defined inputs in construction of numerical solution procedures.

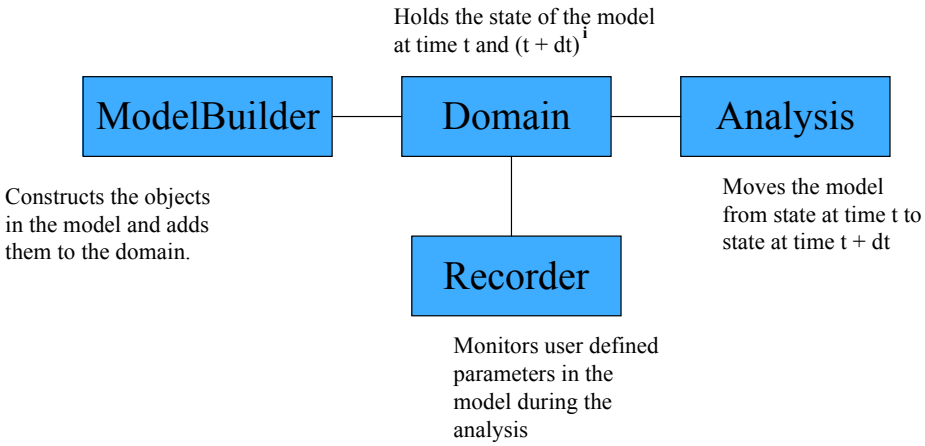

Figure 3.1 The OpenSees framework (source: http://opensees.berkeley.edu).

3.2. Treatment of Numerical Convergence Problems in OpenSees

Convergence problems in a numerical analysis may lead to false results and thus affect the performance of a given collapse assessment method. Therefore, in this study, various solution algorithms, iteration number and tolerance are explored in OpenSees to facilitate numerical convergence during the nonlinear dynamic analysis. Then, an analysis solution procedure has been proposed to efficiently perform IDA by overcoming such convergence problems in numerical analysis, which may occur due to highly nonlinear structural behavior near collapse state. A summary of the steps to handle the numerical convergence issue while performing IDA is described as follows:

- Step1: Choose a solution algorithm, a time step, and an acceptable tolerance. The time step is mostly selected as one tenth of the ground motion time step.
- Step 2: Run the analysis.
- Step 3: If the analysis does not converge, repeat the analysis with a different solution

algorithm.

- Step 4: If the analysis still does not converge, decrease the time step, and start from the beginning.
- Step 5: If the analysis still does not converge, increase the tolerance, and start from the beginning.
- Step 6: If the analysis is completed successfully, i.e., completed without any warning message, check if there is any singularity, e.g., undefined number such as #QNAN or #IND, in the resulting structural responses. If yes, start from the beginning.
- Step 7: Check if the final tolerance is acceptable enough to use the analysis results.

3.3. Component Models Used in the Study

Modeling of structures to simulate incipient dynamic instability followed by dynamic collapse mechanisms of a structure is challenging especially when using coarse macro-models that simplify the structural response through the use of phenomenological moment- thrust-rotation relations or similar. In contrast to advanced high-fidelity analytical models that account for many factors to accurately simulate structural collapse process, macro-models may lack accuracy with respect to structural collapse but less computationally demanding. It is well known that such advanced models may be highly affected by convergence problems that are likely to occur due to the complexity of the modeling details while performing several nonlinear dynamic analyses to assess collapse potential of structures. It is also noted that macro-models are a typical choice for nonlinear analysis at ultimate limit states both for structural design and assessment. It is clear that macro-models are more practical analytical tools in the development of the stochastic framework described in the aims of the research. Therefore, available coarse macro-models that correlate well with experiment results of selected case studies of collapse are considered in this research to develop new collapse criteria, perform large-scale parametric studies in collapse assessment of structures, and assess safety margin against collapse.

Several material models available in OpenSees were considered for calibrating macro-models for the selected case studies through phenomenological incorporation of factors that trigger collapse such as deformation softening, deterioration in strength and softening, and fracture. To simulate these collapse trigging factors, “Steel02”, “Hysteretic”, and “Bilin” material models were then

selected in OpenSees for the test case studies by Kanvinde (2003), Rodgers and Mahin (2004), and Lignos et al. (2008) respectively. A description about the features of these selected component models are available in OpenSees manual as well as in Appendix A.

3.4. Development of Computational Simulation Models of Selected Case Studies

Nonlinear dynamic collapse analyses are performed for selected experimental case studies reported in the literature by use of OpenSees. So far, three cases studies have been performed using advanced capabilities of OpenSees in constitutive models, elements and solution algorithms: Kanvinde (2003), Rodgers and Mahin (2004), and Lignos et al. (2008). In development of the computational simulation models of the selected case studies, emphasis was given on validation of collapse at the "system level" by considering the maximum and residual story drift responses as well as at the "component level" by considering the moment-rotation response obtained at the plastic locations at the element ends.

3.4.1. Shake Table Experiment by Kanvinde (2003)

Kanvinde (2003) conducted shake table tests on a single-story steel specimen configuration measured 12" by 24" in plan (the longer dimension aligned in the direction of motion) and 10" in clear height (shown in Figure 3.2a) to investigate the concept of dynamic instability of structures during earthquakes. The specimen configuration was in the form of four flat steel columns connected to the base plate and a steel mass on top served as a rigid diaphragm as shown in Figure 3.2a. The columns have a cross-section of 1/8" (along the direction of motion) by 1" with 1/2" holes drilled at the column ends (i.e., plastic locations). A structural model in OpenSees was built following the 2-D analytical model details given in Figure 3.2b. Elastic elements were assigned to the columns and beam, and the beam was assumed to behave rigidly. Concentrated nodal masses (totally 0.4143 lbs-s^2/in) were placed at the ends of top beam. A Rayleigh damping of 2% was applied on the mass and on the tangent stiffness of the frame model. Inelastic SDOF zero-length rotational springs were modeled at the plastic locations at the ends of the columns by assuming Giufré-Menegotto-Pinto plasticity model (Menegotto and Pinto, 1973; see "Steel02" in Appendix A) for the spring hysteretic response. The following values for the parameters used in the spring model (see Table A.1) were selected to match with available test experiment results: an initial stiffness of 8.0 kips-in/rad, a yield moment of 0.2398 kips-in, a softening amount of

0.75% after yielding, and a curvature value (R0; see Table A.1) of 16.8 that determines the transition from elastic to plastic branches. The default values were assumed for the remaining parameters in Table A.1. The co-rotational formulation was considered in order to include the nonlinear geometric effects through the specimen. Nonlinear dynamic collapse analyses under the test ground motion (i.e., Obregon Park) were performed to provide the results in Figure 3.2c and Figure 3.3, which are comparable to available experiment data.

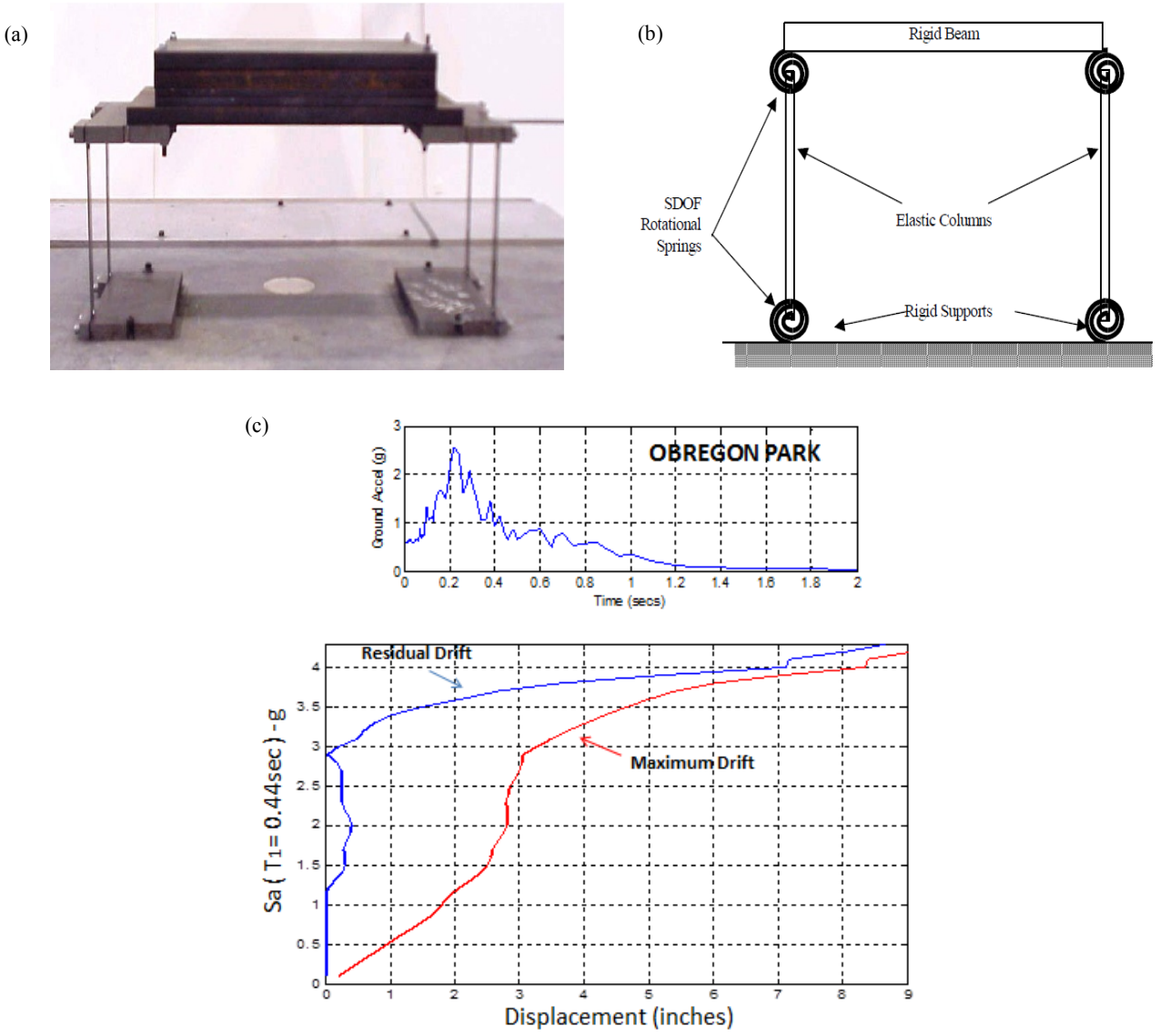

Figure 3.2 a) Specimen configuration (Kanvinde 2003); b) Analytical model details (Kanvinde 2003); and c) IDA results from OpenSees for the ground motion record "Obregon Park".

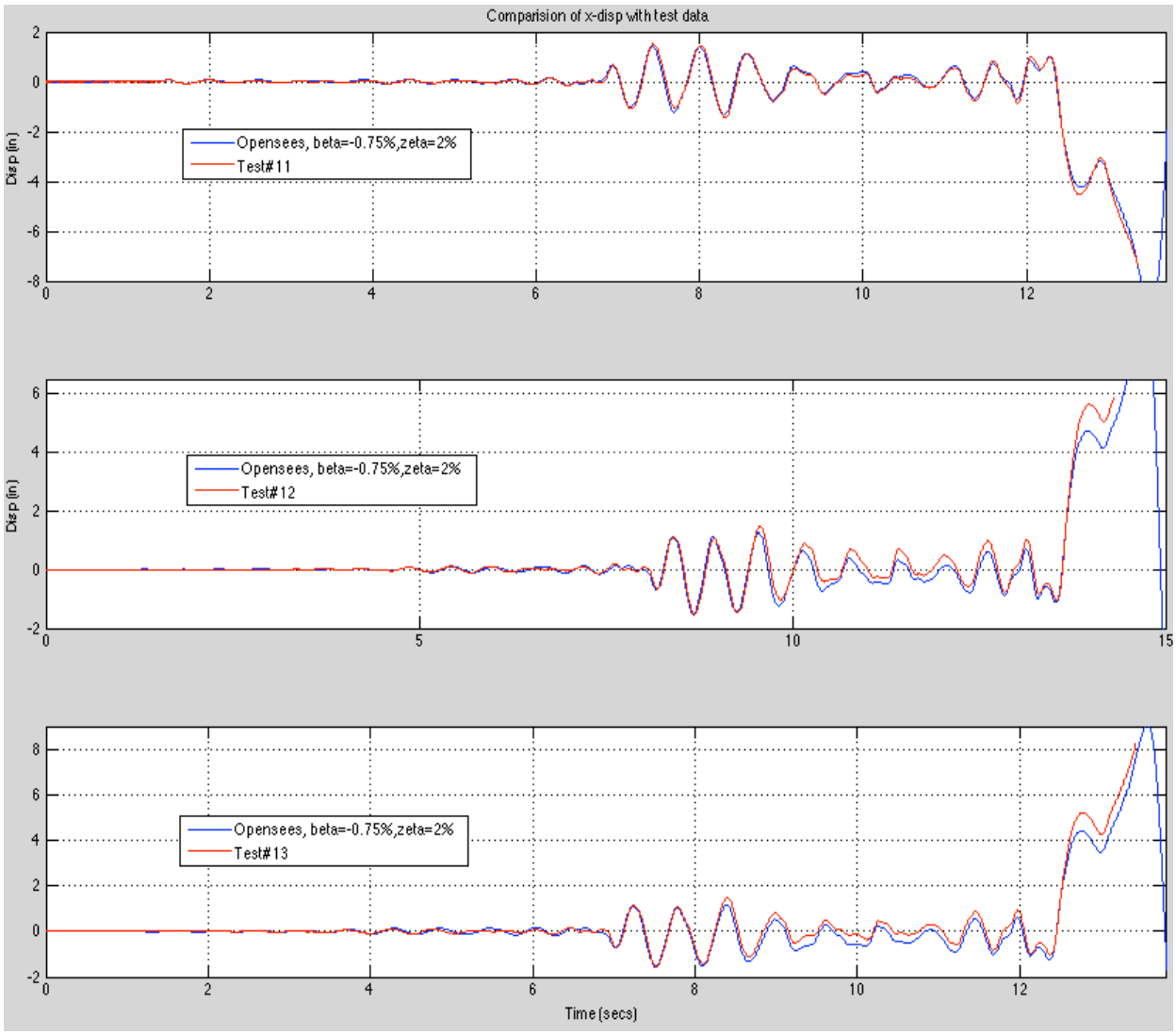

Figure 3.3 Displacement time history results from OpenSees for three test cases under the test ground motion record "Obregon Park" ("beta" and "zeta" in the plots are the softening amount in the springs and damping amount applied to structure).

3.4.2. Shake Table Experiment by Rodgers and Mahin (2004)

Rodgers and Mahin (2004) studied the effects of connection fractures on global behavior of steel moment frames subjected to earthquakes by several shake-test experiments of a one-third scale, two-story, one-bay moment frame. Two simple pin-ended frames were placed parallel to the moment frame, one on each side. Pin ended (clevis) connections were used at the base of each column as shown in Figure 3.4a. Plastic hinge regions at the ends of each beam were represented

by idealized mechanical connections, which were designed to reproduce a wide variety of hysteretic characteristics.

A 2-D clear span analytical model of the moment frame with a bay length of 108" and a clear height of 54" was built in OpenSees comparing the dynamic modal properties such as elastic period and stiffness to available experiment data. Floor masses of 16.045 lbs-s^2/in and 15.010 lbs-s^2/in were assumed at the first and second floors respectively. Rotational masses due to applied floor masses were also included. A Rayleigh damping amount of 4% was applied on the mass and the tangent stiffness of the frame. Co-rotational geometry transformation was considered to include the nonlinear geometry effects on the collapse behavior of the moment frame. Elastic elements were assigned to the beam and columns of the steel frame. Rotational springs were modeled at an offset value of 7.5" from the beam ends considering the same material models in the experiments by Rodgers and Mahin (2004) such as ideally ductile behavior, ductile fracture, brittle fracture, strength degradation, and deformation softening (negative post-yield stiffness) as shown in Figure 3.4b. For example, Figure 3.5 and Figure 3.6 show respectively the ductile behavior and brittle fracture models developed for the experiment under a cosine acceleration pulse with a duration (Tp) of 1.2 s and maximum velocity (Vp) of 25in/s.

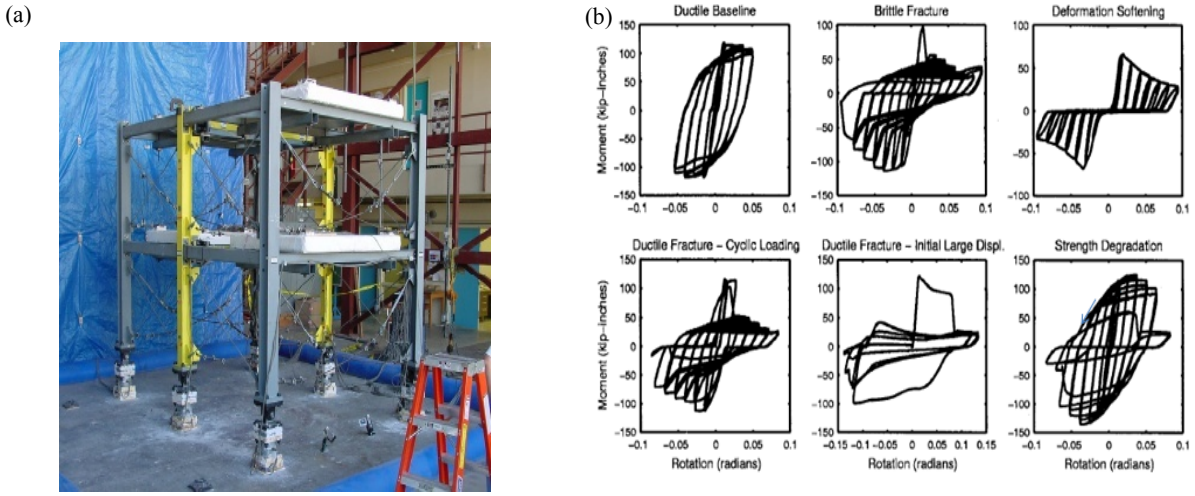

Figure 3.4 a) Shake-table-test of a 1/3 scale 2-story steel frame (Rodgers and Mahin 2004); and b) Material models considered for beam-end connections (Rodgers and Mahin 2004).

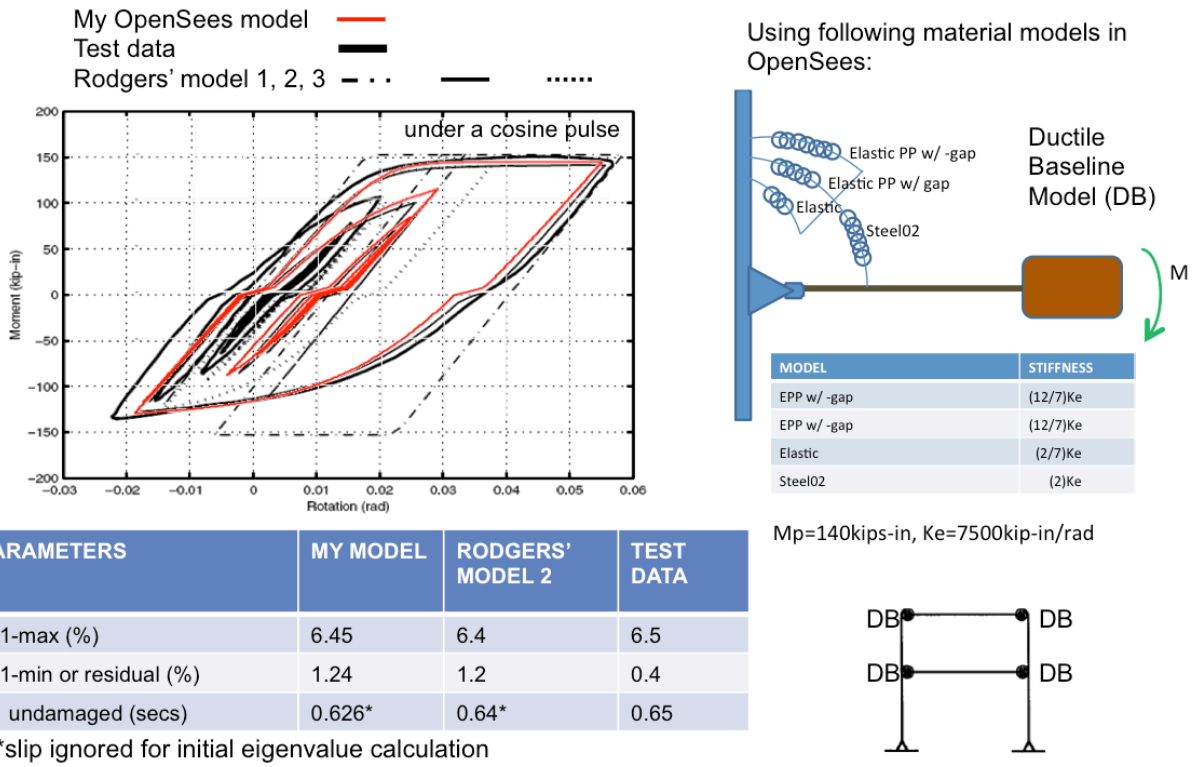

PARAMETERS	MY MODEL	RODGERS' MODEL 2	TEST DATA
ID1-max (%)	6.45	6.4	6.5
ID1-min or residual (%)	1.24	1.2	0.4
T1 undamaged (secs)	0.626*	0.64*	0.65

*slip ignored for initial eigenvalue calculation

Figure 3.5 Ductile baseline model considered for beam-end connections comparing to the test and simulation models by Rodgers and Mahin (2004) (Note that Mp: plastic moment strength, Ke: initial stiffness, EPP: elastic perfectly plastic, ID1: interstory-drift at the first story, T1: the first-mode structural period, and DB: ductile baseline connection).

In Figure 3.5, the ductile connection behavior was modeled using a combination of "Elastic", "ElasticPPGap (i.e., elastic perfectly plastic with gap)", and "Steel02" material models available in OpenSees (see Appendix A for more details about "Steel02"). A gap (i.e., initial slip for rotation) value of 0.002 was assumed in the model. A series combination of elastic and elastic perfectly plastic models with gap in both tension and compression was constructed at first as shown in Figure 3.5. The series combination was then connected with "Steel02" (with zero strain hardening) in parallel to get a total initial stiffness (Ke-total) and a plastic moment (Mp) of 7500 kips-in/rad and 140 kips-in respectively. In order to include a smooth transition from elastic to inelastic region, a curvature R0 value of 8.0 was assumed in "Steel02" model.

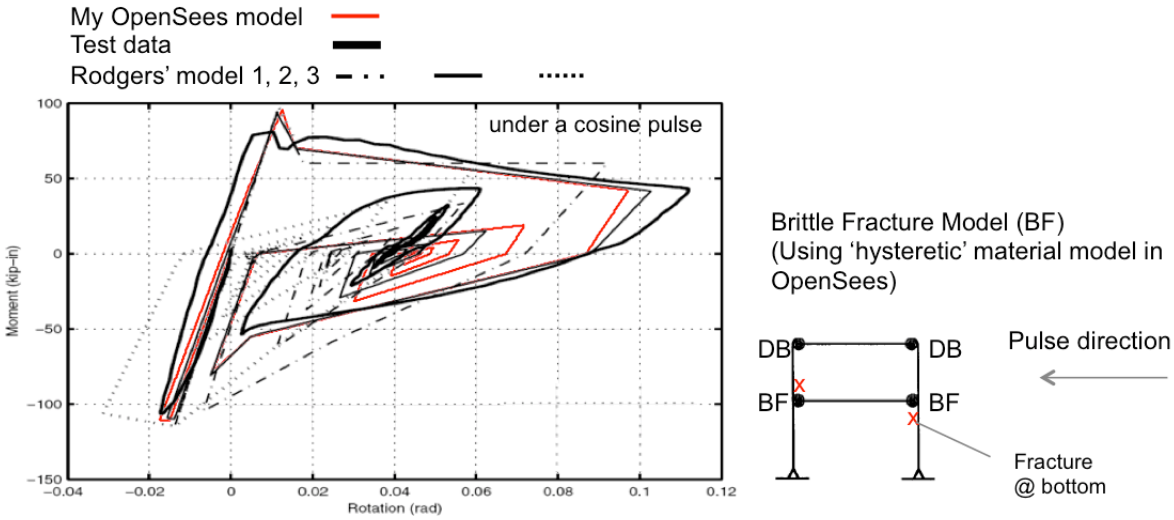

PARAMETERS	MY MODEL	RODGERS' MODEL 2	TEST DATA
ID1-max (%)	9.04	9.5	10.4
ID1-min or residual (%)	3.85	3.3	4.1
T1 undamaged (secs)	0.767	0.75	0.67

Figure 3.6 Brittle fracture model considered for beam-end connections comparing to the test and simulation models by Rodgers and Mahin (2004) (Note that ID1: interstory-drift at the first story, T1: the first-mode structural period, DB: ductile baseline connection, and BF: brittle fracture connection).

Using "Hysteretic" material model available in OpenSees (see Appendix A), a connection model with brittle fracture in tension and plastic behavior in compression was obtained in Figure 3.6. Three following pairs of moment strength and rotation were considered in the model to construct the monotonic backbone curve of the tension side of the spring component: 95 kips-in and 0.0127 rad, 70 kips-in and 0.0160 rad, and 40kips-in and 0.103 rad. A plastic moment of 110 kips and 0.0147 rad were considered on the compression side. Pinching factors of 0.85 and 0.50 during reloading were assumed for rotation and moment respectively in "Hysteretic" model (see Table A.2). Also, a power of 0.3 was used to determine the degraded unloading stiffness based on ductility.

Both models in Figure 3.5 and Figure 3.6 show comparable results (red line) to test data (thick black line) as well as to other results obtained by the three different Rodgers' OpenSees models (other black lines; see the study by Rodgers and Mahin, 2004). The results of IDA employing the constructed OpenSees model also matched those by the experiment.

3.4.3. Shake Table Experiment by Lignos, Krawinkler, and Whittaker (2008)

Lignos et al. (2008) performed a series of collapse shake-table tests of a 4-story, 2-bay steel frame with reduced-beam sections (RBS) in 1/8 scale. Figure 3.7a shows the setup of the test frame on the NEES mass simulator at the University at Buffalo, which consists of elastic members with plastic hinges at the ends. The mass simulator is connected to the test frame by means of axially rigid horizontal links through which the simulator transfers P-Delta effects acting as a leaning column on the test frame. An analytical model for the 1/8 scale 4-story test frame was developed in OpenSees as shown in Figure 3.7b, based on the deterioration parameters and mathematical model properties given by Lignos et al. (2008) (see Appendix B). The rotational springs were used to analytically model the plastic hinges in the frame with a modified Ibarra-Krawinkler deterioration model available in OpenSees (Lignos et al. 2008; see Appendix A), calibrated based on a steel component database of steel beams with RBS under cyclic loading. Moreover, panel zones were modeled at the connections considering the shear distortions. Furthermore, offsets from the panel zones were applied to take RBS into account following the method used by the researchers. Effects of the panel zones on the structural response were explored comparing to those of a developed clear span model. The nonlinear geometry effects were considered using co-rotational transformations.

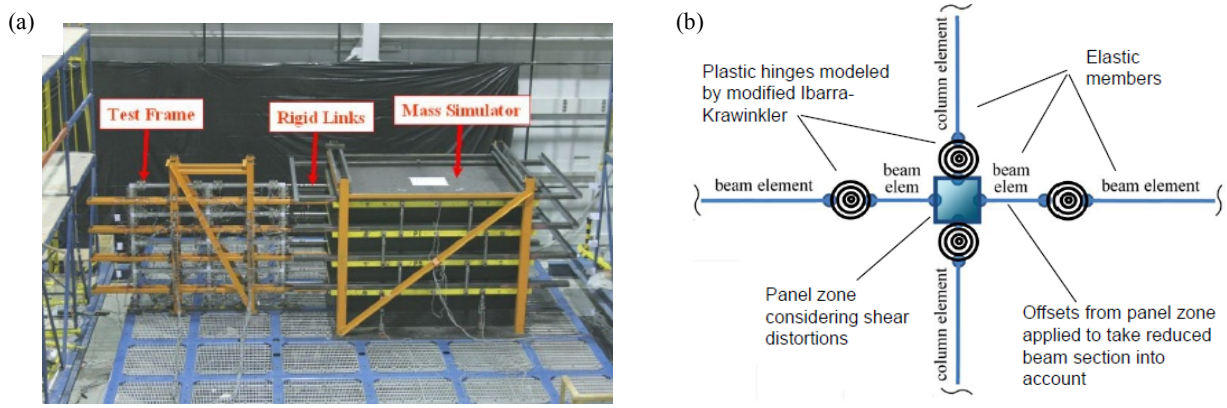

Figure 3.7 a) Shake-table-test of a 1/8 scale 4-story, 2- bay steel frame with reduced beam sections (Lignos et al. 2008); and b) Mathematical model representing the interior sub-assemblage of the 1/8 test frame.

Time history analysis and IDA were performed using the OpenSees model and the results were compared with those by experiment (See Figure 3.8). The developed clear span model was found to be capable to effectively simulate structural collapse comparing to test data (red line) in Figure 3.8; therefore, the clear span model was selected for the following research on structural collapse in the study.

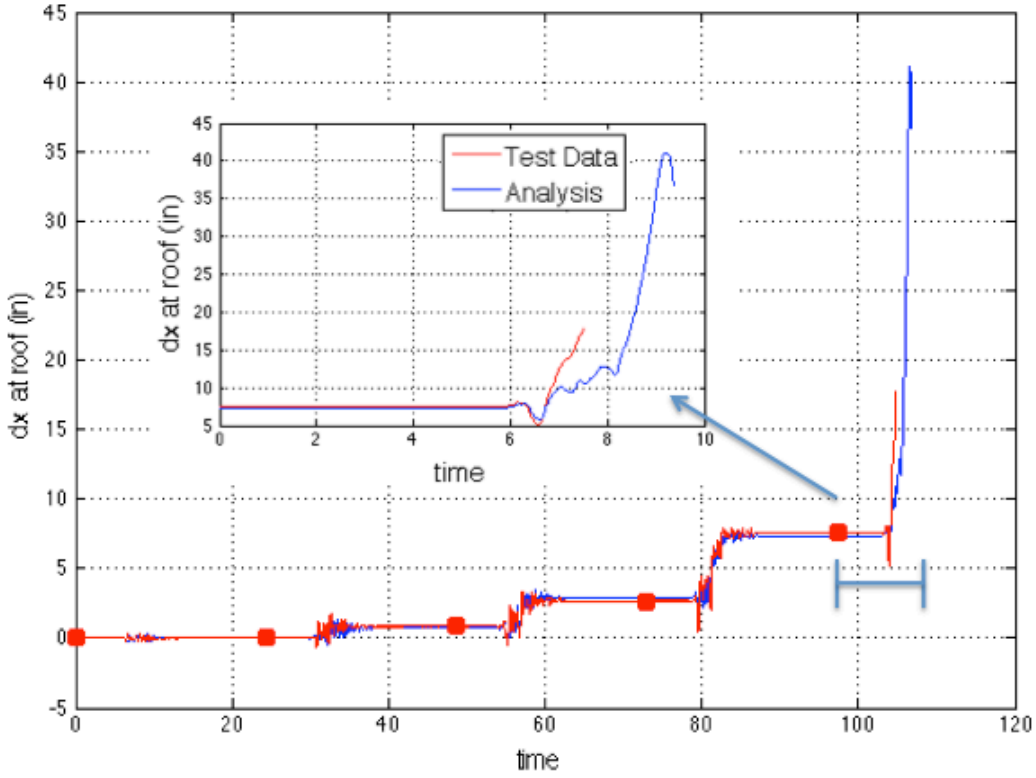

Figure 3.8 Comparison of experimental test results and simulation results of lateral displacement time history at the top of the frame (The simulation model here depends on the clear span model, and was continuously subjected to the ground motion record "Canoga Park" with a scale factor of 0.4, 1.0, 1.5, 1.9, and 2.2).

3.5. Major Findings from Calibration of Case Studies

During the analytical model adjustment of three case studies mentioned above, it was observed that global and local behaviors of structure can be very sensitive against structural model properties at the point where the structure starts to lose stability. For example, Figure 3.9 shows the calibration of the OpenSees analytical model built for Kanvinde's experiment comparing the

lateral displacement time history results at the top to available test data. A small change in the amount of strain hardening/softening (2%, 1%, 0%, -0.75%) assumed in the spring models at the column ends significantly affect the structural behavior towards the end of time-history results (around 13.2s) leading to collapse for elasto-plastic and softening cases, but no-collapse for hardening cases.

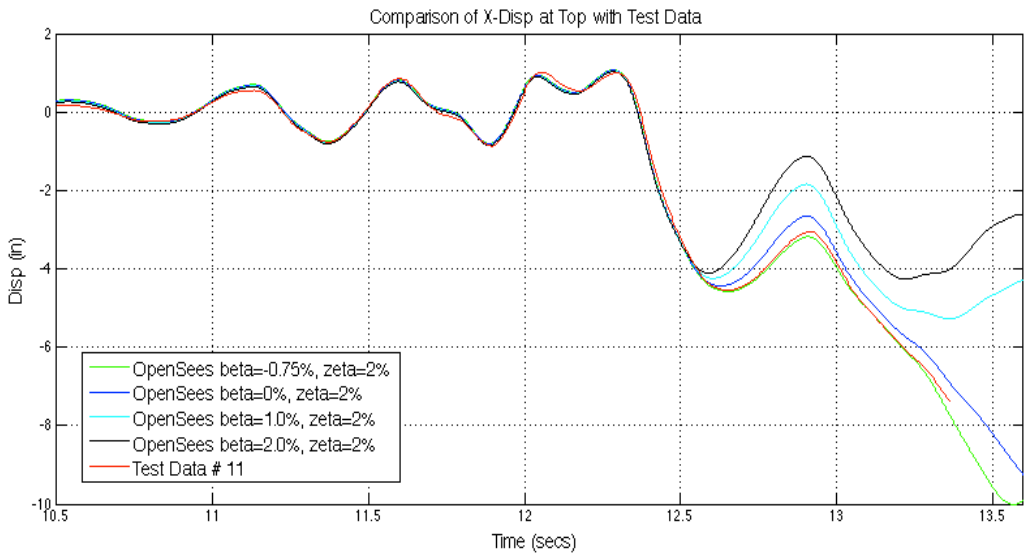

Figure 3.9 Comparison of strain hardening/softening between test results and simulation results of lateral displacement time history at the top of the frame.

It is also noteworthy that application method of the Rayleigh damping on the analytical model may also change the collapse behavior significantly. As seen in Figure 3.10, for the same model, application of the same amount of damping (2%) on initial stiffness or current (tangent) stiffness during the analysis highly affects the structural response under a strong ground motion.

In addition, such sensitivity was also observed for all three cases when the models were developed with linear or different nonlinear geometry transformations (i.e., P-Delta and co-rotational geometry) especially when the scale factors gets larger in an IDA curve. The models with co-rotational transformation were found to be more accurate in matching available experiment data since this transformation type considers high nonlinearities by taking axial deflections into account. Therefore, such models provide more reliable results especially at the collapse level of ground motion intensity.

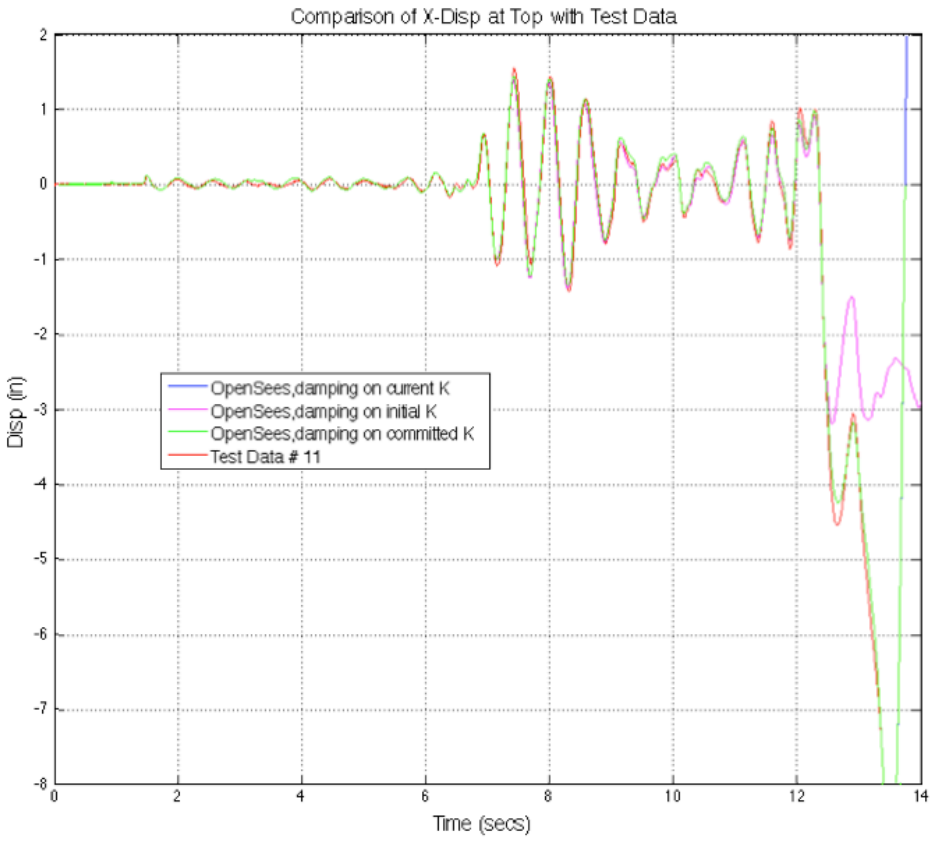

Figure 3.10 Comparison of application of Rayleigh damping between test results and simulation results of lateral displacement time history at the top of the frame.

3.6. Development of Virtual Collapse Simulations

In order to develop a new stochastic framework for identifying collapse limit-state and important parameters in the collapse assessment of structures subjected to seismic loads, extensive IDAs were performed using validated OpenSees simulation models to obtain a large sample for multiple DMs and corresponding IM and for multiple ground motions. Since the ground motions considered in the methodology of ATC-63 project were selected in such a way that the methodology can be generally applied to building structures at any site, the "Far-Field" record set of ATC-63 project (see Appendix C) have been chosen in the development of the stochastic framework. This record set consists of twenty-two ground motion pairs (two-lateral components) recorded at sites located within 10km of fault rupture. Records were selected from strong earthquake ground motions with a magnitude changing from 6.5 to 7.9. Additionally, an

extensive set of the “Far-Field” record set of ATC-63 project has been also considered in order to get more sample data for IMs and DMs. This extensive set includes seventeen more ground motion pairs. Please see Appendix C for more details.

Virtual collapse simulations considering a wide array of geometric and material parameters were also developed based on validated analytical models in order to conduct a parametric study. This study accounts for the impacts of a structural model and a ground motion set selections on the collapse prediction of structures. More details about this study are described in Chapter 7.

4. DEVELOPMENT OF NEW COLLAPSE CRITERIA

This chapter presents a new method to identify collapse limit states of frame structures from their dynamic instability, i.e., the loss of the ability to sustain the gravity loads. Using the OpenSees computational models validated by corresponding experimental results, new dynamic-instability-based collapse criteria have been developed in terms of energy from the input ground motions and the gravity loads. The selected case studies are then used to test the new collapse criteria of a structural system. Next, the collapse predictions by the developed collapse criteria are compared to those by conventional IDAs employing DM-based or IM-based rule.

4.1. Limitations of Collapse Criteria Available in the Literature

In this study, structural collapse is defined as the state of dynamic instability at which the structure is unable to find a new equilibrium configuration, therefore loses the ability to sustain the gravity loads. One of the most widely used methods to identify dynamic instability is to check if the structural system starts to show boundless story drifts. The IDA-based collapse identification approach also relies on this premise: a large increase in the structural response caused by a small increase in the ground motion intensity makes the IDA curve almost flatten, which indicates the collapse of the structural system (Vamvatsikos, 2002). However, it is noted that this procedure may have the following limitations:

- The IDA curve could flatten due to large residual DMs and may not indicate the inability to sustain gravity loads necessarily.
- Most recent research efforts based on the IDA-based approach assume the intensity level of ground motion at which the structure loses the dynamic stability as the collapse capacity. However, the structural collapse capacity should be evaluated based on the maximum intensity level, where the structure still shows resistance before occurrence of dynamic instability (Krawinkler, 2009; Haselton, 2009). The capacity at this intensity level is actual representation of the largest structural resistance against dynamic collapse.
- Collapse criteria of IDA procedure are based on simple rules, such as DM-based rule or IM-based rule, derived from the relationship between a measure of ground motion intensity and an engineering parameter roughly representing structural damage, e.g., peak ground acceleration versus maximum inter-story drift ratio. These collapse criteria are

subjective, and also depend on assumed threshold values instead of the actual occurrence of dynamic instability. Therefore, the collapse capacity (both in terms of IM and DM) identified by these subjective rules could be sensitive to the assumed threshold values.

- IDA curves may show possible chaotic structural behavior such as structural resurrection. In that case, IDA-based rules based on a chaotic IDA curve may provide more than one collapse capacity for the applied ground motion that can cause confusion in identification of simulated collapse.

Dynamic instability is a complex and highly nonlinear phenomenon that may cause non-converge problems in a numerical analysis for nonlinear dynamic analysis of a structure near collapse. In most studies of collapse assessment of structures, numerical non-convergence has been interpreted as an indicator of structural collapse. However, non-convergence of the analysis may not imply the dynamic instability of the structure necessarily if the model is not realistic enough or the non-convergence is caused by issues related with numerical analysis (e.g., step size, algorithm type, etc.) In order to make a reliable collapse assessment, the time-history analysis should be continued until large enough displacement, such as large story drift ratios on the order of 10% to 20% for ductile frame systems, are obtained without any convergence problems (Haselton et al, 2009). Such converge problems need to be handled by an enhanced solution procedure and a well-developed analytical model instead of being used as collapse criteria.

Collapse capacity of structures strongly depends on the collapse-control mechanism (Bernal, 1992, 1994). The significant growth of lateral story drifts may cause the structure to collapse sideways. Attainment of some specific deformation demands, e.g., shear distortion of a joint or drift in a gravity frame, may cause the direct loss of gravity columns or disconnection of slab from the columns, which eventually leads to vertical collapse of the structure (Haselton et al., 2009). Collapse criteria available in the literature do not consider the potential shapes of collapse mechanisms.

Based on the selected performance objective for the structures, the meaning of collapse can be different, which naturally leads to diverse evaluations of collapse capacity. For example, the methodology in ASCE/SEI 41 (2006) describes the occurrence of collapse for existing buildings

under seismic forces as the situation when an individual component in the structure exceeds an allowable demand (e.g., plastic rotation demand). In this approach, re-distribution of loads in the structure is not considered and the structure is not allowed to resist against significantly large deformations before collapse (Krawinkler, 2007). Therefore, such definition of collapse does not actually refer to dynamic instability in many cases and may provide underestimated collapse capacities, therefore leading to conservative collapse assessment of structures (Haselton et al., 2009).

Another collapse assessment method is nonlinear static procedure, which defines the occurrence of collapse as the reduction of base shear to zero. In terms of static structural behavior, this definition makes sense, but structural collapse is a highly nonlinear dynamic behavior with excessive deteriorations in structural components. Thus, such methods are not reliable to get collapse capacity under seismic excitations since these methods neglect: ground motion characteristics obtained by assuming equivalent lateral loads over the height of the structure, load-path dependency of nonlinear structural behavior, and changes in structural parameters (e.g., period and damping) due to dynamic effects (Villaverde, 2007).

All these limitations summarized above show pressing research needs for more rigorous methods to identify structural dynamic instability under variable seismic excitations.

4.2. Research Needs for Identification of Dynamic Instability

The main objective of this section is to explore available definitions of dynamic instability reported in the literature. In order to do such an evaluation, the case study by Kanvinde (2003) is considered. Using the validated computational model of the single-story specimen, nonlinear dynamic analyses were performed under different scales of ground motion of the 1994 Northridge earthquake at Obregon Park, Los Angeles to investigate the dynamic instability of the structure.

The most commonly used criterion for identification of simulated collapse under dynamic loads is boundless drifts towards collapse. For example, Figure 4.1 shows the time histories of the displacement at the top of the frame in horizontal (blue) and vertical (green) direction under the ground motion “Obregon Park” at the scale of 0.8 (Figure 4.1a) and 1.0 (Figure 4.1b). At the

scale of 0.8, the structure converged to a stable state with a residual horizontal displacement of –2.5 inches. On the other hand, at the scale of 1.0, the horizontal displacement at the top showed exponential growth and reached the full column height around 13.5 seconds, which clearly indicates dynamic instability and collapse.

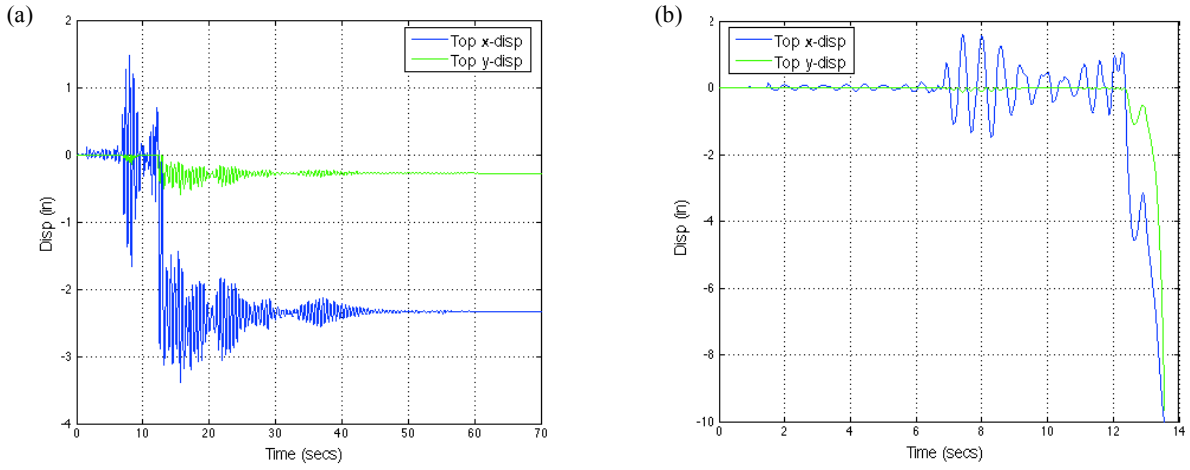

Figure 4.1 Horizontal and vertical displacement time histories at the top of the simulation model developed for Kanvinde's experiment a) at the ground motion-scale of 0.8, and b) at the scale of 1.0.

However, a clear identification of dynamic instability is really challenging. The reason is that reaching an unstable condition such as singular stiffness matrix (representing static instability) may not be sufficient to trigger dynamic instability of structures. Unloading may help overcome such a condition to prevent the structure from dynamic instability (Araki and Hjelmstad, 2000). For example, Figure 4.2 shows structural response of the left-bottom spring of the frame in the phase space (rotation versus rotational velocity) for the scales of 0.8 (Figure 4.2a) and 1.0 (Figure 4.2b). Red circles in the plots indicate negative eigenvalues of tangential system stiffness; hence, indicate static instability at the corresponding time step in the analysis. For the scale of 0.8 (Figure 4.2a), the trajectory at first produces stable paths dissipating around the initial equilibrium state, then exhibits static instability by negative eigenvalues. However, the trajectory converged to another equilibrium state at the end. This result demonstrates that negative eigenvalues do not guarantee dynamic instability. This is because inertia and damping forces can stabilize the structure dynamically (Bernal, 1998). On the contrary, at the scale of 1.0

(Figure 4.2b), the trajectory in the phase space loses static stability first, and then fails to achieve another equilibrium state.

Araki and Hjelmstad (2000) proposed an alternative method to indicate dynamic instability for MDOF cantilevers with elasto-plastic springs. They established collapse criteria based on existence of negative eigenvalues of the Hessian of the system's total potential energy (i.e., tangent stiffness) and consistency of the direction of motion with the loading direction of the elasto-plastic material. However, this method is not applicable to the models such as the simulation models of the case studies considered in this study. To employ such collapse criteria in practical structures, degradation due to softening and the resistance due to damage need to be incorporated into the established collapse criteria (Araki and Hjelmstad, 2000). Load redistribution that may take place in plane or space frames also needs to be considered in the criteria.

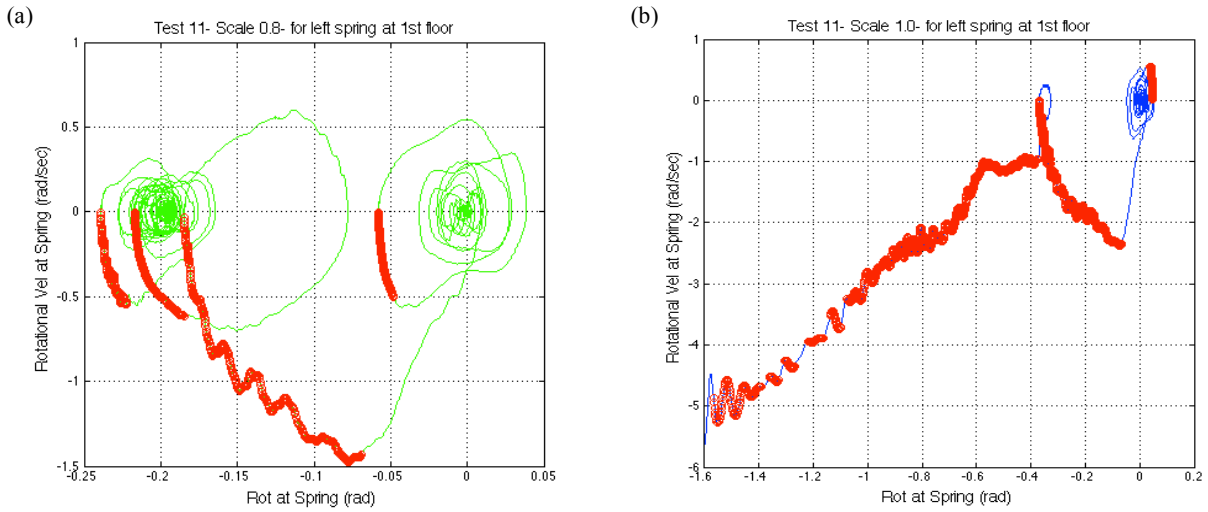

Figure 4.2 Phase plots of structural response of the bottom-right rotational spring in the computational simulation model developed for Kanvinde's experiment a) at the ground motion-scale of a) 0.8 and b) at the scale of 1.0.

4.3. New Dynamic-Instability-Based Collapse Criteria

New collapse criteria based on computational simulations of dynamic instability give rise to new research opportunities to gain better understanding of complex collapse mechanism of structural

systems, identify key parameters that would help describe collapse through comprehensive and accurate measurements, achieve more accurate and systematic prediction of collapse, and allow for incorporating uncertainties into collapse prediction. To this end, in this study, new dynamic-instability-based collapse criteria are developed in terms of energies from the input ground motions, and the gravity loads. First, energy balance of a structural system under seismic excitation is introduced in the following section. Then, details of the new dynamic-instability-based collapse criteria are presented.

4.3.1. Concepts of Seismic Energy Demand and Capacity

The equation of motion at time *t* for an MDOF structure under horizontal earthquake loads and gravity loads is:

$$\underline{M}\ \underline{\ddot{u}}(t) + \underline{C}\,\underline{\dot{u}}(t) + \underline{f_s}(t) = -\underline{M}\,\underline{T}\,\underline{\ddot{u}}_F(t) \qquad (4.1)$$

where $\underline{u}$ is the relative nodal displacement vector, $\underline{\dot{u}}$ is the relative nodal velocity vector, $\underline{\ddot{u}}$ is the relative nodal acceleration vector, $\underline{\ddot{u}}_F$ is the acceleration vector of applied loads, $\underline{M}$ is the structural mass matrix, $\underline{C}$ is the structural damping matrix, $\underline{f_s}$ is the structural restoring force matrix, and $\underline{T}$ is a transformation matrix constructed of 0's and1's with a size of total number of degree-of-freedoms (DOF) in the system (row) by the length of $\underline{\ddot{u}}_F$ (column).

An insight into the dynamic instability of structures can be gained by considering energy balance of a structural system under dynamic and gravity forces. If one takes the integral of each term in (4.1) with respect to $\underline{u}$, the energy balance of the structural system can be derived as (Uang and Bertero, 1990):

$$\int_0^t \left(\underline{M}\ \underline{\ddot{u}}(t)\right).d\underline{u} + \int_0^t \left(\underline{C}\,\underline{\dot{u}}(t)\right).d\underline{u} + \int_0^t \underline{f_s}(t).d\underline{u} = -\int_0^t \left(\underline{M}\,\underline{T}\,\underline{\ddot{u}}_F(t)\right).d\underline{u} \qquad (4.2)$$

The integrals in (4.2) give energy components of a structural system, i.e.,

$$E_K + E_D + E_S = E_I \qquad (4.3)$$

where E_K is the relative kinetic energy, E_D is the damping energy, E_S is the strain energy, and E_I is the relative dynamic input energy.

Using $d\underline{u} = \dot{\underline{u}}(t)\, dt$, the energy components in (4.3) are derived as follows:

$$E_K = \int_0^t \left(\underline{M}\ \ddot{\underline{u}}(t)\right).d\underline{u} = \int_0^t \dot{\underline{u}}(t)^T \underline{M}\ \ddot{\underline{u}}(t)dt = \int_0^t \dot{\underline{u}}(t)^T \underline{M}\ d\dot{\underline{u}} = \frac{1}{2}\ \dot{\underline{u}}(t)^T \underline{M}\ \dot{\underline{u}}(t) \qquad (4.4)$$

$$E_D = \int_0^t \left(\underline{C}\ \dot{\underline{u}}(t)\right).d\underline{u} = \int_0^t \dot{\underline{u}}(t)^T \underline{C}\,(t)\dot{\underline{u}}(t)\, dt \qquad (4.5)$$

$$E_S = \int_0^t \underline{f_s}(t).d\underline{u} = \int_0^t \dot{\underline{u}}(t)^T \underline{f_s}(t)\, dt \qquad (4.6)$$

$$E_I = -\int_0^t \left(\underline{M}\ \underline{T}\ \ddot{\underline{u}}_F(t)\right).d\underline{u} = -\int_0^t \dot{\underline{u}}(t)^T \underline{M}\ \underline{T}\ \ddot{\underline{u}}_F(t)\, dt \qquad (4.7)$$

If Rayleigh damping is assumed, the damping matrix $\underline{C}$ is determined as

$$\underline{C} = a_o\underline{M} + a_1\underline{K}(t) \qquad (4.8)$$

where a_o and a_1 are coefficients determined from the first two dominant frequencies of the structural system, and $\underline{K}$ can be initial stiffness or tangent stiffness. This study uses the tangent stiffness, which is more realistic when the structure is near collapse. Using the model in (4.8), the damping energy E_D can be derived in terms of the mass and stiffness matrices:

$$E_D = \int_0^t \left(\left[a_o\underline{M} + a_1\underline{K_T}(t)\right]\ \dot{\underline{u}}(t)\right).d\underline{u} \qquad (4.9)$$

$$E_D = \int_0^t \dot{\underline{u}}(t)^T a_o\underline{M}\,\dot{\underline{u}}(t)dt + \int_0^t \dot{\underline{u}}(t)^T a_1\underline{K_T}\,(t)\dot{\underline{u}}(t)dt \qquad (4.10)$$

The strain energy E_S can be divided into two parts: elastic strain energy E_E, and hysteretic energy E_H (plastic strain energy), i.e., $E_S = E_E + E_H$. Note that $E_S = E_E$ for linear members. The elastic strain and hysteretic energy are evaluated as follows.

$$E_H = \int_0^t \underline{f_s}(t).d\underline{u_p} = \int_0^t \dot{\underline{u}}_p(t)^T \underline{f_s}(t)\, dt \qquad (4.11)$$

$$E_E = \int_0^t \underline{f_s}(t).d\underline{u_e} = \int_0^t \left(\underline{K_e}\ \underline{u_e}(t)\right).d\underline{u_e} = \frac{1}{2}\underline{u_e}(t)^T \underline{K_e}\ \underline{u_e}(t) \qquad (4.12)$$

While the accelerations for the horizontal earthquake excitation varies over time, the gravity loads applied on the structure remains constant, i.e.,

$$\underline{\ddot{u}}_F = \begin{bmatrix} \ddot{u}_{ground}(t) \\ \ddot{u}_{gravity} \end{bmatrix} \tag{4.13}$$

Consequently, the input energy in (4.3), E_I can be separated into the dynamic input energy due to seismic actions, E_{EQ}, and gravity energy due to the applied gravity loads on the structure, E_G:

$$E_{EQ} = -\int_0^t \underline{M}\,\underline{\hat{T}}\,\ddot{u}_{ground}(t)\,d\underline{u} = -\int_0^t \underline{\dot{u}}(t)^T \underline{M}\,\underline{\hat{T}}\,\ddot{u}_{ground}(t)\,dt \tag{4.14}$$

$$E_G = -\int_0^t \underline{M}\,\underline{\acute{T}}\,\ddot{u}_{gravity}\,d\underline{u} = -\underline{u}(t)^T \underline{M}\;\underline{\acute{T}}\,g \tag{4.15}$$

where $\underline{\hat{T}}$ and $\underline{\acute{T}}$ are transformation column vectors and g is gravity acceleration (–386.2 in/sec^2).

The earthquake energy applied on the structure are dissipated by the work done by the damping and hysteretic forces. Therefore, damping and hysteric energies are irrecoverable, and elastic and kinetic energies are recoverable vibrational energy. If all the individual energy components are gathered together, energy balance of a structure in (4.3) is alternatively described as:

$$E_K + E_D + E_S = E_{EQ} + E_G \tag{4.16}$$

Akiyama (2002) stated that gravity energy can be considered as release of potential energy as result of P-Delta effects, and takes part in the total resistance of a structure against a seismic excitation. Therefore, gravity energy can be also shown on the left side of the energy balance:

$$E_K + E_D + E_S - E_G = E_{EQ} \tag{4.17}$$

4.3.2. Indication of Dynamic Instability by Structural Gravity Energy

Dynamic instability is a complex phenomenon, which cannot be effectively predicted by a ground intensity measure and/or an engineering parameter roughly representing structural damage. The most commonly used criterion for identification of simulated collapse under dynamic loads is boundless drifts towards collapse. However, in this approach, displacement needs to be checked at each DOF, but most studies consider only the roof or story drifts to check the stability of the global structural behavior. Therefore, energy balance of structural systems is studied here to investigate dynamic instability of structural systems, because energy is an indicator that describes the whole system.

The accumulation of permanent lateral drifts during a strong ground shaking may render gravity forces the dominant forces that make the structure collapse under significant P-delta effects due to governing gravity forces (Jennings and Husid, 1968). Therefore, new collapse criteria have been developed to detect collapse by comparing the amount of dynamic energy released by the earthquake to the structure against the amount of gravitational work done by the vertical static loads during the dynamic analysis. The incidence of gravity energy exceeding dynamic energy with a sudden increase can be considered as an indicator of the domination of gravity loads over dynamic loads. For example, Figure 4.3 presents the input-energy-time histories for the validated SDOF model of Kanvinde (2003) under the ground motion record of Obregon Park. At the scale of 1.0 (Figure 4.3a), geometric nonlinearities in the structure become significant near the collapse, causing the frame to show very large displacement in vertical directions and thus result in a sudden increase in gravitational energy as the structure gets close to collapse. On the other hand, if the intensity of the ground motion is not strong enough to trigger the large geometric effects in the frame (e.g., the non-collapse case at the scale of 0.8), the structure obtains a steady state in terms of the gravitational energy, which is found insignificant comparing to the quantity of dynamic input energy coming from the ground motion (Figure 4.3b). Using this energy-based approach, one may not need to check each degree-of-freedom of the structure to check the dynamic instability. Moreover, the approach may facilitate developing a mathematical description of dynamic instability, which can be particularly useful for stochastic analysis of collapse requiring quantitative detection during repeated computational simulations.

The developed method has also been studied using an MDOF example. Figure 4.4 shows the input energy components for the validated MDOF model of the case study by Lignos et al. (2008) under the ground motion record of Canoga Park applied in the experiment. In order to get the energy time histories, the MDOF model of the test frame was continuously loaded for intensity scales of 0.4, 1.0, 1.5, 1.9, and 2.2 following the test procedure. While the gravity energy is steady in the non-collapse case at the scale of 1.9 (Figure 4.4a), it enormously increases and even exceeds dynamic energy in the collapse case at the scale of 2.2, indicating dynamic instability due to loss in resistance against applied gravity loads. Figure 4.5 shows several energy components near collapse for the same MDOF model under the test ground motion with an intensity scale of 2.2. As seen, the potential energy released near structural collapse state far exceeds the earthquake (dynamic) input energy stored in the structure. It is also interesting to

note that a large amount of potential energy released near collapse state is transformed into kinetic energy. The rest of the released potential energy is reintroduced into the structure through damping energy and strain energy during the deformation of the destabilized components.

It is also noteworthy to mention that this criteria works on each three test case studies for almost all 78-ground motions provided by Deierlein and Haselton (2007; see Appendix C) except a few cases. However, in these exception cases, collapse was observed in the following intensity level that allows this criteria to be safely employed on collapse simulation models.

Similarly, Szyniszewski and Krauthammer (2012) consider the change in system's kinetic energy as an indicator of collapse. They recently studied energy flow in progressive collapse of steel framed buildings. They stated that the sudden release of the gravitational energy leads to transient motions and kinetic energy, and a building loses stable configuration if the kinetic energy is not completely dissipated by the structure.

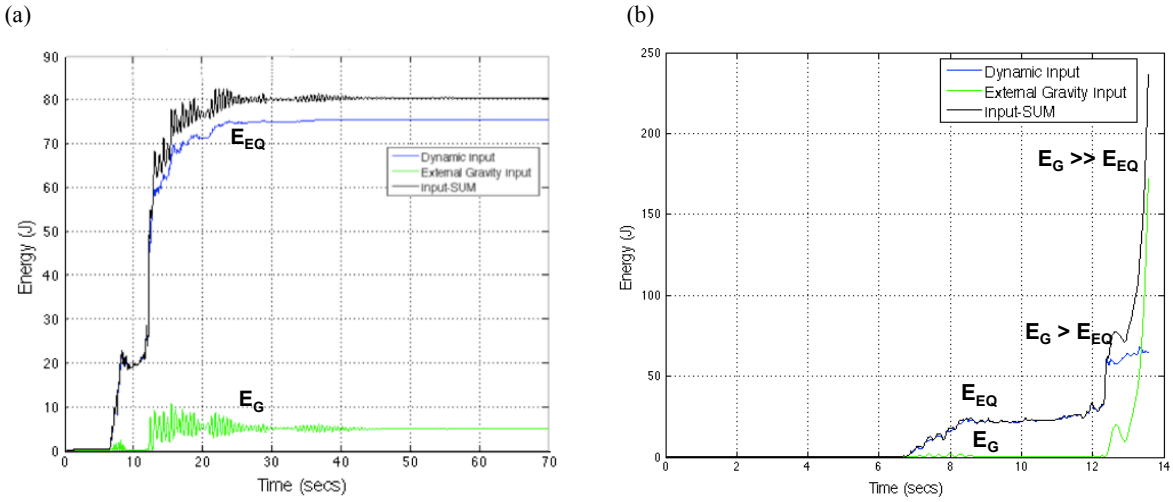

Figure 4.3 Input energy components of Kanvinde's experiment near collapse under the test earthquake of 1994 Northridge earthquake at Obregon Park a) non-collapse case at the ground motion scale of 0.8 and b) collapse case at the ground motion scale of 1.0.

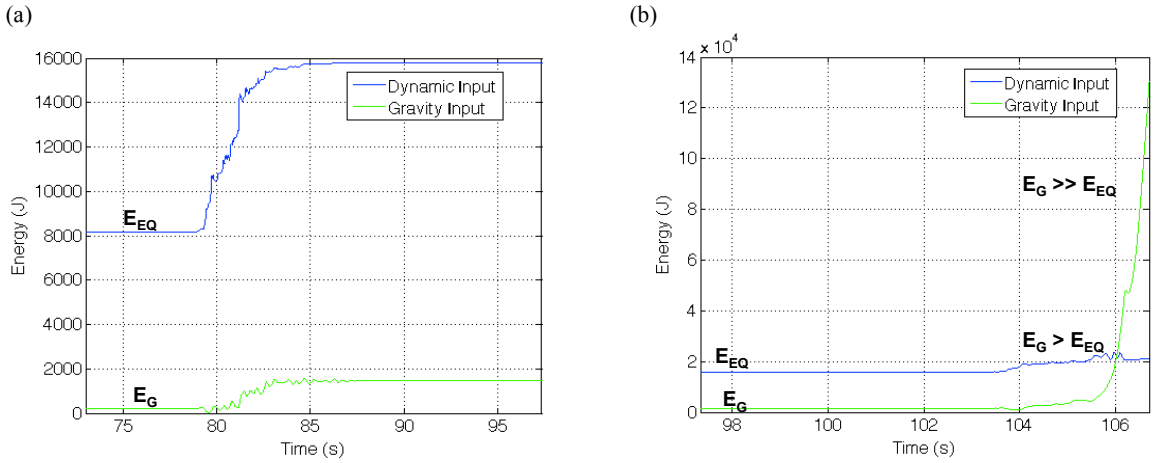

Figure 4.4 Input energy components for the test case by Lignos et al. (2008) near collapse under the test earthquake of 1994 Northridge earthquake at Canoga Park a) non-collapse case at the ground motion scale of 1.9 and b) collapse case at the ground motion scale of 2.2.

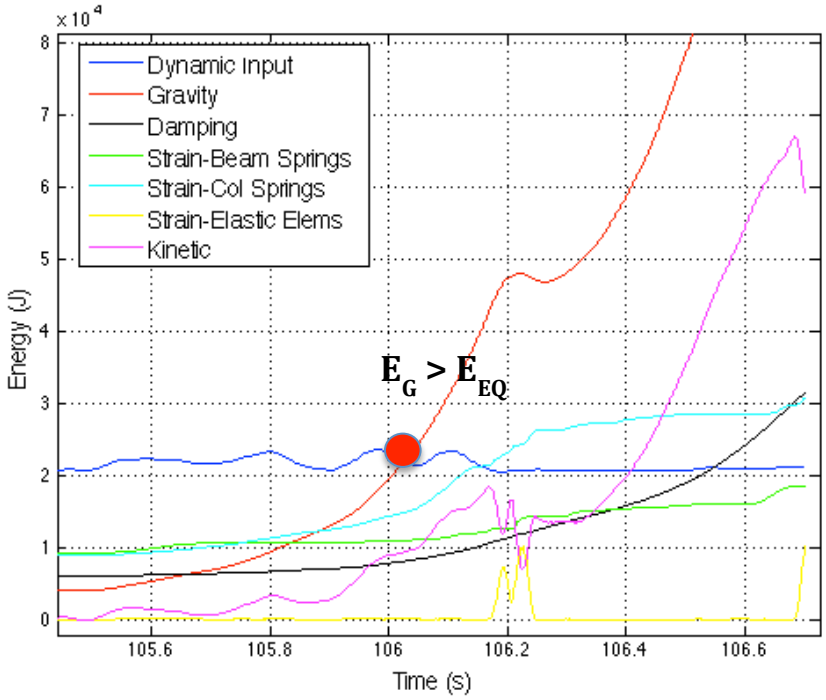

Figure 4.5 Energy components for the MDOF model of the case study of Lignos et al. (2008) near collapse under the test earthquake of Canoga Park at the scale of 2.2.

4.4. Evaluation of Traditional IDA-based Collapse Limit States based on New Collapse Criteria

The collapse capacity of a structure evaluated by the IDA-based approach may be sensitive to a particular selection of ground motions as well as possible chaotic behavior of the IDA curve such as "structural resurrection." Therefore, some deterministic rules have been proposed to handle such unusual behaviors of IDA by Vamvatsikos and Cornell (2002):

- The building's global drift capacity can be assumed as the maximum story drift ratio at which the slope of the curve reduces to 20% of the initial slope (IM-based rule; Figure 4.6a).
- If IDA curve does not fulfill IM-based rule, then the global drift capacity is assumed to be equal to 10% (DM-based rule; Figure 4.6b).

These IDA-based traditional rules depend on simple deterministic values, therefore not sufficient to identify when and how a structure collapses under the effect of variable dynamic loads. Therefore, in this section, these traditional IDA-based collapse limits states are evaluated based on the developed new collapse criteria developed ("energy rule"; Figure 4.6c) for more effective risk assessment using existing approaches.

4.4.1. Comparison of IDA-based Collapse Limit States with New Collapse Criteria

The validated model developed for the case study by Lignos et al (2008) were utilized here to perform nonlinear dynamic analyses using ATC-63 far field set. Figure 4.6d shows the IDA curves of peak ground acceleration (*PGA*) to top lateral displacement obtained from the validated OpenSees model. Traditional IDA-based rules are compared to the new criteria called "energy rule" based on the maximum intensity level observed before the dynamic instability occurs, i.e., gravity energy exceeds dynamic energy. Much variability is observed in collapse capacity level for all rules due to the effect of randomness in the selected ground motions. A more quantitative comparison can be done from histograms of collapse capacities obtained from both IM-based and DM-based rules normalized to those from the energy rule in Figure 4.7 and Figure 4.8 respectively. In both figures, large dispersion is observed in the drift capacity comparing to intensity level but much more in IM-based rule (Figure 4.7b), because deformation capacity from

DM-based rule (Figure 4.8b) depends on a predetermined threshold value giving the same drift capacity for each collapse intensity level. Since DM-based rule provides closer intensity levels (Figure 4.6d-yellow circles) to the ones by the energy rules (Figure 4.6d-red circles), less dispersion is observed in the DM-based intensity levels (Figure 4.8a) comparing to the IM-based intensity levels (Figure 4.7a)

Figure 4.9 and Figure 4.10 show the correlation found between IM-based rule and the energy rule; and DM-based rule and the energy rule, respectively. As expected, a strong correlation is observed in intensity measures, almost 1.0, for both traditional rules (Figure 4.9a and Figure 4.10a). Strong correlation means IM collapse capacities are proportional, but does not mean one can be predicted from the other in a general case. Due to much sensitivity of roof drift capacities to several ground motions, a much less correlation value of 0.1 is found in the drift capacities by IM-based rule (Figure 4.9b). Again, since DM-based rule assumes a strict value as the criterion, no correlation is observed between this rule and the energy rule in terms of deformation capacity (Figure 4.10b). That means it is difficult to predict collapse-level DM based on energy rule using those traditional rules.

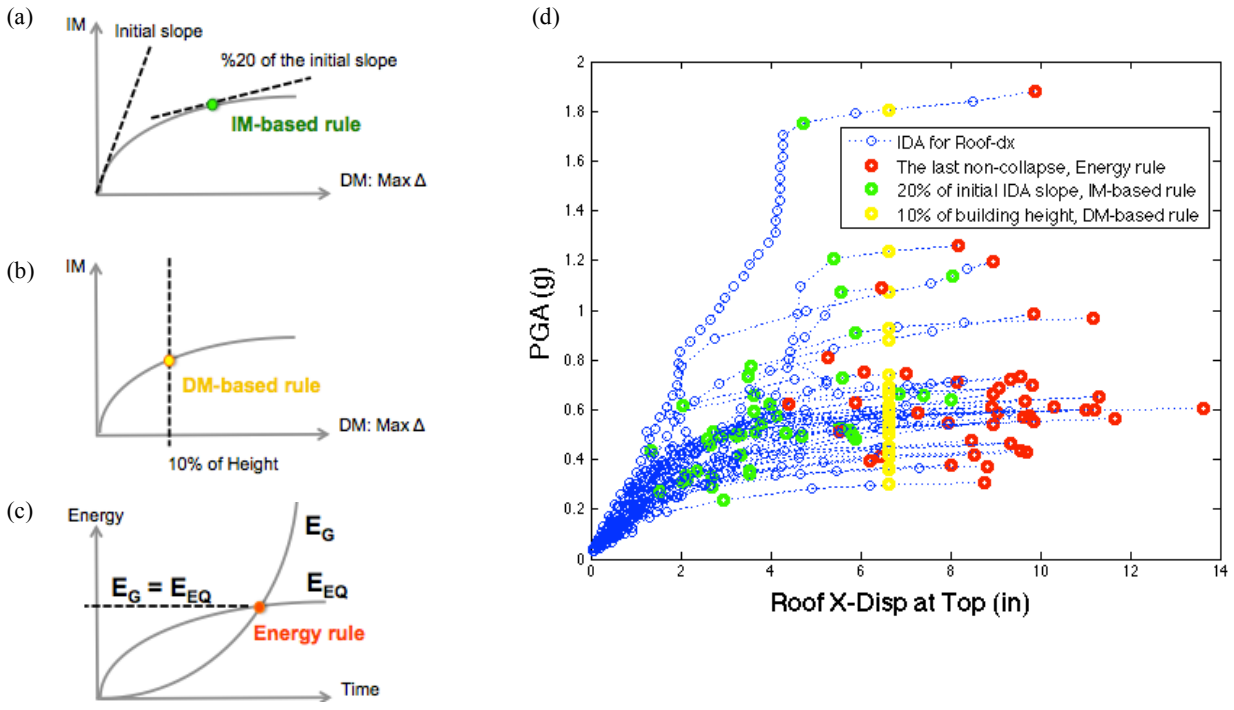

Figure 4.6 a) IM-based, b) DM-based, and c) Energy rules. d) IDA curves obtained for the test case study of Lignos et al. (2008) using ATC-63 far field record set (44 ground motions).

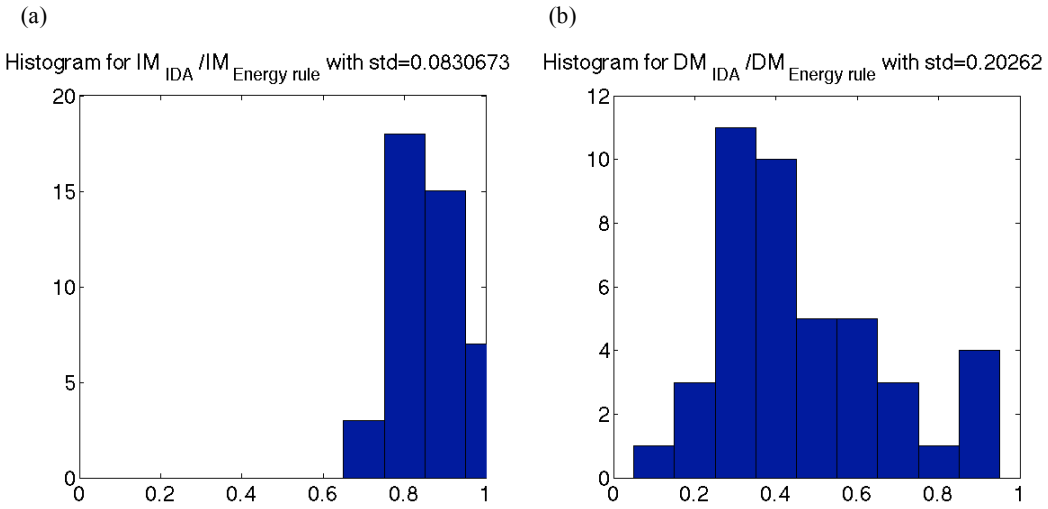

Figure 4.7 Histograms for IM-based rule normalized to the energy rule.

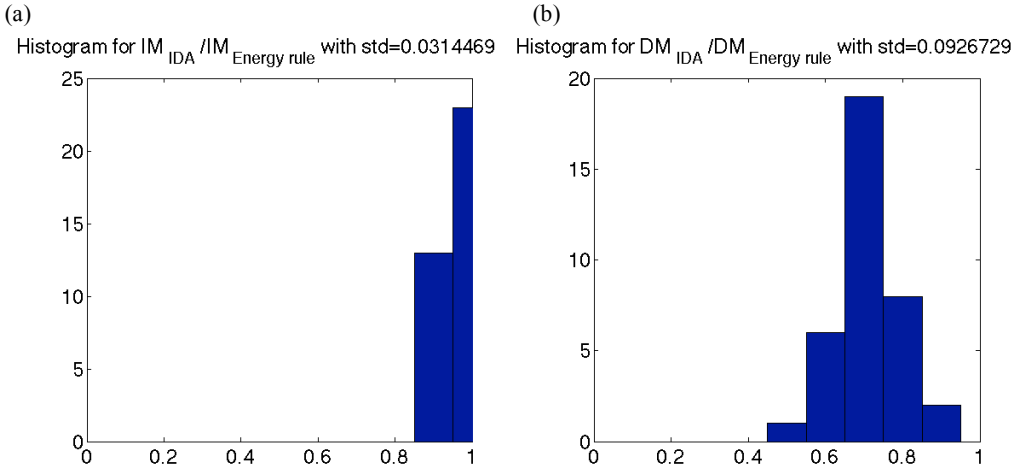

Figure 4.8 Histograms for DM-based rule normalized to the energy rule.

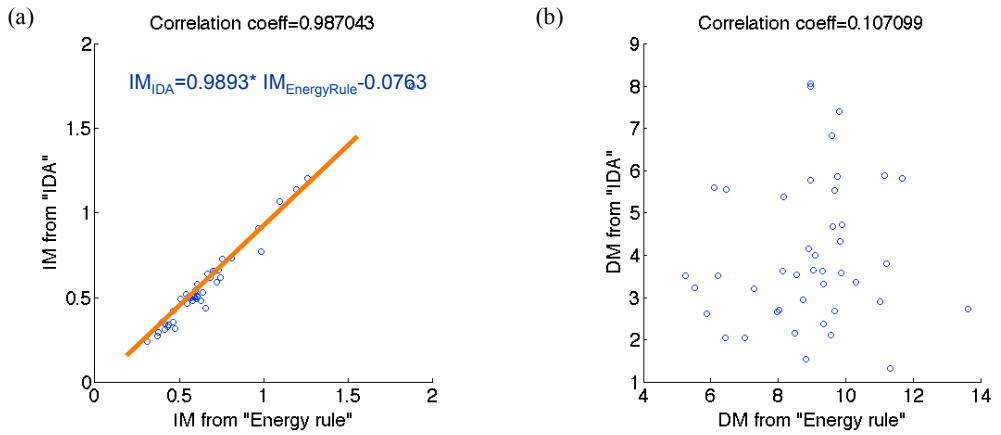

Figure 4.9 Correlation between IM-based rule and the energy rule.

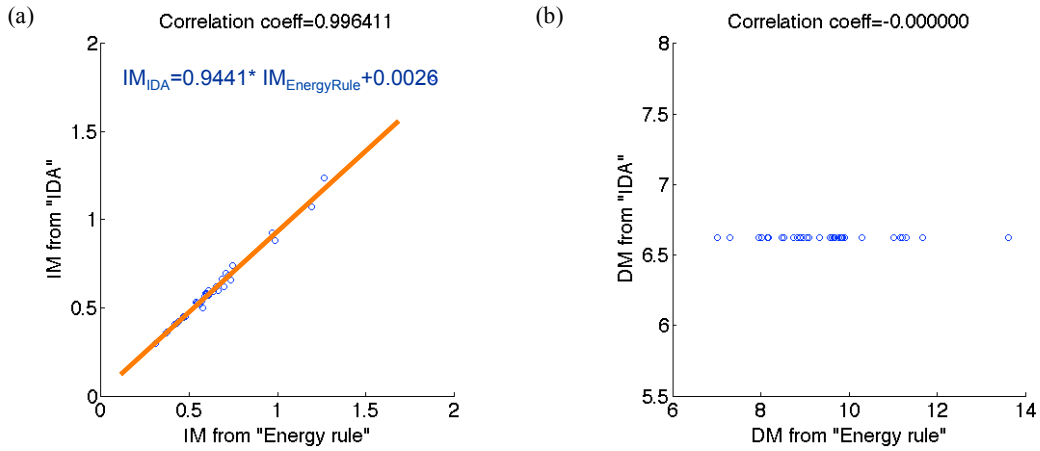

Figure 4.10 Correlation between DM-based rule and the energy rule.

4.4.2. Sensitivity Analysis of IDA-based Collapse Limit States

In order to find the best way to improve the traditional-IDA based rules, sensitive analyses are being performed on IDA results obtained by traditional rules comparing to ones using the energy rule. For example, Figure 4.11 and Figure 4.12 present the sensitivity of IDA results using IM-based rule with a slope percentage value of 10, 20 and 30. Standard deviation in IM levels decreases as the slope of IM-based rules decreases in the histograms of the intensity measure (Figure 4.11), because the intensity measure by IM-based rule gets close to intensity capacity determined by the energy rule. In the histograms of damage measure (Figure 4.12), 10% IM-

based rule shows less standard deviation in DM levels as expected, however, 20 % and 30 % IM-based rules do not show much difference in the deviation. This may be due to chaotic behavior of IDA curves (e.g., structural resurrection) in which slope of the curves may show a sudden increase or decrease towards collapse.

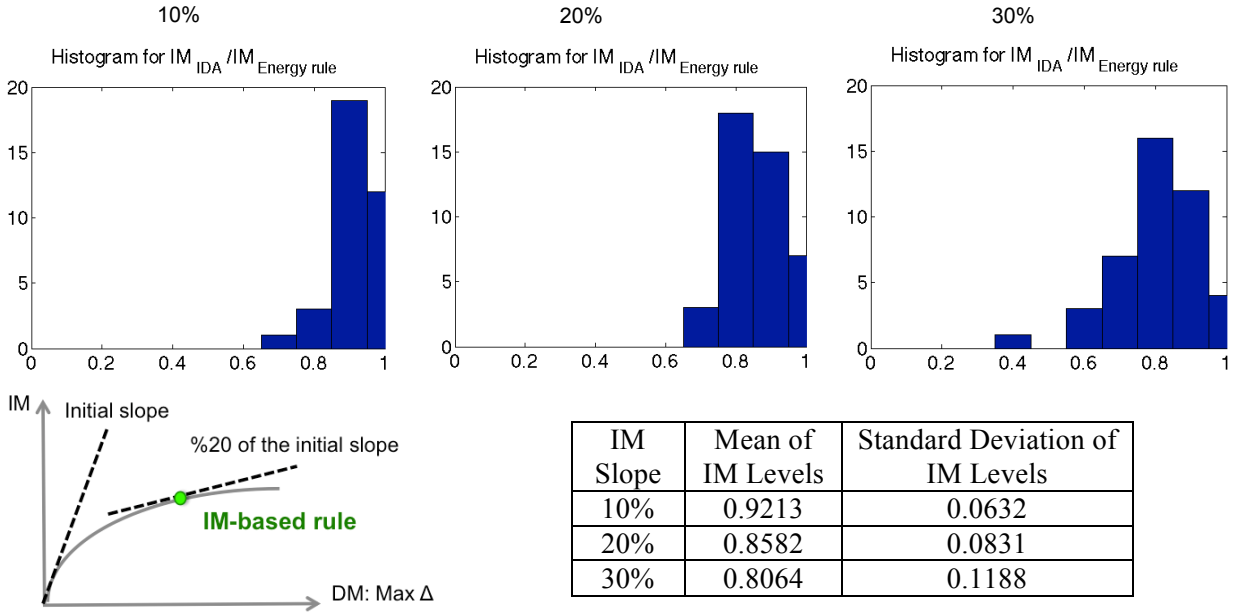

IM Slope	Mean of IM Levels	Standard Deviation of IM Levels
10%	0.9213	0.0632
20%	0.8582	0.0831
30%	0.8064	0.1188

Figure 4.11 Histograms and statistics for IM levels based on IM-based rule with 10%, 20%, and 30 % slopes.

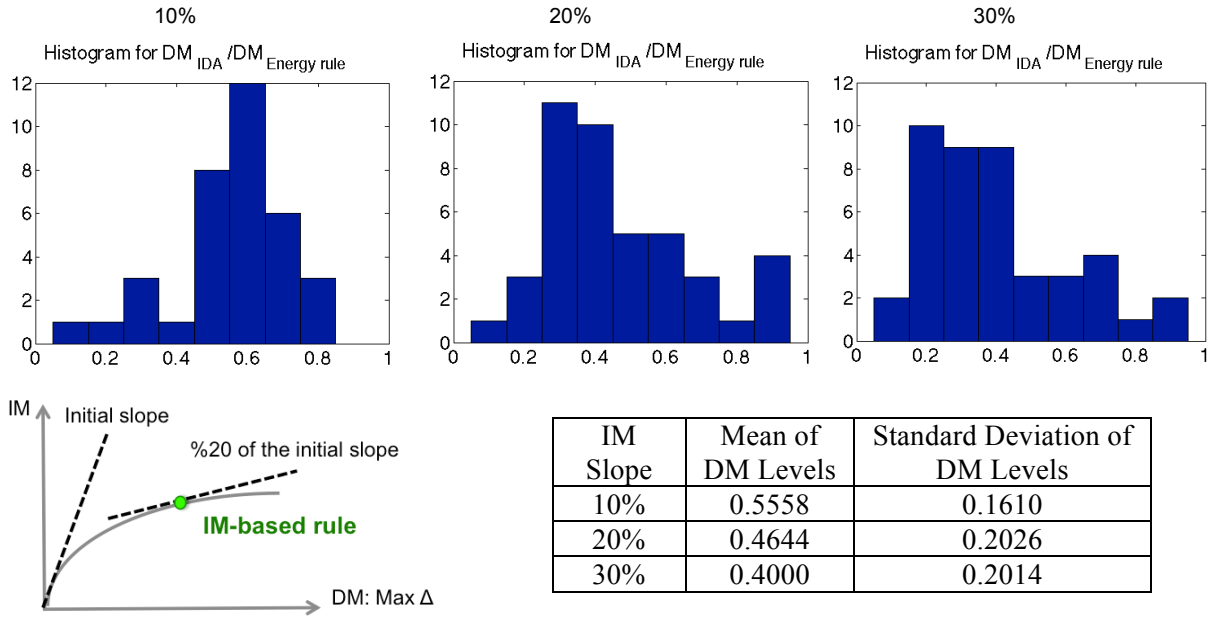

IM Slope	Mean of DM Levels	Standard Deviation of DM Levels
10%	0.5558	0.1610
20%	0.4644	0.2026
30%	0.4000	0.2014

Figure 4.12 Histograms and statistics for DM levels based on IM-based rule with 10%, 20%, and 30 % slopes.

Similarly, sensitivity analysis was performed for DM-based rule with a threshold value of 8, 10, and 12%. Statistics of results shows that deviations of intensity levels increase as the threshold value decreases (Table 4.1), because the intensity capacities determined based on DM-rule are found far from the points obtained based on the energy rule. In the case of damage levels, 8% DM-based rule shows the largest deviation since this threshold underestimates the collapse capacity according to the energy rule.

DM Threshold	Standard Deviation of DM Levels	Standard Deviation of IM Levels
8%	0.1280	0.0508
10%	0.0927	0.0314
12%	0.0939	0.0177

Table 4.1 Amount of dispersion in the levels of measures for DM-based rule with a threshold value of 8%, 10%, and 12 % of the building height.

Sensitivity analyses made in Figure 4.12 and Table 4.1 clearly show that collapse capacities identified by those traditional rules are sensitive to the subjective values assumed for intensity slope and damage thresholds. On the other hand, new energy rule depends the actual occurrence of dynamic instability that makes it more reliable option to be employed in collapse assessment of structures.

4.4.3. Benefits of New Collapse Criteria

The new collapse criteria, i.e., "energy rule" is proposed to predict collapse in terms of dynamic instability due to loss of structural resistance against the gravity loads, instead of the behavior of the IDA curves and subjective threshold values used in the existing IDA-based rules. Input energy components released into the structure due to earthquake shaking and applied gravity loads were compared to develop the new collapse criteria. It was observed that, as the structure approaches the collapse level, the gravity energy shows a large increase, which even exceeds the earthquake energy experienced. Thereby, the new collapse criteria has been defined as a boundless increase in gravity energy. A quantitative indication of structural collapse has been then proposed as gravity energy exceeding dynamic energy with a sudden increase: "$\mathbf{E_G > E_{EQ}}$".

A boundless drift in a structural response is the most commonly used approach in identification of simulated collapse under dynamic loads. However, in this approach, one needs to check response at each degree-of-freedom of the structure to check the dynamic instability. On the other hand, the new approach based on energy rule employs system-level measures, i.e., gravity and dynamic input energies. These energy terms are aggregated quantities of responses of structural components, therefore, can better represent global seismic performance of structural system.

In addition, a boundless increase in a structural response does not represent a realistic structural behavior. The new approach introduces a quantitative description of dynamic instability, which provides a physical boundary on the gravity energy instead of infinity. Moreover, this new quantitative criteria may facilitate developing a mathematical description of dynamic instability, which can be particularly useful as limit-state functions during structural reliability analysis of collapse.

The collapse capacity of a structure evaluated based on the behavior of the IDA curves may be sensitive to variability in ground motions as well as the possible chaotic structural behavior such as structural resurrection. Figure 4.13 shows that IDA-based rules can define more than one collapse capacity for a chaotic case of IDA curves that can cause confusion in identification of simulated collapse. For example, DM-based rule and IM-based rule define three and two collapse points for the cases in Figure 4.13a and Figure 4.13b respectively. This clearly shows that the new energy rule is a better indicator than IDA-based rules in identifying structural collapse, since it depends on dynamic instability not on shapes of IDA curves.

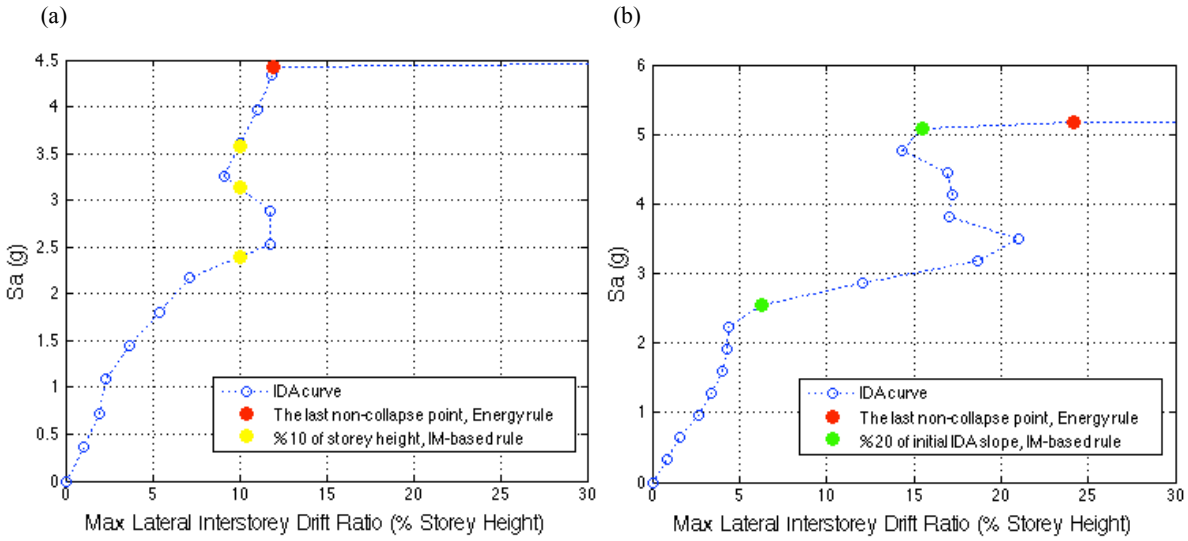

Figure 4.13 Collapse capacity using a) DM-based and energy rules, b) IM-based and energy rules.

5. CRITICAL DESCRIPTORS OF COLLAPSE

This chapter aims to identify critical descriptors for accurate and reliable collapse prediction. First, a literature review is conducted on existing performance measures indicating collapse. Next, extensive IDAs are performed using multiple ground motions on one of the previously validated simulation models in order to obtain a large data sample. Using the energy based-collapse criterion developed in Chapter 4, key parameters that govern collapse capacity of a given type of structure are then identified by statistical analysis of the IDA results.

5.1. Variability in Collapse Capacity

The results of collapse assessment of structures are subject to variability in the set of ground motions and structural model parameters as well as the selection of measures used to describe collapse capacity (Villaverde 2007). There are several measures proposed in the literature to describe the performance of the structures in view of both local and global behaviors during an earthquake. However, most of recent collapse assessment approaches such as IDA use maximum inter-storey or roof drift ratio and elastic spectral acceleration to predict collapse capacity, as illustrated in Figure 5.1.

Each of the IDA curves in Figure 5.1 shows the collapse capacity of the structure for a given ground motion by a red point (i.e., the last no-collapse point on an IDA curve) according to the energy-based collapse criterion developed in the previous chapter. The points show a significant level of variability in terms of intensity levels of ground motions as well as damage thresholds. Often the distributions of intensity and damage levels of collapse data are analyzed in histograms. A lognormal distribution function is often fitted to the collapse data to estimate collapse capacity in terms of either IM or DM that are used to construct the IDA curves. For example, Figure 5.1 shows such fitted collapse capacity models in terms of DM and IM, respectively. The amount of dispersion (lognormal beta value) is found to be larger for IM-based collapse capacity model comparing to DM-based one. However, as the structure gets close to collapse state, the IDA curves usually show a large increase in the structural response for a small increase in the ground motion intensity. This may imply that DM-based collapse capacity model can be notably sensitive near collapse although it may seem to indicate a better model with a smaller value of dispersion.

Large variability and sensitivity observed in collapse capacity indicate that there are research needs to explore alternative performance measures for a more accurate and reliable collapse prediction. Therefore, this study first aims to evaluate the variability of several performance measures available in the literature and then to identify the optimal selections of IM and DM that would effectively reduce the variability and sensitivity. Most IDA-based collapse assessment approaches still use only one DM and one IM, so this chapter also investigates the benefit of having more than one DM or IM for collapse capacity prediction in terms of accuracy and variability.

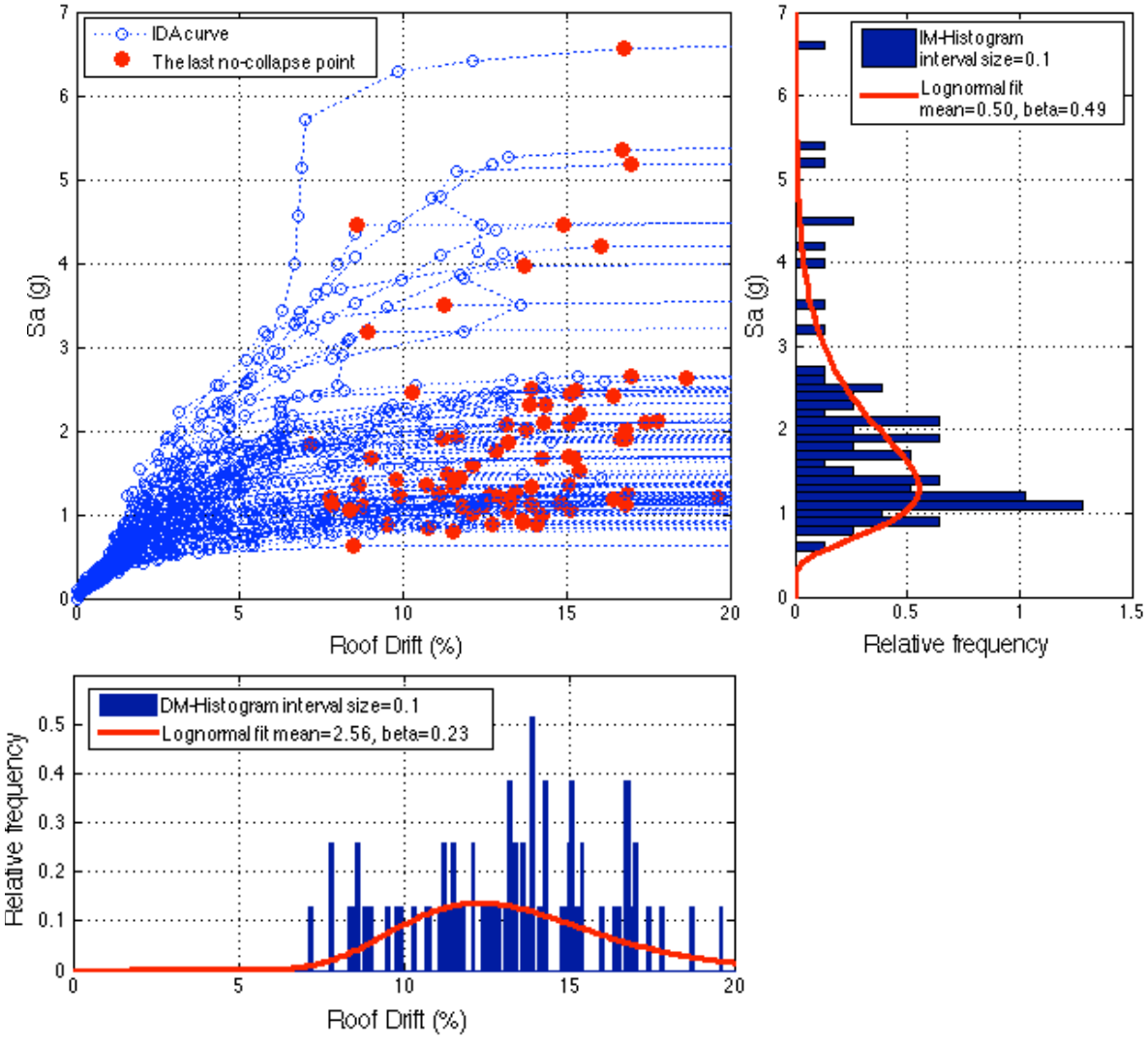

Figure 5.1 IDA curves and histograms for lateral roof drift and elastic spectral acceleration obtained for the case study by Lignos et al. (2008) using far-field ground motion set by Haselton and Deierlein (2007).

5.1.1. Methodology in Evaluation of Performance Measures for Collapse Prediction

A comparative study was conducted on existing performance measures commonly used for collapse prediction. Statistical analysis was performed on damage and intensity levels of collapse (identified by the new energy-based criterion) to quantify the variability and then to identify critical key parameters that effectively describe collapse capacity. One of the most preferred ways to measure dispersion of data is to evaluate sample standard deviation. A larger value of the standard deviation means more dispersed data. However, noting that measures can have different units and scales, this study uses the coefficient of variation (cov) in the following for the purpose of comparison:

$$cov = \frac{\sigma}{\mu} \quad \text{where:} \quad \mu = \frac{\sum_{i=1}^{n} x_i}{n} \quad \text{and} \quad \sigma = \sqrt{\frac{\sum_{i=1}^{n} (x_i - \mu)^2}{n-1}} \tag{5.1}$$

in which σ and μ respectively denote the sample standard deviation and the sample mean (μ), and x_i, $i = 1,\ldots,n$ are the observed values of the measure of interest from IDAs using n ground motions. As seen in (5.1), the cov is a normalized measure of the dispersion, and thus can be a better indicator that provides a fair comparison of variability.

A desirable property of a collapse descriptor is small dispersion since collapse prediction based on a threshold value introduced in terms of the descriptor would predict collapse with more confidence. Moreover, smaller dispersion of IM or DM capacities given IM indicates that a smaller sample of collapse points is necessary to estimate collapse probability. This means fewer non-linear analyses and less ground motions are required for collapse prediction.

Let us consider two performance measures (either damage or intensity) for collapse prediction: PM^1 (μ_1, σ_1) and PM^2 (μ_2, σ_2). Here, "μ_1, σ_1" and "μ_2, σ_2" represent the corresponding mean and standard deviation for the corresponding measures. The most significant numerical descriptor that characterizes relation and linear dependency between pairs of data is the sample correlation coefficient, which can be described for performance measure data points $PM^1{}_i$ and $PM^2{}_i$ (where i=1,…,n and n is the number of data points) as in (5.2). This statistical measure always lies between −1 and 1. The extreme value of −1 and 1 indicate deterministic linear relationship

between the two performance measures. As the correlation gets close to zero, it indicates a weaker linear dependency.

$$\rho_{12} = \frac{\sum_{i=1}^{n}(PM^1{}_i - \mu_1)(PM^2{}_i - \mu_2)}{(n-1)\sigma_1\sigma_2} = \frac{\sum_{i=1}^{n}(PM^1{}_i\, PM^2{}_i) - n\mu_1\mu_2)}{(n-1)\sigma_1\sigma_2} \qquad (5.2)$$

Correlation coefficient can be used for two purposes here. First, it can describe how two damage measures (i.e., DM^1 and DM^2) or two intensity measures (i.e., IM^1 and IM^2) are linearly dependent on each other or how they are different in terms of structural performance (see Figure 5.2). Second, it can be used to check critical intensity indices that correlate well with damage potential of structures (i.e., IM^1 and DM^1).

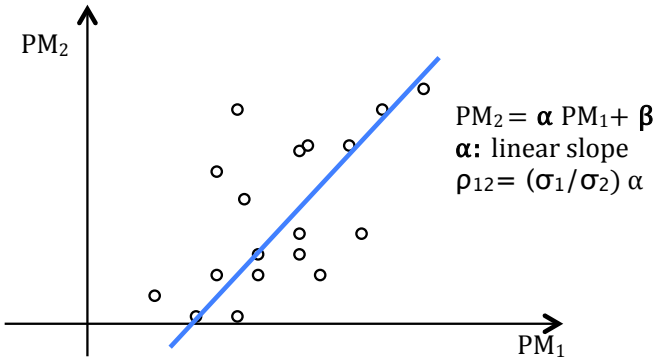

Figure 5.2 Correlation analysis between two performance measures PM^1 (μ_1, σ_1) and PM^2 (μ_2, σ_2).

5.1.2. The Test Case Considered in This Study

The IDA data obtained for the case study by Lignos et al. (2008) is investigated here to study variability in alternative performance measures for collapse prediction. Since enough amount of sample data are needed for reliable statistical results, the IDA curves obtained for Haselton and Deierlein (2007) far-field set (78 ground motion records) has been considered here instead of ATC-63 far field record set (44 ground motion records). This extensive far-field set includes 34 more records in addition to ATC-63 far field record set, all of which fulfill the selection criteria established by ATC-63 project (See Appendix C).

Note that the case study considered here deals with an MDOF frame structure with a dominant period around 0.44 seconds, therefore the results of this study may be generalized to MDOF structures with similar first-mode period and degrading properties with a caution. More detailed study is conducted in Chapter 7 to investigate the structures with different periods and structural parameters.

The new collapse criterion described in Chapter 4, which is the incidence of gravity energy exceeding seismic energy with a "sudden" increase ($E_G >> E_{EQ}$), was applied to indicate collapse. The collapse capacity data are recorded from "the last no-collapse cases" in IDA curves. Statistical analyses were then performed on the levels of IMs (denoted by IM_{col}) and as well as on the levels of DMs (denoted by DM_{col}) to identify critical descriptors for collapse prediction.

5.2. Collapse Capacity by Damage Measures

5.2.1. *Existing Damage Measures for Structural Performance*

The evaluation of damage level of a structural system under seismic forces requires a quantitative descriptor of physical condition of the system, which can be expressed as a function of structural responses. Figure 5.3 describes these responses, which can be the structural forces, deformations, energy or a combination of them on the global and local basis.

Local indicators are needed primarily to assess potential damage localization in the structure. They can be parameters related to stress and strain in fibers or internal forces and deformations in structural components. These indicators are employed to determine the occurrence of local limit states such as yielding, cracking, crushing and buckling. For example, it is necessary to evaluate shear strains to check the occurrence of shear yielding and buckling in steel members.

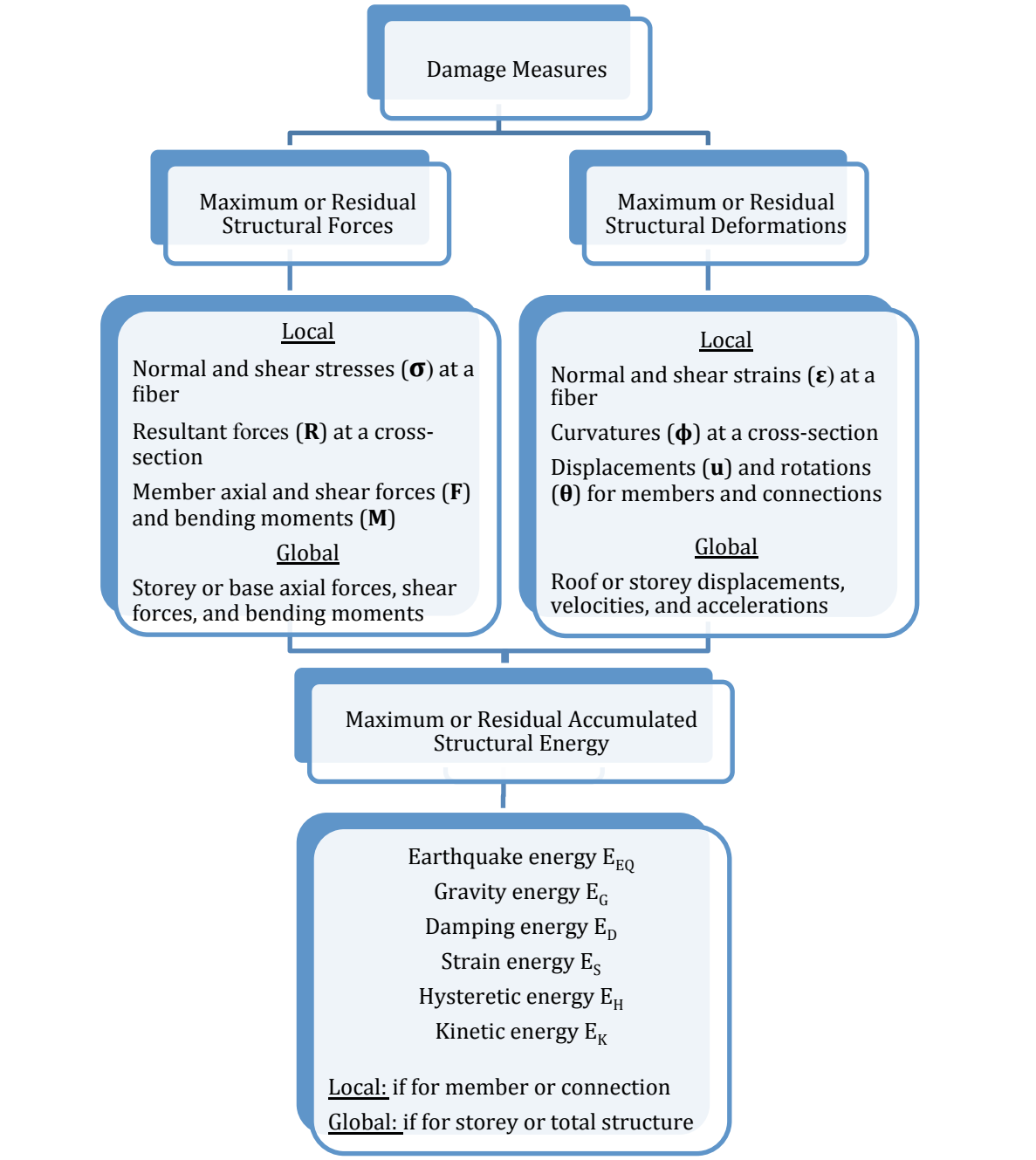

Figure 5.3 Measures of damage state of a structural system on both global and local basis.

On the other hand, global indicators are used to assess system performance and to estimate the fundamental structural response characteristics, e.g., stiffness, strength and ductility of the system. These are parameters related to the contributions of all members at the storey level. For example, peak base/storey moments and shear forces or peak floor displacement, velocity or acceleration are often used as global indicators.

Collapse is traditionally associated with the onset of a target value of inter-storey drift (relative displacement between two floors) or plastic hinge rotation at a structural component (Zareian, 2006). However, such an approach may not accurately represent the seismic performance of structural systems against collapse due to redistribution and variation of damage within the structure.

Collapse assessment based on component damage evaluation ignores redistribution of damage within the structure; therefore, this approach may provide inaccurate estimate of structural resistance against collapse. Figure 5.4 shows the damage level in beam and column springs for the test case study of Lignos et al. (2008) under the test ground motion, which is applied to the frame continuously at scales of 0.5, 1.0, 1.5, 1.9, ad 2.2. At the last intensity scale factor of 2.2, the system starts to show plastic hinges mostly in the first storey just before collapse. If one checks only the spring that first reached ultimate capacity, structural resistance may be then underestimated. However, if one checks only the yielded spring at the top of the right base column near collapse, then structural resistance may be overestimated. Therefore, such local response indicators can only be more appropriate for evaluating losses in resistance of individual elements prior to collapse. These findings indicate that collapse assessment of a structural system requires damage evaluation on a global basis.

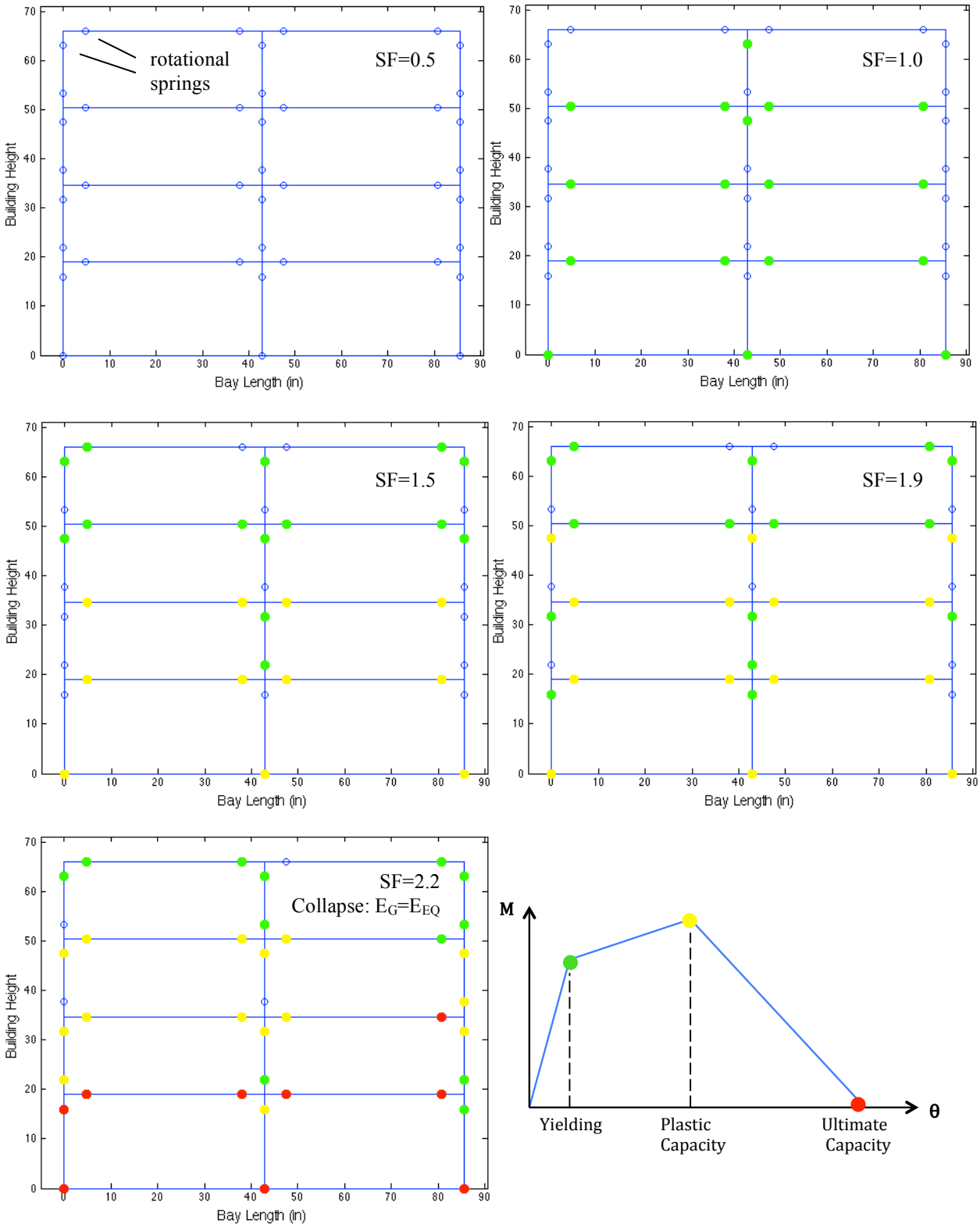

Figure 5.4 Damage distributions in rotational springs for the case study of Lignos et al. (2008) using the test ground motion at scale factors (SF) of 1.0, 1.5, 1.9 and 2.2 (Note: green, yellow, and red marks indicate that yielding, plastic, and ultimate rotational capacities are exceeded respectively).

Damage states of structural components in a system may show variability even if they share the same value of structural response. In other words, the patterns and histories of the structural response may be different. Likewise, for a given damage level of structure (i.e, maximum inter-storey drift), distribution of damage through the structure can vary based on variation in damaged components which may result in different damage state of structural system (i.e, light, moderate, severe, life-safety, or collapse). This variation of damage within the structure requires "cumulative" structural responses instead of "peak" ones in order to accurately estimate seismic performance of structures. These cumulative measures are load-path dependent, therefore can better represent the damage due to cyclic seismic loading. Accumulated plastic deformation and the hysteretic energy are commonly used for calculating cumulative damage indices (Mehannay and Dieierlein, 2000; Kratzig et al., 1989). There are also combined damage measures considering damage due to both excessive deformation and energy absorption (Park and Ang, 1985; see Figure 5.3).

Therefore, for accurate and reliable collapse prediction, one needs both global and cumulative parameters associated with severe structural damage just before collapse. Since energy parameters are aggregated quantities considering each individual component damage, they can be excellent as overall cumulative indicators of structural performance. Since the focus of this chapter is to compare performance measures available in the literature, other damage measures besides energy parameters were also considered in the following statistical analysis. Table 5.1 shows the 24 damage measures selected for comparison in this study.

5.2.2. Statistics of Damage Level of Collapse

From the collapse data points identified by use of the energy-based criterion for 78 ground motions in Figure 5.1 (red points), coefficients of variation were obtained for several damage measures as shown in Table 5.2. Some of these measures are global parameters such as cumulative energy responses for the structural system (e.g., E_{SPR}, E_G, E_{EQ}, E_K) and others are peak story/base responses (e.g., $D_{R,X}$, $IDR_{S,X}$, $F_{B,Y}$, $F_{B,X}$). In addition to these global indicators, the damage measure by Park and Ang (PA_{RBC}) was also included as a local indicator of a column-spring at the base for comparison.

DM_{col}	Unit	Description
$D_{R, X}$ $D_{R, Y}$	%	Maximum lateral (X) and vertical (Y) roof drift over building height
$D_{S, X}$	%	Maximum lateral (X) storey drift through the structure over building height
$IDR_{S, X}$ $IDR_{S, Y}$	%	Maximum lateral (X) and vertical (Y) inter-storey drift ratio through the structure
$V_{S, X}$ $V_{S, Y}$	in/s	Maximum lateral (X) and vertical (Y) storey velocity through the structure
$A_{S, X}$ $A_{S, Y}$	in/s^2	Maximum lateral (X) and vertical (Y) storey acceleration through the structure
$F_{S, X}$	kip	Maximum storey shear (X) force through the structure
$F_{BC, X}$	kip	Maximum shear (X) force at the base-column (BC)
$F_{B, X}$ $F_{B, Y}$	kip	Maximum total shear (X) and axial (Y) force at the base (B)
E_{EQ} $E_{EQ\text{-}rate}$	J, J/s	Cumulative earthquake input energy and its maximum rate
E_G $E_{G\text{-}rate}$	J, J/s	Cumulative gravity energy released into the system and its maximum rate
$E_{K, X}$ $E_{K, Y}$	J	Maximum lateral (X) and vertical (Y) component of kinetic energy absorbed into the
E_K	J	Maximum total kinetic energy absorbed into the system
$E_{SPR, B}$ $E_{SPR, C}$	J	Cumulative strain energy in beam (B) and column (C) springs
E_{SPR}	J	Cumulative total strain energy in beam and column springs
PA_{RBC}	-	Park and Ang (PA) measure for the bottom spring of the right base-column (RBC) with a calibration factor (β) of 0.08 for cyclic damage

Table 5.1 The 24 damage measures considered in statistical analysis for collapse prediction (Note that J: Joules, in: inches, s: second).

DM_{col}	Median	Mean	Cov
$F_{B, Y}$	36.786	37.121	0.038
$F_{B, X}$	10.647	10.886	0.093
$D_{R, X}$	13.642	13.297	0.215
$D_{S, X}$	13.642	13.303	0.216
PA_{RBC}	0.590	0.596	0.217
$IDR_{S, X}$	20.258	19.914	0.226
$F_{BC, X}$	7.567	7.500	0.226
$V_{S, X}$	22.946	25.258	0.347
$D_{R, Y}$	1.221	1.227	0.419
E_G	2590.530	2638.927	0.419
$F_{S, X}$	5.401	6.534	0.428
$IDR_{S, Y}$	2.077	2.113	0.429

DM_{col}	Median	Mean	Cov
$A_{S, X}$	357.295	402.610	0.440
$V_{S, Y}$	1.489	1.643	0.462
$E_{SPR, C}$	7899.076	8492.344	0.462
E_{SPR}	16451.511	18257.613	0.474
$E_{G\text{-}rate}$	4814.126	5366.538	0.482
E_{EQ}	18432.635	20711.983	0.490
$E_{SPR, B}$	8639.646	9765.428	0.493
$E_{K, X}$	1348.868	2045.551	0.818
E_K	1349.177	2050.660	0.819
$E_{EQ\text{-}rate}$	26946.556	39412.707	0.834
$E_{K, Y}$	8.001	12.364	1.363
$A_{S, Y}$	66.725	91.436	2.516

Table 5.2 Statistics of several damage measures at "near-collapse" level for the case study of Lignos et al. (2008) using far-field ground motion set by Haselton and Deierlein (2007).

Although some peak base forces ($F_{B, Y}$ and $F_{B, X}$) give smallest values of cov in Table 5.2, it is seen that force responses are not helpful when used alone to predict the collapse capacity. Once the system starts yielding, which occurs much earlier than collapse, the structure enters into the plastic state and starts to show excessive inelastic deformations under repeated reversed seismic

loads and applied gravity forces. This results in "gradual" change in storey force demands but "rapid" accumulation of storey drift demands. This is the reason why peak values of structural deformation parameters have been widely used in the literature to evaluate the state of structural damage caused by earthquake actions. For example, Figure 5.5a shows that the total base shear $F_{B,X}$ tends to give collapse capacity values around base shear yield, which seems to be around 10 kips. Force quantities such as base shear yield may indicate the initiation of plastic behavior, but may not be helpful to indicate global collapse performance. Similarly, Figure 5.5b indicates that axial forces tend to give values close to the weight of the structure, which is 34.6 kips, as the scale factor of intensity increases. Therefore, these observations support the point that these force measures may provide smaller covs but cannot give any clear sign of collapse comparing to other no-collapse points when the structure enters into the plastic state.

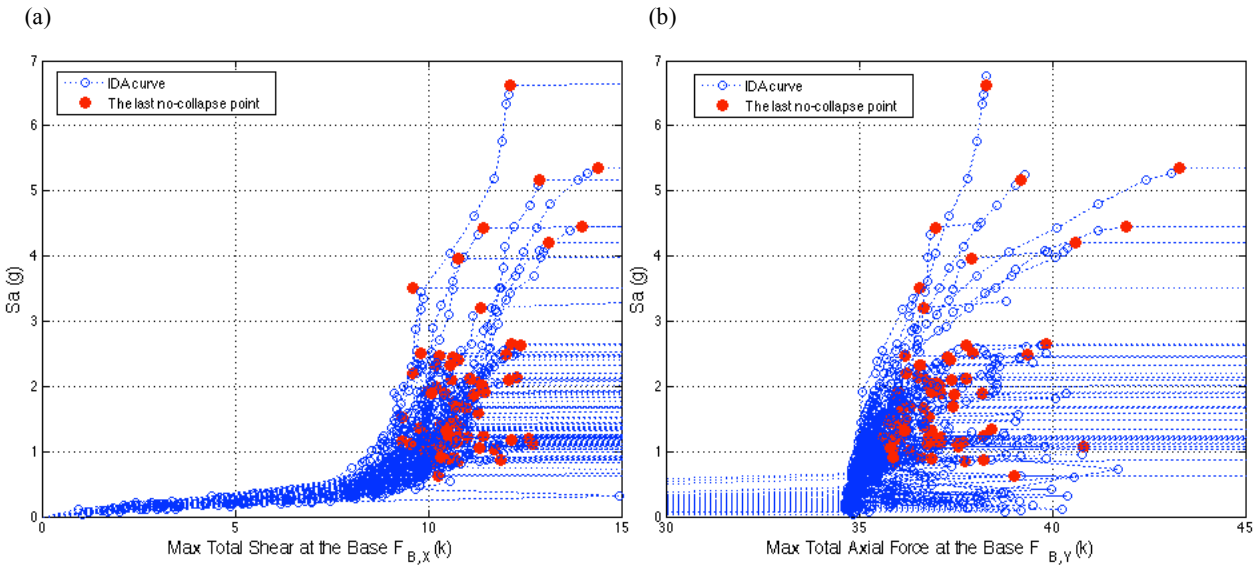

Figure 5.5 IDA curves of a) total base shear and b) total base axial force for the case study of Lignos et al. (2008) using far-field ground motion set by Haselton and Deierlein (2007).

In Figure 5.6, collapse points are identified on IDA curves for structural response at two different structural resolutions: at the level of a structural component by Park and Ang damage measure (PA_{RBC}; Figure 5.6a) and at the level of story by maximum inter-storey drift ratio ($IDR_{S,X}$; Figure 5.6b). While $IDR_{S,X}$ is an indicator of global behavior calculated based on contributions of all members at the storey level, PA_{RBC} can only indicate the local plastic hinge failure at the base spring of the right frame-column. Due to redistribution of forces in such an indeterminate system, even if a base column losses its resistance against local plasticity, it is necessary to form

much more than one plastic hinge to cause the total failure of the structural system. This is the reason why the recent IDA-based studies mostly use story drift ratios such as $D_{R,X}$ or $IDR_{S,X}$ to assess the collapse capacity. Based on 78 far-field ground motions applied on the case study of Lignos et al. (2008), the drift ratios give a cov around 0.22, which is fairly good comparing to others, but not small.

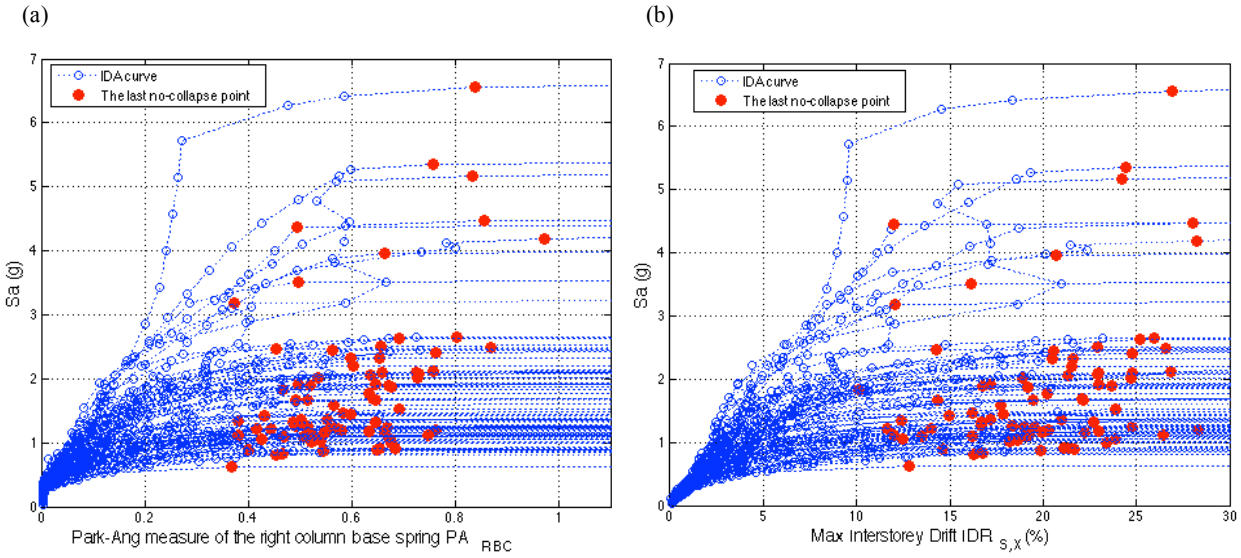

Figure 5.6 IDA curves of a) Park and Ang measure of a base spring and b) maximum IDR for the case study of Lignos et al. (2008) using far-field ground motion set by Haselton and Deierlein (2007).

Energy components mostly provide larger cov comparing to peak structural forces and deformations because these quantities integrate the component damage indices. The energy component E_G here is a direct sum of vertical storey deflections ($D_{R,Y}$) because weight is almost the same at each storey. This is the reason why E_G and $D_{R,Y}$ share the same value of cov (0.42) in Table 5.2. However, E_K depends on square values of $V_{S,Y}$ and $V_{S,X}$ hence giving a larger value of cov around 0.82. Although larger dispersion is observed in most energy quantities, they are cumulative combinations of the response time histories at each degree-of-freedom, thereby, can better represent the structural collapse capacity.

It is also noteworthy that the mean of collapse capacities (i.e., resistance near collapse) for E_G and $E_{K,Y}$ were found to be significantly less then the ones for E_{EQ} and $E_{K,X}$ respectively (see Table 5.2). Once dynamic instability occurs, the structure cannot resist gravity loads anymore, therefore, suddenly releases gravity energy far exceeding the earthquake energy experienced at

collapse. The structure then rapidly transforms most of the released gravity energy into kinetic energy (especially into $E_{K,Y}$) causing the structure to collapse down totally.

IDA curves in Figure 5.5, Figure 5.6, Figure 5.7b, and Figure 5.8 generally show collapse capacities (red circles) on a flat plateau just before any indication of collapse (i.e., $E_G > E_{EQ;}$ the last blue circle on IDA curve). Although a small intensity scale increment (0.05) is chosen in assessment of these collapse capacity points, it was observed that the structural response gives very different results, as the increment gets smaller near collapse. Such sensitivity in structural response to any small increase in intensity (i.e., a large increase in the structural response corresponding to a small increase in the ground motion intensity when the structure is near collapse) can contribute to the variability observed in collapse capacities, for example, for E_G, E_{SPR}, and E_K in Figure 5.7b, Figure 5.8a, and Figure 5.8b respectively. In order to account for the sensitivity issue of the response near collapse, collapse capacity based on E_{EQ} in Figure 5.7a can be considered as a better candidate; however, it shows a larger cov with a value of 0.49 in Table 5.2, therefore does not show a clear separation between no-collapse (blue circles on IDA curve before collapse) and near-collapse points (red circles). Therefore, a critical measure with a smaller cov that handles the sensitivity issue near collapse is pursued in Section 5.4.2 considering the balance of input and dissipated energy within the structure.

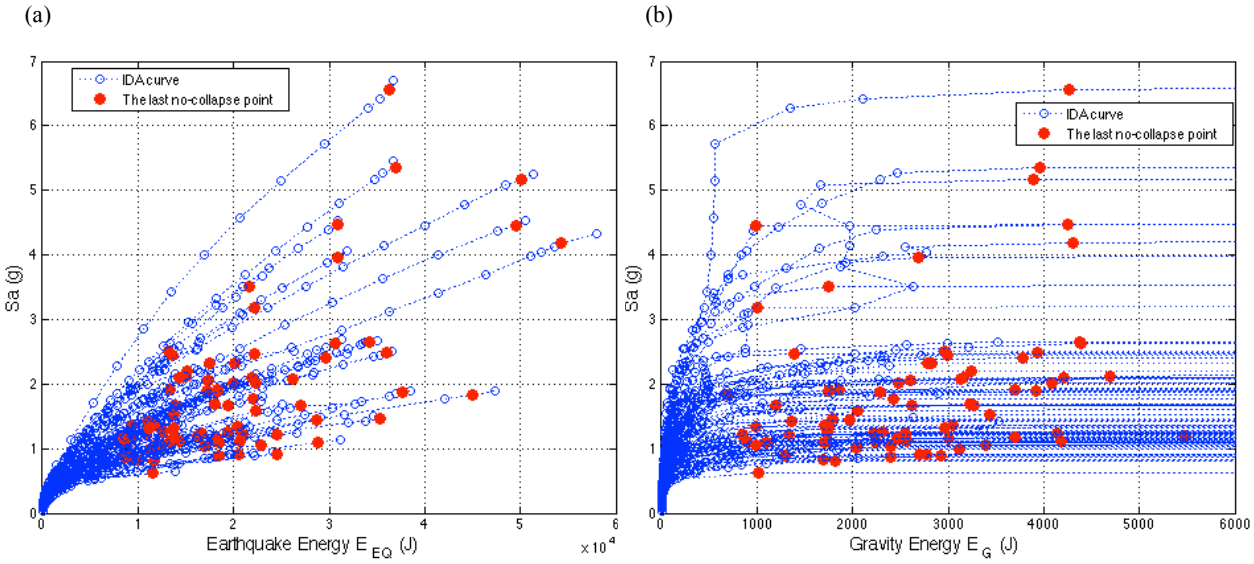

Figure 5.7 IDA curves of released-energy components for the case study of Lignos et al. (2008) using far-field ground motion set by Haselton and Deierlein (2007).

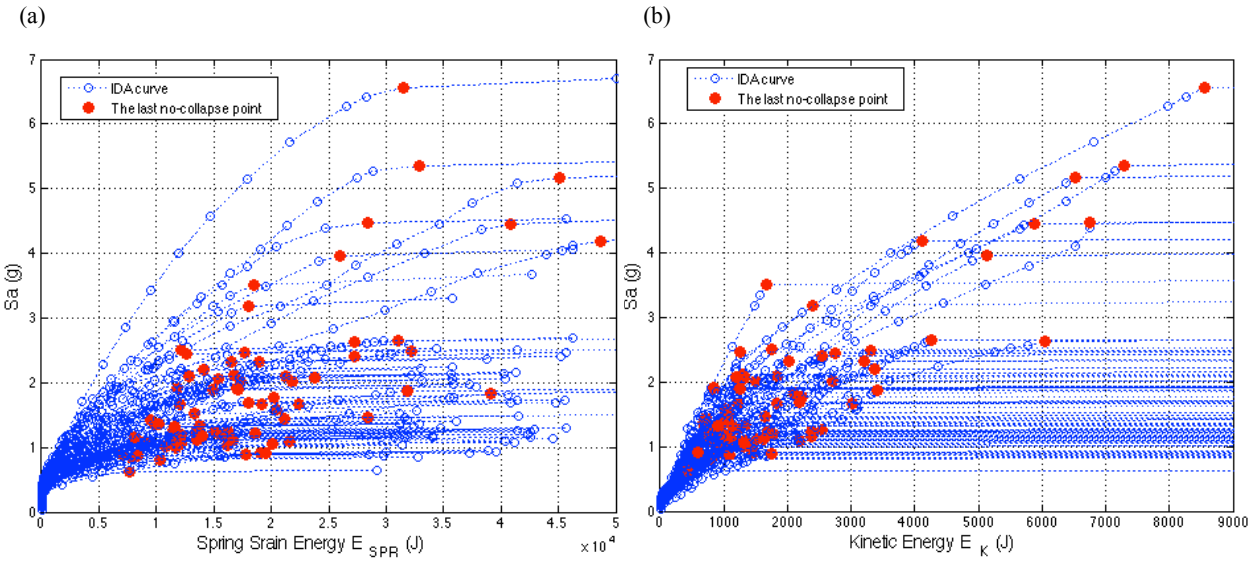

Figure 5.8 IDA curves of absorbed-energy components for the case study of Lignos et al. (2008) using far-field ground motion set by Haselton and Deierlein (2007).

5.2.3. Correlation Analysis on Damage Level of Collapse

Table 5.3 provides correlation analysis results between the 24 damage measures, and Table 5.4 summarizes the measures showing high correlation with each other. Correlation analysis between damage measures can give information about the measure itself and how it is obtained comparing the degree of its linear dependency with other measures. The analysis may also help us to understand the structural response before collapse. For example, the gravity energy component of the structural system E_G shows a strong linear dependency ($\rho \geq 0.95$) on story and roof drifts in both lateral and vertical directions. This indicates that the geometric effects taking place within the structure due to applied gravity forces can be well represented by E_G. Likewise, shear forces at story $F_{S,X}$ and story accelerations $A_{S,X}$ show high correlation since both are directly related through seismic excitations applied on storey-weights. Similarly, E_K components are highly correlated to storey velocities $V_{S,X}$ and $V_{S,Y}$, which also show high correlation with $E_{EQ\text{-}rate}$ and $E_{G\text{-}rate}$ respectively. All of these findings make sense since earthquake shaking releases energy into the system that initiates structural accelerations at each story. Storey acceleration then causes floor movement with a storey drift and a storey velocity that in turn makes the system to release gravity energy and absorb kinetic energy respectively.

Additionally, two more interesting points were observed in Table 5.3 regarding structural collapse behavior: First, high correlation between spring energy components and earthquake energy confirms that E_{EQ} is mostly dissipated as hysteretic energy through springs. Second, E_K is governed by $E_{K,X}$ until collapse and then $E_{K,Y}$ also becomes significant once gravity energy shows an abrupt increase at collapse.

	$D_{R,X}$	$D_{R,Y}$	$D_{S,X}$	$IDR_{S,X}$	$IDR_{S,Y}$	$V_{S,X}$	$V_{S,Y}$	$A_{S,X}$	$A_{S,Y}$	$F_{S,X}$	$F_{BC,X}$	$F_{B,X}$	$F_{B,Y}$	E_{EQ}	$E_{EQ\text{-}rate}$	E_G	$E_{G\text{-}rate}$	$E_{K,X}$	$E_{K,Y}$	E_K	$E_{SPR,B}$	$E_{SPR,C}$	E_{SPR}	PA_{RBC}
$D_{R,X}$	1.00	0.98	1.00	0.95	0.93	0.33	0.48	0.39	0.10	0.33	0.93	0.22	0.38	0.01	0.30	0.98	0.47	0.32	0.33	0.32	0.17	0.12	0.15	0.83
$D_{R,Y}$		1.00	0.99	0.96	0.96	0.36	0.53	0.41	0.10	0.34	0.95	0.28	0.42	0.06	0.35	1.00	0.52	0.36	0.39	0.36	0.22	0.18	0.21	0.86
$D_{S,X}$			1.00	0.95	0.93	0.33	0.48	0.39	0.10	0.33	0.93	0.22	0.38	0.01	0.30	0.98	0.47	0.32	0.33	0.32	0.17	0.12	0.15	0.83
$IDR_{S,X}$				1.00	0.99	0.35	0.55	0.40	0.13	0.33	1.00	0.27	0.46	0.05	0.34	0.98	0.54	0.35	0.41	0.35	0.21	0.18	0.20	0.92
$IDR_{S,Y}$					1.00	0.39	0.57	0.43	0.13	0.36	0.99	0.32	0.49	0.11	0.38	0.98	0.57	0.39	0.44	0.39	0.26	0.24	0.26	0.94
$V_{S,X}$						1.00	0.65	0.89	-0.07	0.84	0.35	0.58	0.55	0.71	0.95	0.37	0.61	0.94	0.53	0.94	0.78	0.68	0.74	0.52
$V_{S,Y}$							1.00	0.55	0.03	0.50	0.55	0.70	0.74	0.34	0.71	0.55	0.99	0.72	0.95	0.72	0.43	0.42	0.43	0.57
$A_{S,X}$								1.00	-0.03	0.95	0.39	0.54	0.56	0.64	0.86	0.42	0.52	0.78	0.44	0.78	0.70	0.62	0.67	0.53
$A_{S,Y}$									1.00	-0.04	0.20	-0.07	0.35	-0.11	-0.07	0.10	0.03	-0.06	0.02	-0.05	-0.08	-0.09	-0.08	0.09
$F_{S,X}$										1.00	0.32	0.56	0.54	0.60	0.84	0.35	0.46	0.74	0.40	0.74	0.65	0.57	0.62	0.46
$F_{BC,X}$											1.00	0.27	0.50	0.06	0.34	0.97	0.55	0.34	0.42	0.34	0.21	0.19	0.20	0.93
$F_{B,X}$												1.00	0.57	0.56	0.64	0.30	0.70	0.61	0.68	0.61	0.59	0.61	0.61	0.41
$F_{B,Y}$													1.00	0.35	0.62	0.45	0.73	0.58	0.73	0.58	0.40	0.39	0.40	0.51
E_{EQ}														1.00	0.69	0.08	0.33	0.66	0.32	0.66	0.97	0.97	0.98	0.40
$E_{EQ\text{-}rate}$															1.00	0.36	0.66	0.97	0.62	0.97	0.75	0.68	0.72	0.50
E_G																1.00	0.54	0.37	0.41	0.37	0.23	0.20	0.22	0.89
$E_{G\text{-}rate}$																	1.00	0.67	0.95	0.67	0.41	0.41	0.41	0.57
$E_{K,X}$																		1.00	0.63	1.00	0.73	0.64	0.70	0.50
$E_{K,Y}$																			1.00	0.63	0.36	0.39	0.37	0.45
E_K																				1.00	0.73	0.64	0.70	0.50
$E_{SPR,B}$																					1.00	0.96	0.99	0.52
$E_{SPR,C}$																						1.00	0.99	0.52
E_{SPR}																							1.00	0.52
$PA_{BC,R}$																								1.00

Table 5.3 Correlation of coefficients of several damage measures at "near-collapse" level for the case study of Lignos et al. (2008) using far-field ground motion set by Haselton and Deierlein (2007) (Note: yellow, green and blue marks indicate $\rho \geq 0.90$, $\rho \geq 0.80$, and $\rho \geq 0.70$ respectively).

Group #	DM_{col}
1	$D_{R,X}$, $D_{R,Y}$, $D_{S,X}$, $IDR_{S,X}$, $IDR_{S,Y}$, $F_{BC,X}$, E_G
2	E_{EQ}, $E_{SPR,B}$, $E_{SPR,C}$, E_{SPR}
3	$V_{S,X}$, $E_{EQ\text{-}rate}$, $E_{K,X}$, E_K
4	$V_{S,Y}$, $E_{G\text{-}rate}$, $E_{K,Y}$
5	$F_{S,X}$, $A_{S,X}$

Table 5.4 Damage measures at "near-collapse" level that show strong correlation ($\rho \geq 0.90$) within each group.

Moreover, eliminating damage measures showing strong correlation with other can reduce the number of parameters to consider during the comparative study. Since system-energy quantities are the best candidates that can represent the global collapse behavior, "E_G, $E_I = E_{EQ}+E_G$, $E_{K,X}$, E_K, E_{SPR}" are selected for further statistical analyses.

5.3. Collapse Capacity by Intensity Measures

5.3.1. Existing Intensity Measures for Ground Motions

Seismic analysis and design of structures demand an adequate measure of intensity of the applied ground motions to describe the severity of the earthquake shaking on structural response. Numerous measures have been proposed to capture important characteristics of strong ground motions such as frequency content, duration and amplitude. Riddell (2007) has recently provided a comprehensive literature review of existing intensity measures of ground motions. Table 5.5 summarizes the measures studied by Riddell (2007) and some other measures proposed in recent studies. These intensity measures can be arranged into the following five groups as shown in Figure 5.9 based on the property of ground motion used in their assessment:

1. *Basic* measures that use only fundamental characteristics of ground motions such as duration (t_T or t_S) and frequency ($f_{v,\ total}$ or $f_{v,\ strong}$)
2. *Peak* amplitudes of ground motion records (e.g, *PGA, PGV*, and *PGD*) or spectral parameters (e.g., *Sa, Sv*, and *Sd*)
3. Cumulative parameters considering the *total behavior* of the ground motion record (e.g., a_{sq}, which takes the integral of square of total ground motion acceleration)
4. Cumulative measures considering the *strong behavior* observed in the ground motion record (e.g., Arias Intensity (AI) is similar to a_{sq} but takes the integral based on strong duration t_S)
5. *Mixed* indices that include more than one property, for example, parameters I_a, I_v, and I_d from Riddell and Garcia (2001) that integrate both strong duration and peak amplitudes

Although various intensity measures have been reported in the literature, most recent research on structural collapse assessment uses elastic spectral acceleration *Sa* at the first dominant structural period or peak ground acceleration *PGA* to represent the potential seismic hazard at a site of interest. One reason is that peak ground motion parameters such as *PGA* are simple and easy-to-compute. Likewise, elastic spectral parameters such as *Sa* are the most practical measures providing information about structural response during earthquake. Moreover, most of the

attenuation relationships developed in earthquake engineering use these intensity quantities to predict the seismicity of the regions.

IM_{col}			Unit	Description
PGA	PGV	PGD	in/s^2, in/s, in	Peak ground motion parameters
Sa	Sv	Sd	in/s^2, in/s, in	Elastic spectral properties at T_1 =0.44s and ξ=2% and 5%
Sa_{ave}	Sv_{ave}	Sd_{ave}	in/s^2, in/s, in	Average spectrum intensities which are the geometric mean of elastic spectral properties from T_1 =0.1 to T_1 =2.5s and ξ=5% (Bianchini et al., 2009)
a_{rms}	v_{rms}	d_{rms}	in/s^2, in/s, in	Root mean square of ground motion time histories (Housner and Jennings, 1964)
a_{sq}	v_{sq}	d_{sq}	in^2/s^4, in^2/s^2, in^2	Square of ground motion time histories (Housner, 1970)
a_{rs}	v_{rs}	d_{rs}	in/s^2, in/s, in	Root square of ground motion time histories (Housner, 1970)
Pa	Pv	Pd	in^2/s^4, in^2/s^2, in^2	Earthquake power indices (Housner, 1975)
Ia	Iv	Id	$in/s^{5/3}$, $(in^2/s)^{1/3}$, in $s^{1/3}$	Riddell and Garcia (2001) parameters
AI			in/s	Arias Intensity for an undamped system (Arias, 1970)
Ic			$in^{1.5}/s^{2.5}$	Characteristic Intensity (Park et al., 1985)
P_D			in/s	Potential Destructiveness (Araya and Saragoni, 1980)
max A_v			in^2/s^3	Maximum incremental velocity which is the maximum area between two zero-crossings in square of ground acceleration history (Kurama and Farrow, 2003)
I_F			$in/s^{3/4}$	Fajfar's index (Fajfar et al., 1990)
I_M			-	Maniatakis index (Maniatakis et al., 2008)
PGV/PGA			-	Ratio of peak ground velocity to acceleration
t_T			s	Total duration of ground motion time history
t_S	t_{45}		s	The instants $\mathbf{t}_5$, $\mathbf{t}_{45}$, and $\mathbf{t}_{95}$ are at which 5%, 45%, and 95% of the total integral of square of ground acceleration time history is obtained. Strong duration $\mathbf{t}_S$ is then the interval between $\mathbf{t}_5$ and $\mathbf{t}_{95}$ (Trifunac and Brady, 1975)
ν_S	ν_T		-	Number of zero crossings of ground acceleration history in t_S and t_T
ν_S^2	ν_T^2		-	Square of number of zero-crossings of ground acceleration history in t_S and t_T
$T_{v,\,strong}$	$T_{v,\,total}$		s	Average period of a zero-crossing in t_S and t_T
$f_{v,\,strong}$	$f_{v,\,total}$		Hz	Average frequency of a zero-crossing in t_S and t_T
CAA	CAV	CAD	in/s, in/s^2, in/s^3	Cumulative absolute parameters
SI			in	Housner's spectral intensity at ξ=2% (Housner, 1952)

Table 5.5 The intensity measures considered in statistical analysis for collapse prediction (**Note:** in: inches, s: second, T_1: first period in seconds, ξ: damping amount in percent).

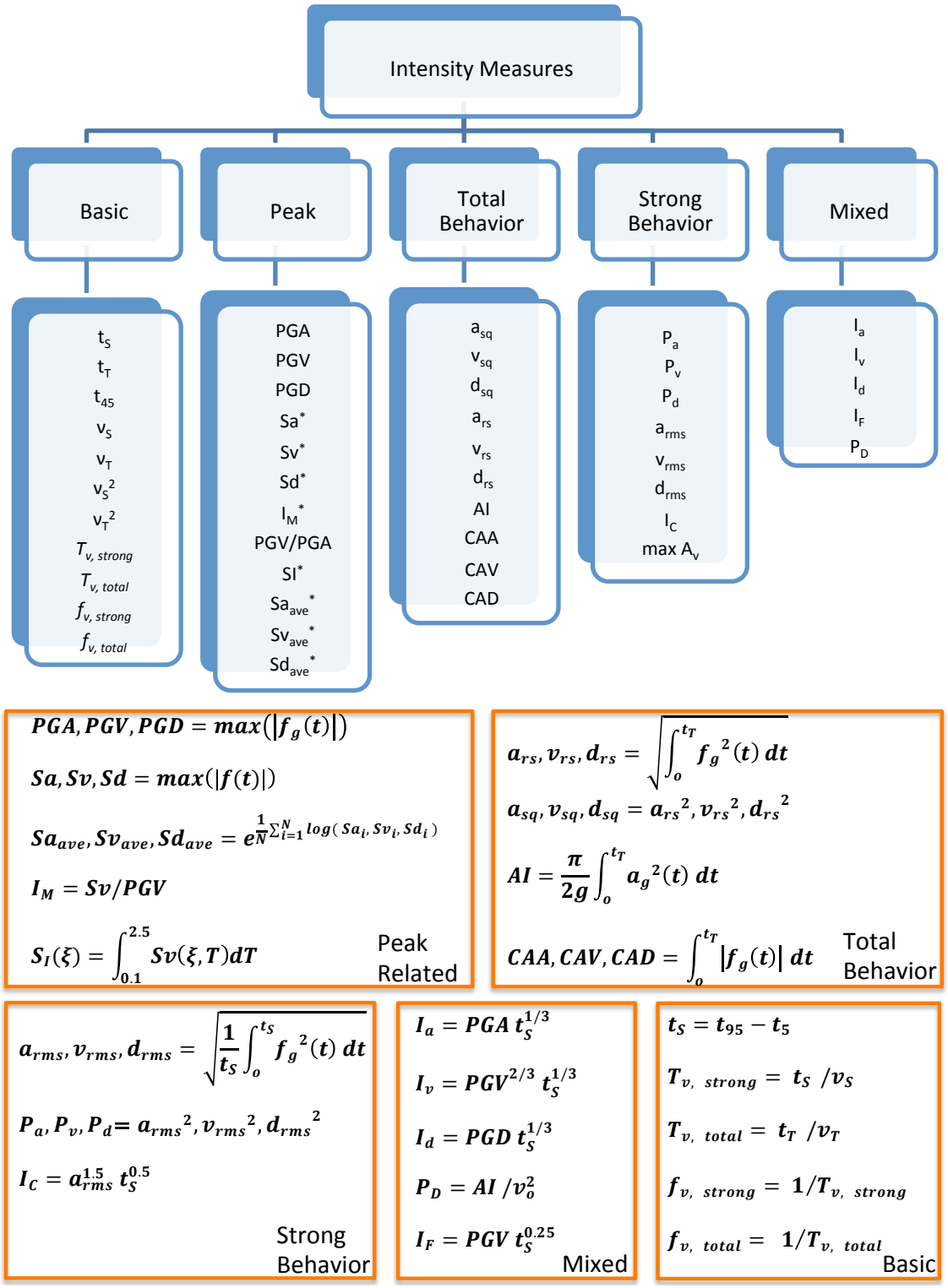

Figure 5.9 Assessment of the intensity measures considered in statistical analysis based on five ground motion properties (**Note:** *: structural response related; g: gravity acceleration; f: acceleration a, velocity v, and displacement d time histories for structure respectively; and f_g: acceleration a_g, velocity v_g, and displacement d_g time histories for ground motion respectively).

While *Sa* and *PGA* are most often used intensity measures in collapse assessment of structural systems, they may not accurately represent severe damage potential of ground motions near structural collapse. In particular, conditioning elastic spectral responses to the first dominant structural period ignore the change in period due to highly inelastic structural response and higher-mode effects that may take place just before collapse. Some recent studies in seismic performance evaluation of structures have proposed to employ combinations of inelastic spectral parameters at the first three dominant periods to take account of such nonlinear structural behaviors (Tothong and Cornell, 2007, 2008). There are much more practical indices in the literature that do not employ inelastic spectrum intensities. These indices are sensitive to both inelastic response and higher-mode effects. For example, Sa_{ave}, which takes the geometric mean of elastic spectral accelerations in a selected range of period, was found to be a more effective predictor than *Sa* and *PGA* especially for degrading MDOF systems (Bianchini et al. 2009).

Damage potential of the structures is also related to input seismic energy that is absorbed during an earthquake-shaking event. Among the indices listed in Table 5.10, cumulative indices may be then considered as better indicators of the released seismic energy than peak parameters. While ground motion parameters like *PGA* provide only the peak amplitudes at a time instant, cumulative indices such as a_{rs} quantify the earthquake behavior during a time interval, thereby give more information about the overall energy of the ground motion, not just the peak amplitudes.

To investigate variability in IM-based collapse capacities, statistical analyses are performed on a total of 50 intensity measures described in Table 5.5 at the collapse state according to the energy-based collapse criterion. Using the findings of these analyses, a more detailed comparison of these measures is provided in the following sections.

5.3.2. Statistics of Seismic Intensity Level at Collapse

Using the collapse data points from 78 ground motions in Figure 5.1 (red points), statistics of totally 50 intensity measures are obtained as shown in Table 5.6 to evaluate variability in IM-based collapse capacity (IM_{col}). Among various IM_{col}'s considered in this comparative study, the Housner's spectral intensity (SI) and the geometric mean of spectral properties (Sa_{ave}, Sv_{ave}, and

Sd_{ave}) were found to give the smallest cov. These measures encompass a period range from 0.1 to 2.5 seconds; therefore can indicate the overall capability of an earthquake that may excite a building structure with a variety of fundamental periods of vibrations. This is why these measures give a small cov (less then 0.3), much smaller than covs found for *Sa* and *PGA* (larger than 0.5). Elastic spectral properties at different damping amounts were also compared in Table 5.6. However, it is found that an increase in damping from 2% to 5% provides a little smaller cov, but does not improve the results much.

IM_{col}	Median	Mean	Cov	IM_{col}	Median	Mean	Cov
SI(2%)	115.665	121.880	0.271	$Sd(T_1,2\%)$	2.826	3.560	0.603
$Sa_{ave}(5\%)$	0.533	0.547	0.283	$Sa(T_1,2\%)$	1.494	1.882	0.604
$Sd_{ave}(5\%)$	5.702	5.839	0.284	t_S	11.458	14.898	0.608
$Sv_{ave}(5\%)$	35.841	38.001	0.296	$Sv(T_1,5\%)$	31.123	37.143	0.622
Iv	21.540	21.495	0.302	$Sv(T_1,2\%)$	40.331	49.525	0.630
CAA	742.576	788.094	0.365	Ic	1398.299	1729.657	0.644
a_{rs}	198.030	223.014	0.366	v_S	90.000	100.436	0.729
PGV	24.813	27.773	0.390	PGD	8.826	12.938	0.800
$f_{v,\ strong}$	6.609	6.963	0.398	a_{sq}	39215.714	56304.313	0.814
I_F	50.978	53.059	0.404	AI	61599.899	88442.609	0.814
$T_{v,\ strong}$	0.151	0.168	0.406	t_{45}	9.995	14.247	0.819
$f_{v,\ total}$	7.870	8.871	0.417	Id	22.761	31.846	0.824
$T_{v,\ total}$	0.127	0.133	0.418	CAD	72.139	107.785	0.893
v_{rms}	8.093	8.589	0.436	d_{rs}	16.905	23.992	0.898
v_{rs}	32.275	34.658	0.450	v_T	295.500	457.372	0.917
PGV/PGA	0.108	0.123	0.463	max A_v	4975.178	7295.489	0.946
Ia	508.350	589.810	0.466	d_{rms}	3.780	5.516	0.987
a_{rms}	53.192	61.295	0.499	v_{sq}	1041.714	1441.033	0.998
$I_M(5\%)$	1.404	1.423	0.499	Pa	2829.765	4680.075	1.167
$I_M(2\%)$	1.898	1.907	0.528	Pv	65.490	87.580	1.188
PGA	218.771	256.734	0.537	P_D	0.781	1.296	1.289
t_T	40.000	47.776	0.553	v_T^2	87326.500	382787.090	1.907
CAV	119.361	143.357	0.562	v_S^2	8104.000	15384.385	2.006
$Sd(T_1,5\%)$	2.197	2.709	0.582	d_{sq}	285.789	1033.337	2.037
$Sa(T_1,5\%)$	1.166	1.438	0.582	Pd	14.293	59.698	2.699

Table 5.6 Statistics of intensity measures at "near-collapse" level for the case study of Lignos et al. (2008) using far-field ground motion set by Haselton and Deierlein (2007).

The Iv index shows the second smallest cov among the indices in the table above. Iv was obtained based on a correlation study carried out by Riddell and Garcia (2001) to identify the ground motion indices that correlate well with energy dissipation of several inelastic SDOF

models during earthquakes. This index includes the effects of duration of ground motion t_S and the peak amplitude *PGV* on the structural response especially for medium-period buildings. Next IMs with the smallest cov are found to be a_{rs} and *CAA*, which can also be good candidates for collapse prediction in addition to others. Since these measures are cumulative quantities, they may better represent the input energy released by earthquakes into the structures.

The dispersion statistics in Table 5.6 also reveal that *PGV* shows a better performance with a cov value of 0.39 comparing to *Sa* and *PGA*. This finding indicates that *PGV* can be also one of the candidates that could give more reliable collapse prediction for this specific type of structure.

Energy dissipation can be recognized as a global representative of structural damage, and thereby plays an important role in the assessment of seismic performance (Riddell and Garcia, 2001; Riddell, 2007; Ye, 2013). In addition to small dispersion, critical intensity measure requires strong correlation with the damage potential of the structure. Therefore, a correlation study between system-energy components and ground motion indices was performed to identify the best intensity candidates that can predict structural collapse with more confidence. More details about this study will be described in section 5.4.3.

5.3.3. Correlation Analysis on Intensity Level of Collapse

The results of correlation analysis between the 50 intensity measures are provided in Table 5.7 – Table 5.9. The most related parameters among these indices are summarized in Table 5.10. As suggested by Riddell (2007), most of these earthquake indices can be separated into three main groups according to sensitivity of the structural response: acceleration-sensitive group (e.g., a_{rs}, *PGA*, and *Ia*), velocity-sensitive group (e.g., v_{rs}, *PGV*, and *Iv*), and displacement-sensitive group (e.g., d_{rs}, *PGD*, and *Id*). According to correlation analysis results in Table 5.7 – Table 5.9, the indices in each of these main groups present fairly strong correlation to each other and show poor correlation with other groups. Only some of the velocity-sensitive indices show good correlation with the displacement-related indices. These main groups can be associated with collapse capacity for buildings in short, intermediate, and long period range respectively (Riddell, 2007; Ye, 2013).

	PGA	$Sa(T_1, 2\%)$	$Sa(T_1, 5\%)$	a_{rms}	a_{sq}	a_{rs}	Pa	Ia	AI	Ic	P_D	CAA	max A_v	Sa_{ave} (5%)	PGV	PGV/ PGA	$Sv(T_1, 2\%)$	$Sv(T_1, 5\%)$	v_{rms}	v_{sq}	v_{rs}	Pv	Iv	I_F	I_M (2%)
PGA	1.00	0.71	0.75	0.89	0.87	0.86	0.86	0.95	0.87	0.90	0.53	0.46	0.90	0.51	0.52	-0.49	0.72	0.76	0.34	0.06	0.09	0.24	0.18	0.35	0.30
$Sa(T_1,2\%)$		1.00	0.98	0.70	0.68	0.68	0.67	0.67	0.68	0.71	0.47	0.33	0.80	0.32	0.32	-0.43	0.99	0.98	0.12	-0.10	-0.05	0.03	0.05	0.18	0.71
$Sa(T_1,5\%)$			1.00	0.73	0.71	0.70	0.70	0.70	0.71	0.74	0.54	0.33	0.82	0.36	0.34	-0.43	0.97	0.99	0.15	-0.10	-0.05	0.05	0.06	0.19	0.66
a_{rms}				1.00	0.90	0.88	0.97	0.77	0.90	0.96	0.70	0.38	0.78	0.47	0.42	-0.48	0.72	0.75	0.33	-0.04	-0.02	0.22	0.01	0.20	0.37
a_{sq}					1.00	0.98	0.91	0.88	1.00	0.98	0.68	0.70	0.80	0.54	0.49	-0.37	0.69	0.71	0.33	0.12	0.19	0.22	0.27	0.38	0.27
a_{rs}						1.00	0.86	0.88	0.98	0.97	0.64	0.76	0.78	0.57	0.51	-0.36	0.69	0.71	0.34	0.15	0.22	0.22	0.31	0.41	0.27
Pa							1.00	0.75	0.91	0.96	0.72	0.41	0.77	0.44	0.42	-0.41	0.69	0.72	0.31	-0.02	0.01	0.20	0.05	0.22	0.32
Ia								1.00	0.88	0.86	0.45	0.64	0.87	0.55	0.56	-0.42	0.67	0.71	0.32	0.16	0.22	0.23	0.36	0.46	0.23
AI									1.00	0.98	0.68	0.70	0.80	0.54	0.49	-0.37	0.69	0.71	0.33	0.12	0.19	0.22	0.27	0.38	0.27
Ic										1.00	0.70	0.60	0.81	0.53	0.49	-0.41	0.72	0.75	0.34	0.07	0.12	0.23	0.18	0.33	0.32
P_D											1.00	0.26	0.47	0.54	0.29	-0.23	0.47	0.52	0.25	-0.04	0.01	0.14	0.04	0.15	0.19
CAA												1.00	0.43	0.41	0.38	-0.04	0.35	0.34	0.21	0.34	0.46	0.12	0.58	0.49	0.04
max A_v													1.00	0.51	0.57	-0.33	0.80	0.83	0.31	0.07	0.13	0.21	0.27	0.42	0.30
Sa_{ave}(5%)														1.00	0.67	0.07	0.31	0.33	0.52	0.32	0.44	0.33	0.53	0.61	-0.21
PGV															1.00	0.39	0.31	0.32	0.87	0.76	0.78	0.76	0.81	0.95	-0.32
PGV/PGA																1.00	-0.45	-0.46	0.44	0.67	0.67	0.40	0.62	0.54	-0.65
$Sv(T_1,2\%)$																	1.00	0.98	0.11	-0.11	-0.07	0.02	0.04	0.17	0.72
$Sv(T_1,5\%)$																		1.00	0.12	-0.12	-0.07	0.03	0.04	0.17	0.68
v_{rms}																			1.00	0.85	0.82	0.94	0.64	0.79	-0.35
v_{sq}																				1.00	0.97	0.85	0.82	0.84	-0.46
v_{rs}																					1.00	0.75	0.89	0.88	-0.49
Pv																						1.00	0.54	0.69	-0.31
Iv																							1.00	0.96	-0.48
I_F																								1.00	-0.42
I_M(2%)																									1.00

Table 5.7 Correlation of coefficients for several intensity measures at "near-collapse" level for the case study of Lignos et al. (2008) using far-field ground motion set by Haselton and Deierlein (2007) (Note: yellow, green, and blue marks indicate $\rho \geq 0.90$, $\rho \geq 0.80$, and $\rho \geq 0.70$ respectively).

	I_M (5%)	CAV	SI (2%)	Sv_{ave} (5%)	PGD	$Sd(T_1, 2\%)$	$Sd(T_1, 5\%)$	d_{rms}	d_{sq}	d_{rs}	Pd	Id	CAD	Sd_{ave} (5%)	t_T	t_S	t_{45}	v_T^2	v_S^2	v_T	v_S	$T_{v,\,total}$	$T_{v,\,strong}$	$f_{v,\,total}$	$f_{v,\,strong}$
PGA	0.36	-0.09	0.57	0.72	0.08	0.71	0.75	0.11	0.08	0.02	0.13	-0.02	-0.06	0.51	-0.26	-0.35	-0.15	-0.13	-0.06	-0.11	-0.03	-0.27	-0.51	0.19	0.53
$Sa(T_1,2\%)$	0.71	-0.15	0.47	0.61	-0.08	1.00	0.98	-0.06	-0.10	-0.11	-0.06	-0.15	-0.15	0.32	-0.19	-0.30	-0.12	-0.08	-0.12	-0.09	-0.11	-0.18	-0.33	0.09	0.28
$Sa(T_1,5\%)$	0.70	-0.17	0.50	0.64	-0.07	0.98	1.00	-0.04	-0.09	-0.11	-0.05	-0.15	-0.16	0.35	-0.21	-0.33	-0.12	-0.08	-0.12	-0.09	-0.12	-0.18	-0.33	0.11	0.31
a_{rms}	0.41	-0.23	0.55	0.69	-0.05	0.70	0.73	0.01	-0.02	-0.11	0.06	-0.16	-0.20	0.47	-0.44	-0.49	-0.32	-0.26	-0.13	-0.27	-0.16	-0.22	-0.47	0.10	0.50
a_{sq}	0.32	0.06	0.61	0.71	0.08	0.68	0.71	0.09	0.08	0.05	0.09	0.02	0.01	0.53	-0.27	-0.14	-0.17	-0.15	0.14	-0.13	0.18	-0.26	-0.49	0.21	0.59
a_{rs}	0.31	0.10	0.64	0.74	0.10	0.68	0.70	0.10	0.08	0.07	0.09	0.05	0.04	0.57	-0.27	-0.09	-0.17	-0.16	0.19	-0.14	0.24	-0.27	-0.52	0.21	0.61
Pa	0.37	-0.16	0.52	0.65	-0.04	0.67	0.70	0.00	-0.01	-0.09	0.04	-0.13	-0.16	0.44	-0.34	-0.39	-0.26	-0.20	-0.12	-0.21	-0.13	-0.20	-0.40	0.11	0.44
Ia	0.29	0.11	0.59	0.71	0.17	0.67	0.70	0.16	0.13	0.13	0.15	0.10	0.09	0.54	-0.13	-0.10	-0.04	-0.04	0.13	-0.01	0.20	-0.29	-0.51	0.24	0.57
AI	0.32	0.06	0.61	0.71	0.08	0.68	0.71	0.09	0.08	0.05	0.09	0.02	0.01	0.53	-0.27	-0.14	-0.17	-0.15	0.14	-0.13	0.18	-0.26	-0.49	0.21	0.59
Ic	0.36	-0.05	0.61	0.73	0.04	0.71	0.74	0.06	0.04	0.00	0.08	-0.04	-0.07	0.53	-0.34	-0.28	-0.23	-0.19	0.03	-0.19	0.05	-0.25	-0.49	0.17	0.57
P_D	0.25	-0.18	0.58	0.63	-0.13	0.47	0.54	-0.10	-0.13	-0.18	-0.07	-0.19	-0.25	0.54	-0.47	-0.30	-0.39	-0.34	-0.16	-0.41	-0.18	0.17	-0.11	-0.18	0.23
CAA	0.04	0.56	0.46	0.44	0.22	0.33	0.33	0.14	0.15	0.28	0.06	0.29	0.37	0.41	0.16	0.55	0.16	0.10	0.55	0.17	0.67	-0.25	-0.32	0.27	0.43
max A_v	0.34	-0.02	0.61	0.75	0.11	0.80	0.82	0.10	0.07	0.05	0.09	0.03	0.00	0.50	-0.17	-0.27	-0.05	-0.07	-0.07	-0.07	-0.06	-0.15	-0.30	0.11	0.33
Sa_{ave}(5%)	-0.19	0.26	0.97	0.92	0.23	0.32	0.36	0.16	0.09	0.16	0.08	0.19	0.11	1.00	-0.23	-0.09	-0.20	-0.23	-0.04	-0.25	-0.01	0.16	-0.05	-0.17	0.14
PGV	-0.31	0.52	0.64	0.65	0.73	0.32	0.34	0.67	0.64	0.66	0.61	0.67	0.56	0.67	-0.07	-0.06	0.17	0.08	-0.09	0.08	-0.02	-0.15	-0.08	0.22	0.17
PGV/PGA	-0.69	0.65	0.01	-0.15	0.60	-0.43	-0.43	0.49	0.52	0.62	0.37	0.70	0.64	0.07	0.29	0.37	0.44	0.32	-0.05	0.30	-0.01	0.08	0.55	0.10	-0.45
$Sv(T_1,2\%)$	0.73	-0.16	0.46	0.60	-0.09	0.99	0.97	-0.07	-0.12	-0.13	-0.07	-0.17	-0.17	0.30	-0.20	-0.30	-0.12	-0.08	-0.11	-0.09	-0.10	-0.20	-0.36	0.10	0.30
$Sv(T_1,5\%)$	0.72	-0.18	0.47	0.62	-0.09	0.98	0.99	-0.07	-0.12	-0.13	-0.07	-0.17	-0.18	0.33	-0.20	-0.32	-0.12	-0.08	-0.10	-0.09	-0.10	-0.20	-0.37	0.11	0.33
v_{rms}	-0.35	0.51	0.45	0.44	0.84	0.12	0.15	0.86	0.82	0.78	0.82	0.74	0.64	0.52	-0.16	-0.14	0.11	0.01	-0.17	0.00	-0.11	-0.10	-0.04	0.18	0.14
v_{sq}	-0.49	0.82	0.24	0.17	0.90	-0.10	-0.10	0.85	0.89	0.91	0.79	0.91	0.87	0.32	0.14	0.29	0.34	0.21	0.05	0.22	0.17	-0.12	0.09	0.25	0.03
v_{rs}	-0.51	0.89	0.38	0.28	0.89	-0.05	-0.05	0.81	0.80	0.90	0.67	0.92	0.88	0.44	0.19	0.38	0.38	0.23	0.09	0.25	0.22	-0.08	0.11	0.23	0.01
Pv	-0.31	0.46	0.25	0.26	0.80	0.03	0.05	0.87	0.89	0.77	0.94	0.70	0.63	0.33	-0.13	-0.11	0.07	-0.01	-0.09	-0.01	-0.05	-0.11	-0.08	0.18	0.18
Iv	-0.49	0.84	0.48	0.40	0.74	0.05	0.06	0.59	0.58	0.73	0.44	0.81	0.75	0.53	0.28	0.48	0.42	0.30	0.21	0.32	0.34	-0.14	0.08	0.27	0.03
I_F	-0.43	0.72	0.57	0.53	0.78	0.18	0.19	0.67	0.65	0.73	0.56	0.79	0.69	0.61	0.11	0.22	0.32	0.21	0.06	0.22	0.17	-0.16	0.00	0.27	0.10
I_M(2%)	0.97	-0.45	-0.08	0.05	-0.45	0.71	0.66	-0.37	-0.36	-0.44	-0.28	-0.50	-0.45	-0.22	-0.16	-0.27	-0.23	-0.15	-0.07	-0.14	-0.10	-0.14	-0.31	-0.01	0.19

Table 5.8 Correlation of coefficients for several intensity measures at "near-collapse" level for the case study of Lignos et al. (2008) using far-field ground motion set by Haselton and Deierlein (2007)(Cont'd.; note: yellow, green, and blue marks indicate $\rho \geq 0.90$, $\rho \geq 0.80$, and $\rho \geq 0.70$ respectively).

	I_M (5%)	CAV	SI (2%)	Sv_{ave} (5%)	PGD	$Sd(T_1, 2\%)$	$Sd(T_1, 5\%)$	d_{rms}	d_{sq}	d_{rs}	Pd	Id	CAD	Sd_{ave} (5%)	t_T	t_S	t_{45}	v_T^2	v_S^2	v_T	v_S	$T_{v, total}$	$T_{v, strong}$	$f_{v, total}$	$f_{v, strong}$
I_M(5%)	1.00	-0.49	-0.06	0.08	-0.47	0.71	0.70	-0.38	-0.38	-0.46	-0.29	-0.52	-0.48	-0.20	-0.17	-0.30	-0.23	-0.13	-0.06	-0.13	-0.09	-0.15	-0.34	0.02	0.24
CAV		1.00	0.22	0.09	0.72	-0.15	-0.17	0.60	0.61	0.79	0.44	0.83	0.89	0.26	0.49	0.70	0.53	0.39	0.25	0.42	0.40	-0.04	0.22	0.22	-0.12
SI(2%)			1.00	0.96	0.16	0.47	0.50	0.09	0.02	0.10	0.00	0.12	0.06	0.97	-0.23	-0.10	-0.20	-0.23	-0.07	-0.25	-0.05	0.17	-0.03	-0.19	0.11
Sv_{ave}(5%)				1.00	0.12	0.61	0.64	0.08	0.01	0.05	0.03	0.05	-0.01	0.92	-0.29	-0.23	-0.24	-0.25	-0.08	-0.27	-0.06	0.07	-0.20	-0.12	0.25
PGD					1.00	-0.08	-0.07	0.96	0.90	0.97	0.82	0.97	0.90	0.23	0.18	0.17	0.45	0.33	-0.01	0.34	0.11	-0.22	0.01	0.38	0.07
$Sd(T_1,2\%)$						1.00	0.98	-0.06	-0.10	-0.11	-0.06	-0.15	-0.15	0.32	-0.19	-0.30	-0.12	-0.08	-0.12	-0.09	-0.11	-0.18	-0.33	0.09	0.28
$Sd(T_1,5\%)$							1.00	-0.04	-0.09	-0.11	-0.05	-0.15	-0.16	0.35	-0.21	-0.33	-0.12	-0.08	-0.12	-0.09	-0.12	-0.17	-0.33	0.10	0.31
d_{rms}								1.00	0.95	0.95	0.92	0.88	0.85	0.16	0.09	0.04	0.36	0.25	-0.03	0.26	0.06	-0.22	-0.07	0.37	0.16
d_{sq}									1.00	0.92	0.96	0.85	0.84	0.09	0.10	0.11	0.34	0.23	0.01	0.25	0.10	-0.24	-0.05	0.37	0.15
d_{rs}										1.00	0.82	0.96	0.96	0.16	0.25	0.29	0.48	0.35	0.07	0.37	0.20	-0.21	0.03	0.38	0.07
Pd											1.00	0.72	0.70	0.08	-0.01	-0.04	0.19	0.11	-0.02	0.13	0.04	-0.21	-0.14	0.30	0.23
Id												1.00	0.93	0.19	0.29	0.35	0.53	0.40	0.07	0.42	0.20	-0.22	0.09	0.40	0.00
CAD													1.00	0.11	0.43	0.47	0.59	0.46	0.16	0.49	0.29	-0.19	0.12	0.39	-0.01
Sd_{ave}(5%)														1.00	-0.23	-0.09	-0.20	-0.23	-0.04	-0.25	-0.01	0.16	-0.05	-0.17	0.14
t_T															1.00	0.60	0.79	0.83	0.18	0.85	0.26	-0.22	0.26	0.35	-0.28
t_S																1.00	0.41	0.32	0.61	0.38	0.71	0.02	0.19	0.09	-0.13
t_{45}																	1.00	0.91	0.06	0.92	0.17	-0.44	0.15	0.65	-0.12
v_T^2																		1.00	0.07	0.98	0.15	-0.49	0.10	0.70	-0.07
v_S^2																			1.00	0.17	0.94	-0.21	-0.30	0.25	0.45
v_T																				1.00	0.25	-0.57	0.03	0.75	-0.01
v_S																					1.00	-0.31	-0.40	0.33	0.52
$T_{v, total}$																						1.00	0.63	-0.89	-0.59
$T_{v, strong}$																							1.00	-0.42	-0.91
$f_{v, total}$																								1.00	0.50
$f_{v, strong}$																									1.00

Table 5.9 Correlation of coefficients for several intensity measures at "near-collapse" level for the case study of Lignos et al. (2008) using far-field ground motion set by Haselton and Deierlein (2007)(Cont'd.; note: yellow, green, and blue marks indicate $\rho \geq 0.90$, $\rho \geq 0.80$, and $\rho \geq 0.70$ respectively).

Group #	IM_{col}
1. Acceleration Sensitive	PGA , Sa , a_{rms} , a_{sq} , a_{rs} , Pa , Ia , AI , Ic, P_D, maxAv
2. Velocity Sensitive	PGV , v_{rms} , v_{sq} , v_{rs} , Pv , Iv , I_F, CAV
3. Displacement Sensitive	PGD, d_{rms} , d_{sq} , d_{rs} , Pd , Id , CAD
4. Acceleration and Spectral Velocity Sensitive	PGA , Sa , a_{rms} , a_{sq} , a_{rs} , Pa , Ia , AI , Ic, P_D, maxAv, Sv, SI, Sv_{ave}
5. Velocity and Displacement Sensitive	PGV, v_{rms} , v_{sq} , v_{rs} , Pv , Iv , I_F , CAV, PGD , d_{rms} , d_{sq}, d_{rs}, Id , Pd, CAD
6. Elastic Spectral Parameters	Sa, Sv, Sd, I_M
7. Average Spectral Parameters	SI, Sa_{ave}, Sv_{ave} , Sd_{ave}
8. Strong Behavior	v_S^2 , v_S , $T_{v, strong}$, $f_{v, strong}$, t_S
9. Total Behavior	v_T^2 , v_T , $T_{v, total}$, $f_{v, total}$, t_{45}
10. Other	PGV/PGA, Iv, Id

Table 5.10 Several intensity measures at "near-collapse" level showing high or almost fairly strong correlation within each group ($\rho \geq 0.50$).

5.4. Critical Performance Measures for Collapse Prediction

Large dispersion observed in collapse-causing intensities of ground motions and damage thresholds has initiated search for alternative performance measures to assess collapse capacity of structures. However, most of recent research on the IDA-based approach still uses only one DM and one IM (mostly maximum story drift ratio and elastic spectral acceleration). This section investigates the benefit of having more than one DM or IM for collapse capacity prediction. As a result, new damage measures are introduced by combining critical performance measures, and then the intensity measure that best describes the collapse capacity is identified along with the new damage measure.

5.4.1. Desirable Performance Measures

Findings of the statistical evaluations described in previous sections show that reliable and accurate collapse assessment requires the following desirable properties for performance measures:

- Global cumulative measures: Global cumulative DMs such as structural energy components at system level consider time history responses at each degree-of-freedom of the structure, thereby, can be the best indicators to describe overall collapse behavior of the structures. Likewise, IMs that correlate well with global cumulative damage measures can be good candidates to present damage potential of structures.
- Small variability: The choice of optimal IM or DM given IM decreases the dispersion due to record-to-record variability, which in turn corresponds to a reduction in uncertainty level associated to collapse probability computation. Therefore, smaller dispersion of IM and DM requires fewer non-linear analysis and less ground motions to estimate collapse probability.
- Scaling robustness near collapse: Structural responses tend to show a large increase correpsonding to any small increment in intensity as the structure gets closer to collapse. This may result in a large difference between the last no-collapse and collapse cases due to scaling sensitivity. Response quantities that are robust to scaling of intensity near collapse as well as sufficient in classifying collapse and no-collapse points are required for more reliable collapse capacity prediction.

- Practical applicability: Dynamic instability is a complex and highly nonlinear phenomenon that may not be exactly described with a single DM. Similarly, a single IM may not be enough to describe the severity of the earthquake shaking. However, single parameter or combined expressions are mostly preferred for performance measures because of its simplicity. Moreover, practical IMs are needed so that they can be easily computed using available attenuation models to assess seismic hazard for a site.

5.4.2. New Damage Measures based on System-Energy Balance

Estimation of seismic performance under earthquake actions may also be derived from the energy balance that takes place between total seismic energy absorbed and retained within structure. This approach is particularly appropriate for collapse assessment because high levels of damage just before collapse are usually associated with high-energy absorption of the structural system, since energy can only be absorbed and dissipated by irreversible deformations.

Earthquake loads applied on the structural system introduces seismic energy into the system. Some part of this input seismic energy (E_{EQ}) is absorbed as kinetic energy (E_K) and strain energy (E_S; i.e., the combined quantity of elastic energy (E_E) and hysteretic energy (E_H)), and the rest is dissipated as damping energy (E_D). As the system experiences loading and unloading during an earthquake, it starts to show highly nonlinear cyclic inelastic behavior and excessive deformations that initiate gravity forces applied on the structure to release gravity energy (E_G). The components of the energy balance can be then described as:

$$E_K + E_D + E_S = E_{EQ} + E_G \qquad OR \quad E_K + E_D + E_E + E_H = E_{EQ} + E_G \tag{5.3}$$

While energy absorption through damping tries to *stabilize* the structural system, energy absorption through stiffness and strength degradation at the structural components contributes to excessive irreversible deformations that try to *destabilize* the system. If the damping forces overcomes and stabilizes the system, the system comes to rest gradually after the earthquake excitation, thus, both kinetic energy (E_K) and elastic strain energy (E_E) become zero. The energy equilibrium then transforms to:

$$E_K = 0,\ E_E = 0, \quad E_S = E_E + E_H = E_H \ \rightarrow \quad E_D + E_H = E_{EQ} + E_G \tag{5.4}$$

However, as the gravity energy keeps increasing as result of progressive accumulation of deformations, the system tries to dissipate this released gravity energy mainly through excessive hysteretic behavior (E_H) at the structural components. Once the gravity forces applied on the structure become dominant, the gravity energy then starts to enormously increase, even exceeds the earthquake energy experienced and eventually causes the structure to collapse.

Considering this energy balance between input energy and absorbed energy shown in (5.3) and (5.4), two new performance measures called "energy ratio (E_R)" and "alternative energy ratio ($E_R{}^a$)" have been proposed in this study for more effective risk assessment of structural collapse.

$$E_R = \frac{E_{Degrading}}{2E_{EQ}}\Big|_{time=at\ the\ end} = \frac{\max\left(E_{Degrading}\right)}{2\ \max\left(E_{EQ}\right)} \tag{5.5}$$

$$E_R{}^a = max\left(\frac{E_{Degrading}}{E_{EQ}+E_G}\right) \tag{5.6}$$

The energy component $E_{Degrading}$ of the system is the total strain energy dissipated from degrading elements in the frame. Since energy components $E_{Degrading}$ and E_{EQ} are cumulative measures, they reach the maximum value at the end of the energy time histories as shown in (5.5).

In the OpenSees model of the test case study by Lignos et al. (2008), since inelasticity is concentrated in flexural plastic hinges at the ends of beams and columns, rotational springs are the only degrading elements. If the strain energy dissipated from inelastic rotational springs is termed as E_{SPR}, then the energy ratios for this test case study become:

$$E_R = \frac{\max\left(E_{SPR}\right)}{2\ \max\left(E_{EQ}\right)} \tag{5.7}$$

$$E_R{}^a = max\left(\frac{E_{SPR}}{E_{EQ}+E_G}\right) \tag{5.8}$$

Energy absorption of a plastic hinge is expressed in terms of the total area enclosed by bending moment versus rotations under load reversals. The total areas for all plastic hinges are then combined to form the global indicator E_{SPR}. Therefore, large inelastic (irreversible) deformations

near collapse require large amounts of input energy dissipation, which significantly depends on available local rotational ductility.

Figure 5.10 shows structural response time histories at the system level for gravity energy (E_G), seismic input energy (E_{EQ}), total input energy (i.e., $E_I = E_{EQ}+E_G$), and strain energy absorbed in springs (E_{SPR}) for the case study by Lignos et al. (2008). The energy analyses were performed for the test ground motion Canoga record at the intensity scale factors of 0.4, 1.0, 1.5, 1.9 (i.e., non-collapse cases), and 2.2 (i.e., collapse case) that were continuously applied on the frame during the experiment. At the scale factor of 0.4, the total input energy, which almost comes from only seismic input energy (i.e., $E_I \approx E_{EQ}$), is dissipated mostly through damping energy ($E_D = E_I - E_{SPR}$). Spring energy then kicks in at the next scale factor of 1.0 and increases its contribution in dissipating seismic energy for the following non-collapse scale factors while gravity energy keeps steady. This is the reason why strain energy time history follows the earthquake energy time history in non-collapse cases (at the scale factors of 1.0, 1.5, and 1.9) with an almost perfect correlation (1.0). At the scale factor of 2.2, gravity energy then starts to enormously increase, even far exceeds seismic input energy stored in the structure in the collapse case. At the same time, strain energy shows a rapid increase following the huge release of gravity energy (i.e., $E_I \approx E_G$ near collapse), therefore provides a decrease in correlation (0.74) with earthquake energy indicating collapse.

Figure 5.11 provides the energy-ratio histories for the ground motion Canoga record that was applied on the case study by Lignos et al. (2008) during the experiment. The pink and green circles indicate the collapse capacities based on E_R defined in (5.7) and E_R^a defined in (5.8) respectively. Although both energy-ratios E_R and E_R^a (red and blue lines respectively) are not significant at the beginning, they increase as the input seismic energy dissipated through hysteretic behavior at the springs gets enormous at the following scale factors. However, the structure does not show any sign of collapse yet due to stabilizing effects of damping forces. At the scale factor of 2.2, E_R shows a significant increase as spring energy far exceeds seismic energy. At the same time, E_R^a shows a remarkable decrease, since excessive release of gravity energy makes the ratio tend to zero once the collapse initiates.

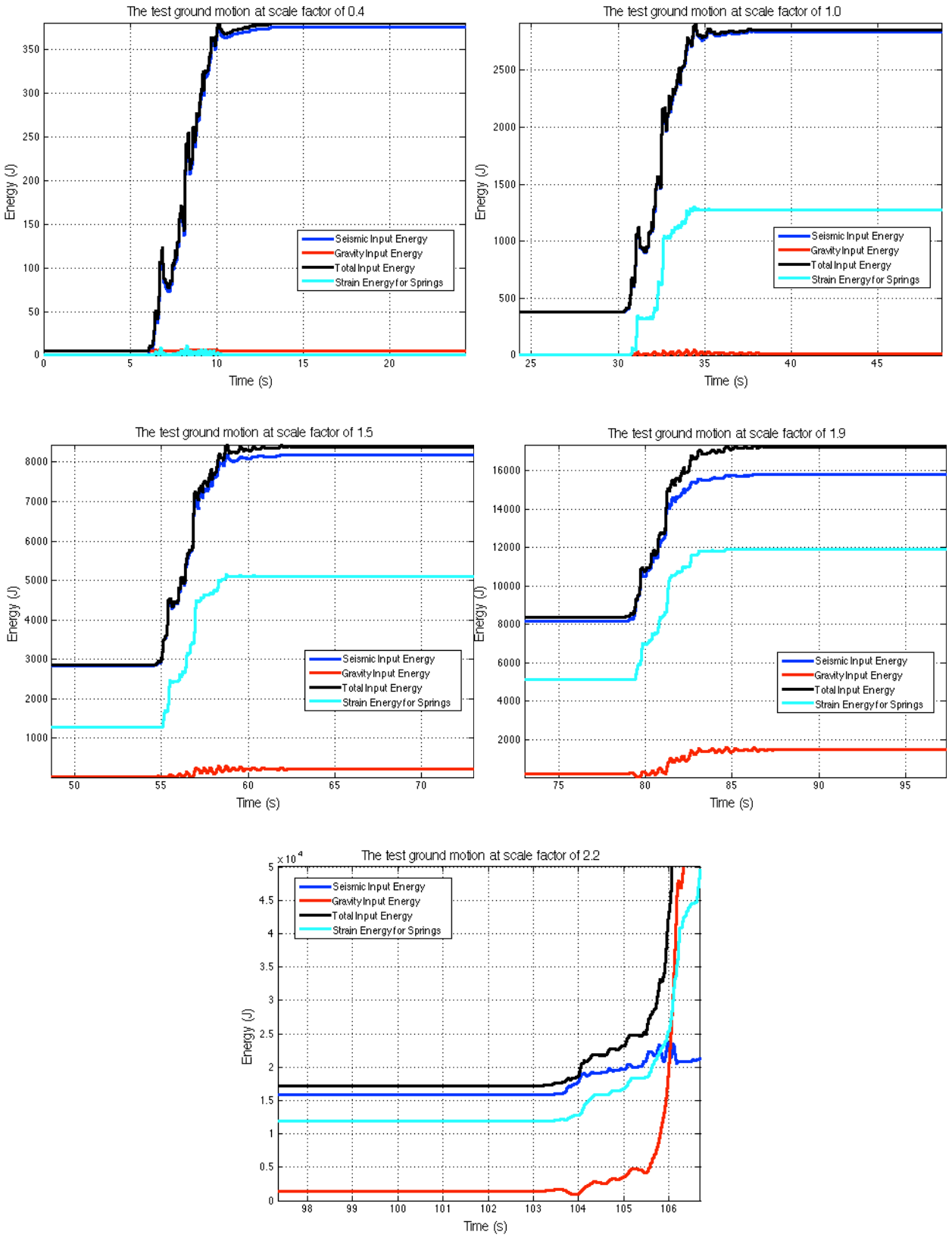

Figure 5.10 Energy histories at the system level for the case study of Lignos et al. (2008) subjected to the test ground motion at scale factors (SF) of 0.4, 1.0, 1.5, 1.9 and 2.2.

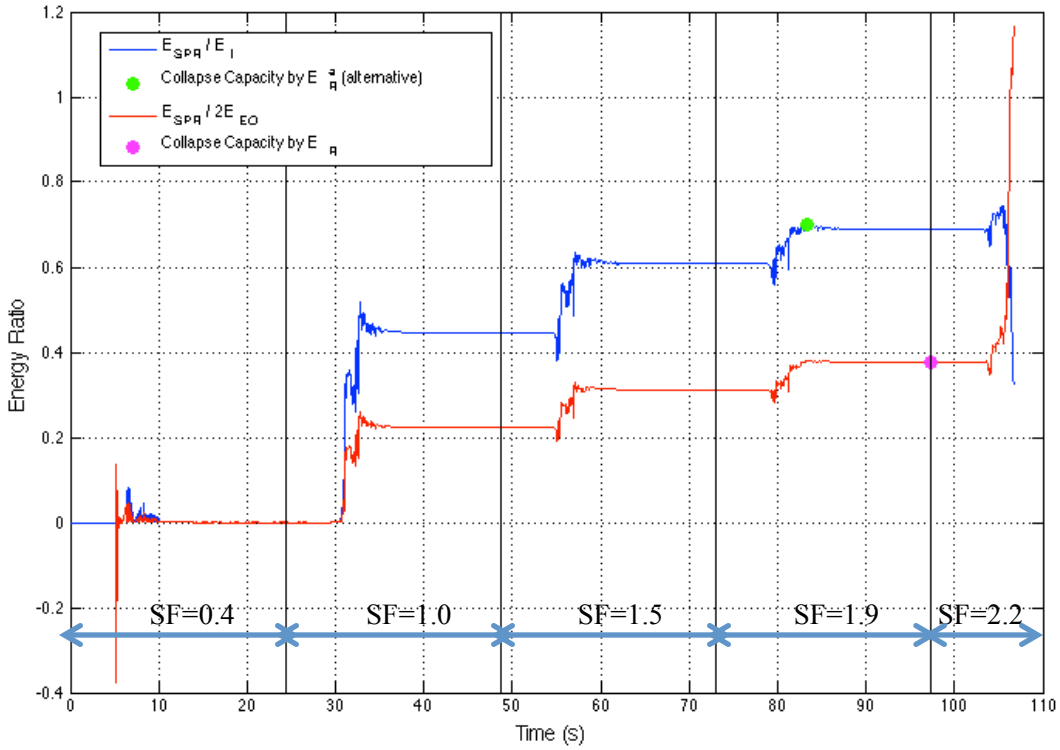

Figure 5.11 Energy-ratio histories for the case study of Lignos et al. (2008) subjected to the test ground motion at scale factors (SF) of 0.4, 1.0, 1.5, 1.9 and 2.2 (Note that circles indicate collapse capacity).

Considering the energy balance in (5.3), it can be proved that "collapse capacity" based on E_R or E_R^a should be less than 1.0. First, the expression in (5.3) can be rearranged as:

$$E_K + E_D + E_S = E_{EQ} + E_G \rightarrow E_S \leq E_{EQ} + E_G \rightarrow \frac{E_S}{E_{EQ}+E_G} \leq 1.0 \qquad (5.9)$$

Remember that E_{SPR}, which is the strain energy absorbed through degrading rotational springs, is only a part of the total strain energy of the structural system (E_S). The ratio in (5.9) then becomes:

$$E_{SPR} \leq E_S \rightarrow \frac{E_{SPR}}{E_{EQ}+E_G} \leq 1.0 \rightarrow {E_R}^a = max\left(\frac{E_{SPR}}{E_{EQ}+E_G}\right) \leq 1.0 \qquad (5.10)$$

which proves that all IDA points for E_R^a should be less than 1.0. If energy-based criterion developed in previous chapter is applied on (5.10) near collapse, the ratio then becomes the "collapse capacity" based on E_R:

$$E_{R_{near\ collapse}} = \frac{E_{SPR}}{E_{EQ}+E_G}\Big|_{E_{EQ}=E_G} = \frac{E_{SPR}}{2E_{EQ}} \leq 1.0 \rightarrow E_{R_{near\ collapse}} = \frac{\max(E_{SPR})}{2\ \max(E_{EQ})} \leq 1.0 \qquad (5.11)$$

Expression in (5.11) clearly shows that energy-ratio E_R exceeding 1.0 indicates collapse according to energy-based collapse criterion.

Figure 5.12 illustrates the IDA curves based on E_R (on the left) and E_R^a (on the right) measures for the 78 far-field ground motion records by Haselton and Deierlein (2007). The IDA points based on E_R in Figure 5.12a can be divided into two main regions: before-collapse region, where the IDA curves show at first a linearly increasing trend until energy-ratio starts to change gradually around a mean of 0.45 for each increment in intensity; and then collapse region, where energy-ratio rapidly diverges for a small increment in intensity leading the structure to collapse. Thereby, this energy-ratio E_R accounts for the sensitivity of the response near collapse with a gradual change in demand before collapse unlike most of the other structural responses. For example, inter-story drift ratio (Figure 5.6b) tends to show a large increase correpsonding to any small increment in intensity as the structure gets closer to collapse. On the other hand, the IDA curves based on E_R show similarity with the curves based on force quantities such as the IDA curves using base shear in Figure 5.5a. However, this energy-ratio E_R integrates both force and deformation demands at each structural component, therefore, it is more representative of severe structural damage observed just before collapse.

In Figure 5.12b, the collapse points indicated by E_R^a (red circles) seem to concentrate around a mean of 0.8, which means that most of the 78 ground motions cause the system to dissipate around 80% of the total input energy through degrading springs, when the structure is near collapse. As clearly seen in Figure 5.12b, unlike the existing response measures studied previously, the collapse capacity points based on E_R^a (red circles) are robust (i.e., not sensitive) to any intensity increment near collapse, even more robust comparing to E_R. However, some blue circles around the mean indicate that there are still no-collapse cases close to collapse cases for some of the ground motions. Therefore, the IDA curves based on E_R^a may not be well enough to show clear collapse boundary, which may cause difficulty later in developing collapse fragility relations. Although this measure is not sufficient alone in classifying collapse and no-collapse points, this mean of E_R^a at least can provide the likelihood about how close the structure can get to collapse.

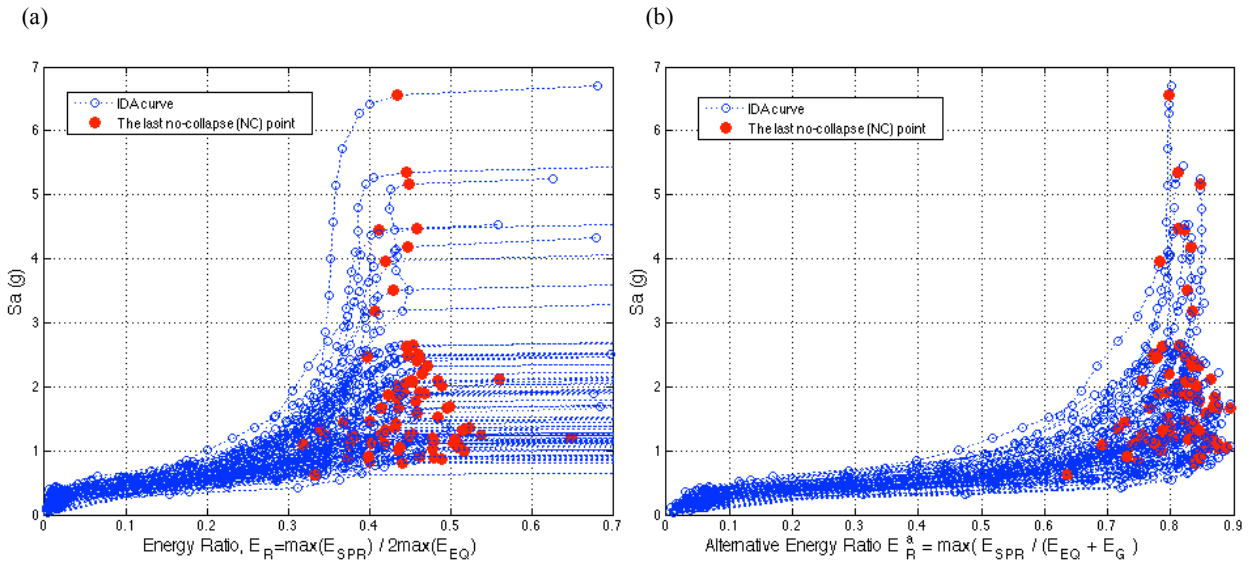

Figure 5.12 IDA curves of energy-ratio E_R (left) and E_R^a (right) for the case study of Lignos et al. (2008) subjected to far-field ground motion set by Haselton and Deierlien (2007).

The variability observed in energy-ratio E_R-based collapse points (red points in Figure 5.12a) can be reduced more using the equivalent-velocity form in IDA curves. Considering the kinetic energy formulation, spring energy and seismic energy in the energy-ratio can be replaced by corresponding equivalent velocities V_{SPR} and V_{EQ} respectively. If m is the mass of the structural system, then the energy-ratio E_R becomes:

$$E_{SPR} = \frac{1}{2} m {V_{SPR}}^2 \quad and \quad E_{EQ} = \frac{1}{2} m {V_{EQ}}^2 \tag{5.12}$$

$$E_R = \frac{\max(E_{SPR})}{2 \max(E_{EQ})} = \frac{\max(\frac{1}{2} m {V_{SPR}}^2)}{2 \max(\frac{1}{2} m {V_{EQ}}^2)} = \frac{\max({V_{SPR}}^2)}{2 \max({V_{EQ}}^2)} \leq 1.0 \tag{5.13}$$

An equivalent velocity-ratio V_R of spring energy to seismic energy can be then introduced by simply taking the square root of energy-ratio E_R in (5.13):

$$V_R = \sqrt{E_R} = \sqrt{\frac{\max(E_{SPR})}{2 \max(E_{EQ})}} = \frac{\max(|V_{SPR}|)}{\sqrt{2} \max(|V_{EQ}|)} \leq 1.0 \tag{5.14}$$

The IDA curves using V_R measure in Figure 5.13 follow a similar trend to E_R-based IDA curves in Figure 5.12a. They first linearly increase until around a mean of 0.65, where it then starts to

shows a gradual increase in ratio followed by enormous rise indicating collapse. Since it is the square root of the energy-ratio, collapse capacity points for V_R measure (red circles in Figure 5.13) are expected to give much smaller variability.

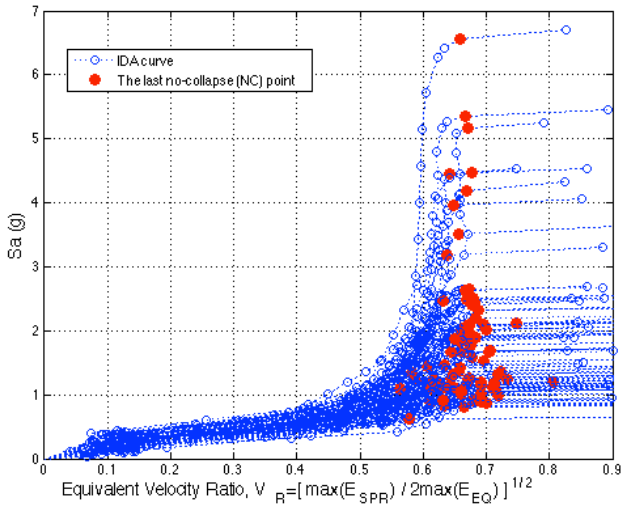

Figure 5.13 IDA curves of equivalent velocity-ratio V_R for the case study of Lignos et al. (2008) subjected to far-field ground motion set by Haselton and Deierlien (2007).

Table 5.11 provides the findings of statistical analyses performed on E_R, $E_R{}^a$, and V_R based collapse capacity using the collapse data in Figure 5.12 and Figure 5.13. According to results, the collapse capacity defined by V_R provides more reliable collapse predictions with a smaller cov of 0.058 comparing to E_R (cov = 0.116) and other existing measures in Table 5.2. For example, cov for lateral IDR is found to be 0.226 in Table 5.2. $E_R{}^a$ also provides almost the same cov (0.059), however, this measure is not sufficient to separate collapse cases (the last blue points on IDA curves) from non-collapse cases. Other energy ratios such as E_{SPR}/E_G, E_G/E_{EQ}, and E_G/E_I were studied as well but they are found to give larger cov's (0.915, 0.609, and 0.506 respectively). Also, the correlation analysis between V_R and existing damage measures show that V_R does not show any high correlation to existing indices reported in Table 5.1 indicating that E_R is a different collapse-related property of structure. It only shows a fairly strong correlation ($0.60 \leq \rho \leq 0.70$) to drift quantities, base shear and gravity energy demonstrating that it has the potential to capture highly nonlinear geometric effects due to gravity forces applied on the structure which eventually causes the structure to collapse.

Moreover, the correlation analysis in Table 5.11 proves that E_R^a measure does not show any strong correlation to existing measures; therefore it indicates that E_R^a represents a unique description of structural collapse that other measures cannot describe. Although it may seem a better measure with a smaller value of dispersion, it is not sufficient alone to separate clearly collapse and no-collapse IDA points. However, the mean of E_R^a at least can help give estimate how close the structure can get to collapse.

DM_{col}	E_R	E_R^a	V_R
Median	0.448	0.822	0.669
Mean	0.448	0.810	0.668
Cov	0.116	0.059	0.058

DM_{col}	Correlation of Coefficient with E_R^a	Correlation of Coefficient with V_R	DM_{col}	Correlation of Coefficient with E_R^a	Correlation of Coefficient with V_R
$D_{R, X}$	0.12	0.66	$F_{B, Y}$	-0.02	0.09
$D_{R, Y}$	0.15	0.68	E_{EQ}	0.14	-0.26
$D_{S, X}$	0.12	0.66	$E_{EQ\text{-}rate}$	0.11	0.00
$IDR_{S, X}$	0.15	0.65	E_G	0.16	0.68
$IDR_{S, Y}$	0.15	0.65	$E_{G\text{-}rate}$	0.23	0.32
$V_{S, X}$	0.14	0.01	$E_{K, X}$	0.14	0.03
$V_{S, Y}$	0.21	0.31	$E_{K, Y}$	0.12	0.17
$A_{S, X}$	0.03	0.00	E_K	0.14	0.03
$A_{S, Y}$	0.12	0.15	$E_{SPR, B}$	0.25	-0.07
$F_{S, X}$	-0.02	-0.08	$E_{SPR, C}$	0.25	-0.09
$F_{BC, X}$	0.17	0.66	E_{SPR}	0.25	-0.08
$F_{B, X}$	0.30	0.05	$PA_{BC, R}$	0.21	0.51

Table 5.11 Statistics for new damage measures for the case study of Lignos et al. (2008) subjected to far-field ground motion set by Haselton and Deierlien (2007).

Response quantities that can describe overall collapse behavior with a smaller value of dispersion are required for more reliable collapse capacity prediction. In addition, they need to be robust to scaling of intensity near collapse as well as still need to show adequacy in classifying collapse and no-collapse cases. Therefore, the new damage measure V_R is later used to develop fragility models in Chapter 6 for the most efficient collapse reliability assessment.

5.4.3. Critical Intensity Measures as Representative of Structural Damage Potential

A practical and appropriate intensity index representative of structural damage capacity is highly desirable in earthquake engineering. This section therefore investigates the existing earthquake

intensity measures reported in Table 5.5 to identify appropriate, comprehensive and practical ones that can reflect the damage potential of structures near collapse. Similar to recent studies by Riddell (2007) and Ye et al. (2013), a correlation analysis between intensity measures and damage measures at collapse level was performed to choose the most critical intensity measures that can represent the severe damage associated with structural collapse. A total of 50 existing intensity measures, which were described previously, were considered to conduct the correlation analysis based on collapse data of 78 ground motion records. 7 critical seismic responses for collapse assessment were selected, which are global cumulative responses representing the energy dissipation and absorption capacity of a structural system. In the correlation analysis, both linear and nonlinear relationships between the possible pairs of intensity and response quantities were considered with and without taking the logarithms of the variables respectively (see Table 5.12 and Table 5.13).

The case study by Lignos et al. (2008), which was considered in this study, is a four-story MDOF model with a dominant period found to be 0.44 sec according to the modal analysis. For this specific type of structure, acceleration parameters in Table 5.12 and Table 5.13 show better correlation results with seismic energy responses. *PGA*, *Sa*, and *max* A_v are the most associated terms with kinetic energy of the system E_K showing ρ larger than 0.8. The intensity indices a_{rs}, a_{sq}, *AI*, and *Ic* give a value of ρ between 0.8 and 0.85 with E_I and E_{SPR}, which are two most significant response terms expressing the damage potential of structure. Among these indices, a_{rs} is found to be the best indicator to be used in IM-based collapse assessment with a minimum cov of 0.366 (see Table 5.6). This measure gives relatively high correlations for E_I and E_{SPR} larger than 0.8. The most widely used intensities *PGA* and *Sa* can be also fairly suitable for collapse estimation with a correlation around 0.65~0.7, however their cov was found to be above 0.5 (see Table 5.6).

The findings of this correlation evaluation are only applicable to the test case study of interest and also can be generalized to similar degrading short period structures. Note that, although acceleration intensity indices show a better correlation for collapse capacity of this model at the specified fundamental period (i.e., the model is sensitive to acceleration indices), they may show poor correlation for similar structures at other periods, even may be no correlation at all. Recent

studies by Riddell (2007) and Ye (2013) indicate that there is no single index that can show satisfactory correlation with response for structures with different periods. They proposed to use acceleration, velocity and displacement-sensitive indices in seismic performance of rigid, intermediate and flexible systems respectively (see Table 5.10). More comprehensive research can be conducted on critical intensity measures with a parametric study considering effect of earthquake characteristics and structural parameters on the collapse capacity of steel frame structures under cyclic loading. Using the parametric collapse data, the effect of acceleration, velocity and displacement-sensitive indices on seismic performance with different dominant periods can be better understood. Therefore, a primary parametric study was performed in Chapter 7 to investigate structural collapse considering several buildings with different geometric and material properties. However, there are pressing research needs for further investigation of effects of ground motion indices on assessment of structural collapse by conducting an extensive building parametric study that covers a wide array of dominant periods.

DMs / IMs	E_G	$E_I \approx E_{EQ}$	$E_{SPR} \approx E_{SPR,B} \approx E_{SPR,C}$	$E_{K,Y}$	$E_K \approx E_{K,X}$	$E_R{}^a$ (alter.)	E_R	V_R
PGA	0.35	0.68	0.68	0.49	0.81	0.05	-0.05	-0.04
$Sa(T_1,2\%)$	0.34	0.70	0.70	0.55	0.87	0.11	-0.01	0.01
$Sa(T_1,5\%)$	0.33	0.71	0.71	0.55	0.89	0.12	-0.01	0.00
a_{rms}	0.39	0.76	0.78	0.42	0.74	0.17	0.01	0.02
a_{sq}	0.29	0.84	0.82	0.37	0.72	-0.05	-0.22	-0.22
a_{rs}	0.24	0.85	0.81	0.36	0.71	-0.09	-0.30	-0.29
Pa	0.40	0.76	0.77	0.39	0.70	0.13	0.00	0.02
Ia	0.25	0.68	0.65	0.45	0.77	-0.10	-0.21	-0.20
AI	0.29	0.84	0.82	0.37	0.72	-0.05	-0.22	-0.22
Ic	0.34	0.83	0.82	0.40	0.75	0.03	-0.14	-0.13
P_D	0.26	0.71	0.73	0.32	0.50	0.26	0.03	0.04
CAA	-0.07	0.64	0.54	0.09	0.33	-0.43	-0.61	-0.62
max A_v	0.33	0.69	0.69	0.62	0.91	0.07	-0.06	-0.05
$Sa_{ave}(5\%)$	0.00	0.56	0.57	0.32	0.45	0.28	-0.14	-0.13
PGV	0.06	0.41	0.41	0.29	0.47	0.14	-0.10	-0.09
PGV/PGA	-0.27	-0.25	-0.25	-0.23	-0.38	-0.04	-0.09	-0.10
$Sv(T_1,2\%)$	0.34	0.70	0.70	0.55	0.87	0.08	-0.02	-0.01
$Sv(T_1,5\%)$	0.34	0.70	0.70	0.54	0.88	0.07	-0.03	-0.02
v_{rms}	0.00	0.25	0.27	0.08	0.21	0.19	-0.04	-0.02
v_{sq}	-0.15	0.06	0.03	-0.10	-0.05	-0.08	-0.20	-0.20
v_{rs}	-0.18	0.15	0.12	-0.09	0.00	-0.11	-0.29	-0.29
Pv	0.01	0.11	0.12	0.03	0.11	0.15	0.02	0.02
Iv	-0.17	0.23	0.18	0.07	0.16	-0.18	-0.37	-0.37
I_F	-0.07	0.31	0.29	0.17	0.31	-0.02	-0.24	-0.24
$I_M(2\%)$	0.22	0.33	0.33	0.25	0.42	0.02	0.03	0.04

DMs / IMs	E_G	$E_I \approx E_{EQ}$	$E_{SPR} \approx E_{SPR,B} \approx E_{SPR,C}$	$E_{K,Y}$	$E_K \approx E_{K,X}$	$E_R{}^a$ (alter.)	E_R	V_R
$I_M(5\%)$	0.22	0.34	0.34	0.25	0.46	0.00	0.02	0.03
CAV	-0.24	0.06	0.00	-0.18	-0.15	-0.29	-0.40	-0.40
SI(2%)	0.04	0.67	0.68	0.38	0.58	0.28	-0.16	-0.15
$Sv_{ave}(5\%)$	0.17	0.72	0.73	0.51	0.72	0.28	-0.08	-0.07
PGD	-0.10	-0.02	-0.04	-0.12	0.00	-0.08	-0.14	-0.14
$Sd(T_1,2\%)$	0.34	0.70	0.70	0.55	0.87	0.11	-0.01	0.01
$Sd(T_1,5\%)$	0.33	0.71	0.71	0.55	0.89	0.12	-0.01	0.01
d_{rms}	-0.02	-0.03	-0.04	-0.11	0.00	-0.02	-0.05	-0.04
d_{sq}	-0.01	-0.04	-0.06	-0.09	-0.04	-0.07	-0.04	-0.04
d_{rs}	-0.09	-0.03	-0.06	-0.17	-0.06	-0.16	-0.17	-0.17
Pd	0.04	-0.06	-0.05	-0.04	0.00	0.03	0.05	0.05
Id	-0.17	-0.05	-0.09	-0.17	-0.09	-0.19	-0.24	-0.24
CAD	-0.12	-0.03	-0.08	-0.20	-0.13	-0.23	-0.23	-0.24
$Sd_{ave}(5\%)$	0.00	0.55	0.56	0.32	0.45	0.28	-0.14	-0.13
t_T	-0.09	-0.23	-0.28	-0.17	-0.25	-0.28	-0.06	-0.08
t_S	-0.32	-0.09	-0.19	-0.26	-0.34	-0.53	-0.52	-0.54
t_{45}	-0.09	-0.15	-0.19	-0.10	-0.14	-0.39	-0.13	-0.14
$v_T{}^2$	-0.01	-0.15	-0.18	-0.09	-0.12	-0.30	0.00	-0.02
$v_S{}^2$	-0.22	0.00	-0.10	-0.13	-0.13	-0.52	-0.53	-0.56
v_T	-0.05	-0.17	-0.21	-0.11	-0.14	-0.37	-0.08	-0.10
v_S	-0.22	0.03	-0.08	-0.14	-0.13	-0.63	-0.57	-0.60
$T_{v,\,total}$	-0.13	-0.07	-0.03	-0.07	-0.14	0.40	0.13	0.14
$T_{v,\,strong}$	-0.21	-0.21	-0.17	-0.19	-0.32	0.30	0.14	0.13
$f_{v,\,total}$	0.06	0.04	0.00	-0.01	0.08	-0.41	-0.15	-0.16
$f_{v,\,strong}$	0.18	0.27	0.23	0.17	0.31	-0.34	-0.19	-0.19

Table 5.12 Correlation results between intensity and energy damage indices at "near-collapse" level for the case study of Lignos et al. (2008) subjected to far-field ground motion set by Haselton and Deierlien (2007).

LOG IMs \ DMs	E_G	$E_I \approx E_{EQ}$	$E_{SPR} \approx E_{SPR,B} \approx E_{SPR,C}$	$E_{K,Y}$	$E_K \approx E_{K,X}$	E_R^a (alter.)	E_R	V_R
PGA	0.31	0.64	0.64	0.47	0.79	0.09	-0.05	-0.03
$Sa(T_1,2\%)$	0.36	0.68	0.70	0.50	0.78	0.17	0.04	0.06
$Sa(T_1,5\%)$	0.34	0.68	0.70	0.52	0.83	0.19	0.05	0.06
a_{rms}	0.34	0.71	0.73	0.41	0.71	0.21	0.01	0.03
a_{sq}	0.17	0.82	0.78	0.33	0.67	-0.13	-0.37	-0.36
a_{rs}	0.17	0.82	0.78	0.33	0.67	-0.13	-0.37	-0.36
Pa	0.34	0.71	0.73	0.41	0.71	0.21	0.01	0.03
Ia	0.19	0.65	0.61	0.41	0.73	-0.12	-0.26	-0.25
AI	0.17	0.82	0.78	0.33	0.67	-0.13	-0.37	-0.36
Ic	0.25	0.82	0.80	0.38	0.72	0.00	-0.23	-0.22
P_D	0.14	0.51	0.54	0.25	0.40	0.35	0.00	0.02
CAA	-0.07	0.63	0.54	0.10	0.34	-0.43	-0.62	-0.62
max A_v	0.27	0.70	0.70	0.55	0.88	0.16	-0.07	-0.05
$Sa_{ave}(5\%)$	-0.01	0.53	0.54	0.29	0.43	0.25	-0.16	-0.15
PGV	0.05	0.44	0.44	0.29	0.49	0.15	-0.11	-0.10
PGV/PGA	-0.29	-0.29	-0.29	-0.25	-0.42	0.03	-0.05	-0.06
$Sv(T_1,2\%)$	0.36	0.68	0.68	0.49	0.78	0.12	0.01	0.03
$Sv(T_1,5\%)$	0.35	0.67	0.68	0.49	0.81	0.12	0.02	0.03
v_{rms}	0.00	0.35	0.37	0.12	0.29	0.21	-0.07	-0.06
v_{sq}	-0.19	0.24	0.20	-0.05	0.07	-0.14	-0.36	-0.35
v_{rs}	-0.19	0.24	0.20	-0.05	0.07	-0.14	-0.36	-0.35
Pv	0.00	0.35	0.37	0.12	0.29	0.21	-0.07	-0.06
Iv	-0.15	0.29	0.24	0.09	0.21	-0.17	-0.38	-0.38
I_F	-0.06	0.37	0.35	0.19	0.35	-0.03	-0.27	-0.27
$I_M(2\%)$	0.29	0.33	0.33	0.25	0.39	0.01	0.09	0.10

LOG IMs \ DMs	E_G	$E_I \approx E_{EQ}$	$E_{SPR} \approx E_{SPR,B} \approx E_{SPR,C}$	$E_{K,Y}$	$E_K \approx E_{K,X}$	E_R^a (alter.)	E_R	V_R
$I_M(5\%)$	0.29	0.32	0.32	0.25	0.41	0.01	0.09	0.10
CAV	-0.25	0.12	0.06	-0.14	-0.07	-0.29	-0.42	-0.43
SI(2%)	0.02	0.64	0.65	0.34	0.54	0.25	-0.18	-0.17
$Sv_{ave}(5\%)$	0.14	0.68	0.69	0.44	0.67	0.28	-0.09	-0.08
PGD	-0.13	0.06	0.04	-0.11	0.06	-0.11	-0.23	-0.22
$Sd(T_1,2\%)$	0.36	0.68	0.70	0.50	0.78	0.17	0.04	0.06
$Sd(T_1,5\%)$	0.34	0.68	0.70	0.52	0.83	0.19	0.05	0.06
d_{rms}	-0.11	0.01	0.00	-0.18	0.01	-0.07	-0.17	-0.16
d_{sq}	-0.16	0.00	-0.05	-0.20	-0.05	-0.21	-0.28	-0.28
d_{rs}	-0.16	0.00	-0.05	-0.20	-0.05	-0.21	-0.28	-0.28
Pd	-0.11	0.01	0.00	-0.18	0.01	-0.07	-0.17	-0.16
Id	-0.19	0.03	-0.02	-0.16	-0.02	-0.21	-0.31	-0.31
CAD	-0.18	-0.05	-0.11	-0.22	-0.10	-0.26	-0.30	-0.30
$Sd_{ave}(5\%)$	-0.01	0.53	0.54	0.29	0.43	0.25	-0.16	-0.15
t_T	-0.21	-0.32	-0.37	-0.22	-0.30	-0.31	-0.14	-0.17
t_S	-0.35	-0.14	-0.23	-0.27	-0.35	-0.53	-0.50	-0.53
t_{45}	-0.13	-0.19	-0.24	-0.09	-0.20	-0.38	-0.15	-0.17
v_T^2	-0.08	-0.18	-0.24	-0.13	-0.13	-0.46	-0.18	-0.20
v_S^2	-0.17	0.05	-0.06	-0.11	-0.08	-0.67	-0.54	-0.56
v_T	-0.08	-0.18	-0.24	-0.13	-0.13	-0.46	-0.18	-0.20
v_S	-0.17	0.05	-0.06	-0.11	-0.08	-0.67	-0.54	-0.56
$T_{v,\,total}$	-0.10	-0.06	-0.01	-0.03	-0.11	0.41	0.14	0.15
$T_{v,\,strong}$	-0.20	-0.25	-0.21	-0.19	-0.33	0.33	0.17	0.16
$f_{v,\,total}$	0.10	0.06	0.01	0.03	0.11	-0.41	-0.14	-0.15
$f_{v,\,strong}$	0.20	0.25	0.21	0.19	0.33	-0.33	-0.17	-0.16

Table 5.13 Correlation results between intensity (in log-scale) and energy damage indices at "near-collapse" level for the case study of Lignos et al. (2008) subjected to far-field ground motion set by Haselton and Deierlien (2007).

6. DEVELOPMENT OF A NEW COLLAPSE FRAGILITY MODEL

This chapter introduces a new approach in probabilistic assessment of structural collapse using the energy-based collapse criterion developed in this study. First, this chapter briefly summarizes current approaches in probabilistic collapse assessment of structures in the context of Performance Based Earthquake Engineering (PBEE), which is then followed by a discussion on the needs for further improvement of such existing approaches. Next, using a large sample of collapse data created using one of the validated simulation models in Chapter 3, effective assessment models for collapse capacity and demand are developed based on the critical performance measures that indicate dynamic instability near collapse defined by the energy-based collapse rule (developed in Chapter 4). Finally, a new method is established to construct collapse fragility models based on the developed collapse demand/capacity framework in order to promote reliable probabilistic evaluation of structural collapse. These fragility models are then compared to those by traditional approaches in evaluation of collapse fragility relations.

6.1. Probabilistic Assessment of Structural Collapse

Uncertainty in structural properties and characteristics of applied ground motions requires probabilistic assessment of structural collapse. Therefore, the probabilistic basis of PBEE framework can be adopted here to integrate these uncertainties into probabilistic description of collapse performance. The following sections first summarize the probabilistic basis of PBEE framework, and then describe collapse assessment of structures in PBEE context.

6.1.1. Probabilistic Basis of PBEE Framework

Several observations of unexpected extensive damage and high repair cost of traditional code-based structures in the 1994 Northridge earthquake and the 1995 Kobe earthquake have initiated the development of PBEE framework by Pacific Earthquake Engineering Research (PEER) Center. PBEE provides a more sustainable, durable, and economic design approach in earthquake engineering while enhancing the life-safety (Mason, 2008; Semih and Mohalem, 2013). Therefore, current seismic provisions are moving towards adopting the PBEE framework.

The PBEE framework aims at improving decision-making process for seismic risk mitigation of structures. The framework describes adequacy of seismic performance of a structural system by achievement of various performance objectives stated in terms of loss of life, disruption to operation, and economic losses. The four basic components of PEER framework to describe the adequacy of structural seismic performance are as follows (Deierlien, et al. 2003; Selim and Mohalem, 2013):

- Seismic hazard analysis: The performance assessment procedure starts with selecting the intensity measure (IM) of ground motion defined by a seismic hazard curve for that intensity. Hazard curve tracks the relationship between the intensity level of ground motion (described in terms of IM such as spectral acceleration, *Sa*) and the mean annual frequency of exceedance of the selected intensity, λ (*Sa*).
- Structural analysis: The next step is to perform nonlinear dynamic analyses under a selected set of ground motions and to obtain structural responses. Then damage measures (DM) are calculated based on the condition of the structure using the resulting structural responses.
- Damage analysis: Among the pre-determined damage states (DS) of a structural system describing the physical condition of the system, the DS matching the engineering responses on the structure is selected. Damage analysis evaluates physical damage at the element- or structure-level and estimates the damage state usually in terms light, moderate, severe, life-safety, or collapse.
- Loss analysis: Finally, loss analysis determines the metrics of risk management decisions variables (DV), which are meaningful to owners such as casualties, economic loss, repair duration and injuries, based on the damage analysis results. The use of DVs rather than structural responses helps owners to make decision more easily about the design of the structure.

If it is assumed that the uncertainties associated with the four components of PBEE probabilistic framework form a Markov chain (i.e., DV is statistically dependent on DS, but independent on the others, DS is dependent only on DM, and DM is dependent only IM), a probabilistic description of performance can be obtained using the total probability theorem (Deierlien, et al.

2003; Selim and Mohalem, 2013). As a result, the mean occurrence rate of decision variable, $\lambda(DV)$ can be then estimated by:

$$\lambda(DV) = \int\int\int G(\mathrm{DV}|\mathrm{DS})\ \mathrm{dG}(\mathrm{DS}|\mathrm{DM})\ \mathrm{dG}(\mathrm{DM}|\mathrm{IM})\ \mathrm{d}\lambda(\mathrm{IM}) \qquad (6.1)$$

where, the term $d\lambda(\mathrm{IM})$ is the differential seismic hazard curve; and other terms, G(DM|IM), G(DS|DM) and G(DV|DS) refer to conditional complementary cumulative distribution function (CDF) of one quantity given another. For example, G(DM|IM) gives the conditional probability of DM exceeding a specified threshold value at a given IM.

6.1.2. Collapse Assessment in PBEE Framework

In view of collapse assessment of structures, the conditional probability of collapse at a given seismic hazard level, P_C or mean annual frequency of collapse, λ_C can be used to describe a performance objective. To assess the collapse performance objectives, it is necessary to evaluate collapse fragility curve and seismic hazard curve. Collapse fragility curve represents the conditional probability of a collapse, P_C for a given intensity level of ground motion. Seismic hazard curve tracks the likelihood of the intensity level for a specific site of building. If seismic hazard curve is integrated into the collapse fragility curve, the collapse performance metric λ_C for a given IM value *im* can be then assessed as follows (Deierlien, et al. 2003; Vamvatsikos and Cornell, 2002; Zareian et al., 2010):

$$\lambda_C = \lambda(DS = C) = \int\int G(C|\mathrm{DM})\ \mathrm{dG}(\mathrm{DM}|\mathrm{IM})\ \mathrm{d}\lambda(\mathrm{IM}) = \int G(C|\mathrm{IM})\ \ \mathrm{d}\lambda(\mathrm{IM}) \qquad (6.2)$$

$$P_C = G(C|\mathrm{IM}) = P(C|IM = im) \qquad (6.3)$$

$$\lambda_C = \int_{all\ IM} P(C|IM = im)\ d\lambda(IM) \qquad (6.4)$$

where "*C*" represents the collapse damage state. Then, the procedure for probabilistic collapse assessment can be summarized by the following steps (Haselton et al., 2011):

1. Determine a ground motion set using available seismic hazard models at a site.
2. Perform nonlinear dynamic analysis subjected to the ground motion set.
3. Construct a collapse fragility function, i.e, the probability of collapse as a function of

ground motion intensity, using the collapse data.

4. Integrate the variability due to structural modeling and ground motions into the collapse fragility.
5. Compute the risk metrics P_C or λ_C for collapse performance.

The purpose of this chapter is to compare available collapse fragility models in the literature and then introduce a new procedure for more reliable and accurate probabilistic prediction of collapse. The next section describes the details of the comparative study performed to compute P_C using methods available for the assessment of collapse fragility relations.

6.2. Evaluation of Available Methods for Collapse Fragility Curves

Assessment of collapse fragility relations is one of the state-of-art approaches to quantity the collapse potential of structures. A collapse fragility curve describes the probability of collapse for a given intensity level of ground motions. There are two ways to get collapse potential of structures (Zareian et al., 2010): so-called "damage measure (DM) based" approach in which the collapse is described in terms of a structural response parameter such as maximum interstory-drift-ratio (IDR) to evaluate the probability of collapse at a specified intensity level; and so-called "intensity measure (IM) based" approach which directly uses an IM of ground motion (such as *Sa*) to describe the collapse limit state. Both methods rely on "demand vs capacity" framework, i.e., the probability of collapse is assessed by the likelihood of the event of the seismic demand exceeding the seismic capacity.

In the following sections, the case study of Lignos et al. (2008) validated in Chapter 3 is considered to investigate two existing approaches to assess collapse fragility curves. For a large sample of IDA-based collapse data obtained using the far-field ground motion set by Haselton and Deierlein (2007), the collapse potential of the structure in the case study is evaluated using the energy-based collapse criterion developed in Chapter 4. Effects of structural modeling options and uncertain characteristics of ground motions on the collapse fragility are studied later in Chapter 7 through an extensive parametric study.

6.2.1. *Assessment of Collapse Fragility Curves with IDA*

In assessing the likelihood of structural collapse, the collapse potential of a structure is often described in terms of a scalar value of DM (e.g., IDR) or IM (e.g., $Sa(T_1)$). In this sense, the IDA is often employed to track the relationship between IM and DM, often termed as "IDA curve" (Vamvatsikos and Cornell, 2002). Then, for a selected combination of DM and IM, and a structural model, statistical characterization of IDA analyses provides collapse capacity. Additionally, IDA curves can give the conditional distribution of DM given IM (Vamvatsikos and Cornell, 2002; Baker, 2007), but this may require a large number of nonlinear dynamic analyses for reliable estimation. Then, the probability of the global collapse event of a structural system for a given intensity level is understood as

$$P(C|IM) = \frac{Number\ of\ Simulations\ Resulting\ in\ Collapse\ at\ the\ intensity\ IM}{Total\ Number\ of\ Simulations\ for\ the\ given\ intensity\ IM} \qquad (6.5)$$

6.2.2. DM-Based Collapse Fragility Curve

The DM-based approach defines the "collapse" in the numerator of (6.5) in terms of a structural response (deformation or force quantity). That is, this approach assumes the occurunce of collapse when the demand for a strucural response (DM_{Demand}) exceeds a specified threshold value ($DM_{Capacity}$). Therefore, the collapse fragility for a given IM value *im* is estimated as:

$$P_C = P(C|IM = im) \ = P\left(DM_{Demand} \geq DM_{Capacity} \middle| IM = im\right) \qquad (6.6)$$

If the uncertainty in $DM_{Capacity}$ is also taken into account, using total probability theorem, the probability of collapse is then obtained as

$$P_C = \int_{all\ x} P\left(DM_{Demand} \geq DM_{Capacity} \middle| DM_{Capacity} = x, IM = im\right) f_{DM_{Capacity}}(x)\, dx \qquad (6.7)$$

where, $f_{DM_{Capacity}}$ denotes the probability distribution function of $DM_{Capacity.}$ The first term in the integral of (6.7) is the probabilty of the structural demand exceeding *x* at a given intensity level *im* of ground motion; and the second term then gives the probability density function of the capacity being equal to *x*. Assuming the capacity is statistically independent of the demand, this equation can be reduced as follows (Jalayer and Cornell, 2003; Zareian et al., 2010):

$$P_C = \int_{all\ x} P(DM_{Demand} \geq x \,|IM = im)\ f_{DM_{Capacity}}(x)\, dx \qquad (6.8)$$

$$P_C = \int_{all\ x} \left[1 - F_{DM_{Demand}|IM}(x\,|im)\right] f_{DM_{Capacity}}(x)\, dx \qquad (6.9)$$

where $F_{DM_{Demand}|IM}$ denotes the conditional CDF of DM_{Demand} given an IM.

The expression in (6.9) requires evaluating the conditional complementary distribution of structural demand (DM_{Demand}) given IM and as well as quantifying the uncertain structural capacity $DM_{Capacity}$ in a stochastic manner. Partial descriptors such as conditional mean and variance of DM_{Demand} given IM can be obtained through linear/nonlinear regression analysis. Such regression models provide probabilistic estimation of the structural demand for a given intensity level. On the other hand, often a probability distribution function is simply fitted on the collapse data (DM_{col}) obtained from IDA curves to evaluate probability of $DM_{Capacity}$.

In (6.9), the maximum interstorey drift ratio (IDR) is often selected as the DM to represent the global behaviour of structural system (FEMA, 2000; Cornell et al., 2002). Following this convention, the relationship between structural demand IDR_{Demand} and Sa_{Demand} is investigated by use of a scatter plot in Figure 6.1. Usually linear regression is applied on logarithms of IDR to find the conditional mean and variance in the 2000 SAC/FEMA methodology (FEMA, 2000; Cornell et al., 2002). Using the same approach, the ratio of the conditional standard deviation of the error of logarithms of IDR_{Demand} by the linear regression analysis to the logarithmic mean of IDR_{Demand} is estimated 0.406, which shows much variability. Although logarithms are applied on collapse data to obtain an approximate linear relationship with "constant" variance, it seems variance increases with intensity. This is expected from the fact that the sensitivity of IDR increases as the IDA curve becomes almost flat near collapse as observed in Chapter 5.

In Figure 6.2a, the conditional distribution of structural collapse resistance IDR_{col} (or $IDR_{Capacity}$) given IM_{col} is obtained by the value of IDR when the structure "collapses" according to the energy-based criteria proposed in this study. Figure 6.2a shows that the relationship between logarithms of IDR_{col} and logarithms of Sa_{col} is not significant providing a low correlation of 0.294, which indicates that the probabilistic distribution of $DM_{Capacity}$ given in max IDR does not need to be described as the conditional distribution function of IM. Therefore, usually a

lognormal distribution function is employed on the collapse data (DM_{col}) to evaluate probability of $DM_{Capacity}$ in a stochastic manner as shown in Figure 6.2b. However, Medina and Krawinkler (2003) found out that the location of maximum IDR changes from upper stories to lower stories as the intensity level of a specific ground motion increases. DM-based approach for computing collapse probability then requires $DM_{Capacity}$ being at least a function of the storey number despite the assumption made in (6.7) (Zareian et al., 2010).

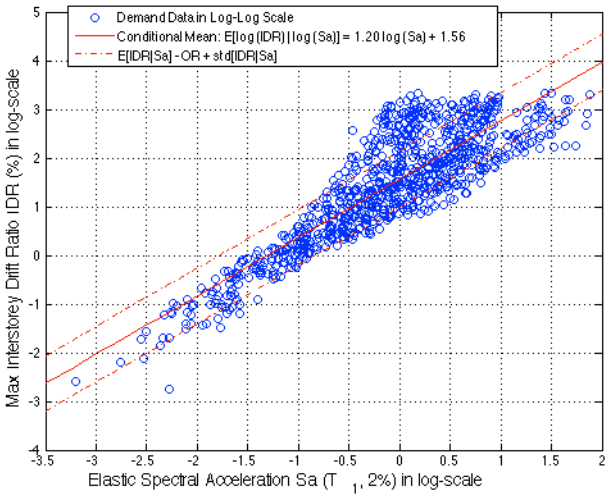

Figure 6.1 Relationship between IDR_{Demand} and Sa_{Demand} for the case structure of Lignos et al. (2008) subjected to the far-field ground motion set by Haselton and Deierlien (2007).

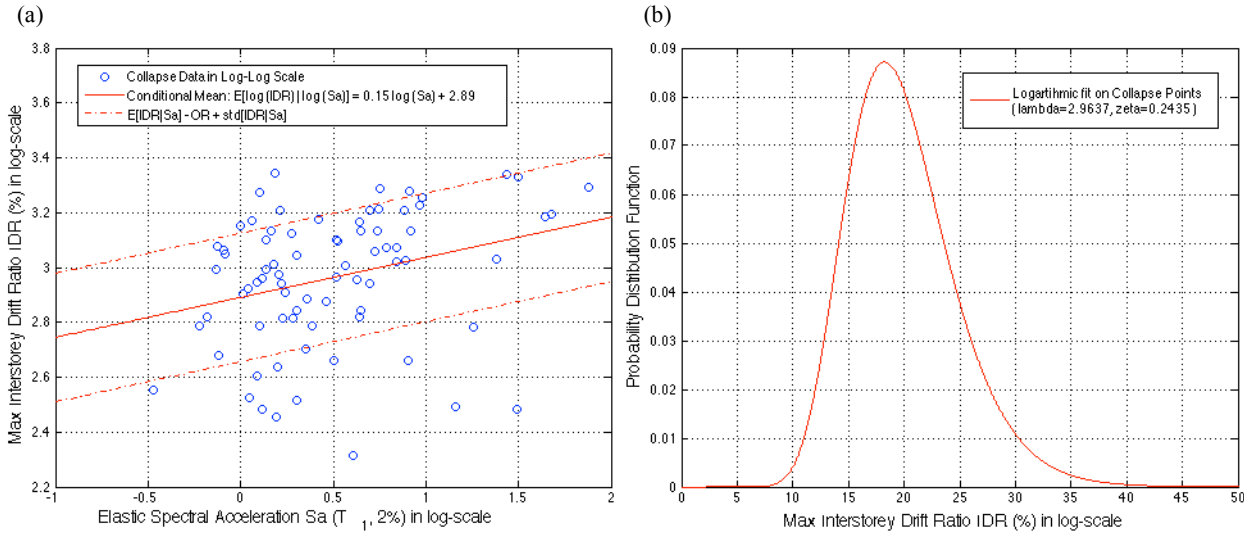

Figure 6.2 Relationship between IDR_{col} (or $IDR_{Capacity}$) and Sa_{col} (or $Sa_{Capacity}$) for the case structure of Lignos et al. (2008) subjected to the far-field ground motion set by Haselton and Deierlien (2007).

6.2.3. IM-Based Collapse Fragility Curve

The IM-based approach in collapse fragility curves has been introduced first by Ibarra et al. (2002). The approach defines the occurrence of collapse as the event that the collapse capacity of a structure specified in terms of an intensity measure ($IM_{Capacity}$) is exceeded by the given intensity demand (IM_{Demand}). $IM_{Capacity}$ here can be defined as the ground motion intensity level at which structural collapse is observed according to the collapse criteria. Then, the probability of collapse is estimated by the probability that the intensity capacity is less than a given demand value "im", i.e., the cumulative distribution function of $IM_{Capacity}$:

$$P_C = P(C|IM = im) = P(IM_{Capacity} < IM_{Demand} = im) = F_{IM_{Capacity}}(im) \qquad (6.10)$$

Collapse fragility is then defined as the probability distribution of collapse capacity, which can be generally obtained using the IDA simulations for a suit of ground motions possible at the site. Using the collapse intensities from IDA curves for Lignos et al. (2008) under 78 ground motions, empirical cumulative distribution functions (CDF) for IM_{col} identified by the energy rule are presented in Figure 6.3. The CDFs of IM_{col} are obtained for various IMs such as peak ground acceleration (*PGA*), peak ground velocity (*PGV*), peak ground displacement (*PGD)*, spectral acceleration for 2% damping, *Sa (2%)*, undamped intensity of Arias, *AI (0%)* (Arias 1970), root of integral of square of ground acceleration-time history (a_{rs}), average cycle of zero-crossings in the strong part of accelerogram ($T_{v,strong}$, where strong duration is based on definition by Trifunac & Brady (1975)), and average spectral acceleration for 5% damping (Sa_{ave} (5%)). For a fair comparison of their variability, IM_{col}'s are normalized by their mean values before the construction of the CDFs. These CDF curves allows for a visual comparison of probabilistic distributions of the identified IM collapse capacities. In order to make a numerical comparison, the coefficient of variations (cov) of IM_{col}'s are computed, as shown in Table 5.6. The IMs with the smallest cov's are Sa_{ave} *(5%)* and a_{rs}. According to the correlation analysis in Table 5.12, a_{rs} correlates better with the damage potential of the structure, and thus allows for more confidence in collapse prediction comparing to other IM candidates.

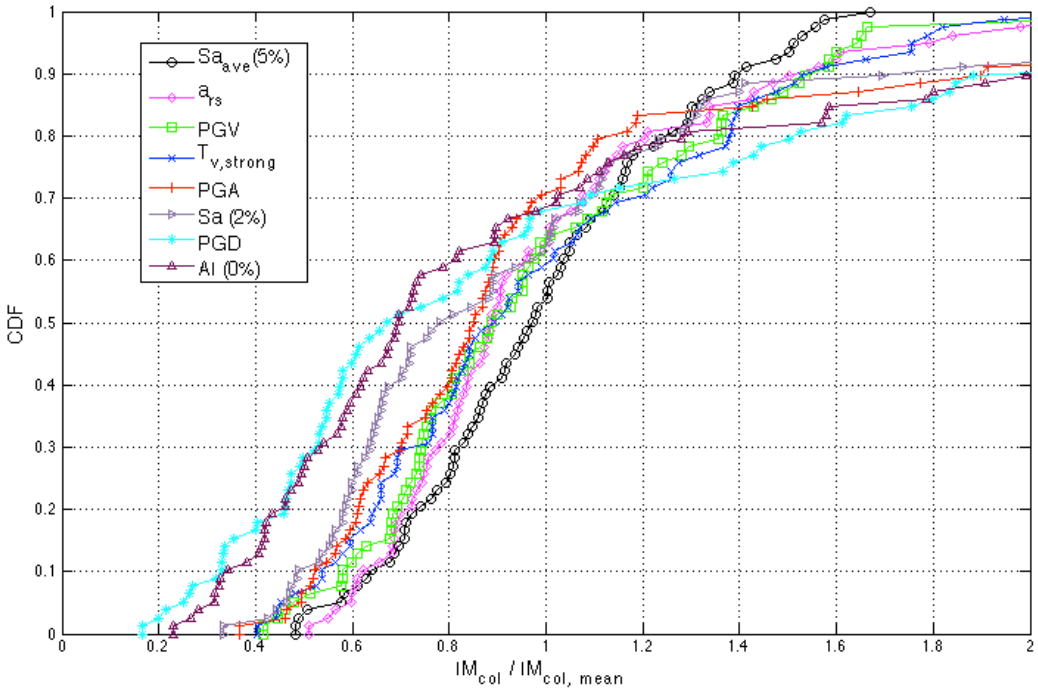

Figure 6.3 Cumulative distribution functions of IM-collapse level for the test case of Lignos et al. (2008) subjected to 78 far-field ground motions by Haselton and Deierlein (2007).

A lognormal CDF is often employed to fit empirical fragility curves by a smooth function that relates the probability of collapse with the ground motion intensity (Ibarra and Krawinkler, 2005; Bradley and Dhakal 2008; Ghafory-Ashtiany et al. 2011). If $IM_{Capacity}$ follows a lognormal distribution with the distribution parameters λ and ξ (Ang and Tang, 2007), i.e., LN (λ, ξ), then from (6.10), the fragility is derived as:

$$P_C = \boldsymbol{\Phi}\left[\frac{ln\, im - \lambda_{IM_{Capacity}}}{\xi_{IM_{Capacity}}}\right] \qquad (6.11)$$

Figure 6.4 shows the fragility models developed by use of the lognormal CDFs of collapse intensities in terms of *Sa* and a_{rs} at the collapse level. $IM_{Capacity}$ models for both measures seem well fitted to collapse data points. The model based on a_{rs} provides smaller dispersion (smaller zeta in Figure 6.4) as discussed above.

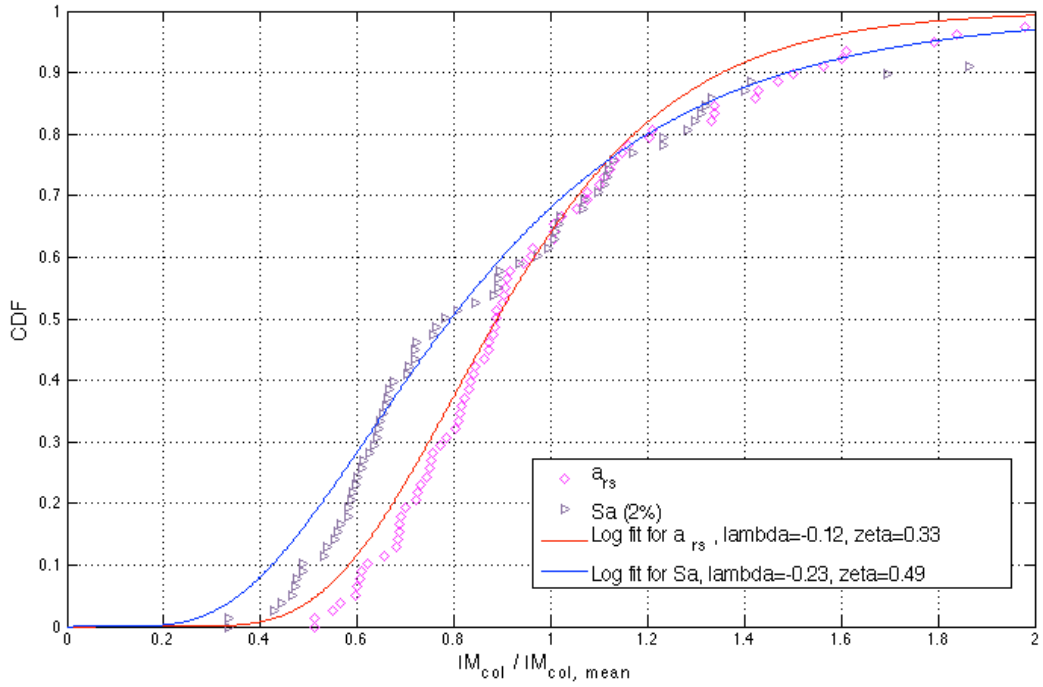

Figure 6.4 Lognormal cumulative distribution function fitted for a_{rs} and *Sa* at collapse level for the test case of Lignos et al. (2008) subjected to 78 far-field ground motions by Haselton and Deierlein (2007).

Assumptions made for the DM-based approach, e.g., dependency between capacity and demand and approximations in assessment of conditional distributions of DM given IM (i.e., linear/nonlinear conditional regression models) may make the IM-based approach seem like a more reliable method to get collapse estimates. However, the IM-based approach relies on "demand vs capacity" framework considering uncertainty only in seismic capacity, which may provide less reliable collapse prediction. On the other hand, using more representative global structural responses with a small cov that are robust to scaling sensitivity near collapse can improve DM-based approach that traditionally uses IDR measure. Thereby, considering uncertainty in both seismic demand and seismic capacity, this study focuses on DM-based approach using energy parameters for the development of a new fragility model as presented in the following sections.

6.3. Collapse Capacity Model

In the literature, there is a concern about validity of nonlinear dynamic analyses results obtained using records that have been scaled (Vamvatsikos and Cornell, 2002). The concern arises from

whether ‘weaker’ records can represent the characteristics of ‘stronger’ ones after scaled. This issue is investigated herein by using multiple unscaled ground motions for collapse capacity prediction. The main idea here is that several records originated from the same earthquake event, but at different stations are “naturally” scaled at different intensity levels, which thus provide true relationship between ground motion characteristics and the intensity level. The relationship between those for artificially scaled ground motions can be tested through comparison.

Therefore, this section first analyzes collapse capacities at the scaled intensity and original intensity in terms of the equivalent velocity ratio “V_R”, i.e., square root of ratio of energy dissipated through degrading elements to total input energy, which was introduced in Chapter 5. The outcomes for collapse capacity analyses are then compared to evaluate the validity of structural collapse performance using scaled ground motions.

6.3.1. Comparison of Collapse Assessments at Original and Scaled Intensities

Usually collapse simulations (i.e., nonlinear dynamic analyses where structural failure occurs) tend to give divergence in results (i.e., enormous increases in structural responses), which may lead to unrealistic estimates in collapse prediction. In order to overcome this issue and to get collapse prediction from simulations at especially “original intensities” where structural failure occurs, the response time histories are considered only up to occurrence of energy collapse criterion (i.e., $E_{EG}=E_G$) to find V_R for such collapse cases. The collapse points for scaled intensities are obtained as well in the same way for fair comparison of the two approaches. However, note that energy-based collapse criterion determines the collapse capacity based on “the last no-collapse cases” on IDA curves, where the structure shows the largest resistance against dynamic collapse.

Figure 6.5 compares the collapse capacities in terms of V_R for Chi-Chi earthquakes obtained by two different approaches: collapse analysis using the natural (original) scale of the ground motions and collapse analysis using scaled ground motions until collapse is observed, i.e., IDA. Note that collapse points (green and blue plus points) are found from the failure time histories considered only up to the point where gravity energy starts to far exceed seismic energy. “The last no-collapse cases” on IDA curves (red star points) are identified as well for comparison. The IDA was performed using the 12 Chi-Chi earthquake records existed in the far-field set provided

by Haselton and Deierlein (2007). Collapse analysis at the natural scale was performed using the same 12 ground motion records and also 28 more Chi-Chi ground motion records at other stations. These extra Chi-Chi earthquakes chosen from the PEER database fulfilling the same selection criteria established by ATC-63 project.

In Figure 6.5, it is observed that the a few scaled records used in IDA (blue plus points or red star points) show collapse at extremely large *Sa* values that were not observed in naturally scaled records (green plus points). This observation may be considered as a preliminary evidence that ground motion records incrementally scaled up to collapse may not represent well enough the characteristics of real strong ground motions at the different intensity levels of collapse. Similarly, using all 78 records in the far-field set provided by Haselton and Deierlein (2007), collapse capacities at original (green points) and at scaled (blue points) intensity levels for each record were compared in Figure 6.6. Two approaches show different trends (i.e., blue points showing larger *Sa* values) implying increasing differences in collapse capacity V_R given *Sa* as the intensity level increases.

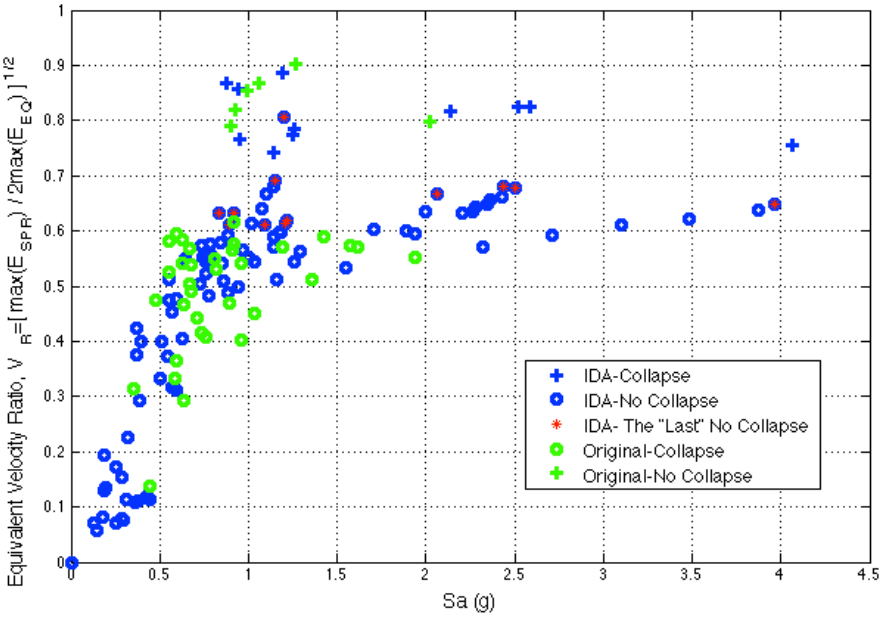

Figure 6.5. Collapse analyses using 40 Chi-Chi records at natural scale (green points) and 12 Chi-Chi records with scaling (blue points).

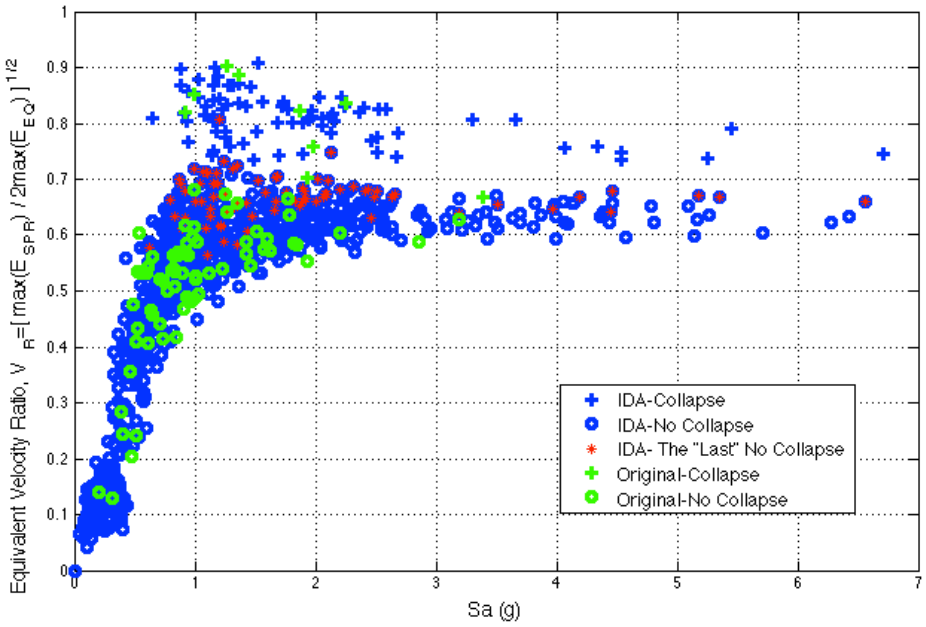

Figure 6.6. Collapse analyses using full records of Deierlein and Haselton (2007) at natural scale (green points) and scaled records (blue points).

Collapse points in both Figure 6.5 and Figure 6.6 (blue and green plus points) represent the "failure" cases where the structure loses its dynamic instability as well as the collapse capacity at the corresponding intensity level. Since the structural capacity should be assessed based on the maximum intensity level, where the structure still shows resistance before occurrence of dynamic instability, "the last no-collapse cases" obtained by IDA (red star points) are more actual representative of the largest structural resistance against dynamic collapse. Therefore, these last no-collapse points (red points) should be considered in assessment of collapse capacity while the failure points (plus points) and no-collapse points (circle points) can be treated as upper and lower boundaries respectively in collapse prediction. The following sections further compare the two approaches using scaled and original intensities in evaluation of collapse capacity models.

6.3.2. Collapse Capacity Analysis at Scaled Intensity

In Chapter 5, "Equivalent Velocity Ratio (V_R)" in (5.5) was introduced as a new performance measure to consider the energy balance between input and absorbed in a structural system in estimating the collapse potential or capacity of a structure under earthquake excitation. In detail,

the measure is the square root of the ratio of the maximum dissipated energy from degrading components ($E_{Degrading}$) to the maximum total input energy released into the system ($E_I=E_{EQ}+E_G$) from a given earthquake time history. Statistical analyses on V_R-based collapse capacity using IDA data (i.e., "the last no-collapse cases" on IDA curves based on energy collapse criterion) show that this measure can describe the collapse capacity of a structure with a smaller cov (0.058) than most of other existing measures tested in this study (see Section 5.4.2). Additionally, this ratio is relatively less sensitive near collapse point and is a unique global energy property of the entire structural system that can better describe structural collapse capacity.

For more effective risk assessment of structural collapse, V_R is considered to develop structural collapse capacity. For a given level of velocity ratio "v", the probability of collapse is:

$$P(C|V_R = v) = P(V_{R_{Capacity}} < V_{R_{Demand}} = v) = F_{V_{R_{Capacity}}}(v) \qquad (6.12)$$

Based on the IDA-collapse capacity data obtained in Figure 6.7a (red points) for the far-field ground motion records by Haselton and Deierlein (2007), the fragility function in (6.12) is developed using a fitted lognormal and normal distributions as shown in Figure 6.7b.

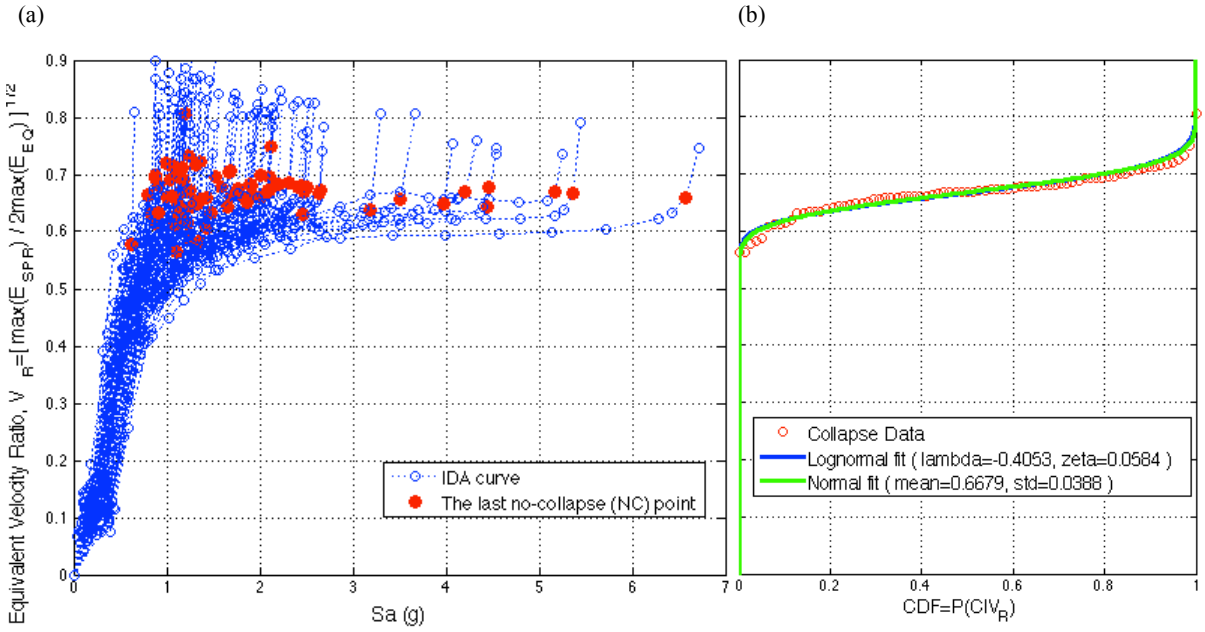

Figure 6.7 Structural collapse capacity based on V_R at scaled intensity level of ground motions.

As shown in Figure 6.7, the maximum energy ratio V_R can describe the collapse capacity of a structure with small variability (small "zeta" and "std" value for deviation of lognormal and normal capacity models respectively). Therefore, both the lognormal and normal fits can be considered as candidate capacity models for later use in collapse fragility assessments.

6.3.3. Collapse Capacity Analysis at Original Intensity

Figure 6.8 shows the relationships between intensity values of *Sa* and V_R for the 78 far-field ground motion records at original scales provided by Haselton and Deierlein (2007). Only 9 records (pink plus points in Figure 6.8) out of this far-field set have been found to cause collapse of the model of the test case study by Lignos et al. (2008). The collapse capacity based on V_R for these 9 ground motions gives a small cov value of 0.10 with a mean of 0.81. Even though there is a less number of collapse sample points at the original intensity, this still proves that V_R as a performance measure can be a good candidate even for collapse capacity analysis at the natural scale of the ground motions.

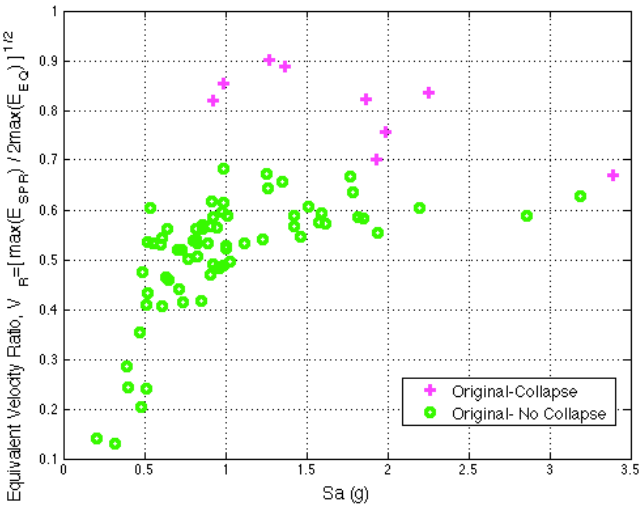

Figure 6.8 Results of nonlinear dynamic analyses for the test case of Lignos et al. (2008) subjected to 78 far field-ground motion records provided by Haselton and Deierlein (2007) at original scale.

In recent studies by Gardoni et al. (2002), Song et al. (2007), and Kim et al. (2007), a Bayesian parameter estimation methodology was successfully applied to develop probabilistic capacity models of various types of structural components based on experimental observations. Similarly, four different probabilistic capacity models based on V_R are constructed as shown in Figure 6.9

by applying the Bayesian methodology to the data obtained in Figure 6.8 for the validated test case study by Lignos et al. (2008). Not only 9 'collapse' cases, but also the effects of the 69 'no-collapse' cases were also considered on the capacity models using the merit of Bayesian approach. The capacity models in Figure 6.9 were obtained using: only 9 collapse cases with Bayesian approach (blue curve; assumed collapse occurred exactly at the original scale), 9 collapse and 69 non-collapse (i.e., lower bound) cases with Bayesian approach (yellow curve), 9 upper bounds and 69 lower bound cases with Bayesian approach (green curve; considering that the collapse may have occurred at the lower scale than the original), and only 9 collapse cases using a fitting logarithmic model (red curve). All models except the green one show a similar mean of V_R capacity around 0.79, but only for green model in Figure 6.9, the mean is a little shifted down (around 0.68) as the result of interpreting the collapse cases as upper bound on the collapse capacity. It is also noted that the models except the green case show a similar level of variability, which indicates that the equality information from the 9 failure cases makes dominant impact on the capacity distribution although the structure may collapse at the lower intensity than the observed one. In that sense, the green model seems to provide most reasonable estimate on the capacity of the structure against dynamic instability. It is also noted that the green model is free from the potential bias caused by the scaling of the ground motion time histories.

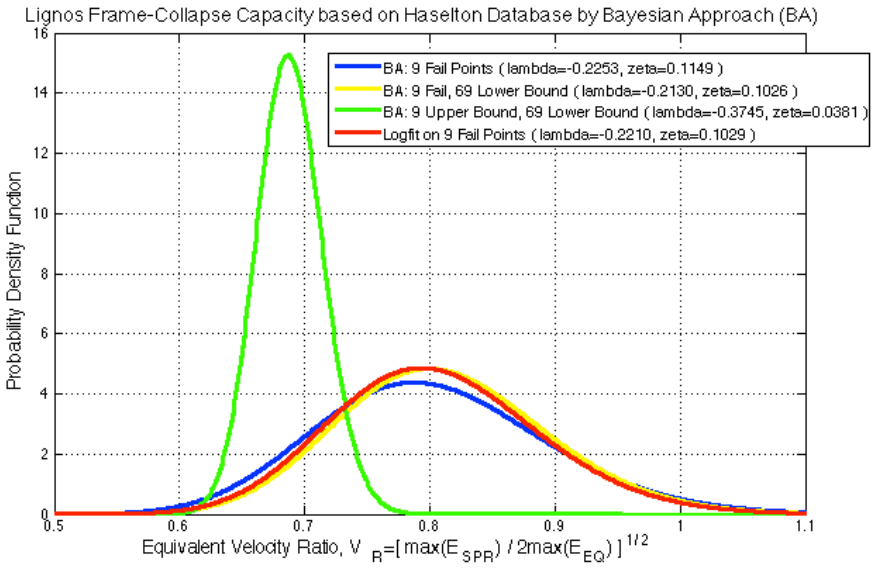

Figure 6.9. Lognormal capacity models based on nonlinear dynamic analyses for the test case of Lignos et al. (2008) subjected to far field-ground motion records provided by Haselton and Deierlein (2007) at original scale.

In order to investigate the potential impact of scaling on the collapse capacities, Figure 6.10 compares the collapse capacities obtained for the same set of 78 ground motions at natural and scaled levels. The black curve shows the lognormal model fitted for the collapse capacities identified by scaled ground motions, i.e., IDA, which is developed in Figure 6.7b previously. The green curve is the same as the one in Figure 6.8 using the Bayesian approach without scaling. The distribution identified from 78 ground motion using scaling (black curve) shows more dispersion and lower mean value than the one not using scaling (green curve). If the structure is subjected to a low seismic intensity, the collapse probability, i.e., the probability that the capacity is lower than the given demand, is overestimated because of the scaling. On the other hand, the probability may be underestimated if the seismic intensity is high. This can be considered as another preliminary evidence that the scaling in IDA would impact the identified collapse capacities and fragilities. Therefore, there is a pressing need of further research on scaling effect of ground motions to have more accurate prediction of the collapse capacities and probabilities.

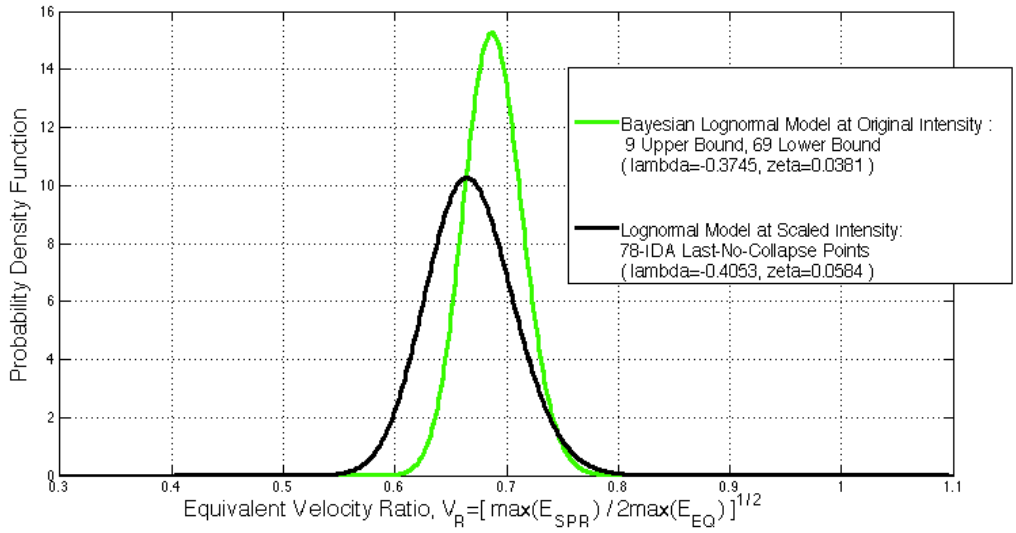

Figure 6.10 Structural collapse capacity models based on V_R at original and scaled intensities of 78 far field-ground motion records provided by Haselton and Deierlein (2007).

6.4. Collapse Demand Model

In order to characterize conditional distribution of structural demand DM_{Demand} for a given intensity measure IM, empirical demand models can be obtained by directly fitting cumulative distribution functions to IDA points without doing any assumption on relationship between DM and IM. However, this method would require a very large sample of IDA data, thereby several

other potential approaches regarding probabilistic estimation of DM given IM are introduced in the literature (Baker, 2007). The most practical one among these approaches is to employ linear/nonlinear regression models on IDA-based data points to quantify the uncertain structural demand DM_{Demand} given IM in a stochastic manner.

For more effective risk assessment of structural collapse, V_R is found to be the best indicator as representative of global damage potential of structures near collapse. In addition, S_a is one of the mostly used practical measures in seismic hazard assessments. Therefore, this section aims to find the most practical and effective linear demand model using V_R given S_a (elastic spectral acceleration value at first period with 2% damping) to later use in development of a new DM-based fragility model. First, the statistical methodology used in this study, linear regression analysis is briefly explained. Then, a new demand model is developed by applying linear regression on the IDA data described in the plane of V_R and S_a, which is obtained using energy-based collapse criterion.

6.4.1. Linear Regression Model with Stationary Conditional Variance

In order to find the conditional distribution of structural demand in V_R given seismic demand S_a, a linear regression model is developed on V_R as in (6.13) to find the conditional mean (6.14) and variance (6.15). Logarithms are applied to S_a before the regression in order to achieve an approximate linear relationship with constant variance:

$$V_{R_{Demand}} = V_R{}' = \mathrm{k}_1 \ln S_a + \mathrm{k}_2 + \sigma\varepsilon \tag{6.13}$$

$$E[V_{R_{Demand}} | \ln S_a] = \mathrm{k}_1 \ln S_a + \mathrm{k}_2 \tag{6.14}$$

$$Var\left[V_{R_{Demand}} | \ln S_a\right] = \sigma^2 \tag{6.15}$$

where, $V_{R_{Demand}}$ or in short $V_R{}'$ is the structural demand in equivalent velocity ratio obtained from approximate linear relationship for a given level of $\ln S_a$, k_1 and k_2 are coefficients found based on linear regression, ε is a normal random variable with zero mean and unit variance, and finally σ represents the magnitude of the linear regression error.

The conditional probability of structural demand exceeding a given level of the capacity v at a

given spectral elastic acceleration level s of ground motion can be described as:

$$P_{V_{R_{Demand}}|\ln S_a} = P(V_{R_{Demand}} \geq v|\ln S_a = \ln s) = 1 - F_{V_{R_{Demand}}|\ln S_a}(v\,|\ln s) \qquad (6.16)$$

Since ε has a normal distribution and other terms in (6.13) (i.e., coefficients k_1 and k_2, the given intensity level $\ln S_a$, and the regression error σ) are deterministic, the structural demand V_R becomes a normal random variable as well. If V_R given an intensity level $\ln S_a$ follows a normal distribution $N(\mu_{V_{R_{Demand}}|lnS_a}, \sigma_{V_{R_{Demand}}|lnS_a})$, the conditional CDF of structural demand based on V_R measure in (6.16) can be then written as:

$$F_{V_{R_{Demand}}|\ln S_a} = \boldsymbol{\Phi}\left[\frac{v-\mu_{V_{R_{Demand}}|\ln S_a}}{\sigma_{V_{R_{Demand}}|\ln S_a}}\right] \qquad (6.17)$$

$$where,\ \mu_{V_{R_{Demand}}|lnS_a} = k_1 \ln S_a + k_2\ \ and\ \ \sigma_{V_{R_{Demand}}|\ln S_a} = \sigma \qquad (6.18)$$

The total absolute error for a sample of observed data points can be presented by the total cumulative squared error Δ^2. If the sample data pairs are given as $\ln S_{a_i}$ and V_{R_i} (where $i = 1, \ldots, n$ and n is the number of data points), then the constant conditional variance σ^2 can be found from the total squared error for regression points $V_{R_i}{}'$ as following:

$$\sigma^2 = \frac{\Delta^2}{n-2}\ ,where\ \ \Delta^2 = \sum_{i=1}^{n}(V_{R_i} - V_{R_i}{}')^2 \qquad (6.19)$$

Using the least squared error method, the coefficients of the linear regression k_1 and k_2 can be found by minimizing the total absolute error Δ^2 as following (Ang and Tang, 2007):

$$\frac{\partial \Delta^2}{\partial k_1} = \sum_{i=1}^{n} -2\ln S_{a_i}\left(V_{R_i} - k_1 \ln S_{a_i} - k_2\right) = 0 \qquad (6.20)$$

$$\frac{\partial \Delta^2}{\partial k_2} = \sum_{i=1}^{n} -2\left(V_{R_i} - k_1 \ln S_{a_i} - k_2\right) = 0 \qquad (6.21)$$

$$k_1 = \frac{\sum(\ln S_{a_i} - \mu_{\ln S_a})(V_{R_i} - \mu_{V_R})}{\sum(\ln S_{a_i} - \mu_{\ln S_a})^2} = \frac{\sum \ln S_{a_i} V_{R_i} - n\mu_{\ln S_a}\mu_{V_R}}{\sum \ln S_{a_i}{}^2 - n\mu^2{}_{\ln S_a}} \qquad (6.22)$$

$$k_2 = \mu_{V_R} - k_1 \mu_{\ln S_a} \qquad (6.23)$$

where, $\mu_{\ln S_a}$ and μ_{V_R} are the mean values for the observed data pairs $\ln S_{a_i}$ and V_{R_i} of a size n.

Following the linear regression procedure described above, a linear demand model was developed based on IDA-data points in Figure 6.11 obtained for the test case of Lignos et al. (2008) subjected to 78 far field-ground motion records. Note that collapse points (i.e, failure points) are not included in the data for an accurate estimate of structural demand. In addition, a limited *Sa* range is considered in the linear regression to get a better model fitting to IDA points. Studying the histogram of S_a values in Figure 6.12, the limited range of S_a is then determined as:

$$S_{a_{Range}}: \mu_{S_a} - \sigma_{S_a} \leq S_a \leq \mu_{S_a} + \sigma_{S_a} \qquad (6.24)$$

Therefore, only "dark" blue circles, which remain in $S_{a_{Range}}$ (i.e., $0.22\text{g} \leq S_a \leq 2.23\text{g}$ corresponding to 79 percent of "all" blue circles) in Figure 6.11, are considered to develop the demand model for the test case of Lignos et al. (2008).

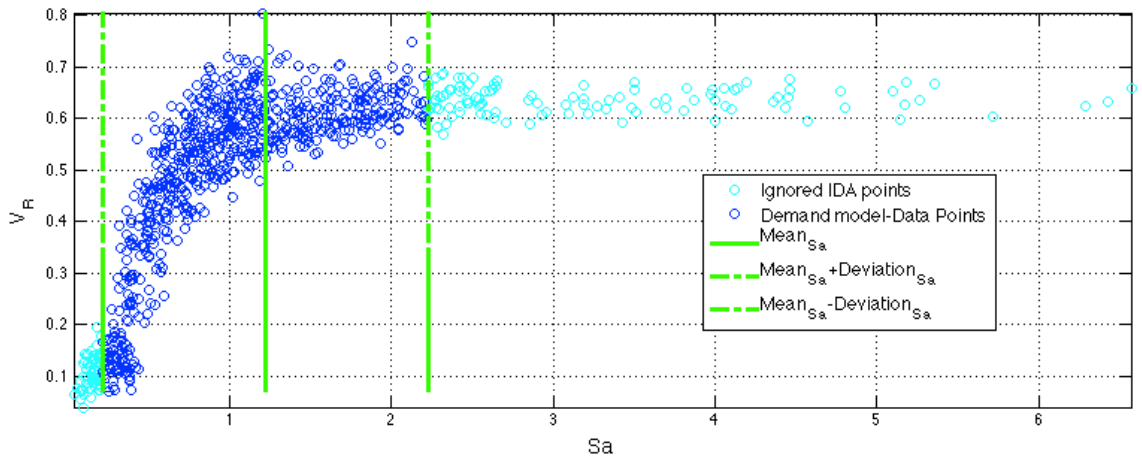

Figure 6.11. Non-collapse data points obtained from IDA results for the test case of Lignos et al. (2008) subjected to 78 far field-ground motion records of Deierlein and Haselton (2007).

Validity of the linear approximation made for the conditional distribution $P(V_R|\ln S_a)$ depends on assumption of a constant conditional variance (the so-called "homoskedasticity" assumption). Therefore, the linear relationship between V_R and $\ln S_a$ is obtained in Figure 6.13 using the "dark" blue data points (i.e., the non-collapse IDA points in $S_{a_{Range}}$) to check this assumption. The linear regression shows approximate constant variance for a limited intensity range, but such models can be acceptable because they have the benefits of practical applicability and reducing computational expense of estimation (Baker, 2007).

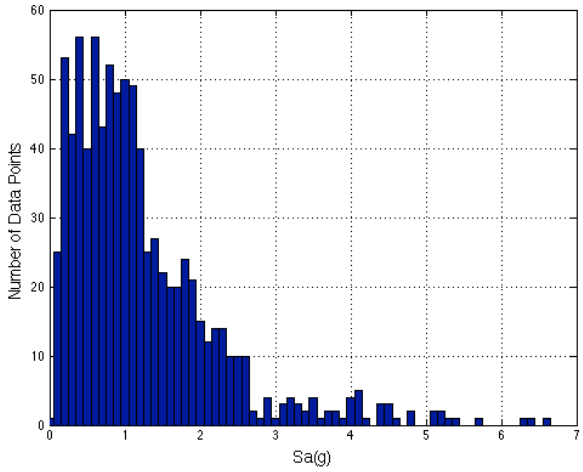

Figure 6.12. Histogram of *Sa* points (with an increment of 0.1) obtained from non-collapse cases based on IDA curves for the test case of Lignos et al. (2008) subjected to 78 far field-ground motion records of Deierlein and Haselton (2007).

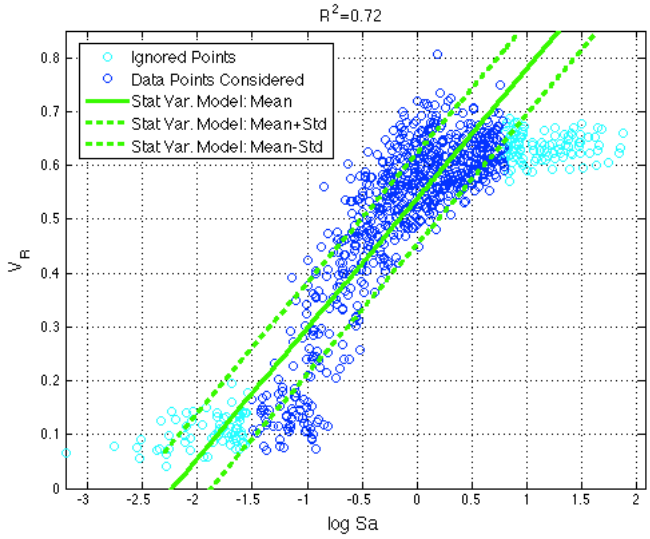

Figure 6.13 The linear regression model with stationary variance between the logarithms of S_a and original V_R data for the test case of Lignos et al. (2008) subjected to 78 far field-ground motion records.

In the development of the collapse demand model, linear or nonlinear regression trials using a full S_a range showed a significant arbitrary bias in collapse predictions by attempting a better fit at the extreme cases (i.e., $S_a > \mu_{S_a} + \sigma_{S_a}$ and $S_a < \mu_{S_a} - \sigma_{S_a}$). This is the main reason why the trend in the middle range was focused here in the development of the linear model. Moreover, it was previously found that nonlinear dynamic analyses results obtained using scaled records may give a misleading trend in collapse capacity estimate, especially as the intensity level increases (see section 6.3.1). Similarly, the IDA-based non-collapse points at higher intensity levels (i.e.,

the "light" blue data points on the right side in Figure 6.13 corresponding to $S_a > \mu_{S_a} + \sigma_{S_a}$) might mislead the demand model if a full S_a range had been considered in the development of the model. Therefore, choosing a limited S_a range in (6.24) for this demand model probably reduces this misleading effect and moreover pushes the demand model to the left (overestimating demand) so providing collapse estimates probably on the safe side. Since the occurrence of global dynamic instability is more probable at higher intensity levels, excluding the IDA-based non-collapse points at smaller intensity levels (i.e., the "light" blue points at the left in Figure 6.13 corresponding to $S_a < \mu_{S_a} - \sigma_{S_a}$) in development of the demand model may not affect accuracy of collapse predictions. Thereby, although this linear demand relation may not be valid for an entire range, it may be appropriate for a limited intensity range, especially near collapse. However, further research is needed to investigate and confirm the misleading and accuracy effects of these extreme cases on collapse prediction.

Using the linear regression tool within the same limited range for S_a, three more other options were considered as well in terms of nonlinear transformation of the data plane given in "V_R and S_a" i.e., taking logarithmic of data or not. Figure 6.14 shows these three options (Figure 6.14b, Figure 6.14c, and Figure 6.14d) together with the developed one above (Figure 6.14a) for the test case of Lignos et al. (2008) subjected to 78 far field-ground motion records. Visual comparisons performed in Figure 6.14 prove the developed model (Figure 6.14a) shows more satisfactory performance in fitting to the data points with an approximate constant variance comparing to other three options. It also seems that taking logarithms of S_a data works better with this linear regression model, because the linear models based on the original S_a data as in Figure 6.14c and Figure 6.14d intersect V_R above zero, indicating a structural demand when S_a equals to zero, which is not realistic. Since earthquake energy is dissipated mostly through damping instead of spring energy at smaller intensities, V_R (i.e., the equivalent velocity ratio of spring energy to earthquake energy) is expected to start at a small intensity level larger than zero as in the models observed in Figure 6.14a and Figure 6.14b.

A practical comparison of efficacy of the demand models for DM given IM can be done by comparing their statistical parameters R^2 and conditional cov, which are given by:

$$R^2 = 1 - \frac{{\sigma^2}_{DM|IM}}{{\sigma^2}_{DM}} \quad and \quad \text{cov} = \frac{\sigma_{DM|IM}}{\mu_{DM}} \tag{6.25}$$

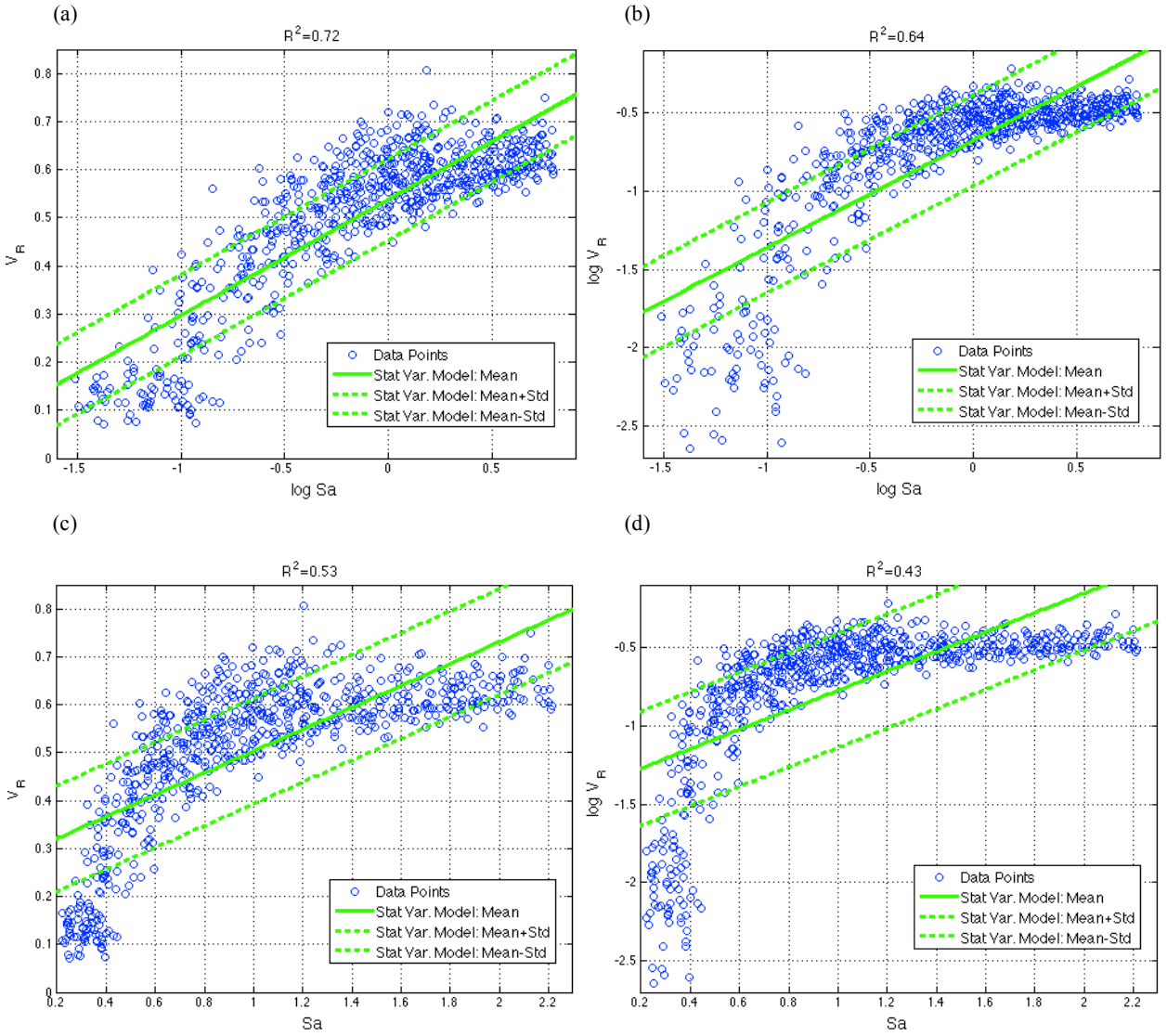

Figure 6.14 Linear regression models between V_R and S_a using a) the logarithms of S_a and original V_R data, b) the logarithms of both V_R and S_a data, c) original data, and d) the logarithms of V_R and original S_a data for the test case of Lignos et al. (2008) subjected to 78 far field-ground motion records.

The statistical parameter R^2 always lies between 0 and 1 while the lower and upper bounds represent no and perfect linear relationship respectively. A summary of these statistical results is provided in Table 6.1. As expected from visual observation in Figure 6.14, the linear model based on the logarithms of S_a and original V_R data (Figure 6.14a) provides smaller cov and larger R^2 values (0.168 and 0.72 respectively) comparing the other models in Figure 6.14. Moreover, the statistical values for this model is compared with the linear demand models based on traditional measure IDR (i.e., maximum inter-story drift ratio) considering both full range and the same limited range for S_a, as seen in Table 6.1. Although IDR based models are found to

provide similar R^2 values, they give more conditional varibility (cov value around 0.4) due to their sensitivity to intensity scaling at higher intensity levels. Therefore, the linear model based on V_R in Figure 6.14a can give more reliable prediction of structural demand and may provide better estimate of collapse probability.

Linear Regression Models	DM	IM	IM Range	R^2	Conditional cov
Figure 6.14a	V_R	log Sa	Limited	0.72	0.168
Figure 6.14b	log V_R	log Sa	Limited	0.64	0.575
Figure 6.14c	V_R	Sa	Limited	0.53	0.218
Figure 6.14d	log V_R	Sa	Limited	0.43	0.723
Figure 6.1	log IDR	log Sa	All	0.76	0.406
Figure 6.1	log IDR	log Sa	Limited	0.61	0.391

Table 6.1 Comparison of several structural demand models for the test case of Lignos et al. (2008) subjected to 78 far field-ground motion records.

6.4.2. *Linear Regression Model with Non-stationary Conditional Variance*

The distribution of data points in Figure 6.14a indicates a variation in the degree of scatter of data points with increasing intensity level. Therefore, linear regression tool with an option of "non-stationary" conditional variance can be applied to improve the demand model developed in previous section. For this purpose, the conditional variance for (6.13) can be described in terms of S_a as:

$$\sigma^2{}_{V_{R_{Demand}}|lnS_a} = \sigma^2 = {\sigma_o}^2 g^2(S_a) \qquad (6.26)$$

where, σ_o is an unknown constant and $g(S_a)$ is a predetermined function of S_a. In this case, V_R given an intensity level $\ln S_a$ then follows a normal distribution with a varying variance $N(\mu_{V_{R_{Demand}}|lnS_a}, \sigma_{V_{R_{Demand}}|lnS_a} = \sigma_o g(S_a))$.

It can be reasonably assumed that the data points in the region of smaller variance should have higher "weights" comparing to ones in the region of larger variance. Then, the weights w can be assigned as inversely proportional to the function $g(lnS_a)$, given by:

$$w = 1/g^2(S_a) \tag{6.27}$$

If w_i is the weight assigned for each sample data pair $\ln S_{a_i}$ and V_{R_i} (where $i = 1, \dots, n$ and n is the number of data points), the total squared error for this regression option and the unknown constant σ_o then become:

$$\Delta^2 = \sum_{i=1}^{n} w_i (V_{R_i} - V_{R_i}')^2 \quad and \quad {\sigma_o}^2 = \frac{\Delta^2}{n-2} \tag{6.28}$$

The total absolute error Δ^2 in (6.28) can be minimized to evaluate the coefficients of the linear regression k_1 and k_2 in (6.13), which are found as (Ang and Tang, 2007):

$$\mathrm{k}_1 = \frac{\sum w_i (\sum w_i \ln S_{a_i} V_{R_i}) - (\sum w_i \ln S_{a_i})(\sum w_i V_{R_i})}{\sum w_i (\sum w_i \ln {S_{a_i}}^2) - (\sum w_i \ln S_{a_i})^2} \tag{6.29}$$

$$\mathrm{k}_2 = \frac{\sum w_i V_{R_i} - \mathrm{k}_1 \sum w_i \ln S_{a_i}}{\sum w_i} \tag{6.30}$$

Since the variance of data points in Figure 6.14a seems to increase as the level of intensity increases, the following expressions are assumed for the functions $g(\mathrm{S_a})$ and w with a coefficient of c larger than zero:

$$g(\mathrm{S_a}) = {\mathrm{S_a}}^c \quad and \quad w = 1/g^2(\mathrm{S_a}) = {\mathrm{S_a}}^{-2c} \tag{6.31}$$

Figure 6.15 shows several linear regression trials with different non-stationary variances (red models) and compares them with the stationary model (green model, which is the model developed in Figure 6.14a) to find the optimal selection for the coefficient c. Note that when c equals to zero, variance becomes constant and the model becomes exactly the same as the stationary model (green models in Figure 6.15); and when c gets larger, so does the variance. It appears that an increase in c pushes the model-mean (trend) to right at lower intensities getting close to data points; and to left at higher intensities providing estimates on safe side for collapse predictions. Although the model with a larger value of c such as 1.0 in Figure 6.15a seems to better fit with the scatter of data points, the increase in variance may underestimate demand at higher intensity levels, thereby may affect the accuracy of collapse prediction. The linear models in Figure 6.15 are transformed to the original data plane of V_R- S_a to better understand the trends of each model. As clearly seen in Figure 6.16a and Figure 6.16b, a value of 1.0 and 0.75 for c

respectively may cause the demand model to have unrealistic small values in demand (0.5~0.6) at higher intensity levels due to increasing variance. As a result, the demand models with a smaller value of c, as in Figure 6.16c (c =0.5) and Figure 6.16d (c =0.25), provide slightly better demands comparing to demand for stationary model. Therefore, these models together with the model based on stationary variance are selected as candidates for the development of collapse fragility relations in the following sections.

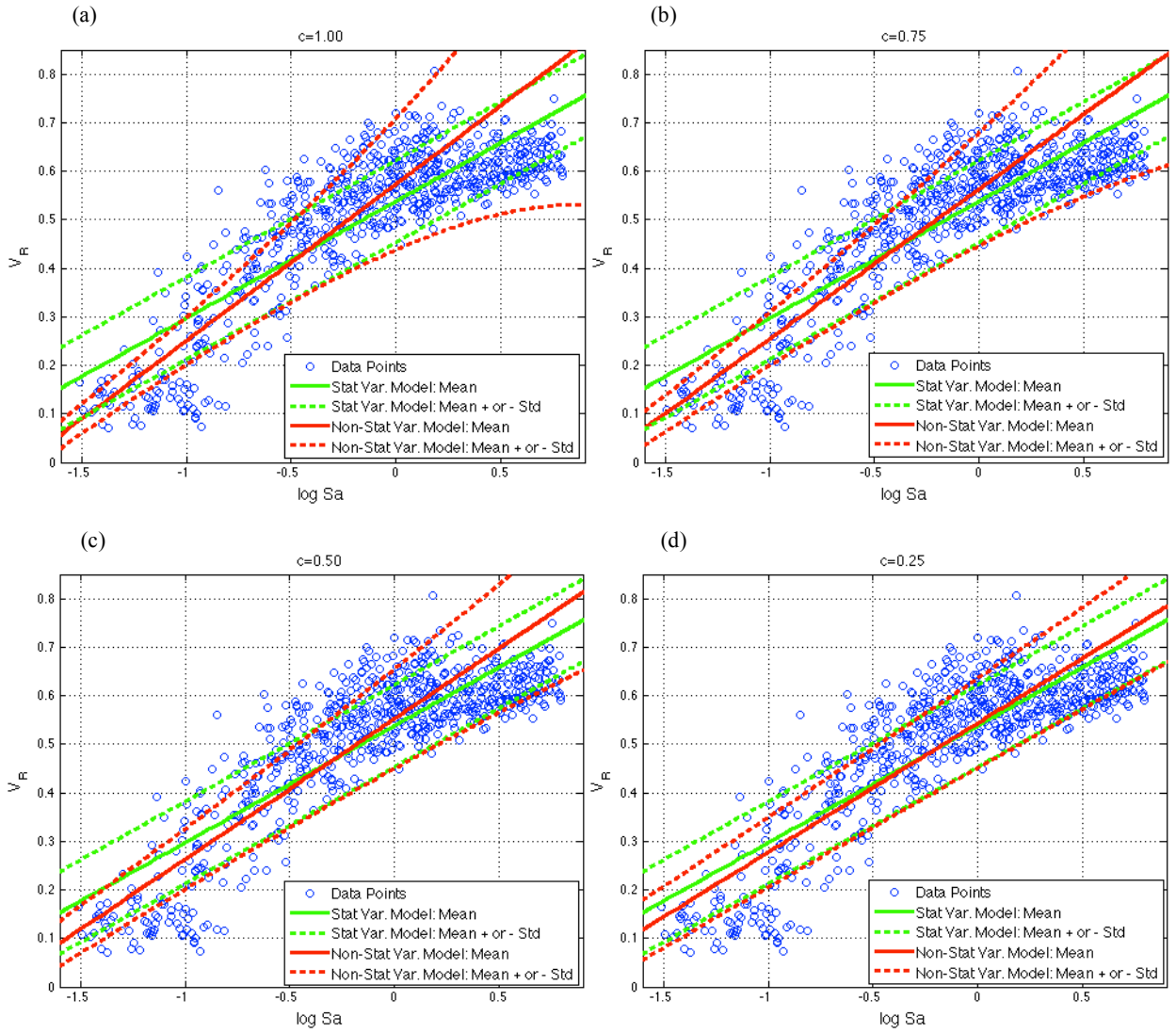

Figure 6.15 The linear regression models with different non-stationary variance between the logarithms of S_a and original V_R data for the test case of Lignos et al. (2008) subjected to 78 far field-ground motion records.

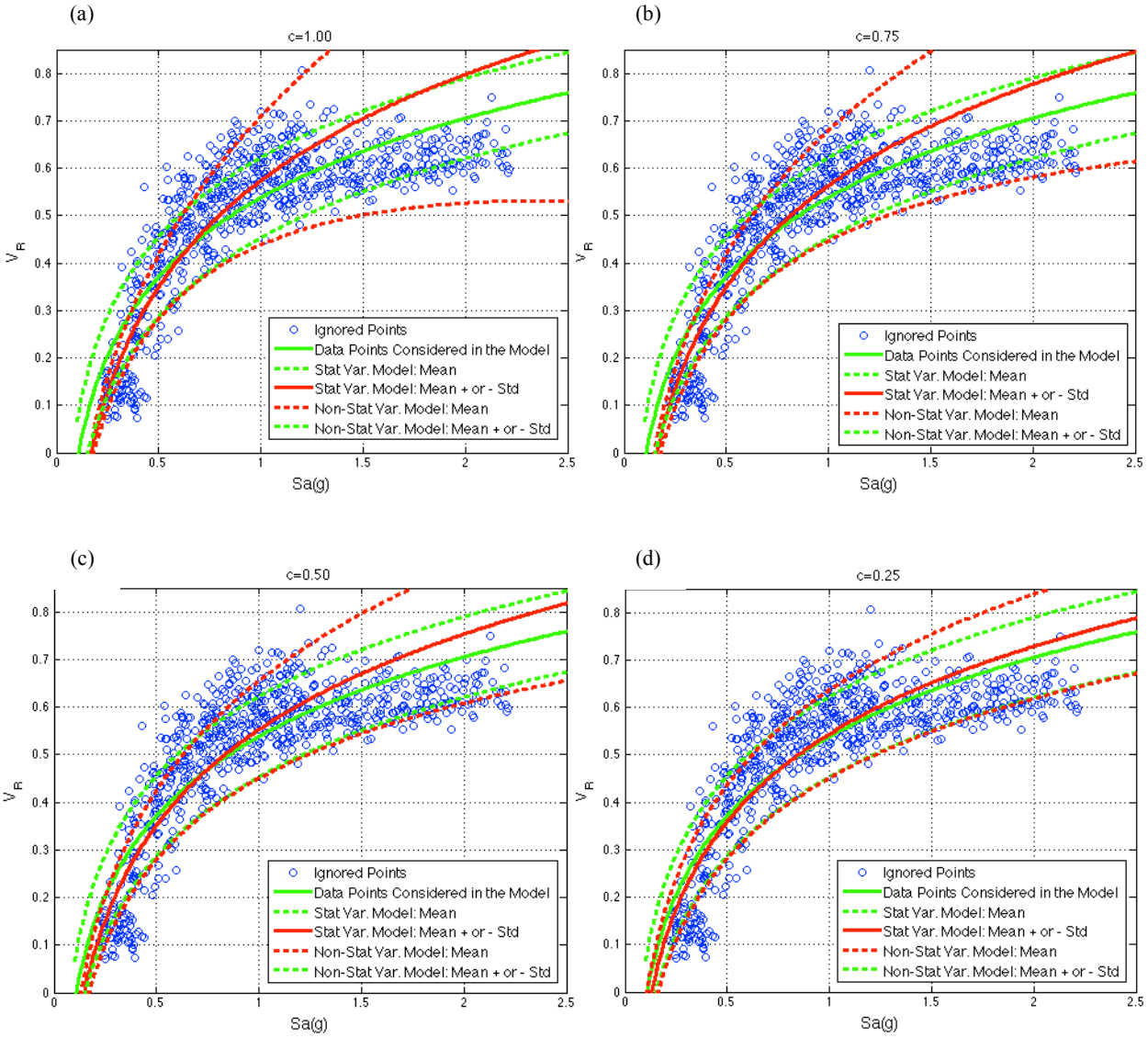

Figure 6.16 Transformation of the linear regression models with different non-stationary variance between the logarithms of S_a and original V_R data onto the original data plane for the test case of Lignos et al. (2008) subjected to 78 far field-ground motion records.

6.5. New Collapse Fragility Models

In Section 6.4, the collapse probabilities are derived for a given collapse capacity level. Since the collapse capacity also has significant uncertainties as shown in Section 6.3, this study develops a DM-based fragility model by considering uncertainty in both seismic demand and seismic

capacity. A demand/capacity framework using energy-based collapse criterion proposed in this study is utilized in the following sections to develop new collapse fragility curves.

As discussed above, efficient and reliable collapse risk assessment requires using more representative global structural responses with a small cov that are robust to scaling sensitivity near collapse. Thereby, rather than using traditional models such as those based on IDR, new capacity (Section 6.3) and demand models (Section 6.4) based on V_R are selected instead to assess new collapse fragility relations. The proposed methodology is demonstrated using the test case study by Lignos et al. (2008) and a ground motion set of 78 records. The developed collapse fragility curves are then compared to other available models.

6.5.1. Development of a New Collapse Fragility Model using Safety Margin.

In a probabilistic manner, structural collapse can be identified in a demand/capacity format considering randomness in both demand and capacity. Therefore, a new model for collapse fragility is developed in this section based on safety margin approach using the most efficient performance measure V_R. In (6.32), safety margin of a structural system can be defined in terms of V_R as the difference between capacity $V_{R_{Capacity}}$ and demand $V_{R_{Demand}}$:

$$M_{V_R} = V_{R_{Capacity}} - V_{R_{Demand}} \tag{6.32}$$

Here, if the safety margin M_{V_R} is a random variable, then probability of collapse becomes the probability of safety margin being less than zero (i.e., demand exceeding capacity) at an intensity level "im":

$$P_C = P(C|IM = im) = P\left(M_{V_R} \leq 0 \middle| IM = im\right) \tag{6.33}$$

Most recent research on collapse assessment use practical IMs such as S_a and *PGA* to use the available attenuation models to assess seismic hazard at a site of interest. Therefore, S_a (elastic spectral acceleration value at first period with 2% damping) was selected here to describe collapse probability. The equation in (6.33) then becomes:

$$P_C = P(C|S_a = s) = P\left(M_{V_R} \leq 0 \middle| S_a = s\right) \tag{6.34}$$

In the previous sections, new collapse capacity and demand models were identified using the equivalent velocity ratio V_R along with S_a for a better description of structural collapse. A normal collapse capacity model was fitted to IDA-collapse capacity data using energy-based collapse criterion in Figure 6.7b. It is found that capacity prediction based on IDA show more dispersion comparing to estimate at original intensities, however still may provide conservative results. Although this evidence is preliminary, collapse capacity based on scaled intensities is still used here, but note that more research is needed to investigate this scaling effect.

In order to find the best demand model using V_R, linear regression analyses were performed considering constant and varying variance as explained in previous sections. Several nonlinear transformations of IDA data were considered, and the best linear fit was obtained by taking logarithms of only S_a. As a result, the normal demand model based on linear regression with stationary variance in Figure 6.14a, and the normal models considering varying variance in Figure 6.15c and Figure 6.15d are found the most efficient ones for a limited range of S_a. Although these models are valid for a limited range, they are found to provide conservative demand at higher intensities near collapse, therefore give collapse estimates on the safe side.

Therefore, using the "normal" collapse capacity and "normal" demand candidate models identified above, a description of conditional joint "normal" distribution of ($V_{R_{Capacity}}$, $V_{R_{Demand}}$) is then required to assess the probability of the failure event $M_{V_R} \leq 0$. However, one can reasonably assume that demand and capacity are statistically independent events at a given intensity level. In any case, if demand and capacity are normal variables, any linear combination of them such as M_{V_R} also becomes a normal random variable.

If structural capacity and demand in terms of V_R given an intensity level ln S_a have the following normal distributions in (6.35) and (6.36) respectively and if they are statistically independent events, then M_{V_R} follows a normal distribution $N\left(\mu_{M_{V_R}}, \sigma_{M_{V_R}}\right)$, where the mean and deviation of M_{V_R}can be assessed as in (6.37) and (6.38) correspondingly:

$$V_{R_{Capacity}} \sim N\left(\mu_{V_{R_{Demand}}|lnS_a}, \sigma_{V_{R_{Demand}}|lnS_a}\right) \quad (6.35)$$

$$V_{R_{Demand}} \sim N\left(\mu_{V_{R_{Capacity}}}, \sigma_{V_{R_{Capacity}}}\right) \quad (6.36)$$

$$\mu_{M_{V_R}} = \mu_{V_{R_{Capacity}}} - \mu_{V_{R_{Demand}}|lnS_a} \quad (6.37)$$

$$\sigma_{M_{V_R}} = \sqrt{\sigma_{V_{R_{Capacity}}}^{\ 2} + \sigma_{V_{R_{Demand}}|lnS_a}^{\ 2}} \quad (6.38)$$

where, mean ($\mu_{V_{R_{Capacity}}}$) and standard deviation ($\sigma_{V_{R_{Capacity}}}$) for the normal capacity model are found as 0.668 and 0.039 respectively in Figure 6.7b. For the linear demand models with non-stationary variance, both mean ($\mu_{V_{R_{Demand}}|lnS_a}$) and deviation ($\sigma_{V_{R_{Demand}}|lnS_a}$) varies with spectral acceleration. At intensity levels of 1g and 2g, the statistics for the linear demand models are obtained in Table 6.2.

Normal Demand Models		c=0.50 Figure 6.15c	c=0.25 Figure 6.15d	c=0 (Stationary) Figure 6.14a
Sa=1g	Mean	0.5527	0.5438	0.5382
	Std	0.1028	0.0926	0.0847
Sa=2g	Mean	0.7533	0.7286	0.7052
	Std	0.1454	0.1101	0.0847

Table 6.2 Comparison of statistics of linear demand models at elastic spectral acceleration intensity levels of 1g and 2g for the test case of Lignos et al. (2008) subjected to 78 far field-ground motion records.

Using the statistics information in Table 6.2, probability density functions for capacity and demand models are compared visually in Figure 6.17. Although the difference between demand models is little at the intensity level of 1g, it increases at the level of 2g as expected. If one considers the distributions for capacity and demand in Figure 6.17, the area under the distribution curves for both coincide indicates a nonzero probability of collapse. In this case, it is noted that it is "highly" likely that the structural collapse occurs at the intensity level of 2g for all demand models. To quantify this probability of collapse, one needs to evaluate the normal cumulative distribution of M_{V_R} at the given spectral elastic acceleration level of $\ln s$:

$$P_C = P\left(M_{V_R} \leq 0 \middle| \ln S_a = \ln s\right) = F_{M_{V_R}|\ln S_a}(0 \,|\, \ln s) \quad (6.39)$$

$$P_C = \boldsymbol{\Phi}\left[-\frac{\mu_{M_{V_R}}(S_a)}{\sigma_{M_{V_R}}(S_a)}\right] \quad (6.40)$$

Using the expression in (6.40), the probability for collapse using different demand models is obtained in Figure 6.18 at the intensity levels of 1g and 2g. Structural collapse occurs when the safety margin becomes less than zero. In this case, the probabilities of collapse are evaluated around 0.10 and 0.70 for all demand models at the intensity levels of 1g and 2g respectively.

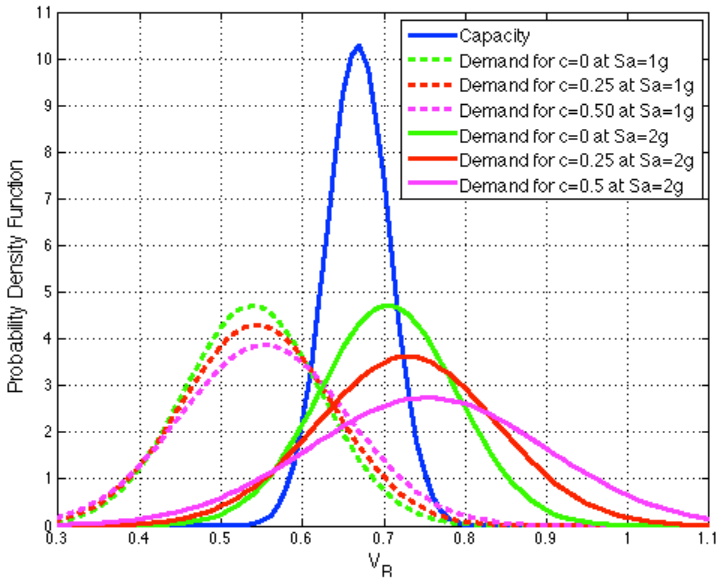

Figure 6.17 Probability density functions for capacity and demand models obtained for the test case of Lignos et al. (2008) subjected to 78 far field-ground motion records.

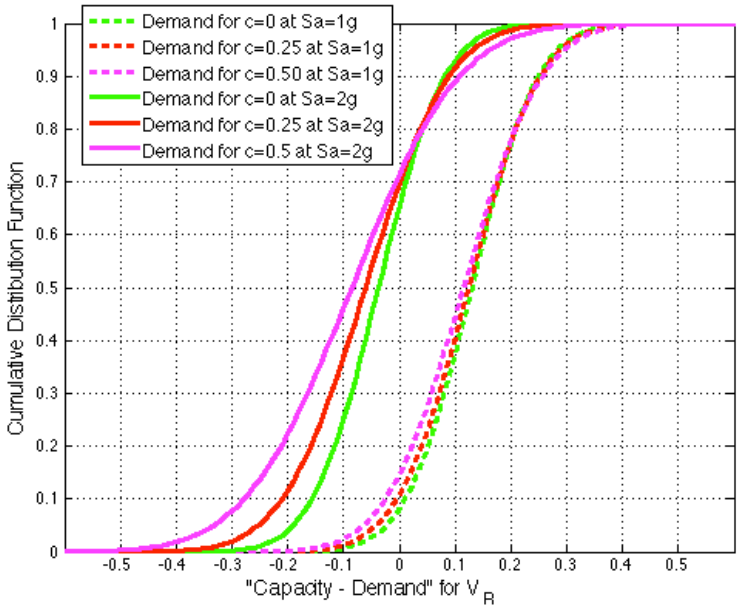

Figure 6.18 Cumulative distribution functions for safety margin using different demand models obtained for the test case of Lignos et al. (2008) subjected to 78 far field-ground motion records.

If one evaluates (6.40) for a range of spectral acceleration values, collapse fragility relations can be obtained. Figure 6.19 compares the new collapse fragility models using the three different demand models: stationary variance model (c=0) and non-stationary variance models (c=0.25 and 0.50). Figure 6.20 provides a closer look at the same fragility models until a level of 2.5 g for elastic spectral acceleration. All fragility models are obtained for the test case of Lignos et al. (2008) subjected to 78 far field-ground motion records using energy-based collapse criteria. It seems that although the linear demand model with a non-stationary variance coefficient (c) of 0.5 (pink curve) shows little higher probability of collapse at first, it starts to give smaller values after 2.2 g comparing the other models, and even does not converge to 1.0 at higher intensities because of increasing variance existed in the model. This point can be more clearly seen in Figure 6.21a, which provides the demand model for c=0.5. Therefore, this indicates that this model with c=0.5 may not be a good choice to describe collapse fragilities.

On the other hand, the fragility model based on demand with c=0.25 (red curve) seems to give reasonable results, converging to 1.0 at the end. With a little larger fragility slope at first, this fragility model gives less variance until a level of 2.2 g for spectral acceleration comparing to the one based on stationary demand model (green curve) as seen clearly in Figure 6.20. Therefore, it provides a little larger collapse probabilities until 2.2g, which can be also seen from the trend (red curve) in Figure 6.21b. Therefore this model can be a better selection with slight difference to describe collapse probability of this specific structure in a more reliable way.

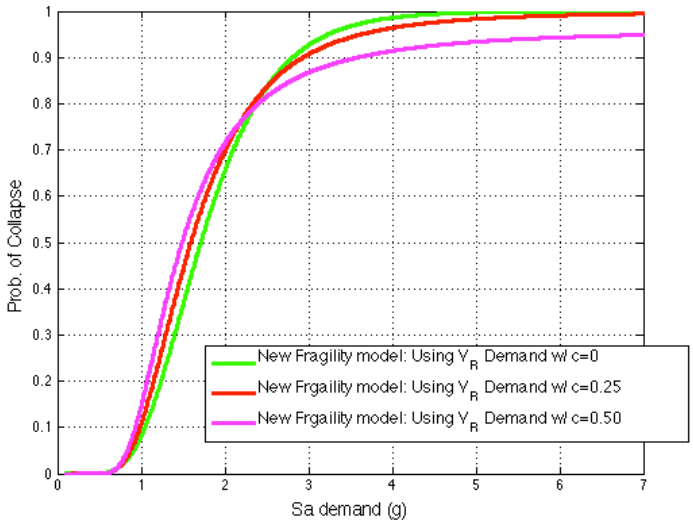

Figure 6.19 Collapse fragility relations obtained by energy-collapse criteria for the test case of Lignos et al. (2008) subjected to 78 far field-ground motion records.

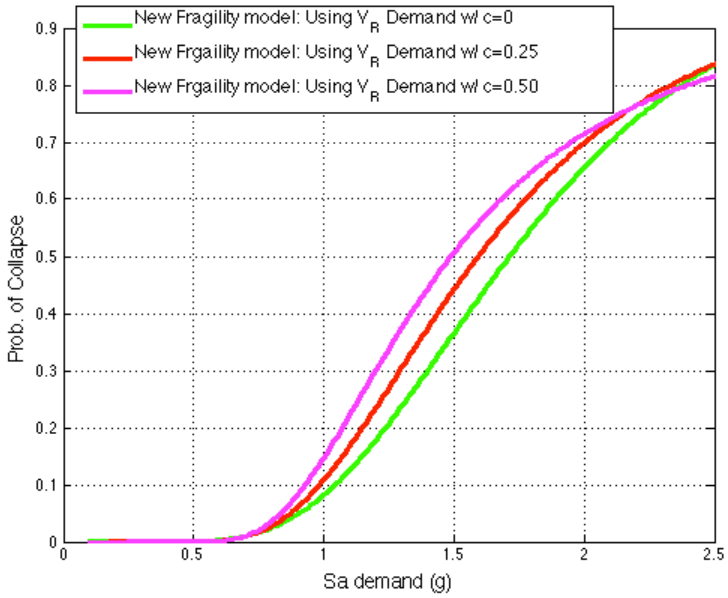

Figure 6.20 A larger version of collapse fragility relations obtained by energy-collapse criteria for the test case of Lignos et al. (2008) subjected to 78 far field-ground motion records.

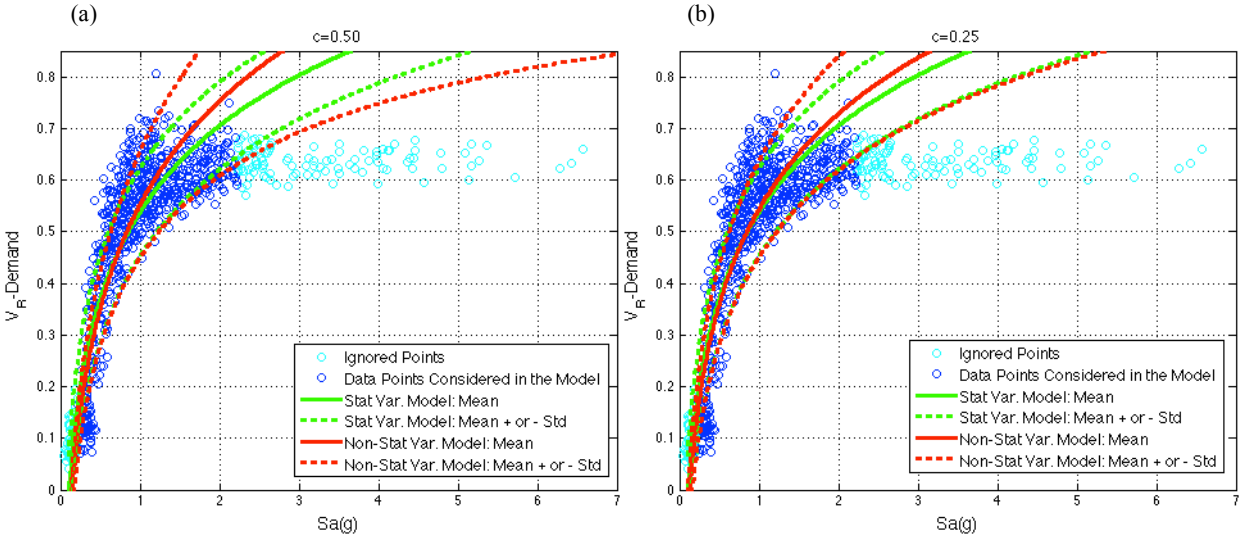

Figure 6.21 The linear demand models used in collapse fragilities for the test case of Lignos et al. (2008) subjected to 78 far field-ground motion records.

Sensitivity of structural demand and capacity to scaling effect at higher scaled intensities was proved previously. Therefore, if IDA-based no-collapse points indicated as “light blue circles” in Figure 6.21b had been included into the development of demand model, it might affect the

accuracy of collapse predictions due to unrealistic no-collapse points at higher intensity levels, pushing the structural demand down, therefore giving unsafe collapse predictions. Although the this demand model is developed for a limited intensity range, collapse fragility relations based on this demand option can be reliable and appropriate especially near collapse. Thus, this model option is selected for further study in the following section.

6.5.2. Comparison of New Collapse Fragility Model with Traditional Models

Often a lognormal CDF of the elastic spectral acceleration "*Sa*" is employed into the empirical fragility curves to evaluate collapse probabilities as a function of intensity for the given type of structure (Ibarra and Krawinkler, 2005; Bradley and Dhakal 2008; Ghafory-Ashtiany et al. 2011). This method is called IM-based fragility model based on *Sa*, which was studied previously in Figure 6.3 for the test case of Lignos et al. (2008). In this figure, 78 far field-ground motion records were considered to get IDA-based collapse point for each record using energy-collapse rule (i.e, gravity energy far-exceeding earthquake energy).

Another common approach to get collapse fragility curves is the 2000 SAC/FEMA methodology that adopts a DM-based fragility procedure using interstory-drift ratio "IDR" in both demand and capacity assessment. This methodology uses a power law to describe the relationship between structural demand in IDR and intensity in *Sa* (FEMA, 2000; Cornell et al., 2002). This fragility model was also investigated previously using energy-rule, and demand and capacity models based on IDR were assessed for the test case of Lignos et al. (2008) subjected to 78 far field-ground motion records in Figure 6.2 and Figure 6.3 respectively.

A new collapse fragility model was developed in previous section based on the demand/capacity format described in V_R (red curve in Figure 6.19) using energy-collapse rule. In this section, this new fragility model is then compared to these traditional fragility models described above in two ways: first, using the energy based collapse criterion for all models; second, using traditional rules (such as IM-rule and DM-rule) for traditional models and energy-rule for the new model.

Figure 6.22 compares the new fragility model (red curve) with common approaches such as "IM-based fragility model using lognormal CDF of *Sa* (blue curve)" and "DM-based fragility model using IDR (black curve)". All fragility models were obtained for the test case of Lignos et al.

(2008) subjected to 78 far field-ground motion records using energy-based collapse criteria. As seen clearly, the DM-based fragility model using IDR (black curve) underestimates so much because of its large dispersion amount (a conditional cov of 0.406 was found in Table 6.1 for the demand model based on IDR) as well as its high sensitivity to intensity scaling near collapse, thereof, does not work for the energy-collapse rule. As a note, the same method for the black curve is assessed for the maximum roof drift ratio (D_R) as well, which gave almost the same black curve obtained for IDR. On the other hand, IM-based fragility model using *Sa* (blue curve) seems to slightly overestimate collapse probabilities in general comparing to the new fragility model (red curve). The reason of this slight overestimate can be due to not accounting for uncertainty in seismic demand in the development of the collapse fragility (blue curve).

The new fragility model uses V_R as a more representative measure of global performance with small cov and less scaling sensitivity near collapse. This new model also integrates uncertainties in both capacity and demand due to variety of structural and ground motions parameters. If one underestimates these uncertainties, then less conservative collapse predictions are expected in general. Thus, the new model (red curve) can give more reliable and accurate collapse predictions comparing to other approaches in Figure 6.22.

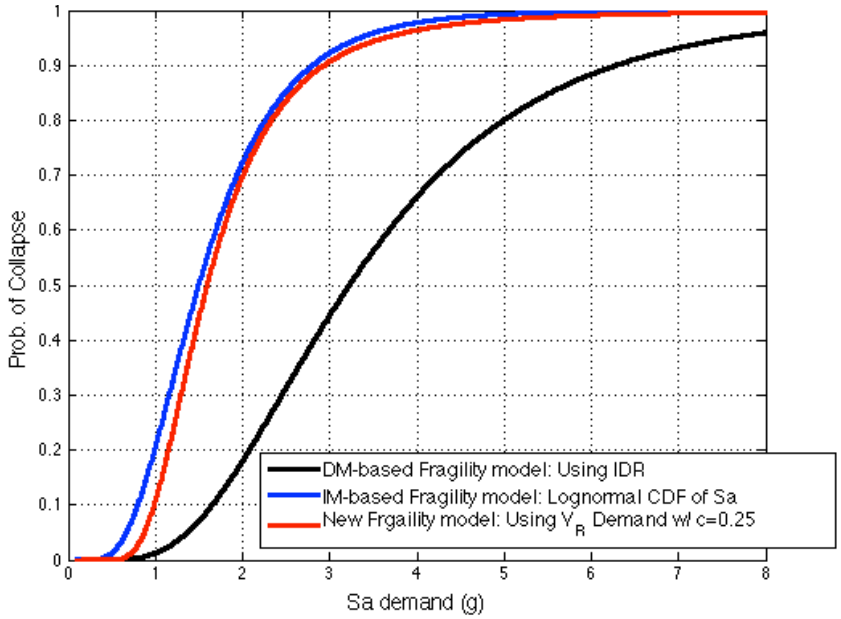

Figure 6.22 Comparison of new collapse fragility to traditional fragility relations obtained by energy-collapse criteria for the test case of Lignos et al. (2008) subjected to 78 far field-ground motion records.

Figure 6.23 shows the collapse data for IDR and *Sa* obtained for different rules from IDA curves for the test case of Lignos et al. (2008) subjected to 78 far field-ground motion records: Energy-rule (i.e, $E_G >> E_{EG}$), IM-based rule (i.e., exceedance of 20% of the initial IDA slope), and DM-based rule (i.e., exceedance of 10% of the total building height). In Figure 6.24, the new fragility model using energy-rule (red curve) is then compared with the common fragility approaches using traditional rules: "IM-based fragility model using lognormal CDF of *Sa* with DM-rule (blue curve) and IM-rule (dashed blue curve); and "DM-based fragility model using IDR with DM-rule (black curve) and IM-rule (dashed black curve)". As seen in Figure 6.23, there is a large difference between collapse points obtained by the three collapse rules. It is important to indicate that energy-rule assesses the collapse capacity at the maximum intensity before the structure loses its dynamic instability. However, DM-rule is based on a pre-determined threshold value (ignoring variance in capacity), while IM-rule is based on a simple deterministic rule using shape of IDA curves, which can be chaotic due to possible hardening in structural behavior. Therefore, these traditional rules have been found not sufficient to identify when and how a structure collapses under the effect of variable dynamic loads.

In Figure 6.24, IM-based fragilities using DM-rule and IM-rule (blue and dashed blue curves respectively) are found to overestimate the collapse probability comparing to the new fragility model (red curve). This may be because of IM-based fragility not accounting uncertainties in structural demands. Here, IM-based fragility using IM-rule overestimates more for $Sa < 2.5$g because in this region IM-rule determines collapse capacity data at points much lower than the ones by the other rules (see Figure 6.23). On the other hand, DM-based fragilities with DM-rule (black curve) or with IM-rule (dashed black curve) underestimates collapse probability in general.

In Figure 6.25 and Figure 6.26, similar comparison can be made for the demand and collapse data based on maximum drift ratio (D_R) and *Sa* obtained by the three collapse rules from IDA curves for the test case of Lignos et al. (2008) subjected to 78 far field-ground motion records. In this case, both IM-based fragility models (blue and dashed blue curves) overestimate again with a slight difference comparing to the ones in Figure 6.24, but both DM-based fragility models (black and dashed black curves respectively) underestimate the collapse predictions more according to the new fragility model (red curve). Therefore, it is noteworthy that both IM-rule and DM-rule are sensitive to the chosen damage measure used in assessment of IDA curves. On

the other hand, new energy rule depends the actual occurrence of dynamic instability that makes it more reliable option to be employed in collapse assessment of structures.

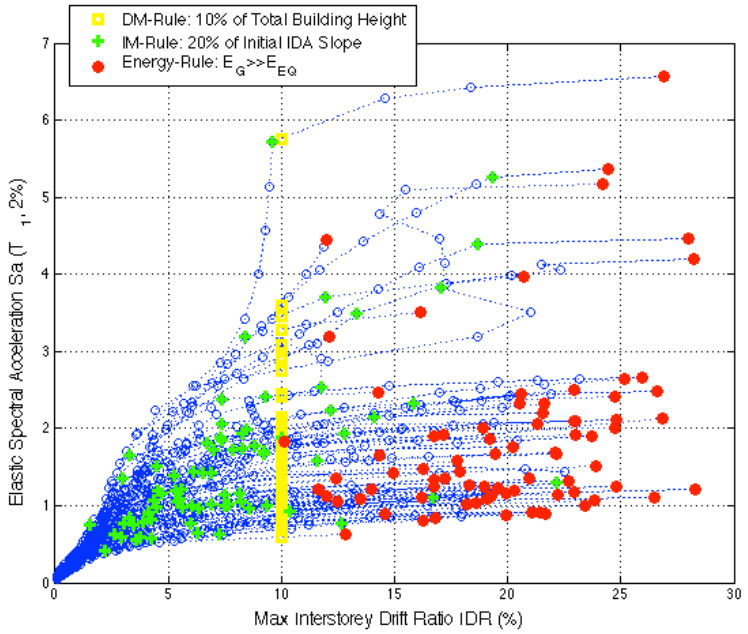

Figure 6.23 Comparison of collapse data for *Sa* and IDR obtained by different collapse rules for the test case of Lignos et al. (2008) subjected to 78 far field-ground motion records.

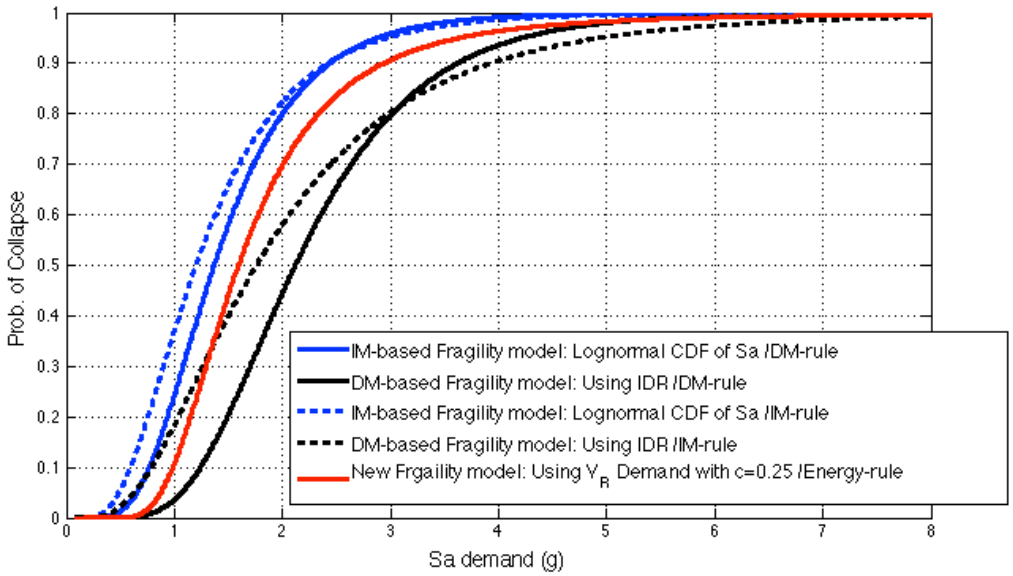

Figure 6.24 Comparison of new collapse fragility by energy-rule to traditional fragility relations by IM-rule and DM-rule based on IDA data for *Sa* and IDR obtained for the test case of Lignos et al. (2008) subjected to 78 far field-ground motion records.

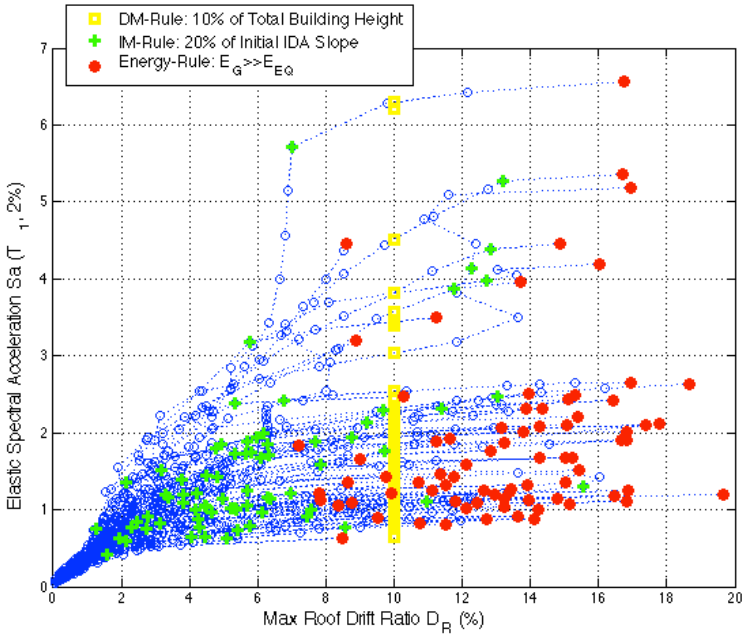

Figure 6.25 Comparison of collapse data for *Sa* and D_R obtained by different collapse rules for the test case of Lignos et al. (2008) subjected to 78 far field-ground motion records.

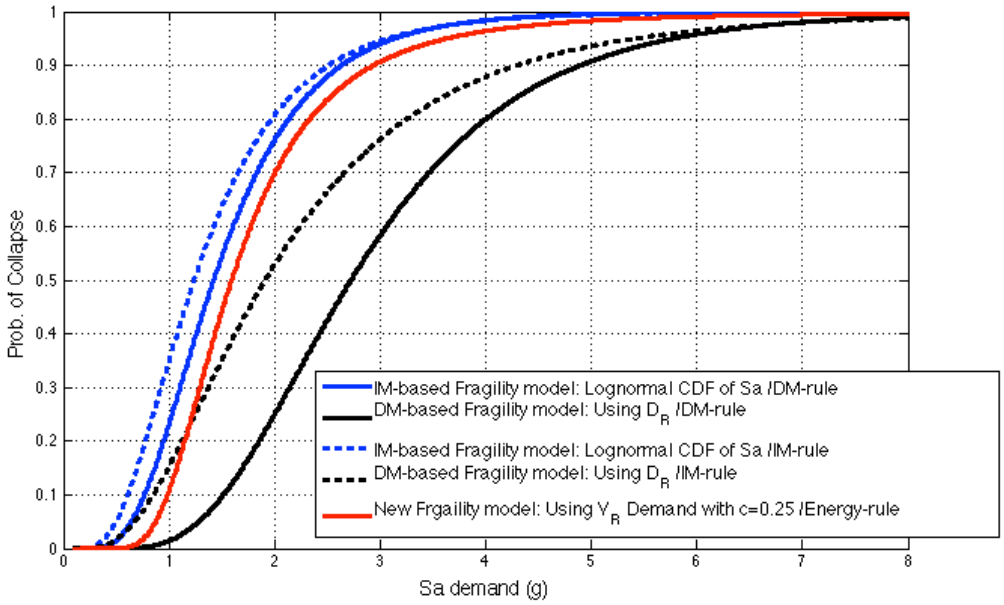

Figure 6.26 Comparison of new collapse fragility by energy-rule to traditional fragility relations by IM-rule and DM-rule based on IDA data for *Sa* and D_R obtained for the test case of Lignos et al. (2008) subjected to 78 far field-ground motion records.

6.5.3. Enhanced Collapse Fragility Model

Baker and Cornell (2005) suggested to use a vector-valued IM, e.g., in the form of (S_a, ε) to represent the seismic hazard for a building. ε is a measure between S_a of the ground motion considered and the predicted S_a from the attenuation relationship for a seismic hazard level. Haselton (2006), Zareian and Krawinkler (2007) indicate that, by using a vector-valued IM (S_a, ε) instead of using S_a only, one can reduce epistemic variability in estimation of seismic hazard.

Similarly, the concept of vector-valued IM was investigated here to enhance the fragility models presented in previous sections, especially those based on a linear demand model with stationary variance (green curve in Figure 6.19) assuming that more information about ground motion characteristics is available. One can then evaluate the probability of structural collapse at a given intensity level of S_a and a secondary intensity measure.

Several multi-linear regression analyses are performed on IDA-data obtained by energy-collapse rule to try different secondary IM candidates in Table 5.5 and identify the best combinations with the smallest conditional cov. However, as seen in Table 6.3, cov for numerous regression trials (0.143~0.168) was not improved much, comparing to the originally proposed demand model with a cov value of 0.168 (see Table 6.3). Therefore, the correlation of coefficients were studied in Table 6.3 to find the most unrelated secondary measure to the parameters already used in the original regression model (i.e, V_R and S_a).

The index $T_{v,strong}$, which is average period between two zero-crossings in the strong part of accelerogram, was found to be best candidate among the indices in Table 6.3, which is another unique property that can represent damage potential of the structure**.** The strong part of accelerogram is determined by the interval between instants where 5% and 95% of the total integral of square of accelerogram are obtained (Trifunac and Brady, 1975). The linear regression model with stationary variance then becomes:

$$V_R{}' = \mathrm{k}_1 \ln S_a + \mathrm{k}_2 \ln T_{v,strong} + \mathrm{k}_3 + \sigma\varepsilon \qquad (6.41)$$

$$\mu_{V_{R\,Demand}|ln\mathrm{S_a}} = E[V_R{}'] = \mathrm{k}_1 \ln S_a + \mathrm{k}_2 \ln T_{v,strong} + \mathrm{k}_3 \qquad (6.42)$$

$$\sigma^2_{V_{R_{Demand}}|lnS_a} = Var[V_R{}'] = \sigma^2 \qquad (6.43)$$

Demand IMs (in log)	Correlation coeff. with Demand V_R	Correlation coeff. with Demand Sa(T_1,2%) (in log)	Conditional linear reg. cov
max A_v	0.853	0.811	0.142
Sv_{ave}(5%)	0.834	0.777	0.143
Sd(T_1,5%)	0.888	0.976	0.144
Sa(T_1,5%)	0.888	0.976	0.144
SI(2%)	0.812	0.743	0.145
Sa_{ave}(5%)	0.787	0.711	0.146
Sd_{ave}(5%)	0.786	0.710	0.146
I_M(2%)	0.012	0.292	0.149
PGV	0.729	0.642	0.150
v_{rms}	0.697	0.608	0.152
Pv	0.697	0.608	0.152
I_F	0.681	0.604	0.154
I_M(5%)	0.024	0.257	0.155
Iv	0.618	0.552	0.158
$T_{v,\,strong}$	0.097	-0.092	0.159
$f_{v,\,strong}$	-0.097	0.092	0.159
$v_S{}^2$	-0.182	-0.011	0.159
v_S	-0.182	-0.011	0.159
v_{sq}	0.611	0.551	0.159
v_{rs}	0.611	0.551	0.159
a_{rms}	0.792	0.817	0.159
Pa	0.792	0.817	0.159
Ic	0.798	0.835	0.160
PGA	0.773	0.798	0.160
PGV/PGA	-0.005	-0.177	0.161

Demand IMs (in log)	Correlation coeff. with Demand V_R	Correlation coeff. with Demand Sa(T_1,2%) (in log)	Conditional linear reg. cov
a_{sq}	0.780	0.821	0.162
a_{rs}	0.780	0.821	0.162
AI	0.780	0.821	0.162
PGD	0.459	0.387	0.162
$T_{v,\,total}$	0.103	-0.038	0.162
$f_{v,\,total}$	-0.103	0.038	0.162
Ia	0.751	0.786	0.163
Sv(T_1,5%)	0.854	0.968	0.163
CAV	0.518	0.478	0.163
Id	0.410	0.349	0.164
d_{rms}	0.435	0.380	0.164
Pd	0.435	0.380	0.164
P_D	0.599	0.592	0.164
Sv(T_1,2%)	0.826	0.991	0.164
Sd(T_1,2%)	0.850	1.000	0.165
d_{sq}	0.385	0.348	0.165
d_{rs}	0.385	0.348	0.165
CAA	0.684	0.731	0.165
CAD	0.349	0.313	0.166
v_T	-0.094	-0.044	0.167
$v_T{}^2$	-0.094	-0.044	0.167
t_S	-0.131	-0.094	0.167
t_T	-0.035	-0.097	0.167
Sa(T_1,2%)	0.849	1.000	0.168
t_{45}	-0.066	-0.072	0.168

Table 6.3 Correlation coefficients between logarithms of intensity demands and structural demand V_R as well as between logarithms of intensity demands and logarithms of *Sa* demands, shown in the order of minimum to maximum conditional cov obtained from multi-linear regression analysis (Note that blue mark indicates ρ ≤0.1 and pink mark indicates the originally proposed model).

Figure 6.27 shows the conditional collapse probability of the test case study by Lignos et al. (2008) as a function of S_a at four different values for $T_{v,strong}$. All four models have the same dispersion amount (a deviation value of 0.0889) but varying median collapse probability, as expected from (6.42) and (6.43). Although the reduction in dispersion is not much (little less than the dispersion of original model which has a deviation value of 0.0932), the conditional mean is apparently affected. As $T_{v,strong}$ gets smaller, the average zero-crossing period of the earthquake

ground motion decreases so does the probability of collapse. The green curve with a $T_{v,strong}$ value of 0.15 s was found to be very close to the originally developed collapse fragility model (green curve) because of the mean value of $T_{v,strong}$ being around 0.153 s. Effect of $T_{v,strong}$ on the fragility model gets decreasing as the values decreases, but becomes significant on the collapse probability as the value gets close to the structural first dominant period, which is 0.44 sec.

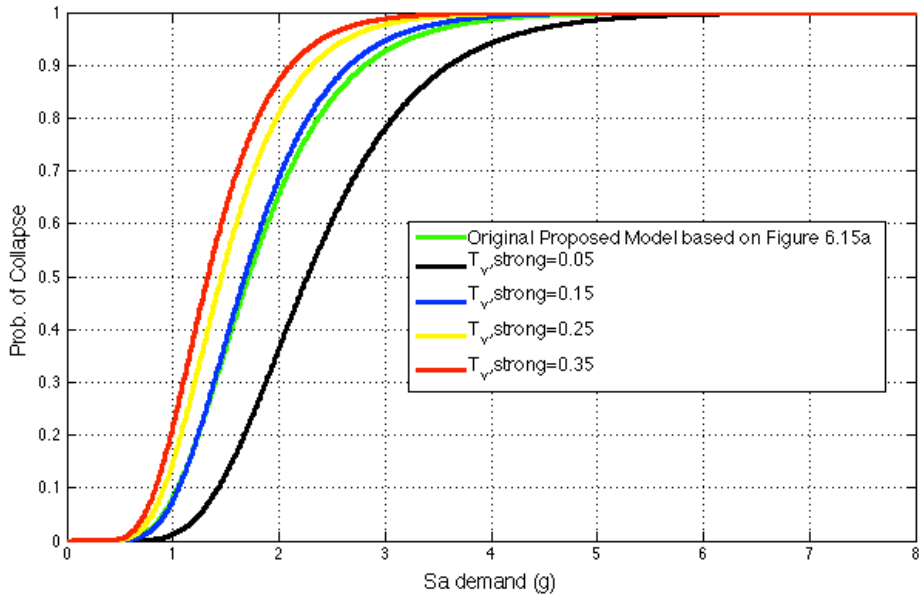

Figure 6.27 Enhanced collapse fragility relations at four different values of $T_{v,strong}$ (s) using energy-collapse criterion for the test case of Lignos et al. (2008) subjected to 78 far field-ground motion records.

Moreover, conditional collapse fragility contours are obtained for the given two conditions of ground motions considered in the collapse assessment. For example, Figure 6.28 represents the same information in Figure 6.27 with a larger range for $T_{v,strong}$. Similarly, fragility contours in Figure 6.29 are provided for maximum incremental velocity ($\max A_v$), which is the maximum area between two zero-crossings in square of ground motion acceleration time history. This index shows impulsive characteristics of ground motion, therefore may indicate the damage potential of structure more comparing to $T_{v,strong}$ as proved by the strong correlation to damage parameters obtained in Table 5.12. Sensitivity of $\max A_v$ to S_a (i.e., degree of correlation) can be also observed by the gradual changes between two contours when compared to rapid changes for $T_{v,strong}$ in Figure 6.28. This is the reason why $\max A_v$ gives the smallest conditional cov in

Table 6.3 when used as the second condition in the multi-linear regression model.

Since most of seismic hazard relations are obtained using peak parameters of ground motions such as PGA, PGV, and PGD in addition to S_a, the collapse fragility contours for these measures as a second condition are evaluated as well in Figure 6.30, Figure 6.31, and Figure 6.32 respectively. Therefore, one can estimate probability of collapse easily from these contours for this specific structure when more information about ground motions are available. Unlike the fragility contours for PGA and PGV, the ones for PGD mostly seem parallel to y-axis, indicating less correlation to Sa. Therefore, PGD seems to give more unique information about the ground motion characteristics comparing to PGA and PGV.

In summary, integrating the available information about ground motion characteristics into collapse fragility models may decrease the dispersion (i.e., slope of fragility curve) due to record-to-record variability, which in turn corresponds to a reduction in uncertainty level associated to collapse probability computation. Collapse assessment of structures then requires fewer non-linear analysis and less ground motions to estimate collapse probability.

However, as in the case of $T_{v,strong}$ in Figure 6.27, the reduction of dispersion in fragility model due to addition of second intensity measure may be sometimes minimal but its impact on fragility analysis may still be significant because of varying conditional mean. This indicates high sensitivity of fragilities to uncertainties in selected ground motion intensity parameters used in the collapse assessment. Therefore, effect of variability in ground motion records on collapse assessment is explored more in Chapter 7 by developing several ground motion subsets for a selected measure of ground motion severity.

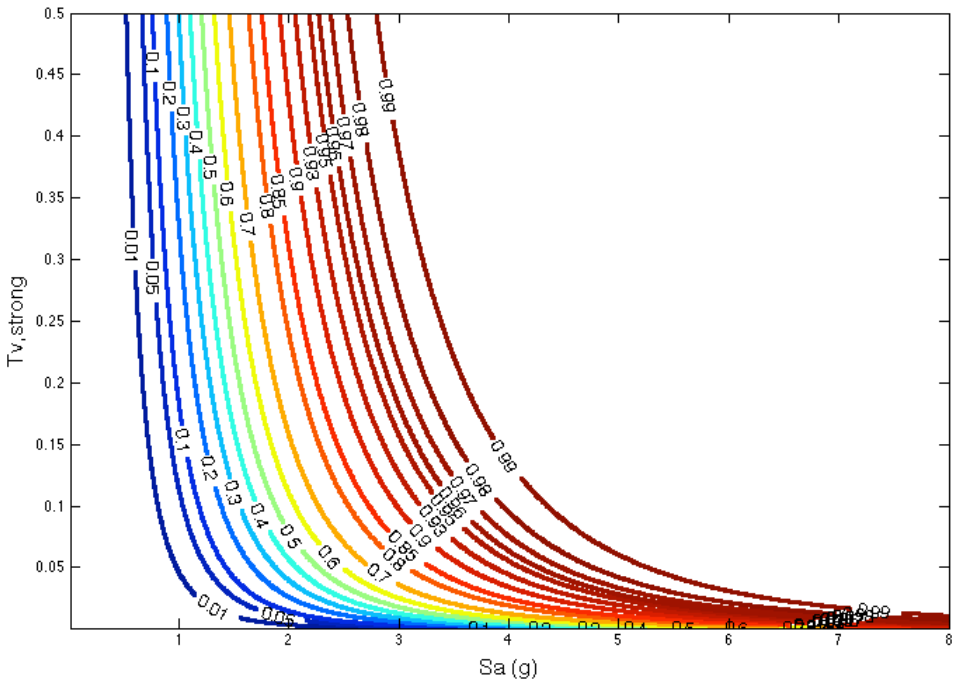

Figure 6.28 Collapse fragility contours for $T_{v,strong}$ (s) and S_a (g) using energy-collapse criterion for the test case of Lignos et al. (2008) subjected to 78 far field-ground motion records.

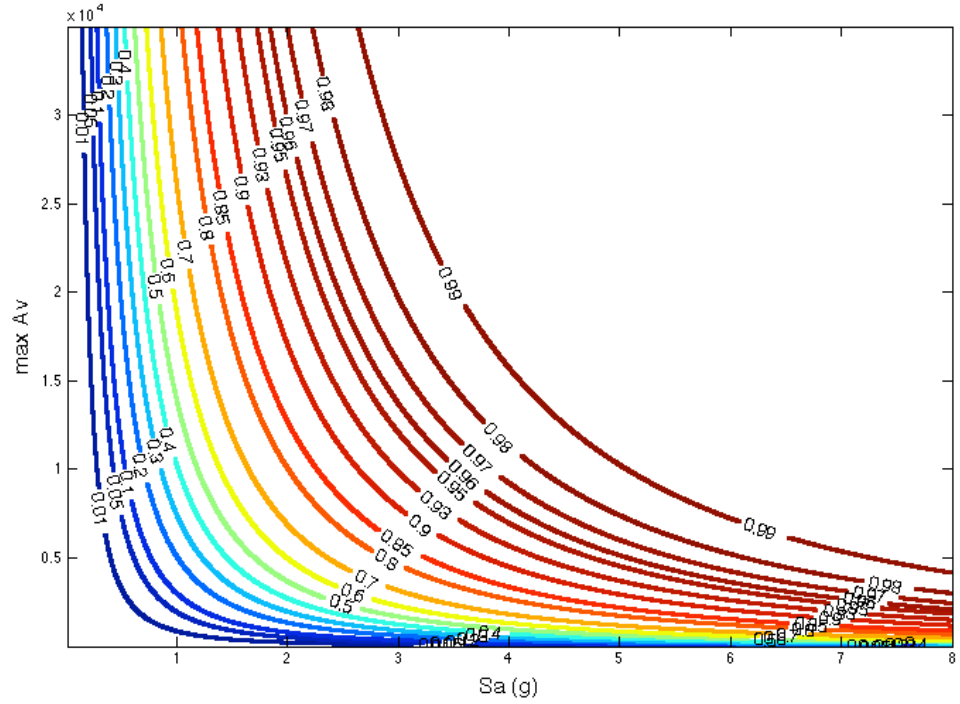

Figure 6.29 Collapse fragility contours for max Av (in^2/s^3) and S_a (g) using energy-collapse criterion for the test case of Lignos et al. (2008) subjected to 78 far field-ground motion records.

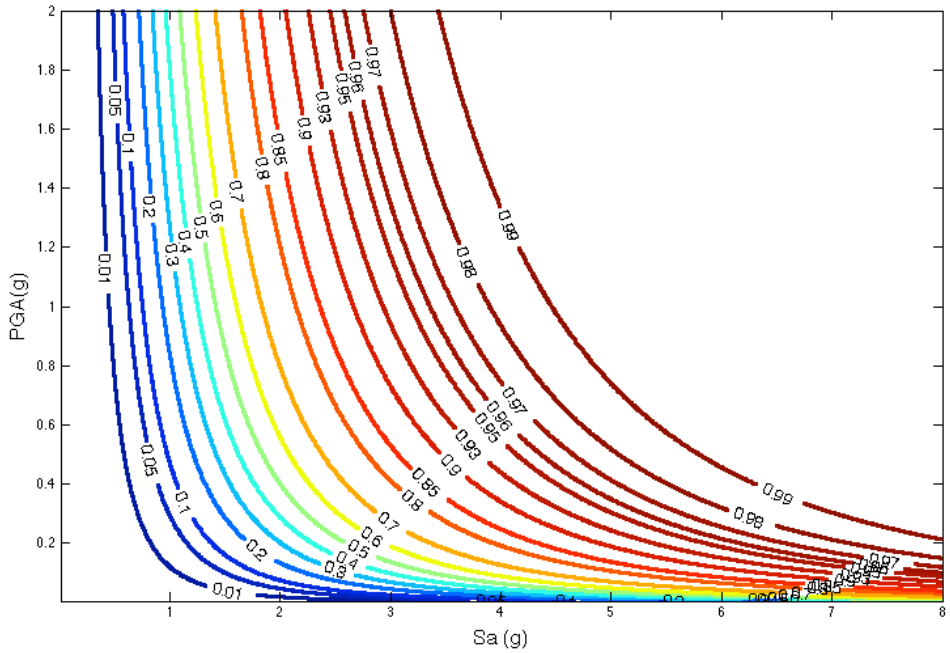

Figure 6.30 Collapse fragility contours for PGA (g) and S_a (g) using energy-collapse criterion for the test case of Lignos et al. (2008) subjected to 78 far field-ground motion records.

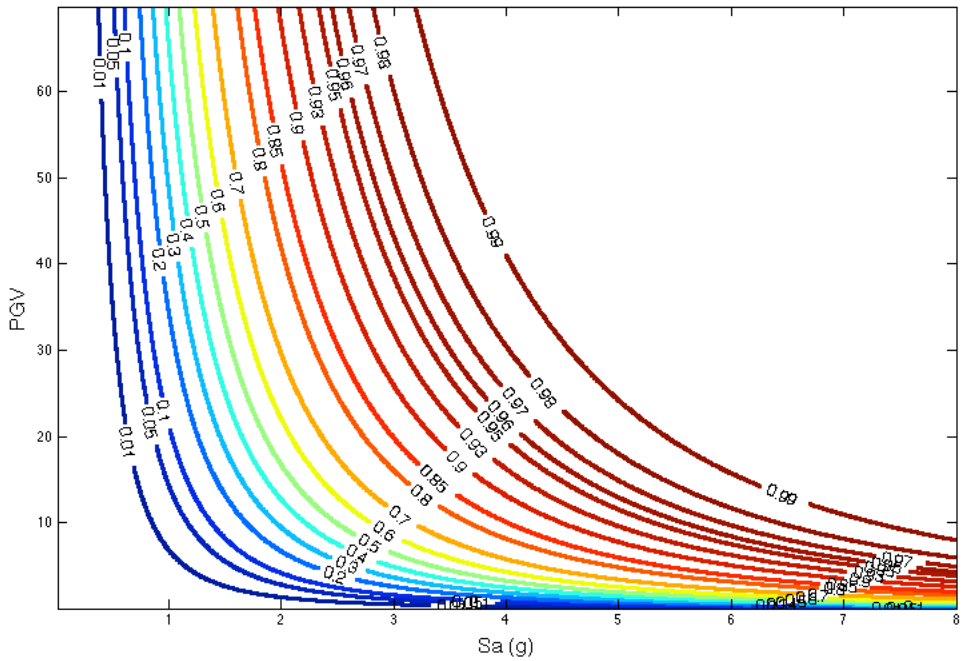

Figure 6.31 Collapse fragility contours for PGV (in/s) and S_a (g) using energy-collapse criterion for the test case of Lignos et al. (2008) subjected to 78 far field-ground motion records.

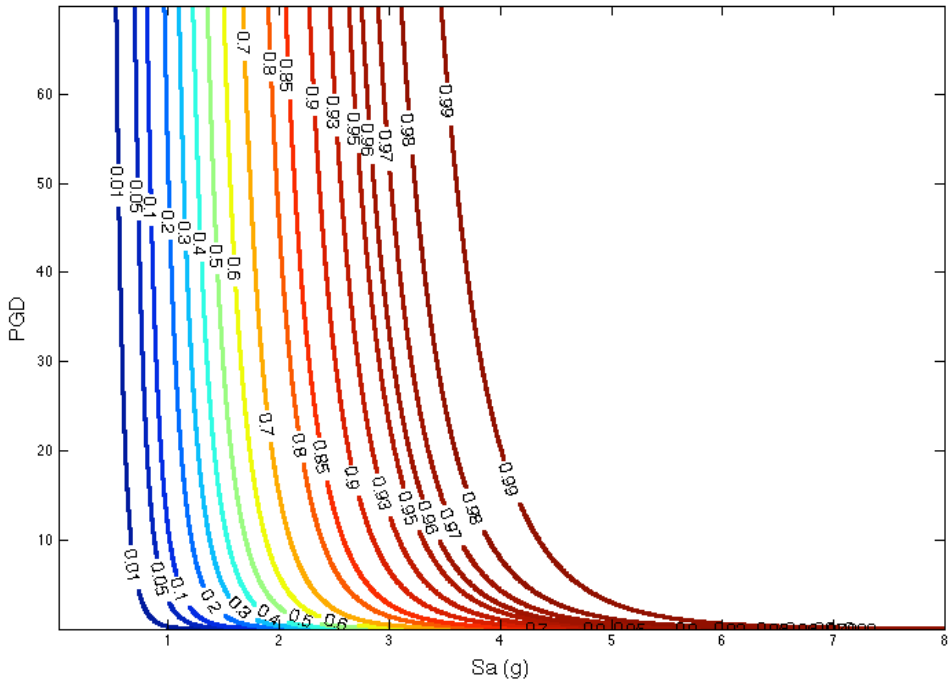

Figure 6.32 Collapse fragility contours for PGD (in) and S_a (g) using energy-collapse criterion for the test case of Lignos et al. (2008) subjected to 78 far field-ground motion records.

7. PARAMETRIC STUDY ON COLLAPSE FRAGILITY

The focus of this chapter is to investigate the effect of earthquake characteristics and structural parameters on the collapse capacity of steel frame structures under cyclic loading for the purpose of estimating and improving structural reliability against collapse. To this end, several nonlinear dynamic analyses are performed for the validated test case study of Lignos et al. (2008) using the far-field set of ground motions by Haselton and Deierlein (2007). The collapse data obtained using energy based-collapse criteria are used to study the effect of parameters on collapse fragility relations.

7.1. Effect of Structural Model Parameters on Collapse Assessment

During the analytical model adjustment of three case studies in Chapter 3, it was observed that global and local behaviors of structure can be very sensitive to structural model properties especially at the collapse level of ground motion intensity. A small change in the amount of strain hardening/softening or Rayleigh damping on the analytical model may change the collapse behavior significantly. For example, see Figure 3.9 and Figure 3.10. Such sensitivity was also observed for all cases in which the models were developed with linear or nonlinear geometry transformations especially at the point where the structure starts to lose stability. Therefore, such effects of structural parameters on the collapse capacity need to be further investigated to gain insights to enhance the structural reliability against collapse.

Effects of structural parameters on collapse capacity can be investigated by repeating nonlinear dynamic analyses while varying material or geometrical properties of the structural elements. For this purpose, virtual collapse simulations are performed using the validated analytical model of the test case study by Lignos et al. (2008) considering a wide array of structural parameters to account for the impacts of a structural model selection on the collapse prediction of structures. The following structural parameters are considered for the parametric study that may have significant effect on the system especially near collapse: material properties such as yield moment, stiffness, and degrading amount; factors that affects distribution of damage through structure such as the ratio of beam-strength to column-strength; system properties such as damping and mass; and geometrical data such as bay and storey height. Table 7.1 summarizes all these structural parameters considered in this study and shows the adjustment factors for each

parameter studied to measure sensitivity of collapse assessment. Totally, 10 different model parameters are considered in this study with a total number of 26 adjusted models. Note that some adjustment factors applied for the parameters here may not be realistic in view of structural building design requirements, but help us to understand the trend in collapse assessment for extreme cases.

NO	Parameter	Description	Original Value	Adjustment Factors
MP1	My	Yield moment strength of all (i.e, all column and all beam) springs	See Table B.2	0.50, 0.75, 1.25, 1.5
MP2	Mc/My	Ratio of capping moment to yield moment for all springs (or post-yielding moment ratio)	See Table B.2	0.95, 1.10
MP3	ThetaP	Plastic rotational capacity of all springs	See Table B.2	0.5, 1.5
MP4	ThetaPC	Post-capping rotational capacity of all springs	See Table B.2	0.5, 1.5
MP5	Myb	Yield moment of all beam springs	See Table B.2	0.25, 0.75, 1.25, 1.5
MP6	BeamKi	Initial stiffness of all beam springs	See Table B.2	0.50, 1.5
MP7	damping	Damping applied on system	1.5%	0, 2, 3
MP8	(Roof) Mass	Roof mass applied on 4^{th} floor	8.8 kips/g	0.5, 1.5, 2.0
MP9	Building Height	Clear storey height (1^{st} and 2^{nd} -3^{rd} -4^{th})	19.75in and 15.75in	0.5, 1.5
MP10	Bay Length	Clear bay length	42.75in	0.5, 1.5

Table 7.1 The 10 model parametric (MP) sets with a total of 26 different analytical models considered for the parametric study on structural model parameters for collapse assessment.

In order to better understand parameters considered in this study, a summary of the spring component model is described in Figure 7.1, which is assumed at the end of elastic beam and column elements for the test case study of Lignos et al. (2008). The modified Ibarra-Krawinkler model is adapted to model rotational springs in the frame. The parameters of the spring model are defined in terms of moment and rotation quantities. In Figure 7.1, the monotonic backbone curve of the spring component can be defined by seven parameters: yield moment strength (My) and initial stiffness **(**Ki) in elastic region; ratio of capping moment strength to yield strength (Mc/My) and plastic rotational capacity (thetaP) in post-yielding region; residual moment strength (Mr) and post-capping rotational capacity (thetaPC) in post-capping plastic region; and

finally ultimate rotation (thetaU). Since strain-hardening ratio (α_s) is also an important parameter that needs to be considered during this parametric study, the relation between strain hardening and other parameters are described by the following equation:

$$\alpha_s = \frac{(Mc/My-1)\,My}{thetaP \;\; Ki} \tag{7.1}$$

Note that ductile rotational springs are assumed for the behavior of connections for the test case study of Lignos et al. (2008). The most important parameters affecting ductility and damage potential of structures in Figure 7.1 are considered in the parametric study as given in Table 7.1.

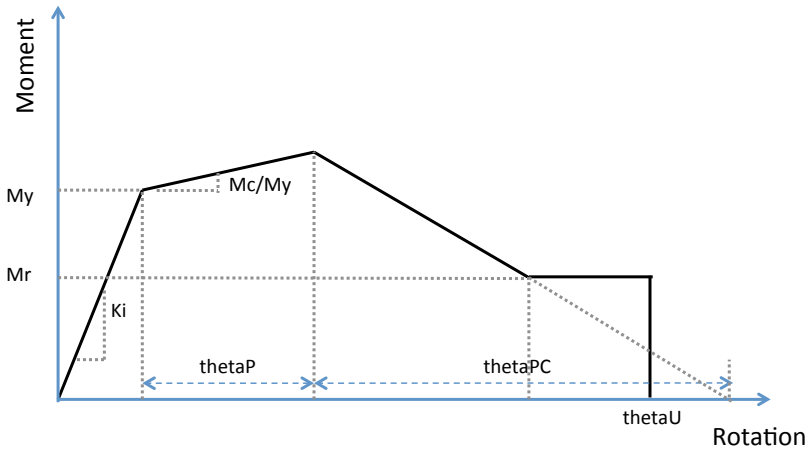

Figure 7.1 The spring-component model for the test case study of Lignos et al. (2008).

It is important to check if the demand/capacity procedure developed based on the original model in Chapter 6 can be generalized to these adjusted models or not. Therefore, using the statistical methodology developed previously, both two collapse demand models considering linear regression with stationary and non-stationary variance (variance coefficient c equals to 0 and 0.25 respectively) are obtained in the plane of V_R and S_a . Note that a limited range for spectral acceleration, which is within one standard deviation from the mean of IDA-based spectral acceleration values (i.e., $\mu_{S_a} - \sigma_{S_a} \leq S_a \leq \mu_{S_a} + \sigma_{S_a}$), is considered to evaluate demand models for a more reliable collapse assessment. These two demand models developed within the limited S_a range are then compared and checked if the non-stationary model is still appropriate to be used for collapse assessment of the adjusted structural models with variations in structural properties.

In order to understand how comprehensive the parametric study is, the first dominant period of the adjusted models is evaluated in Table 7.2 to see the range of period of structural buildings (i.e., short-period, mid-period, and long-period) considered in this study. Moreover, since the statistical procedure for fragility assessment uses spectral acceleration S_a as the intensity level to describe collapse risk of structures, the first dominant period of the adjusted models is required to apply the developed procedure. As the structures become taller, they are expected to be more flexible. Therefore, the maximum and minimum period (0.71 and 0.20 sec respectively) are observed with a 50% increase and a 50% decrease in the building height parameter correspondingly.

NO	Parameter	Adjustment Factors	T1 (sec)
MP6	beamKi	0.5	0.45
		1.5	0.43
MP8	(Roof) Mass	0.5	0.38
		1.5	0.49
MP9	Building Height	0.5	0.20
		1.5	0.71
MP10	Bay Length	0.5	0.36
		1.5	0.50
Other MP's	-	-	0.44

Table 7.2 The first dominant period in seconds found for the adjusted models.

In the following sections, collapse fragility relations for the test case study by Lignos et al. (2008) are provided using 78 far field-ground motion records for each adjusted model based on "non-stationary" demand model (variance coefficient c =0.25). In addition, a summary of sensitivity of collapse capacity with respect to a change in parameters is provided at the end by evaluating corresponding changes in statistics (mean and variability) of collapse capacity. Note that the findings of these parametric studies below are only applicable to this specific structure or other structures with similar dominant structural periods and degrading properties.

7.1.1. Yield Moment Strength of All Springs

In the OpenSees model of the test case study by Lignos et al. (2008), inelasticity is concentrated only in flexural plastic hinges at the ends of beams and columns. The equivalent velocity amount of energy dissipated through these degrading elements to the total input energy defines the velocity ratio $V_{R,}$ which is a critical performance measure used to describe the new collapse-prediction methodology developed in Chapter 5. Energy dissipation of the system significantly depends on available local energy absorption of a plastic hinge, which is expressed in terms of the total area enclosed by bending moment versus rotations under load reversals. One of the parameters that define the relationship between spring's bending moment versus rotation is the yield moment level selected in the material modeling. Therefore, sensitivity of system's overall collapse capacity of the test case study is first investigated with regard to a change in the yield moment of all rotational springs. If the yield moment used in each rotational spring of the original model of the case study is My, then the following levels were considered with an increment of 0.25 My for the sensitivity analysis: 0.50 My, 0.75 My, My, 1.25 My, and 1.50 My.

Using the same statistical methodology, i.e., linear regression with stationary variance (variance coefficient c =0) as well as non-stationary variance (variance coefficient c =0.25), demand models are obtained for each of the four different structural models using "V_R and S_a." Figure 7.2 shows the demand results obtained for the four different models together with the original one (Figure 7.2a) based on nonlinear dynamic analysis results obtained for the 78 far field-ground motion records. Note that the IDA-data points in "dark blue circles" are considered in the demand analysis. The reason why the light blue circles are excluded is to have a better and unbiased estimate of structural demand as well as to eliminate the possible misleading effect of scaled intensities on collapse capacity (see Section 6.3.1; note that more investigation on scaling of ground motions is needed to confirm this misleading effect on collapse assessment).

In Figure 7.2, as the adjustment factors increases, the trends (means) in the demand models are shifted up, which indicates that the model gets stronger comparing to the original one. Also Figure 7.2 clearly indicates that the demand model curves with varying variance (red curves) for each adjustment factor show better performance comparing to the demand models with constant variance (green curves) by giving closer trend to dark blue data points.

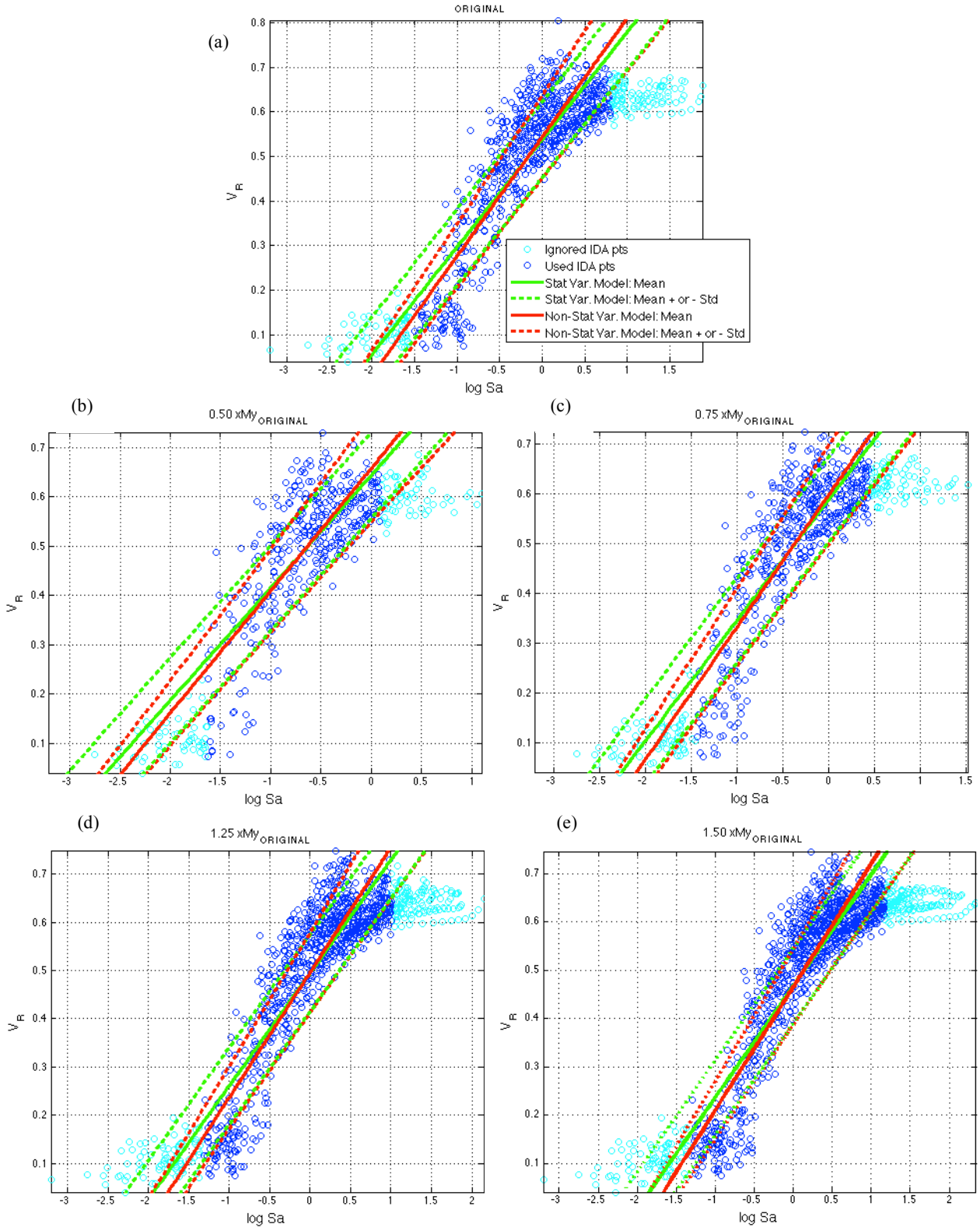

Figure 7.2 Application of linear regression on nonlinear dynamic analysis results for the test case of Lignos et al. (2008) subjected to 78 far field-ground motion records for the following yield moment values of rotational springs: a) Original model, b) 0.50 My, c) 0.75 My, d)1.25 My, and e)1.50 My.

It is interesting to note that the linear model with varying variance (red curves) in Figure 7.2 fit much better to dark blue IDA-points for larger adjustment factors such as 1.25 and 1.5. However, for smaller factors like in the case of 0.5 and 0.75, the linear trends at lower *Sa* values are pushed down to the left from dark blue points. However, occurrence of collapse is more likely at higher intensity levels, therefore, the demand models with non-stationary variance found in Figure 7.2 can be reliably used for collapse assessment.

In order to assess the effect of yield moment of all springs on collapse performance, the collapse capacities based on V_R are compared for these adjusted models in Figure 7.3a. It is observed that increasing the yield moment does not affect much the capacity means. However, a decrease in yield moment causes a noticeable decrease in the means. The collapse fragility relations using the non-stationary demand model are obtained in Figure 7.3b for the adjusted models as well as for the original model. The curve for 1.50 My (black line) has a smaller slope, which indicates that increasing the yield moment decreases the probability of collapse as expected. If one checks the median collapse probability, while the curve for original model (red line) gives this probability at a *Sa* level of 1.6g, the curves for 0.50 My (pink line) and 1.50 My (black line) correspond to a value of 0.8 g and 2.2 g. This finding indicates that the same amount of decrease or increase in yield moment does not mean the same degree of sensitivity on collapse prediction.

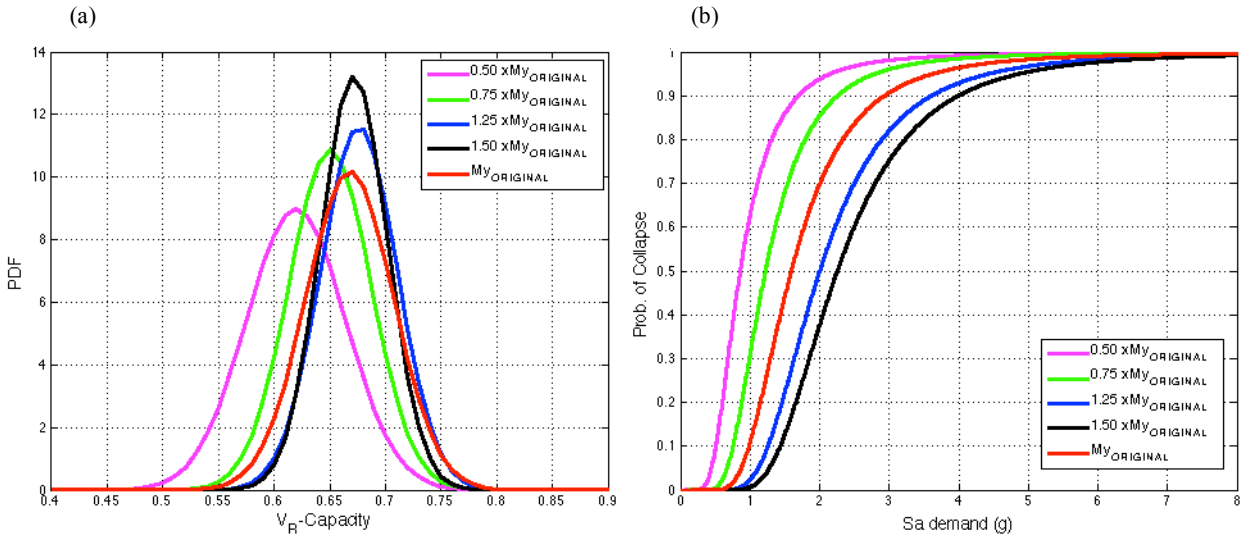

Figure 7.3 a) Collapse capacity probability distributions and b) collapse fragility relations for the test case of Lignos et al. (2008) with different My values for rotational springs subjected to 78 far field-ground motion records.

7.1.2. Post-yielding Moment Ratio of All Springs

Another factor that affects the local energy absorption of a plastic hinge is the post-yielding moment ratio, which is the ratio of capping moment to yield moment (i.e., Mc/My in short) and defines the maximum (capping) moment of the backbone curve in Figure 7.1. This ratio is significant because this defines post-yielding hardening (i.e., the ratio of post-yielding stiffness to initial stiffness) which influences geometric effects that occurred in the structure after yielding (Medina and Krawinkler, 2005).

Sensitivity of collapse prediction with respect to this post-yielding ratio is studied considering a 5% decrease and 10% increase in this parameter, which are 0.95 Mc/My and 1.10 Mc/My respectively considering that Mc/My is the original level. According to original values given in A3.1, both modified values 0.95 Mc/My and 1.10 Mc/My are still larger than 1.0, therefore the structural model still shows hardening after yielding in the backbone curve in Figure 7.1 First, the demand models are obtained in Figure 7.4, in which the model with non-stationary seems to better fit to IDA points comparing to stationary model. Then probability distributions of collapse capacities as well as the collapse fragility results for different post-yield ratios are provided in Figure 7.5.

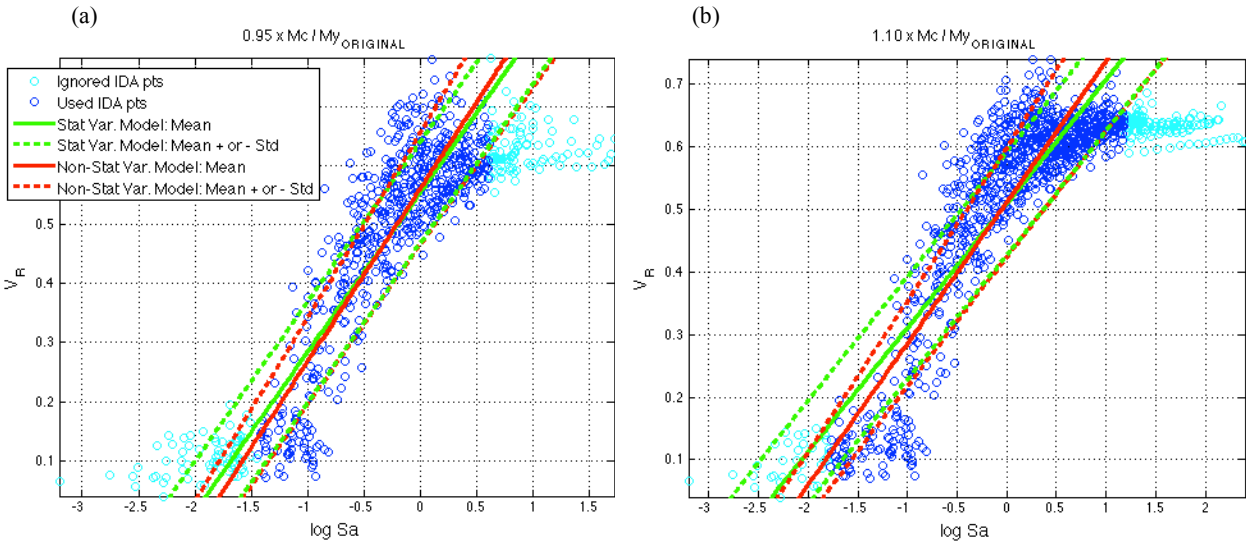

Figure 7.4 Application of linear regression on nonlinear dynamic analysis results for the test case of Lignos et al. (2008) subjected to 78 far field-ground motion records for the following post-yielding moment ratios of rotational springs: a) 0.95 Mc/My, and b)1.10 Mc/My.

In Figure 7.5a, although the collapse capacity for the smaller post-yielding ratio (the light blue line for 0.95 Mc/My) has a little more variability, all cases for Mc/My values (0.95 and 1.0, and 1.10 Mc/My) seem to have similar means of collapse capacities to the original case (red line), which is larger than the mean for 0.75My (green line). This may be the reason why collapse fragility curve for 0.95 Mc/My (light blue line) in Figure 7.5b shows lower collapse probabilities comparing to the case of 0.75 My (green line). This is also obvious from Table 7.3 that both 0.95 Mc/My and 1.10 Mc/My cases have more capping moment strength (Mc).

An increase in post-yielding ratio definitely increases the resistance, but it is interesting that an increase in Mc/My can be more effective than an increase in My in terms of resistance. As seen in Figure 7.5b, a 10% increase in Mc/My ratio amount almost equals to the case of yield strength with an increase between 25% and 50%. Although, 1.10Mc/My case has smaller Mc values comparing to the ones for 1.25My and 1.50My in Table 7.3, it has larger value for strain hardening, which makes it still stronger against collapse.

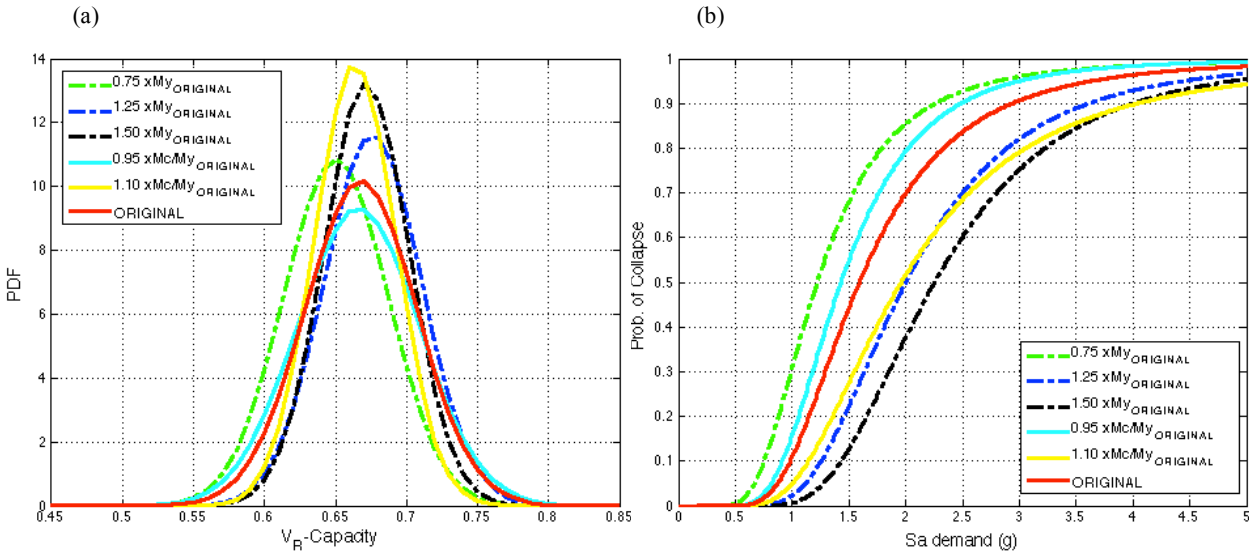

Figure 7.5 a) Collapse capacity probability distributions and b) collapse fragility relations for the test case of Lignos et al. (2008) with different Mc/My and My values for rotational springs subjected to 78 far field-ground motion records.

Parametric Case / Spring Location	Original Case	0.95 x Mc/My	1.10 x Mc/My	0.75 x My	1.25 x My	1.50 x My
C1B	38.0	36.1	41.7	28.5	47.4	56.9
C1T, C2, C3B	29.7	28.2	32.7	22.3	37.1	44.6
C3T, C4	15.3	14.6	16.9	11.5	19.2	23.0
B1, B2	21.8	20.7	24.0	16.3	27.2	32.7
B3, B4	15.3	14.6	16.9	11.5	19.2	23.0

Table 7.3 Capping-moment strengths (Mc) in the adjusted spring models (B and C represent "beam" and "column" springs; see Figure A.1 for locations).

7.1.3. Plastic Rotational Capacity of All Springs

The term "ductility" refers to the ability of a component or a system to dissipate large amounts of energy by showing excessive inelastic deformations without significant deterioration in strength or stiffness. Plastic rotational capacity after yielding is one of the factors that affects the dissipated amount of energy, which is the total area enclosed by bending moment versus rotations under load reversals. In addition, it significantly affects the strain-hardening ratio of the spring model as stated in (7.1) that determines the deterioration rate in strength or stiffness after yielding. In order to better understand such effect on collapse prediction, the structural model for the test case study of Lignos et al. (2008) is adjusted at two different levels of plastic rotational capacities 0.50 ThetaP and 1.50 ThetaP assuming that ThetaP is the original level.

Based on the demand models using linear regression with non-stationary variance (red lines) in Figure 7.6, the collapse capacity and collapse fragilities are assessed in Figure 7.7. Not only the results for ThetaP cases (pink line for 0.50 ThetaP and green line for 1.50 ThetaP) are provided in Figure 7.7, but the previous results obtained for the two different Mc/My levels (blue line for 0.95Mc/My and black line for 1.10 Mc/My) are shown for comparison. Although both 0.50 ThetaP and 1.50 ThetaP cases have similar mean for capacity in Figure 7.7a, an increase in ThetaP (green line) results in smaller strain-hardening ratio, therefore provides less lateral strength against seismic actions giving large probability of collapse in Figure 7.7b. However, collapse fragilities for both 0.50 ThetaP and 1.50 ThetaP remain between 0.95 Mc/My and 1.10 Mc/My cases, following each other based on the order of strain hardening values given in Table 7.4. 0.95 Mc/My is almost the same with 1.50 thetaP, which slightly gives smaller probabilities

due to slightly larger values in strain hardening. Lastly, although the strain-hardening ratios for 0.5 ThetaP and 1.10 Mc/My are close to each other in Table 7.4, 1.10 Mc/My has more rotational capacity therefore provide more area under the backbone curve in Figure 7.1, resulting in a significant increase in resistance in Figure 7.7b.

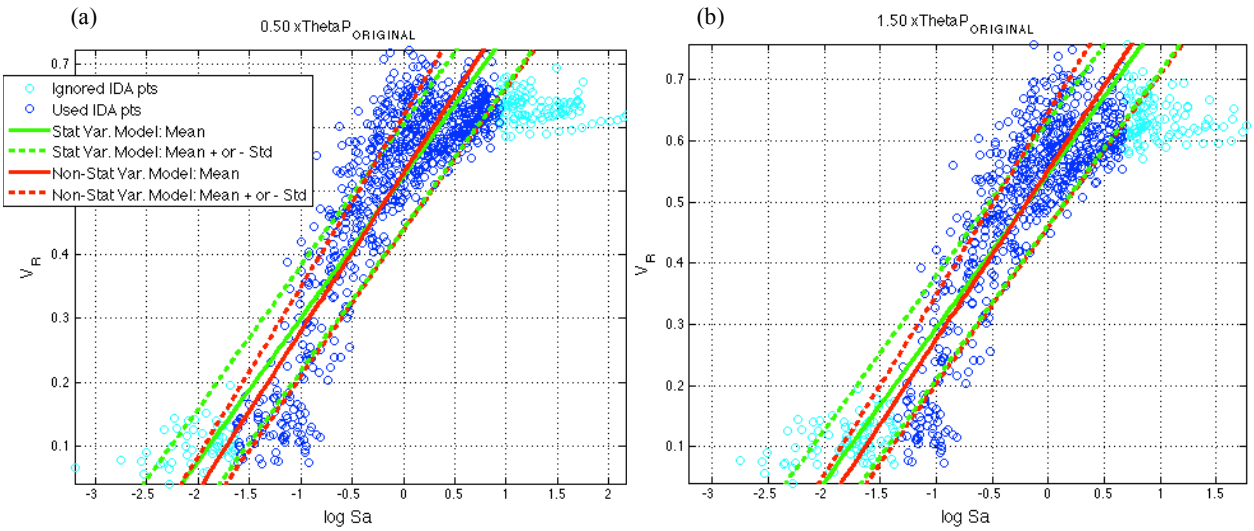

Figure 7.6 Application of linear regression on nonlinear dynamic analysis results for the test case of Lignos et al. (2008) subjected to 78 far field-ground motion records for the following plastic rotational capacity values of rotational springs: a) 0.5 ThetaP and b)1.5 ThetaP.

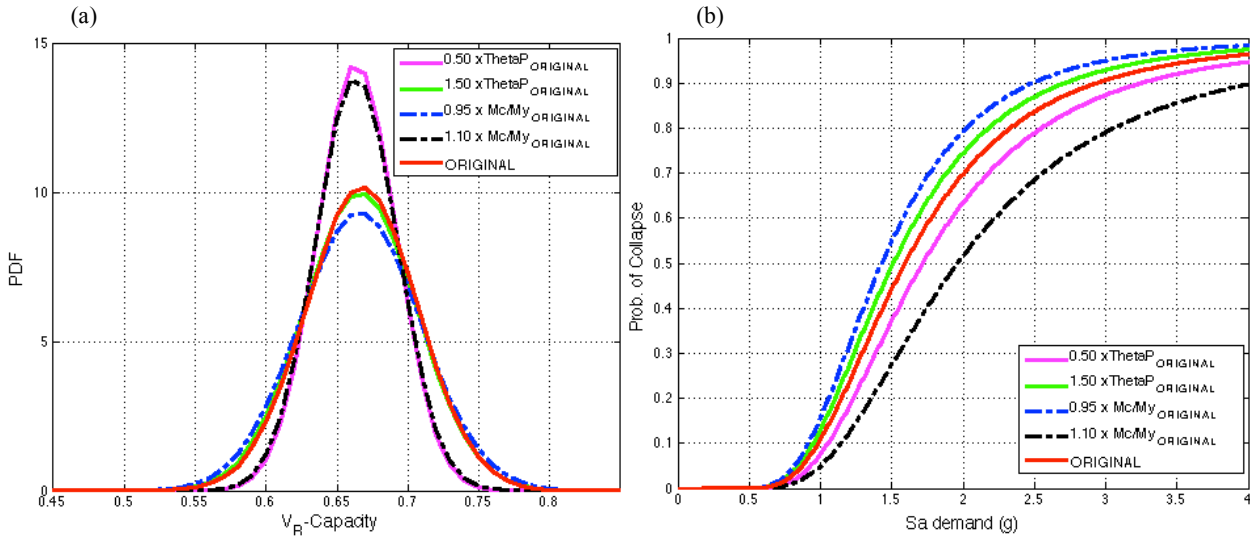

Figure 7.7 a) Collapse capacity probability distributions and b) collapse fragility relations for the test case of Lignos et al. (2008) with different ThetaP and Mc/My values for rotational springs subjected to 78 far-field ground motion records.

Parametric Case / Spring Location	Original Case	0.50 x ThetaP	1.50 x ThetaP	0.95 x Mc/My	1.10 x Mc/My
C1B	0.0027	0.0054	0.0018	0.0012	0.0056
C1T, C2, C3B	0.0026	0.0052	0.0017	0.0012	0.0055
C3T, C4	0.0018	0.0037	0.0012	0.0006	0.0043
B1, B2	0.0030	0.0061	0.0020	0.0014	0.0064
B3, B4	0.0018	0.0037	0.0012	0.0006	0.0043

Table 7.4 Strain hardening ratios in adjusted spring models (B and C represent "beam" and "column" springs; see Figure A.1 for locations).

7.1.4. Post-capping Rotational Capacity of All Springs

Post-capping plastic rotation is the difference between rotation at maximum moment (i.e., capping moment) and rotation at complete loss of strength (ultimate rotation). Thus, it is one of the important factors affecting the total area enclosed under the backbone curve in Figure 7.1. Moreover, it determines the softening after post-capping point in Figure 7.1. Two adjustment factors for ThetaPC are considered in this section: 0.50 and 1.50. After applying linear regression on IDA-results to find the demand model with non-stationary variance (red curves in Figure 7.8), the collapse capacities and collapse fragility curves are found in Figure 7.9 and are then compared to the results for ThetaP obtained in previous section.

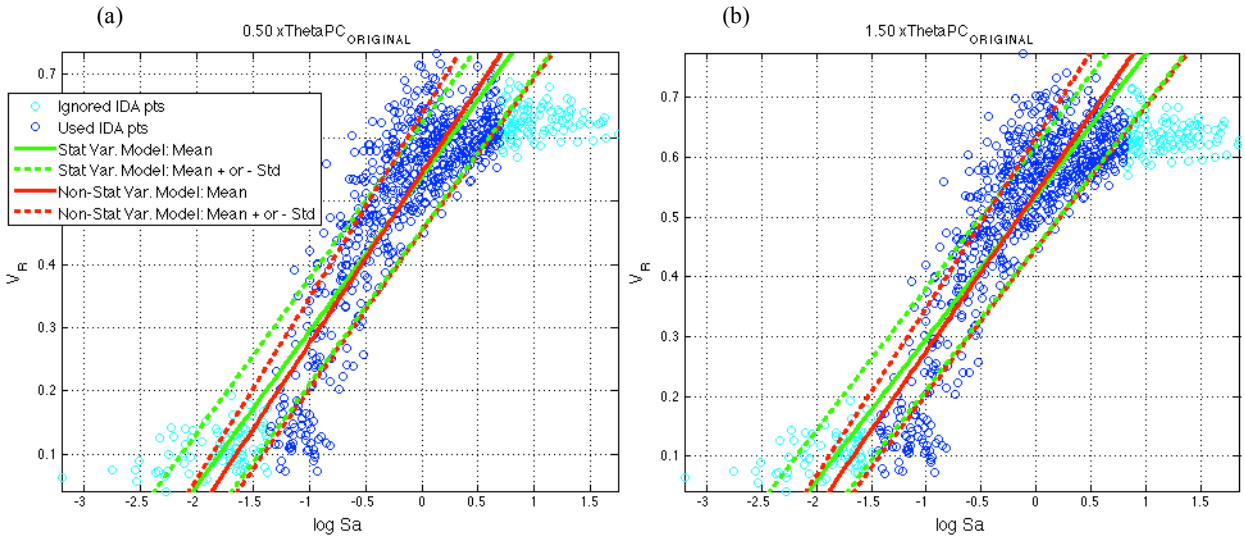

Figure 7.8 Application of linear regression on nonlinear dynamic analysis results for the test case of Lignos et al. (2008) subjected to 78 far field-ground motion records for the following post-capping rotational capacity values of rotational springs: a) 0.5 ThetaPC and b) 1.5 ThetaPC.

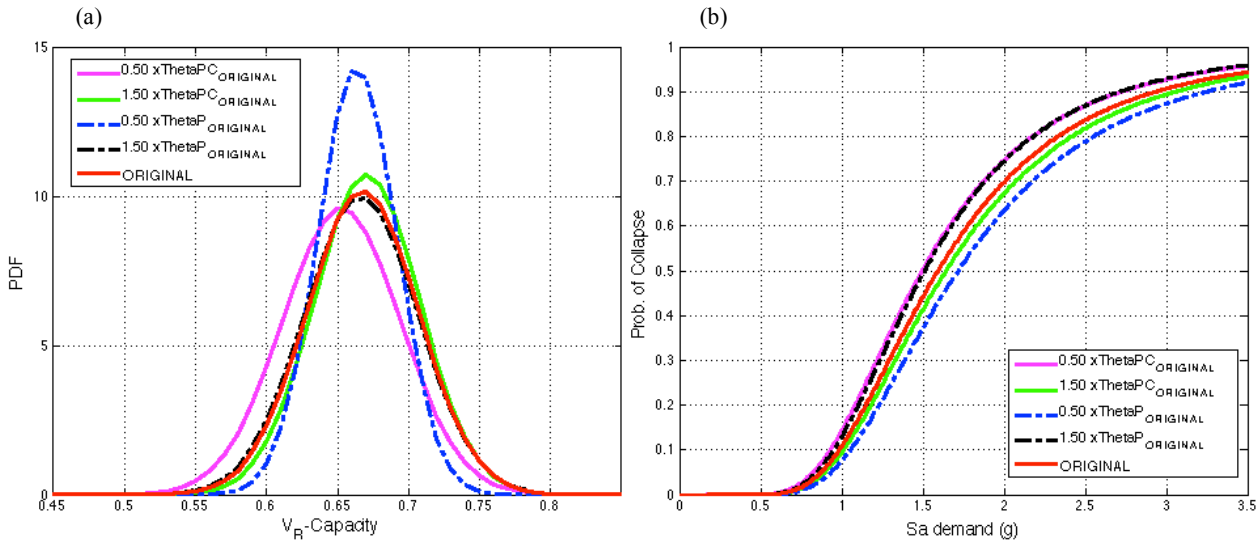

Figure 7.9 a) Collapse capacity probability distributions and b) collapse fragility relations for the test case of Lignos et al. (2008) with different ThetaPC and ThetaP values for rotational springs subjected to 78 far field-ground motion records.

In Figure 7.9a, a decrease in ThetaPC causes a little loss in collapse resistance capacity of the structural system. However, an increase in ThetaPC is not effective as much as in the case of decrease when comparing green line to red line. Figure 7.9b also confirms that the difference between the two ThetaPC cases indicates that the collapse prediction is more sensitive to any decrease in post-capping rotational capacity.

The case of 0.50 ThetaPC (pink line) gives the same results as the case of 1.50 ThetaP (black line). While the strain-hardening ratio for pink line stays the same with the original case, it is almost halved for black line (see Table 7.4), which indicates the importance of a decrease in strain-hardening ratio on collapse prediction. This can be supported with an example from the time history analysis obtained using the test ground motion for the case study. As seen in Figure 7.10, although 0.50 ThetaPC and 1.50 ThetaP goes to collapse following the original case, 0.50 ThetaP case still resists seismic actions because of its large strain-hardening ratio so that the structure comes to rest at the end. In other terms, the probability of collapse for 0.50 ThetaP case seems to be more sensitive to a change in strain-hardening ratio than a change in the plastic rotational capacity.

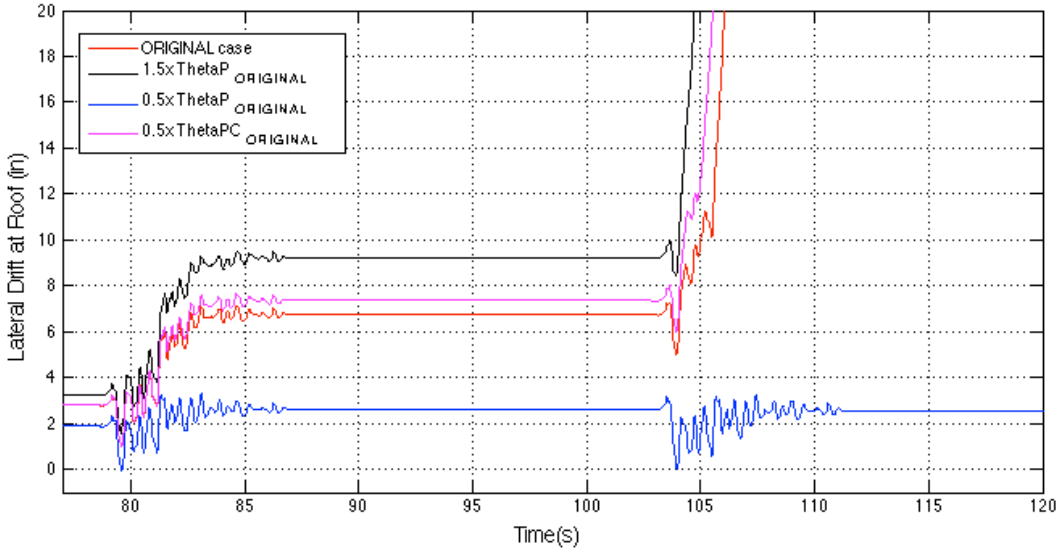

Figure 7.10 Time history analysis for the test case of Lignos et al. (2008) with different ThetaP and ThetaPC values for rotational springs subjected to the test ground motion continuously at the scale factors of 0.4, 1.0, 1.5, 1.9 and 2.2.

7.1.5. Yield Moment Strength of Beam Springs

Distribution of strength and stiffness within the structure influence the seismic actions applied on the components, therefore affects the location and degree of damage concentrations in the structure. This section therefore studies two variations in yield moment strength only considering beam rotational springs: 0.5 Myb and 1.5 Myb assuming that Myb is the original level. The linear demand models are obtained in Figure 7.11. The stationary model in the case of 0.5 Myb (green lines) shows poor performance especially at lower intensity levels. This proves one more time the effectiveness of the red lines, which can better fit to the data points with a varying variance. Therefore, using the red models in Figure 7.11, which is ones with non-stationary variance option, the collapse capacities and fragilities are provided in Figure 7.12 for the two variations in Myb together with the adjustment factors of 0.5, 0.75, and 1.5 for My.

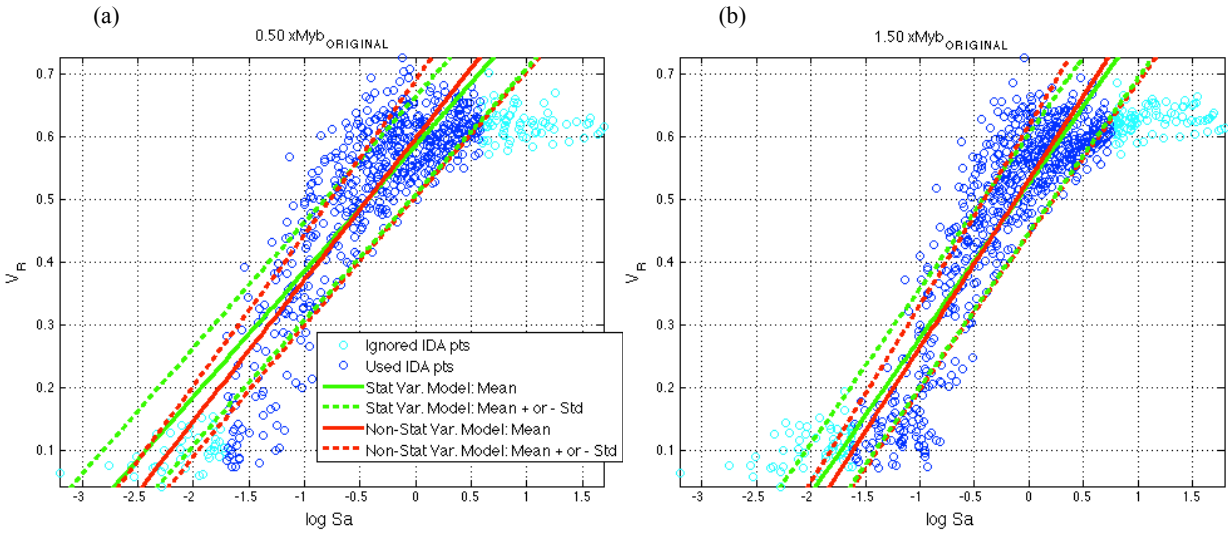

Figure 7.11 Application of linear regression on nonlinear dynamic analysis results for the test case of Lignos et al. (2008) subjected to 78 far field-ground motion records for the following Myb values of rotational springs: a) 0.5 Myb and b)1.5 Myb.

As expected in Figure 7.12, the collapse capacities and fragilities of the two variations for Myb of beam springs (pink and green lines for 0.5Myb and 1.5Myb respectively) stay between the two same variations for My of all springs (dark blue and light blue lines for 0.5My and 1.5My respectively). In Figure 7.12b, the fragility curves for Myb cases give higher potential of collapse risk comparing to the original case (red line), even still higher for the case of 50% increase in Myb (green line). This can be also confirmed from Figure 7.12a that both 0.5 Myb and 1.5 Myb give a capacity mean lower than the original case and close to the mean for 0.75 My case (black line). This is due to distribution of damage within the structure. As Myb increases, the beam springs become stronger but the ratio of strong column to weak beam (i.e., SCWB ratio which is the ratio of column's flexural strength to adjacent beam's flexural strength) reduces, even becomes smaller than 1.0 as indicated in Table 7.5. This means the flexural strength in the connection is governed by the columns, which in turn makes column springs first form plastic hinges instead of adjacent beam ones.

On the other hand, as Myb decreases, it increases the SCWB ratio as well (see Table 7.5). However, this increase in ratio does not significantly improve collapse-related performance because beam springs become hinges much earlier than the original case as result of decrease in flexural strength, therefore increases the collapse risk of structures.

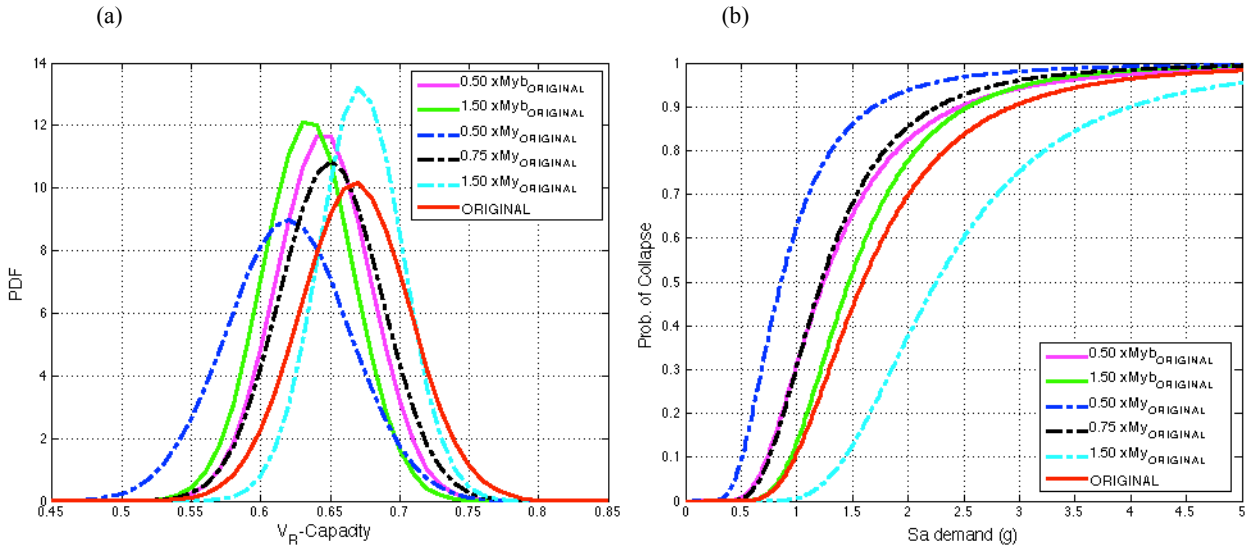

Figure 7.12 a) Collapse capacity probability distributions and b) collapse fragility relations for the test case of Lignos et al. (2008) with different Myb and My values for rotational springs subjected to 78 far field-ground motion records.

Parametric Case / Spring Location	Original Case	All My Cases	0.50 x Myb	1.5 x Myb
{C1T, C2, C3B} to {B1,B2}	1.36	1.36	2.72	0.91
{C3T, C4} to {B3, B4)}	1.00	1.00	2.00	0.67

Table 7.5 The ratios of column-moment strength to beam-moment strength in adjusted spring models (B and C represent "beam" and "column" springs; and springs in "{}" carry the same properties; see Figure A.1 for locations).

In summary, if a higher SCWB ratio is assumed in the design by providing necessary flexural strength for beams, the columns become stronger so it gives a chance to structural system to spread the damage within structure through strong columns. As a result, this increases involvement of number of stories to collapse mechanism, therefore, improves energy absorption as well as collapse capacity of structural system (Haselton et al., 2011).

7.1.6. Initial Stiffness of Beam Springs

Similar to the previous section, a change in the initial stiffness (Ki) of beam spring is investigated here to understand the effect of the damage distribution of stiffness in the springs on

collapse capacity. Using the linear demand model with varying variance in Figure 7.13, the fragility curves and collapse capacity distributions are obtained in Figure 7.14 and compared with the results of Myb cases studied in previous section.

In Figure 7.14a, an increase or decrease for Ki in beam springs does not almost make any change in collapse capacities comparing to the original case. However, the Beam-Ki cases have higher capacities comparing to ones for Myb cases, which in turn, makes the Beam-Ki cases stronger against collapse potential in Figure 7.14b. The collapse fragilities given in Figure 7.14b also shows that a decrease in Beam-Ki does not improve the collapse performance much since the case of 0.5 Beam-Ki (pink curve) almost gives the same collapse performances with the original case. On the other hand, an increase in Beam-Ki worsen the performance as indicated by the case of 1.5 Beam-Ki (green line) showing almost identical results with the case of 1.5Myb (black line).

In summary, a decrease in stiffness for beam springs may lead to late yielding of beam springs, therefore may reduce damage concentration on beams. However, nearby columns become much stiffer this time comparing to beams and takes more damage, which in turn, causes earlier plastic hinging at the column ends. Therefore, a decrease in Ki for beam springs does not significantly improve collapse performance.

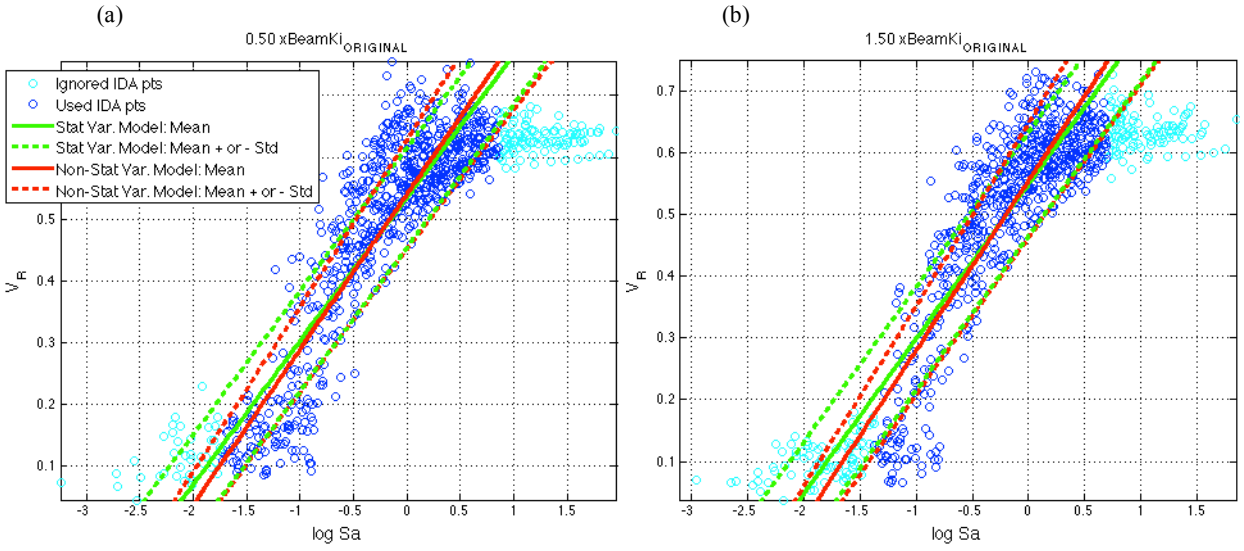

Figure 7.13 Application of linear regression on nonlinear dynamic analysis results for the test case of Lignos et al. (2008) subjected to 78 far field-ground motion records for the following post-yield values of rotational springs: a) 0.5 beamKi and b) 1.5 beamKi.

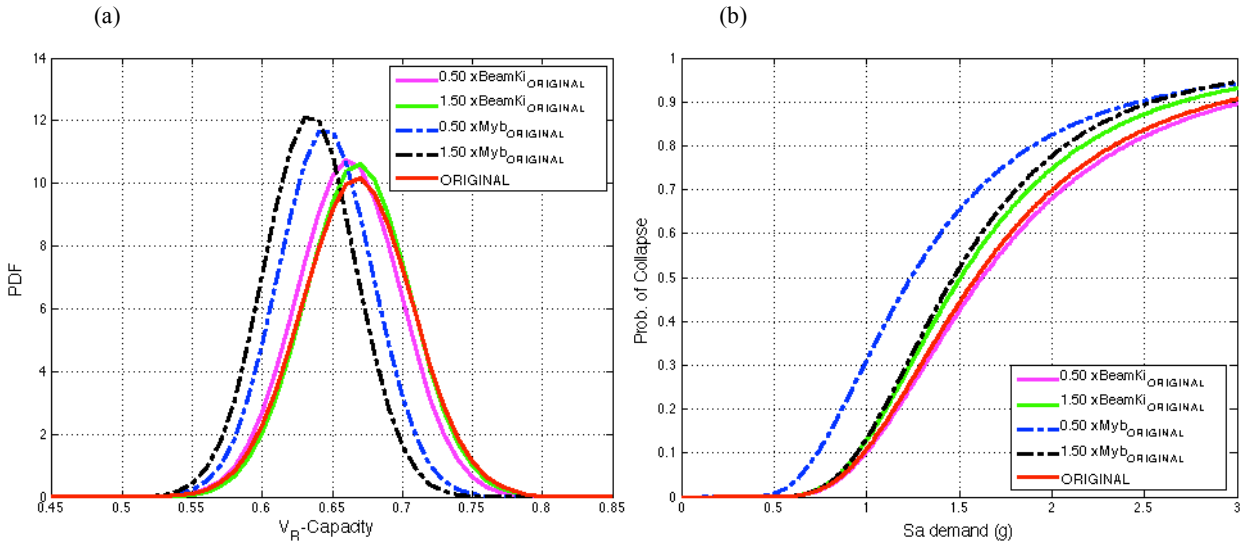

Figure 7.14 a) Collapse capacity probability distributions and b) collapse fragility relations for the test case of Lignos et al. (2008) with different Beam-Ki and Myb values for rotational springs subjected to 78 far field-ground motion record.

7.1.7. Damping of the Structural System

All building structures have inherent damping mostly due to internal friction in the structural materials and interaction of components. While the system is subject to loading and unloading during an earthquake, the structure tries to stabilize the system by dissipating most of seismic energy through damping. As the structure experiences excessive irreversible deformations through component degradation, more seismic energy is dissipated through damping in proportion to the displacement amplitude. If the damping forces overcome hysteretic forces, and are able to stabilize the system, the system gradually comes to rest after the earthquake excitation. Therefore, an increase in damping yields to larger resistance against excessive deformations near collapse.

During the development of analytical models for the three case studies in Chapter 3, it was observed that application of damping on initial or current stiffness during analysis results in significant differences in the analysis results. It is found that damping proportional to initial stiffness can give large errors especially near collapse (see Figure 3.10). Therefore, the analytical model developed for the test case study of Lignos et al. (2008) is adjusted to the three following values of damping by applying damping on current stiffness to see the change in structural

collapse behavior: zero damping, 1.5% damping (original level), 3% damping, and 4.5% damping (with an adjustment factor of 0, 1, 2, and 3 respectively).

Using the demand models with non-stationary option (red cures in Figure 7.15) in development of collapse prediction, the capacities in Figure 7.15a and fragility curves in Figure 7.16b are obtained. As seen in collapse capacity distributions, more damped the system is, more resistance against collapse can be observed. This can be also observed if one checks collapse fragilities. For example, at a value of 2g for spectral acceleration, the blue curve with three times the original damping (4.5% damping) has around 60% collapse likelihood, while undamped system (0% damping) has 77% possibility.

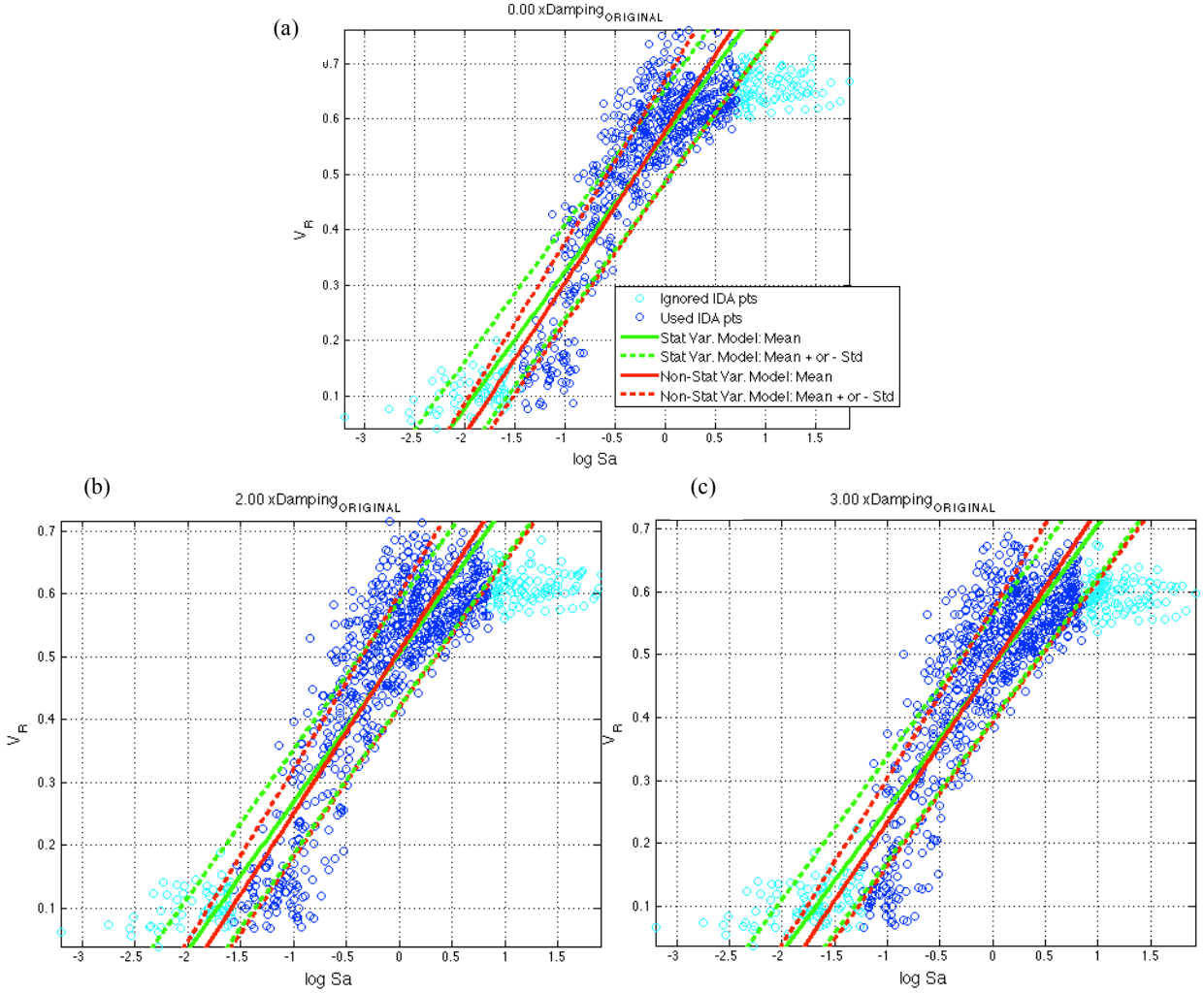

Figure 7.15 Application of linear regression on nonlinear dynamic analysis results for the test case of Lignos et al. (2008) subjected to 78 far field-ground motion records for the following damping values: a) 0%, b) 3%, and c) 4.5%.

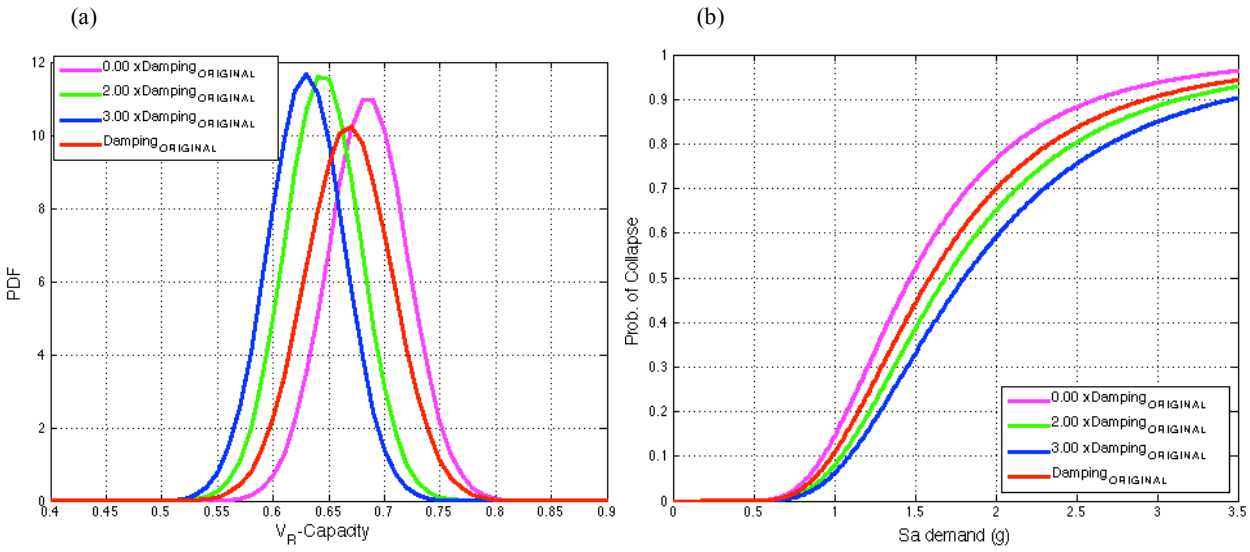

Figure 7.16 a) Collapse capacity probability distributions and b) collapse fragility relations for the test case of Lignos et al. (2008) with different damping values subjected to 78 far field- ground motion records.

7.1.8. Roof Mass Applied on The Structure

Reducing structural mass ensures economic designs as well as may decrease seismic demand induced on the structure. This is because an increase in the mass (or weight) of the structure increases the inertial effects as well as geometric effects due to increased gravity loads on the structure. Moreover, an increase in mass of structure means a shift in period too. The first dominant period elongates as the mass of structure increases that may put the structure into a lower part of response spectrum. However, a decrease in mass may move the structural period closer to that of the excitation, which in turn may cause resonance in structure.

The linear demand models obtained in Figure 7.17 for roof masses at two different variations: 0.5 Mass and 1.5 Mass, where Mass is the original level for roof. Note that as the roof mass increases so do the gravity loads applied on the roof. As seen, the dark blue points at smaller intensities are not well covered by the linear demand models. Despite this observation, the demand models are still reliable to make collapse prediction, because collapse occurs usually at higher intensities.

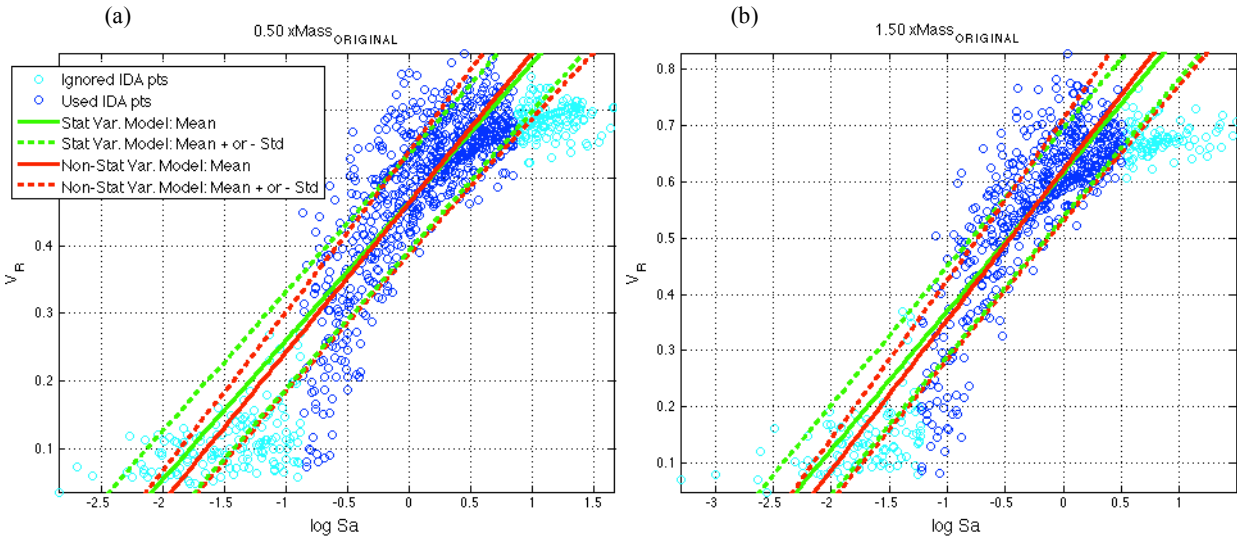

Figure 7.17 Application of linear regression on nonlinear dynamic analysis results for the test case of Lignos et al. (2008) subjected to 78 far field-ground motion records for the following roof mass values: a) 0.5 (Roof) Mass and b) 1.5 (Roof) Mass.

In Figure 7.18, the results for in roof mass are compared with the previous results obtained for a damping. First, as the roof weight decreases, so does the collapse capacity in Figure 7.18a. If the collapse probabilities at 2g are evaluated in Figure 7.18b, it can be noticed that a 50% reduction and 50% increase in roof mass yield to 50% and 80% likelihood for collapse, while the original case gives 70% probability of collapse. It is clear that a decrease in roof mass/weight causes more sensitivity on collapse performance comparing to the same of amount of increase in roof mass, which may be due to differences in natural period of the structure corresponding to the two variations in roof mass (see Table 7.2).

In summary, seismic loadings applied on structure are in proportion with seismic weight at each floor. Especially the roof mass has a potential to create more overturning geometry effects once the gravity load applied on the structure become dominant as result of progressive accumulation of deformations. Comparing the results for variation in damping and roof mass, it is seen that seismic protection can be provided more efficiently by reducing the seismic weight of the structure instead of increasing the inherent damping applied on the structure.

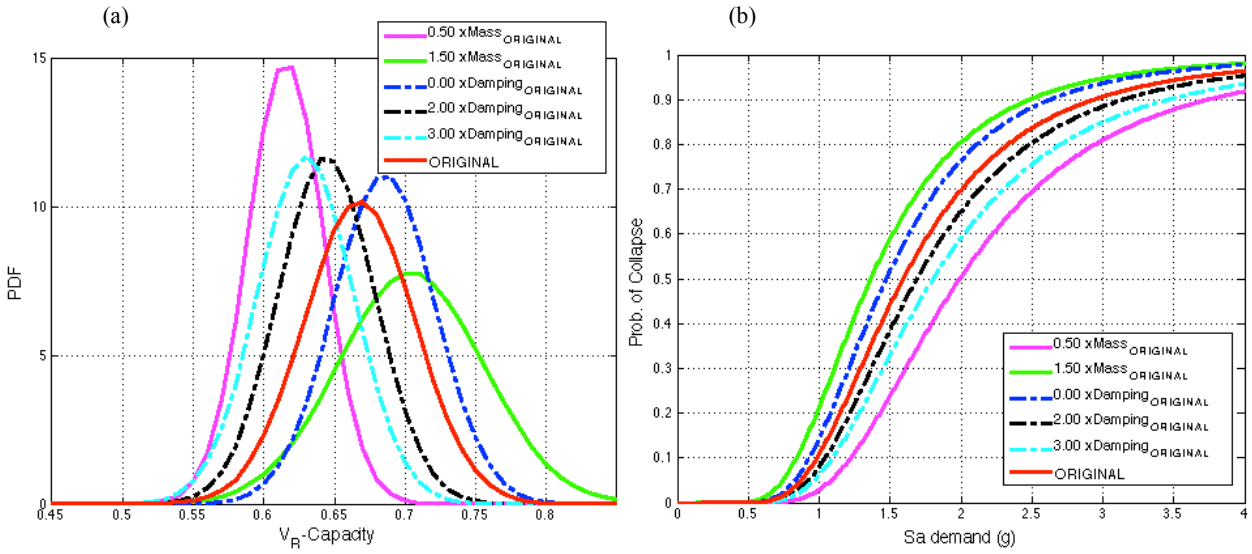

Figure 7.18 a) Collapse capacity probability distributions and b) collapse fragility relations for the test case of Lignos et al. (2008) with different roof mass and damping values subjected to 78 far field-ground motion records.

7.1.9. Building Geometry of the Structural System

Building/storey height and bay length are the two main dimensions that define the building geometry for 2D–frames. They are the two main system parameters that affect response motion during seismic excitation. In order to better understand the influence of building geometry on structural performance near collapse, this section investigates a change in building/storey height and bay length on collapse prediction by performing fragility analyses considering the following variations: 0.5 and 1.5 times the building (or story) height and, 0.5 and 1.5 times the bay length.

First, the demand models with non-stationary variance for each change in geometry are obtained in Figure 7.19, which show reasonable fit within the limited range of spectral acceleration. Choosing the demand model with varying stationary, the collapse capacities and fragilities are provided in Figure 7.20.

As expected, increasing the building height makes the structure more flexible by shifting the first natural period from 0.44 sec to 0.71 sec. Therefore, there is more collapse risk for this adjusted model. On the other hand, the structural model with an half of the original building height shows very large resistance, even so large that it shows 50% probability of collapse around 4g of

spectral acceleration. Note that this value may not be realistic for building design requirements, however it at least gives an idea about this extreme case for this specific structure.

Any change in bay length does not seem to make any significant impact on collapse predictions, almost providing the same results with the original case. Changes in column spacing can affect the joint shear demand on connections (Haselton et al., 2011). However, since this shear effect is ignored in the development of the structural model, this may cause the results observed in Figure 7.20b.

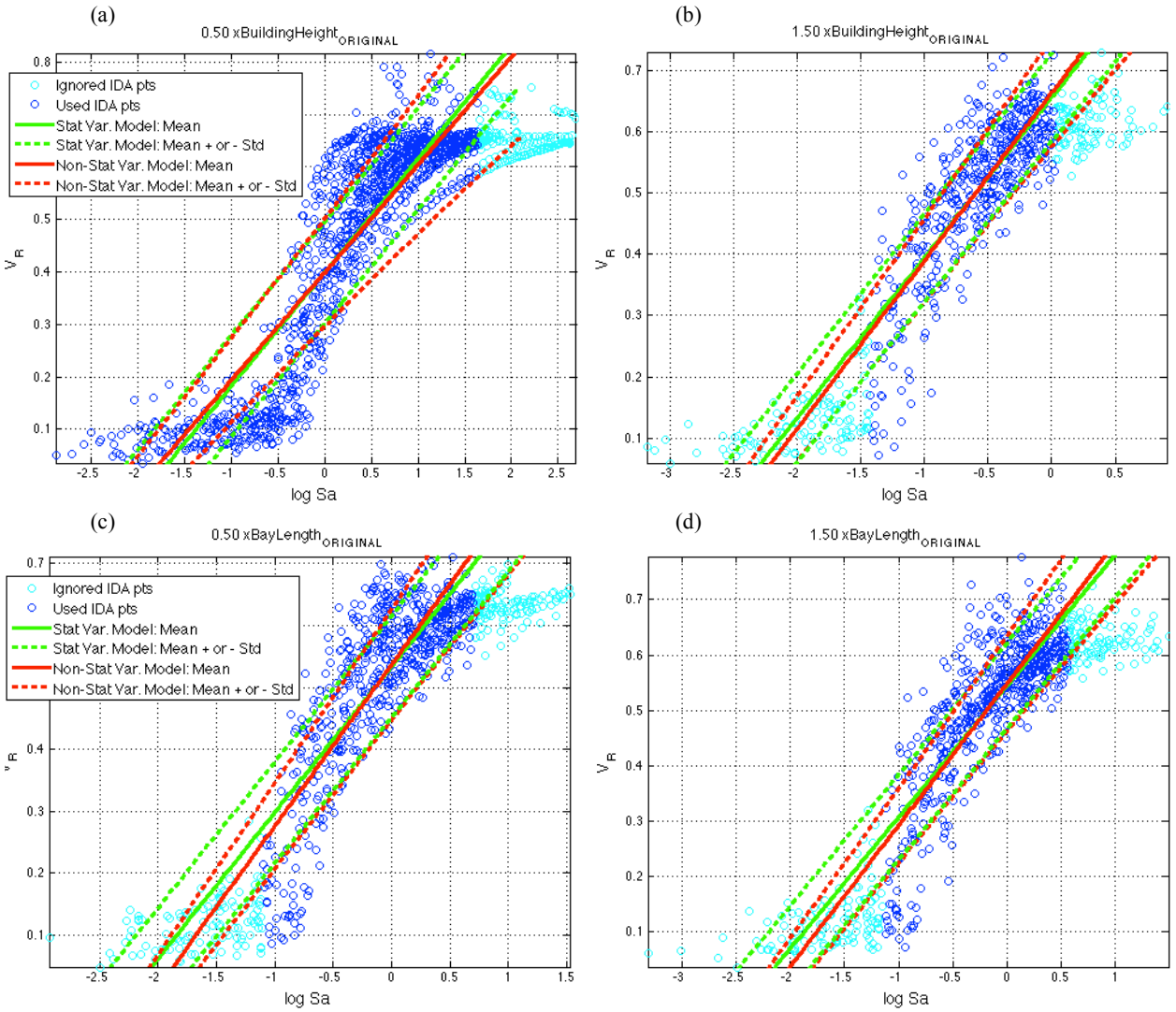

Figure 7.19 Application of linear regression on nonlinear dynamic analysis results for the test case of Lignos et al. (2008) subjected to 78 far field-ground motion records for the following values of building dimensions: a) 0.5 Building Height, b) 1.5 Building Height, c) 0.5 Bay Length , and d) 1.5 Bay Length.

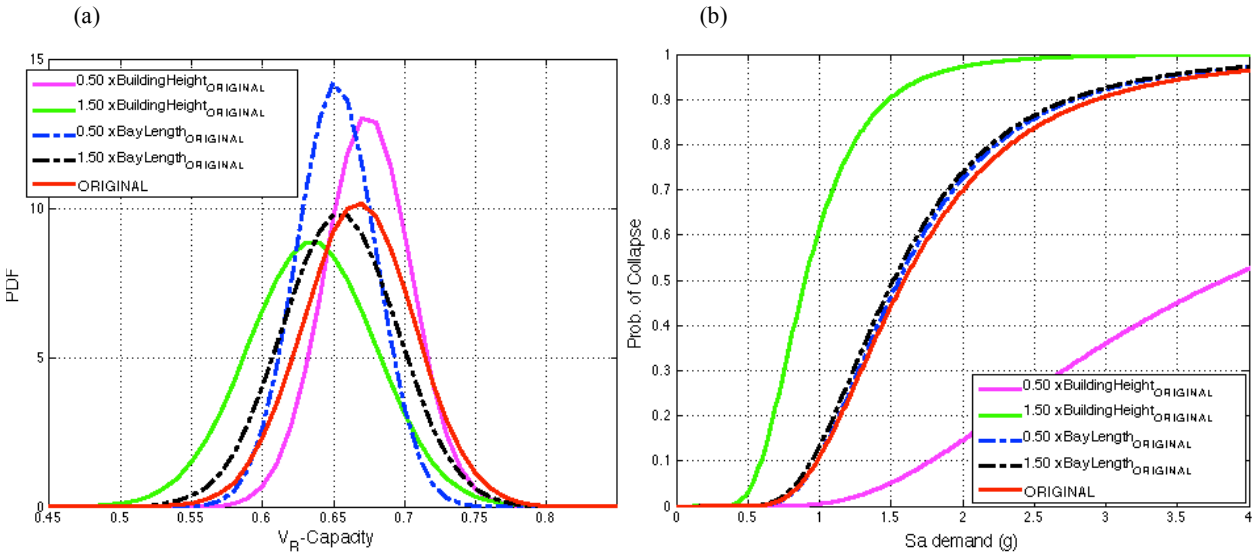

Figure 7.20 a) Collapse capacity probability distributions and b) collapse fragility relations for the test case of Lignos et al. (2008) with different building dimensions subjected to 78 far field-ground motion records.

A summary of sensitivity analyses of collapse capacity to a change in all structural model parameters is shown in Table 7.6. Mean of collapse capacities based on V_R measure shows smaller sensitivity comparing to the results giving for roof drift D_R, which indicates efficiency of V_R measure in describing collapse performance of structures.

		Equivalent Velocity Ratio		Roof Drift Ratio	
Parametric Cases	**Change in parameter %**	**Change in mean %**	**Change in cov %**	**Change in mean %**	**Change in cov %**
ORIGINAL	-	**(Value=0.668)** -	**(Value=0.059)** -	**(Value=13.261)** -	**(Value=0.216)** -
0.50 My	-50	-7.2	22.4	-53.5	22.7
0.75 My	-25	-2.6	-3.8	-26.3	-0.7
1.25 My	25	1.3	-13.4	22.7	-2.9
1.50My	50	0.6	-23.5	28.9	4.3
0.95 Mc/My	-5	-0.2	9.7	-4.4	2.7
1.10 Mc/My	10	-0.6	-26.1	6.7	-12.4
0.5 ThetaP	-50	-0.6	-28.4	-2.0	-2.6
1.5 ThetaP	50	-0.2	2.2	-1.3	19.1
0.5 ThetaPC	-50	-2.2	8.6	-13.0	11.2
1.5 ThetaPC	50	0.5	-5.3	3.1	0.3
0.50 Myb	-50	-3.4	-10.4	-18.6	26.9
1.50 Myb	50	-5.0	-12.0	-51.0	29.6
0.50 beamKi	-50	-0.9	-4.6	-3.1	5.0
1.50 beamKi	50	0.1	-4.4	-0.2	-2.0
0 damping	-100	2.6	-10.4	-3.4	3.2
2 damping	100	-3.5	-9.7	-2.3	1.2
3 damping	200	-5.7	-7.5	-0.6	5.5
0.50 (Roof) Mass	-50	-7.8	-25.7	3.1	-6.6
1.50 (Roof) Mass	50	5.4	24.3	-14.2	18.7
0.50 Building Height	-50	-0.8	122.6	-30.6	171.2
1.50 Building Height	50	-4.9	20.6	2.6	-9.2
0.50 Bay Length	-50	-2.4	-26.5	-52.3	20.6
1.50 Bay Length	50	-2.0	5.7	-0.6	11.1

Table 7.6 Statistical analyses on sensitivity of collapse capacity to a change in model parameters for the test case of Lignos et al. (2008) subjected to 78 far -field ground motion records.

7.2. Effect of Variability in Ground Motion Sets on Collapse Assessment

A large record set is usually chosen in recent collapse assessment approaches such as IDA to represent the record-to-record variability in structural response (Krawinkler et al., 2003; Delgado et al., 2010). However, it takes a great deal of time to perform nonlinear dynamic analyses for a specific structure subjected to a large set of ground motions. In order to reduce the number of

ground motions needed for collapse assessment, it is required to investigate effects of uncertain characteristics of ground motions to develop guidelines regarding selection of a suite of ground motions to be used in nonlinear collapse analyses.

In this section, two-ground motion database are adopted to develop fragility curves: ATC-63 far field-ground motion set (FEMA 2009; 44 records) and an expanded set by Haselton and Deierlein (2007; 78 records). Basic ground motion characteristics such as ratios of peak ground motion parameters, frequency, and duration are selected to conduct several sensitivity analyses on collapse capacity. The proposed methodology is to form a few subsets from the ground motion database considering these parameters, and to use each subset for the collapse simulation on the test case study to evaluate the effect on collapse capacity.

The following parameters, which are unaffected from intensity scaling, are selected among indices given in Table 5.5 to construct ground motion subsets:

- Strong duration between t_5 and t_{95} at which 5% and 95% of the total integral of square of accelerogram is obtained: t_S (Trifunac and Brady, 1975)
- The instant where 45% of the total integral of square of accelerogram is obtained: t_{45}
- Average period of a zero-crossing in t_S: $T_{v,strong}$
- Number of zero crossings of accelerogram in strong duration: v_S
- Ratio of peak ground motion velocity to peak ground acceleration: *PGV/PGA*
- Ratio of peak ground motion displacement to peak ground velocity: *PGD/PGV*
- Ratio of peak ground motion displacement to peak ground acceleration: *PGD/PGA*
- Ratio of spectral velocity to peak ground velocity: I_M (Maniatakis et al., 2008)

Three ground motion subsets are formed for each parameter in the list above considering three following ranges which creates sufficient number of data points (at least 14 points) in each range:

$$IMrange_1 < \mu_{IM} - \frac{\sigma_{IM}}{3} \tag{7.2}$$

$$\mu_{IM} - \frac{\sigma_{IM}}{3} \leq IMrange_2 < \mu_{IM} + \frac{\sigma_{IM}}{3} \tag{7.3}$$

$$\mu_{IM} + \frac{\sigma_{IM}}{3} \leq IMrange_3 \quad (7.4)$$

Using the ranges above for the selected ground motion characteristics, several subsets are formed based on 78 far field-ground motion records. The statistical results for these ranges (or subsets) for each ground motion parameter are provided in Table 7.7. All parameters have an increasing mean from $IMrange_1$ to $IMrange_3$.

	IM-mean			IM-cov		
Parametric Cases	**IM Range 1**	**IM Range 2**	**IM Range 3**	**IM Range 1**	**IM Range 2**	**IM Range 3**
$\mathbf{t_S}$	9.292	14.424	28.729	0.208	0.126	0.314
$\mathbf{t_{45}}$	7.275	13.310	35.357	0.245	0.157	0.302
$\mathbf{T_{v,strong}}$	0.112	0.166	0.250	0.197	0.080	0.179
$\mathbf{v_S}$	49.419	98.067	197.647	0.295	0.126	0.507
PGV/PGA	0.080	0.122	0.182	0.161	0.085	0.195
PGD/PGV	0.255	0.440	0.746	0.260	0.103	0.265
PGD/PGA	0.025	0.056	0.138	0.375	0.206	0.309
$\mathbf{I_M}$ **(2%)**	0.945	1.849	2.879	0.295	0.098	0.284

Table 7.7 The developed subset means and covs for selected intensity parameters using far field-ground motion set by Haselton and Deierlein (2007).

The original model of the test case study of Lignos et al. (2008) is considered here to investigate the effects of established ground motion subsets on collapse performance. The statistical results of sensitivity analyses on structural collapse capacity using totally 24 different ground motion subsets are provided in Table 7.8 and Table 7.9.

In Table 7.8, mean of V_R based capacity gives larger values for shorter t_S and t_{45}; smaller number of v_S; smaller peak ratios such as *PGV/PGA*, *PGD/PGV*, and *PGD/PGA*; and lastly for larger $T_{v,strong}$ and I_M. The cov values for collapse capacity obtained in Table 7.9 shows that V_R based capacity is less sensitive to selected ground motions used in each subset for collapse assessment comparing the results for roof drift. In Table 7.9, while V_R gives a cov around 0.092 at largest, D_R gives a maximum cov around 0.270. This may be an indication of efficiency of V_R measure and promotes its use in collapse prediction instead of drift ratios, which are found to be highly

sensitive to the ground motion details near collapse.

	Capacity Mean for Equivalent Velocity Ratio (V_R)			Capacity Mean for Roof Drift Ratio (D_R)		
Parametric Cases	**IM Range 1**	**IM Range 2**	**IM Range 3**	**IM Range 1**	**IM Range 2**	**IM Range 3**
ALL SET: 78 GMs	**0.668**			**13.261**		
ATC-63 SET: 44GMs	**0.667**			**13.174**		
t_S	0.681	0.670	0.634	14.092	12.661	11.783
t_{45}	0.674	0.669	0.650	13.342	13.643	12.305
$T_{v,strong}$	0.665	0.652	0.683	14.151	11.785	12.893
v_S	0.683	0.669	0.637	13.281	13.685	12.500
PGV/PGA	0.669	0.669	0.666	13.976	13.426	12.001
PGD/PGV	0.673	0.671	0.658	13.466	13.457	12.674
PGD/PGA	0.676	0.662	0.659	13.797	13.196	12.050
I_M (2%)	0.667	0.662	0.676	12.408	13.412	14.214

Table 7.8 Mean of collapse capacities at "near-collapse" level for the case study of Lignos et al. (2008) using several subsets of far field-ground motion set by Haselton and Deierlein (2007).

	Capacity cov for Equivalent Velocity Ratio			Capacity cov for Roof Drift Ratio		
Parametric Cases	**IM Range 1**	**IM Range 2**	**IM Range 3**	**IM Range 1**	**IM Range 2**	**IM Range 3**
ALL SET: 78 GMs	**0.059**			**0.216**		
ATC-63 SET: 44GMs	**0.056**			**0.208**		
t_S	0.036	0.038	0.092	0.184	0.212	0.270
t_{45}	0.038	0.068	0.088	0.222	0.192	0.254
$T_{v,strong}$	0.047	0.064	0.065	0.188	0.187	0.249
v_S	0.040	0.054	0.072	0.207	0.206	0.253
PGV/PGA	0.047	0.066	0.071	0.187	0.192	0.266
PGD/PGV	0.053	0.076	0.047	0.220	0.227	0.207
PGD/PGA	0.045	0.081	0.050	0.201	0.237	0.216
I_M (2%)	0.072	0.046	0.049	0.258	0.188	0.177

Table 7.9 Coefficient of variations of collapse capacities at "near-collapse" level for the case study of Lignos et al. (2008) using several subsets of far field-ground motion set by Haselton and Deierlein (2007).

In order to better compare effects of variability of ground motion sets on collapse performance, the collapse fragility curves are obtained for each selected 8 parameters in Figure 7.21 and Figure 7.22 using the statistical methodology developed before in Chapter 6 (i.e., the safety margin approach built on the IDA-based collapse capacity and the linear collapse demand model with a non-stationary variance coefficient of 0.25). Also, collapse performances based on the general data sets by ATC-63 (44 records) and by Haselton and Deierlein (78 records) are provided for comparison.

Duration related ground motion indices such as t_S, t_{45}, and $T_{v,strong}$ are parameters that indicate damage potential of ground motions. As expected, they show larger collapse probability from the first range to the third range (i.e., as the duration related intensity value increases) in Figure 7.21a, Figure 7.21b, and Figure 7.21c respectively. Similarly, it is more probable for the structure to collapse as the impulsive characteristics of ground motions such as *PGV/PGA*, *PGD/PGV*, and *PGD/PGA* get larger in Figure 7.22a, Figure 7.22b, and Figure 7.22c respectively. Here, only exception is I_M (the ratio of *Sv* to *PGV*; Maniatakis et al., 2008), which shows smaller probability of collapse as I_M increases indicating that *PGV* has more effect on collapse comparing to *Sv*.

From the results, it is clearly seen that records in ATC-63 set is so well selected from the expanded 78-record set that they show almost the same collapse performance. In Figure 7.21 and Figure 7.22, among the fragility sets for each 8 parameters, v_S (the number of zero crossing in strong duration) shows the least difference (Figure 7.21d) between the collapse performances of the three ranges, while I_M (the ratio of *Sv* to *PGV*; Maniatakis et al., 2008) shows the largest one (Figure 7.22d). Note that this difference represents the record-to-record variability. If one wants to decrease this variability in collapse prediction, then v_S can be a good candidate in selection of record sets. However, since most of attenuation relationships use peak ground motion parameters, *PGD/PGV* (Figure 7.22b) can be then the most practical choice with being one of the indices showing small differences in collapse fragilities between ranges.

This parametric study describing herein clearly shows that model uncertainties as well as ground motions uncertainties would impact the estimate of collapse capacities and fragilities. Therefore, a more complete analytical study including more variations in structural model parameters using

more ground motions is needed to better quantify the influences of uncertainties in these parameters. In order to have a more accurate prediction of the collapse probabilities, further research is needed to develop statistical methodologies to integrate these uncertainties into collapse fragility curves.

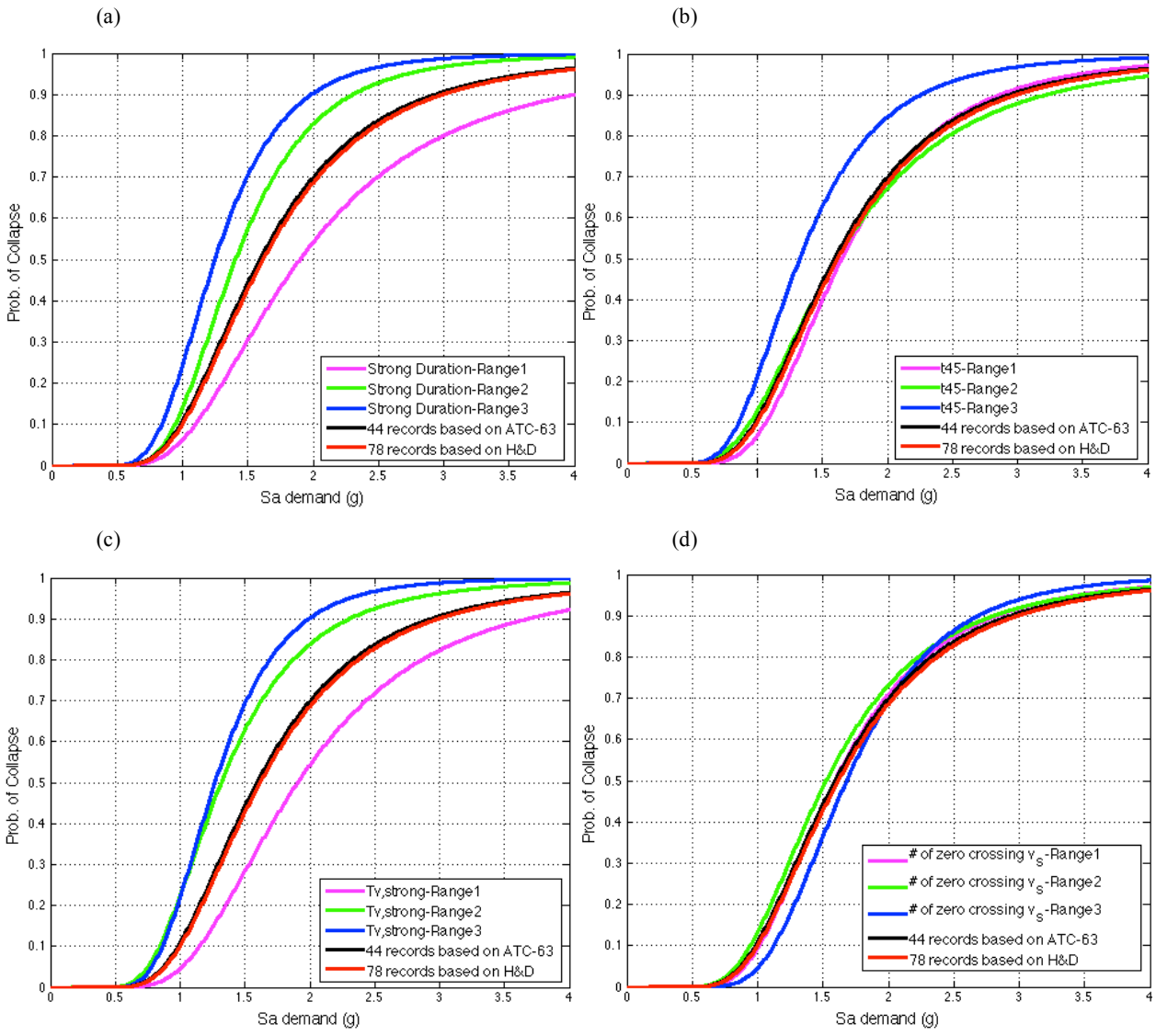

Figure 7.21 Collapse fragility relations for the test case of Lignos et al. (2008) with different ground motion subsets using 78 far field-ground motion records.

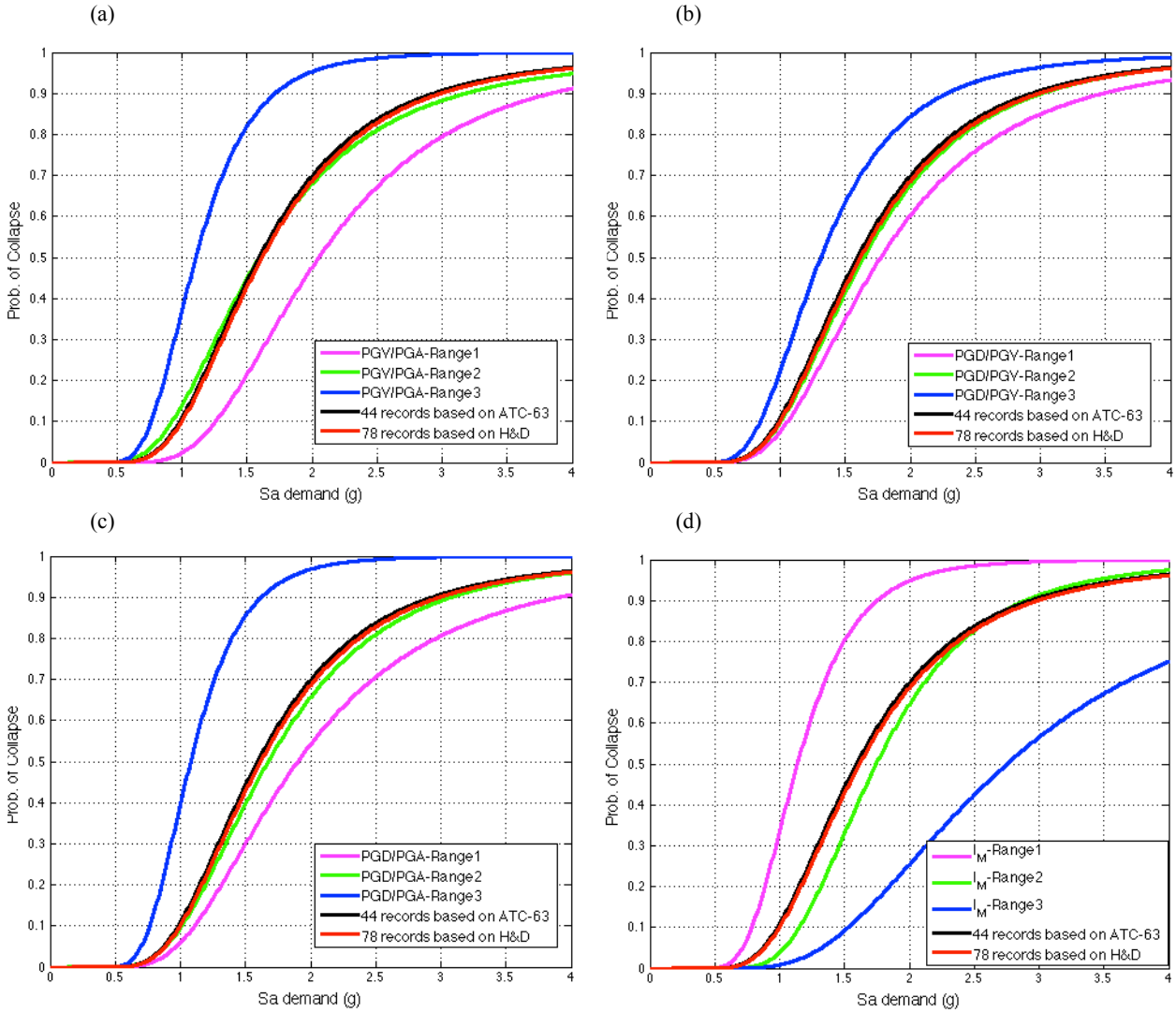

Figure 7.22 Collapse fragility relations for the test case of Lignos et al. (2008) with different ground motion subsets using 78 far field-ground motion records.

8. CONCLUSIONS

8.1. Summary and Main Findings

Collapse criteria of IDA procedure in the literature are usually based on simple rules, such as DM-based rule or IM-based rule, derived from the relationship between a measure of ground motion intensity and an engineering parameter roughly representing structural damage, which are traditionally elastic spectral acceleration versus maximum inter-story drift ratio. These collapse criteria are subjective or based on engineering judgment, and also depend on assumed threshold values instead of the actual occurrence of dynamic instability. Therefore, a new collapse criterion, i.e., "energy rule" has been proposed to predict collapse in terms of dynamic instability caused by loss of structural resistance against the gravity loads, instead of the behavior of the IDA curves. Input energy components released into the structure due to earthquake shaking and applied gravity loads were compared to each other in developing the new collapse criteria. It was observed that, as the structure approaches the collapse level, the gravity energy shows a large increase, which even exceeds the earthquake energy experienced. Thereby, the new collapse criterion has been defined as a boundless increase in the gravity energy. A quantitative indication of structural collapse has been also proposed as gravity energy exceeding dynamic energy with a sudden increase.

In order to develop a new stochastic framework that can validate new collapse limit-state, identify important parameters, and compute the collapse probabilities of structures under cyclic dynamic loadings, it was necessary to develop validated computational models of structural collapse. There is a dearth of collapse experiments reported in the literature because of economic reasons and complexity of collapse test procedure. This study selected three steel frame experimental case studies (Kanvinde, 2003; Rodgers and Mahin, 2004; Lignos *et al.*, 2008) to develop validated computational models. OpenSees models were built for each test case study, and then validated by corresponding experimental tests results. The new collapse criterion was then tested and confirmed by performing energy based collapses analyses on the validated computational models subjected to the test ground motions.

There are several measures reported in the literature to provide quantitative description of the performance of the structures in view of both local and global behaviors during an earthquake.

However, most recent research on the IDA-based approach has selected only one DM and one IM (mostly maximum story drift ratio and elastic spectral acceleration) and lacks thorough investigation on selection of multiple performance measures that best describe collapse capacity and on the benefit of having more than one DM or IM for collapse capacity prediction in terms of accuracy and variability. Moreover, traditional selections for DM such as inter-storey drift or plastic hinge rotation at a structural component for collapse assessment ignores redistribution and variation of damage within the structural system, therefore may not accurately represent structural resistance against collapse. Therefore, extensive IDAs were performed on validated collapse simulation models using 79 far-field records provided by Haselton and Deierlein (2007) in order to obtain a large sample for several performance measures. Based on this large sample and on the new collapse criterion, key parameters that govern collapse capacity of the test case study by Lignos et al. (2008) were identified with a statistical analysis.

Findings of the statistical evaluations on performance measures reveal that reliable and accurate collapse assessment requires global cumulative performance measures that are associated with severe structural damage just before collapse. Since energy parameters represent aggregated damage of individual components, they can better account for distribution and variation of damage within structure. Therefore, considering the energy balance of a structural system, several practical combinations of energy parameters were investigate to develop new performance candidates that have small variability as well as have robustness to intensity scaling near collapse. As a result, an equivalent velocity ratio of the system's dissipated energy to input seismic energy was found the most effective collapse descriptor representative of history of global behavior of the structure. Unlike the traditional selection for DM such as inter-story drift ratio, this new collapse descriptor based on energy was found to show much smaller variability and less sensitivity to intensity scaling near collapse.

The fragility approaches in collapse assessment are generally based on IM-based or DM-based fragility method. While both approaches rely on "demand vs capacity" framework to construct fragilities, IM-based approach considers uncertainty only in seismic capacity, which may provide less reliable collapse prediction. On the other hand, DM-based fragility accounts for uncertainties in both seismic capacity and seismic demand but requires approximations in assessment of conditional distributions of DM given IM. DM-based approach traditionally uses IDA curves

mostly between maximum inter-story drift ratio and elastic spectral acceleration to evaluate the conditional distribution of structural demand. However, conditional distributions for inter-story drift ratio are found to give larger variability because of its sensitivity to intensity scaling near collapse (i.e., enormous increase in structural response corresponding to a small scale increment in intensity). Thereby, considering uncertainty in both seismic demand and seismic capacity, the new collapse descriptor "equivalent energy ratio" was utilized in this study to develop new collapse fragility curves using energy based collapse criterion for a more reliable and accurate collapse prediction.

Linear regression analyses with stationary/varying variance were performed to develop demand models based on the new equivalent velocity ratio at a given level of seismic intensity. Spectral acceleration was chosen here to describe intensity of ground motions since it is one of the most practical measures widely used in seismic hazard assessments. Capacity models were constructed fitting normal distributions to IDA collapse data points obtained using "energy rule". Using safety margin approach, uncertainties in developed collapse capacity and demand models were then combined to get more reliable and appropriate new collapse fragility curves for use in performance-based design and collapse assessment.

Moreover, new conditional collapse fragilities (i.e, fragility contours) were obtained extending the new fragility approach to include one more ground motion characteristics. Integrating the available information about ground motion characteristics into fragility models may decrease the dispersion due to record-to-record variability, which in turn corresponds to a reduction in uncertainty level associated to collapse probability computation. Therefore, when more information about ground motion characteristics is available, one can then estimate structural collapse probability at a given intensity level of spectral acceleration and a secondary intensity measure using fewer non-linear analysis and less ground motion time histories.

Large-scale parametric studies were also performed in collapse assessment of structures considering uncertainties in model parameters. For this purpose, virtual collapse simulations were performed using the validated analytical model of the test case study by Lignos et al. (2008) considering a wide array of structural parameters to account for the impacts of a structural model selection on the collapse prediction of structures. The following parameters that

significantly affect ductility and damage potential of the test case study were selected in the parametric study to adjust the analytical model: material properties such as yield moment, stiffness, and degrading amount; factors that affects distribution of damage through structure such as the ratio of beam-strength to column-strength; system properties such as damping and mass; and lastly geometrical data such as bay and storey height. The new fragility approach was successfully generalized to all adjusted analytical models of the test case study to perform sensitivity analyses of collapse performance. It has been observed that ductile connection model parameters related to strain-hardening ratio and deterioration rate after yielding can result in remarkably different collapse estimates. The results of sensitivity analyses applied on collapse capacity indicate that equivalent velocity ratio is the most efficient measure in describing collapse performance of structures showing smaller sensitivity to a change in structural model parameters comparing to roof drift ratio.

Lastly, the effect of earthquake characteristics on the structural collapse capacity of steel frame structures under cyclic loading was also studied for the purpose of estimating and improving structural reliability against collapse. In order to better understand the record-to record variability of ground motion records on collapse performance, the collapse fragility curves for the test case study of Lignos et al. (2008) were obtained for several number of subsets of ground motions using 78 far-field record set by Haselton and Deierlein (2007). The ratio of peak ground displacement to peak ground velocity, which is unaffected from intensity scaling, was found the most practical index that can be utilized in selection of a suite of ground motions to be used in nonlinear collapse analyses. The results showed small differences in collapse prediction between subsets of ground motions constructed based on this parameter reduces the epistemic uncertainty significantly and thus enable risk assessment of structural collapse with enhanced confidence. Therefore, the number of ground motions needed for collapse assessment can be reduced significantly if one chooses this index to describe collapse assessment for the test case study of Lignos et al. (2008).

8.2. Limitations of the Study

The list below summarizes the limitations as well as assumptions considered in the study:

- Advanced high-fidelity analytical models are desired for more accurate and reliable

simulation of structural collapse considering many important factors. However, they are computationally demanding and highly sensitive to numerical convergence issues in general. Therefore, practical macro-models that correlate well with experiment results of selected case studies of collapse were used in this research to perform large-scale parametric studies in collapse assessment of structures and assessment of safety margin against collapse.

- Since there are only a few available collapse experiments in the literature, only three case studies for steel frame experiments were considered in this study to develop the new stochastic framework described in previous section. Collapse models of these steel moment resisting frames were built in 2D-plane and were developed by using elastic elements for girders and columns, coupled with the use of uniaxial moment-rotation relations at the element ends.
- Sidesway collapse mechanism was the dominant failure mode in the three-collapse experiments selected in this study. Therefore, the new energy collapse criterion developed for more reliable collapse assessment was only checked and validated for this particular collapse mode.
- Only 78 far-field strong ground motions provided by Haselton and Deierlein (2007) were considered to develop the probabilistic collapse assessment procedure. Near-field records and bilateral or vertical ground motions were not considered in this study.
- The findings of the study such as key descriptors that govern collapse capacity were found using the test case study of Lignos et al. (2008). Parametric studies were also conducted on the same case study assuming variations in hysteretic behaviors of ductile connections at the element ends. Therefore, the findings of this study cannot be realistically considered to cover the broader class of steel moment-frame buildings, but can be only applicable to the test case study of Lignos et al. (2008) and can be generalized to similar degrading short period structures.
- In the parametric studies using the test case study of Lignos et al. (2008), variations selected for some of the structural model parameters might not be realistic in view of structural design requirements. However, it helps to understand the trends in collapse performance for such extreme cases.

8.3. Future Work

The new collapse criteria based on computational simulations of dynamic instability give rise to new research opportunities to gain better understanding of complex collapse mechanism of structural systems, identify key parameters that would help describe collapse through comprehensive and accurate measurements, achieve more accurate and systematic prediction of collapse, and allow for incorporating uncertainties into collapse prediction. Therefore, the stochastic procedure developed for collapse assessment in this study can be applied to other structural systems as well to investigate their collapse performance. In summary, the following list provides potential topics for future research:

- Energy-based collapse criterion can be applied to other structural system to assess collapse capacity for other failure modes such as vertical collapse mechanism due to the direct loss of gravity columns or disconnection of slab from the columns; or both vertical and sidesway collapse mechanisms that may take place especially in a high-rise building.
- Moreover, one or several structural components of a building may fail due to an earthquake excitation but the structure may still be able to maintain its integrity. For example, a gravity column may fail in compression, or shear transfer may be lost between a beam and a column, however such local failures may not trigger the global instability of the structure. Therefore, research is needed to explore such unconventional progressive collapse mechanisms especially for three-dimensional structural systems.
- Other constitutive models that have capability to include combined shear and flexural failures as well as failures due to brittle fracture can be adopted in steel frames or concrete frames and impacts on collapse capacity can be investigated through the developed framework for probabilistic collapse assessment.
- More realistic building structures with three-dimensional irregular structural systems can be studied using the developed stochastic framework to investigate torsional effects on collapse behavior.
- It has been shown that that the scaling in IDA would impact the identified collapse capacities as well as structural demands. Therefore, this indicates that there is a need of further research on scaling effect of ground motions, as this is an important topic in earthquake engineering. Moreover, it has been observed that there are not many several

strong ground motion databases that can cause structural collapse at original intensity levels. For this purpose, artificial ground motions can be developed to simulate strong ground motions to be used in nonlinear collapse analyses.

- The findings of the parametric studies can be employed as primary results to further develop guidelines regarding selection of a suite of ground motions to be used in nonlinear collapse analyses.
- The parametric study describing herein clearly shows that model uncertainties as well as ground motions uncertainties would impact the estimate of collapse capacities and fragilities. Therefore, a more complete analytical study including more realistic variations in structural model parameters around the nominal values and including more buildings of various heights is needed to better quantify uncertainties in these parameters. In addition to gravity loads, effects of potential variations in live loads on collapse assessment can be also studied to see the effects on collapse capacity.
- More comprehensive research can be conducted on critical collapse intensity measures using the parametric data on structural parameters to study the effect of acceleration, velocity and displacement-sensitive indices on collapse performance with different dominant periods.
- Further research is required to develop statistical methodologies to integrate record-to-record variability in ground motions and variability in model parameters into collapse fragility curves to be used in PBEE framework. This is necessary for a more accurate and reliable prediction of the collapse probabilities.

APPENDIX A

COMPONENT MODELS USED IN THE STUDY

In the OpenSees manual, "Steel02", "Hysteretic", and "Bilin" material models were selected for the test case studies by Kanvinde (2003), Rodgers and Mahin (2004), and Lignos et al. (2008) respectively. In the following, description about the features of these selected component models are summarized:

- The material model for "Steel02" constructs a uniaxial Giuffre-Menegotto-Pinto steel material object with isotropic strain hardening. Table A.1 gives the command function and summarizes input values for this material model.
- The material model for "Hysteretic" constructs a uniaxial bilinear hysteretic material object with pinching of force and deformation, damage due to ductility and energy, and degraded unloading stiffness based on ductility. The command function and input values for this model are provided in Table A.2.
- The material model for "Bilin" simulates the modified Ibarra-Krawinkler deterioration model with bilinear hysteretic response. It considers cyclic energy dissipation to include deterioration in stiffness and strength of components under large cyclic inelastic displacements. The developed phenomenological models consider cyclic deterioration in four component parameters: yield strength, post-capping strength, unloading stiffness, and reloading stiffness. Moreover, different rates of cyclic deterioration in the two loading directions can be chosen, and residual strength can be assumed to consider asymmetric component hysteric behavior. Table A.3 shows the command function and input values for this model.

uniaxialMaterial Steel02 $matTag $Fy $E $b $R0 $cR1 $cR2 <$a1 $a2 $a3 $a4 $sigInit>	
$matTag	integer tag identifying material
$Fy	yield strength
$E0	initial elastic tangent
$b	strain-hardening ratio (ratio between post-yield tangent and initial elastic tangent)
$R0 $cR1 $cR2	parameters to control the transition from elastic to plastic branches. Recommended values: $R0=between 10 and 20, $cR1=0.925, $cR2=0.15
$a1	isotropic hardening parameter, increase of compression yield envelope as proportion of yield strength after a plastic strain of $a2*($Fy/E0). (optional)
$a2	isotropic hardening parameter (see explanation under $a1). (optional default = 1.0).
$a3	isotropic hardening parameter, increase of tension yield envelope as proportion of yield strength after a plastic strain of $a4*($Fy/E0). (optional default = 0.0)
$a4	isotropic hardening parameter (see explanation under $a3). (optional default = 1.0)
$sigInit	Initial Stress Value (optional, default: 0.0)

Table A.1 The input parameters for "Steel02" component model
(Ref: http://opensees.berkeley.edu/wiki/index.php/Steel02_Material).

uniaxialMaterial Hysteretic $matTag $s1p $e1p $s2p $e2p <$s3p $e3p> $s1n $e1n $s2n $e2n <$s3n $e3n> $pinchX $pinchY $damage1 $damage2 <$beta>	
$matTag	integer tag identifying material
$s1p $e1p	stress and strain (or force & deformation) at first point of the envelope in the positive direction
$s2p $e2p	stress and strain (or force & deformation) at second point of the envelope in the positive direction
$s3p $e3p	stress and strain (or force & deformation) at third point of the envelope in the positive direction (optional)
$s1n $e1n	stress and strain (or force & deformation) at first point of the envelope in the negative direction
$s2n $e2n	stress and strain (or force & deformation) at second point of the envelope in the negative direction
$s3n $e3n	stress and strain (or force & deformation) at third point of the envelope in the negative direction (optional)
$pinchx	pinching factor for strain (or deformation) during reloading
$pinchy	pinching factor for stress (or force) during reloading
$damage1	damage due to ductility: D1(mu-1)
$damage2	damage due to energy: D2(Eii/Eult)
$beta	power used to determine the degraded unloading stiffness based on ductility, mu-beta (optional, default=0.0)

Table A.2 The input parameters for "Hysteretic" component model
(Ref: http://opensees.berkeley.edu/wiki/index.php/Hysteretic_Material).

uniaxialMaterial Bilin $matTag $K0 $as_Plus $as_Neg $My_Plus $My_Neg $Lamda_S $Lamda_C $Lamda_A $Lamda_K $c_S $c_C $c_A $c_K $theta_p_Plus $theta_p_Neg $theta_pc_Plus $theta_pc_Neg $Res_Pos $Res_Neg $theta_u_Plus $theta_u_Neg $D_Plus $D_Neg <$nFactor>	
$matTag	integer tag identifying material
$K0	elastic stiffness
$as_Plus	strain hardening ratio for positive loading direction
$as_Neg	strain hardening ratio for negative loading direction
$My_Plus	effective yield strength for positive loading direction
$My_Neg	effective yield strength for negative loading direction (negative value)
$Lamda_S	Cyclic deterioration parameter for strength deterioration
$Lamda_C	Cyclic deterioration parameter for post-capping strength deterioration
$Lamda_A	Cyclic deterioration parameter for acceleration reloading stiffness deterioration (is not a deterioration mode for a component with Bilinear hysteretic response).
$Lamda_K	Cyclic deterioration parameter for unloading stiffness deterioration
$c_S	rate of strength deterioration. The default value is 1.0.
$c_C	rate of post-capping strength deterioration. The default value is 1.0.
$c_A	rate of accelerated reloading deterioration. The default value is 1.0.
$c_K	rate of unloading stiffness deterioration. The default value is 1.0.
$theta_p_Plus	pre-capping rotation for positive loading direction (often noted as plastic rotation capacity)
$theta_p_Neg	pre-capping rotation for negative loading direction (often noted as plastic rotation capacity) (positive value)
$theta_pc_Plus	post-capping rotation for positive loading direction
$theta_pc_Neg	post-capping rotation for negative loading direction (positive value)
$Res_Pos	residual strength ratio for positive loading direction
$Res_Neg	residual strength ratio for negative loading direction (positive value)
$theta_u_Plus	ultimate rotation capacity for positive loading direction
$theta_u_Neg	ultimate rotation capacity for negative loading direction (positive value)
$D_Plus	rate of cyclic deterioration in the positive loading direction (this parameter is used to create asymmetric hysteretic behavior for the case of a composite beam). For symmetric hysteretic response use 1.0.
$D_Neg	rate of cyclic deterioration in the negative loading direction (this parameter is used to create asymmetric hysteretic behavior for the case of a composite beam). For symmetric hysteretic response use 1.0.
$nFactor	elastic stiffness amplification factor, mainly for use with concentrated plastic hinge elements (optional, default = 0).

Table A.3 The input parameters for "Bilin" component model
(Ref: http://opensees.berkeley.edu/wiki/index.php/Bilin_Material).

APPENDIX B

COMPONENT MODEL PARAMETERS USED FOR BILIN MODEL

The case study of Lignos et al. (2008) is a 4-story, 2-bay steel frame in 1/8 scale with reduced-beam sections (RBS). An analytical model for the test frame was developed in OpenSees as shown in Figure B.1, which consists of elastic members with plastic hinges at the ends. The rotational springs were used to analytically model the plastic hinges at element ends with a modified Ibarra-Krawinkler deterioration model (Lignos et al. 2008) available in OpenSees. The mathematical model properties and deterioration parameters used in the analytical model are given in Table B.1 and Table B.2. More details about the element section dimensions and properties can be found in the study by Lignos and Krawinkler (2012).

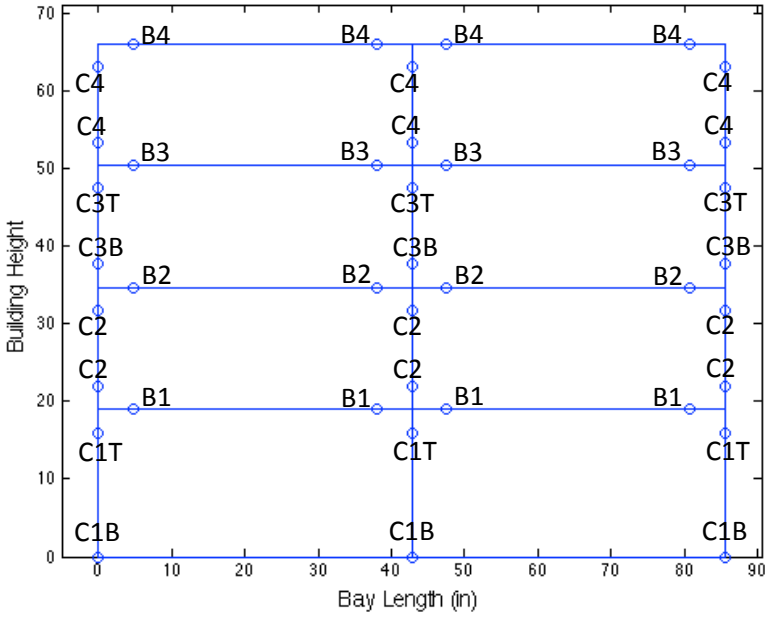

Figure B.1 The analytical model developed for the test case study by Lignos et al. (2008) (Note that circles indicate the location of rotational springs at the element ends).

System Parameters	Values
Damping	1.5% applied on mass and tangent (current) stiffness
Period	0.44 sec
Story Weight	8.6 kips (for 1st , 2nd , and 3rd story)
Roof Weight	8.8 kips
Clear Storey Height	19.75 in (1st story) and 15.75in (1st, 2nd, and 3rd story)
Clear Bay Length	42.75 in

Table B.1 The system parameters assumed for the test case study by Lignos et al. (2008).

Location	My	Ki	Mc/My	L	ThetaP	ThetaPC	Mr	ThetaU	D	c
C1B	34.5	25700	1.10	26.0	0.050	2.0	0	0.4	1	1
C1T, C2, C3B	27.0	20631	1.10	26.0	0.050	2.0	0	0.4	1	1
C3T, C4	14.2	11200	1.08	18.2	0.055	2.4	0	0.4	1	1
B1, B2	19.8	13000	1.10	36.0	0.050	1.6	0	0.4	1	1
B3, B4	14.2	11200	1.08	18.2	0.055	2.4	0	0.4	1	1

Table B.2 The rotational springs parameters assumed for the test case study by Lignos et al. (2008) (Note that My: yield moment strength, Ki: initial stiffness, Mc/My: post-yielding moment ratio; L: cyclic deterioration parameter, ThetaP: plastic rotational capacity, TehtaPC: post-capping rotational capacity, Mres: resiudual strength, ThetaU: ultimate rotation, D: rate of cyclic component deterioration, and c: rate of component deterioration).

APPENDIX C

THE FAR-FIELD GROUND MOTION SET RECORDS

The far-field ground motion set considered in this study includes 39 pairs of horizontal ground motion records (totally 78 records) provided by Haselton and Deierlein (2007). The selection criteria in this ground motion set are determined to form a large sample of extreme strong ground motion records that may cause structural collapse of modern buildings. Therefore, the following search criteria were imposed on PEER database (Haselton and Deierlein, 2007) to find the far-field ground motion set records given in Table C.1 and Table C.2:

- Magnitude > 6.5
- Distance from source to site > 10 km (average of Joyner-Boore and Campbell distances)
- Peak ground acceleration > 0.2g AND peak ground velocity > 15 cm/sec
- Soil shear wave velocity, in upper 30m of soil, greater than 180 m/s (NEHRP soil types A-D; note that all selected records happened to be on C/D sites)
- Limit of six records from a single seismic event; if more than six records pass the initial criteria, then the six records with largest *PGV* are selected, but in some cases a lower *PGV* record is used if the *PGA* is much larger.
- Lowest useable frequency < 0.25 Hz, to ensure that the low frequency content was not removed by the ground motion filtering process
- Strike-slip and thrust faults (consistent with California)
- No consideration of spectral shape
- No consideration of station housing, but PEER-NGA records were selected to be "free-field"

			Event Information				Site Information				Record Information		
EQ Index	EQ ID	PEER-NGA Rec. Num.	Mag.	Year	Event	Fault Type	Station Name	Vs_30 (m/s)	Campbell Distance (km)	Joyner-Boore Distance (km)	Lowest Useable Freq. (Hz)	Horizontal Acceleration Time History Files	
1*	12011	953	6.7	1994	Northridge	Blind thrust	Beverly Hills - 14145	356	17.2	9.4	0.25	NORTHR/MUL009.at2	NORTHR/MUL279.at2
2*	12012	960	6.7	1994	Northridge	Blind thrust	Canyon Country - W Lost Cany	309	12.4	11.4	0.13	NORTHR/LOS000.at2	NORTHR/LOS270.at2
3	12013	1003	6.7	1994	Northridge	Blind thrust	LA - Saturn St	309	27.0	21.2	0.13	NORTHR/STN020.at2	NORTHR/STN110.at2
4	12014	1077	6.7	1994	Northridge	Blind thrust	Santa Monica City Hall	336	27.0	17.3	0.14	NORTHR/STM090.at2	NORTHR/STM360.at2
5	12015	952	6.7	1994	Northridge	Blind thrust	Beverly Hills - 12520	546	18.4	12.4	0.16	NORTHR/MU2035.at2	NORTHR/MU2125.at2
6*	12041	1602	7.1	1999	Duzce, Turkey	Strike-slip	Bolu	326	12.4	12.0	0.06	DUZCE/BOL000.at2	DUZCE/BOL090.at2
7*	12052	1787	7.1	1999	Hector Mine	Strike-slip	Hector	685	12.0	10.4	0.04	HECTOR/HEC000.at2	HECTOR/HEC090.at2
8*	12061	169	6.5	1979	Imperial Valley	Strike-slip	Delta	275	22.5	22.0	0.06	IMPVALL/H-DLT262.at2	IMPVALL/H-DLT352.at2
9*	12062	174	6.5	1979	Imperial Valley	Strike-slip	El Centro Array #11	196	13.5	12.5	0.25	IMPVALL/H-E11140.at2	IMPVALL/H-E11230.at2
10	12063	162	6.5	1979	Imperial Valley	Strike-slip	Calexico Fire Station	231	11.6	10.5	0.25	IMPVALL/H-CXO225.at2	IMPVALL/H-CXO315.at2
11	12064	189	6.5	1979	Imperial Valley	Strike-slip	SAHOP Casa Flores	339	10.8	9.6	0.25	IMPVALL/H-SHP000.at2	IMPVALL/H-SHP270.at2
12*	12071	1111	6.9	1995	Kobe, Japan	Strike-slip	Nishi-Akashi	609	25.2	7.1	0.13	KOBE/NIS000.at2	KOBE/NIS090.at2
13*	12072	1116	6.9	1995	Kobe, Japan	Strike-slip	Shin-Osaka	256	28.5	19.1	0.13	KOBE/SHI000.at2	KOBE/SHI090.at2
14	12073	1107	6.9	1995	Kobe, Japan	Strike-slip	Kakogawa	312	3.2	22.5	0.13	KOBE/KAK000.at2	KOBE/KAK090.at2
15	12074	1106	6.9	1995	Kobe, Japan	Strike-slip	KJMA	312	95.8	0.9	0.06	KOBE/KJM000.at2	KOBE/KJM090.at2
16*	12081	1158	7.5	1999	Kocaeli, Turkey	Strike-slip	Duzce	276	15.4	13.6	0.24	KOCAELI/DZC180.at2	KOCAELI/DZC270.at2
17*	12082	1148	7.5	1999	Kocaeli, Turkey	Strike-slip	Arcelik	523	13.5	10.6	0.09	KOCAELI/ARC000.at2	KOCAELI/ARC090.at2
18*	12091	900	7.3	1992	Landers	Strike-slip	Yermo Fire Station	354	23.8	23.6	0.07	LANDERS/YER270.at2	LANDERS/YER360.at2
19*	12092	848	7.3	1992	Landers	Strike-slip	Coolwater	271	20.0	19.7	0.13	LANDERS/CLW-LN.at2	LANDERS/CLW-TR.at2
20	12093	864	7.3	1992	Landers	Strike-slip	Joshua Tree	379	11.4	11.0	0.07	LANDERS/JOS000.at2	LANDERS/JOS090.at2

* This marks the records that are included a smaller (22 record) far-field set (selected with a maximum of 2 records per event).
This smaller set was used in the Applied Technology Council Project 63.

Table C.1 Far-field ground motion set by Haselton and Deierlein (2007)
(Ref: http://www.csuchico.edu/structural/researchdatabases/ground_motion_sets.shtml).

			Event Information				Site Information				Record Information		
EQ Index	EQ ID	PEER-NGA Rec. Num.	Mag.	Year	Event	Fault Type	Station Name	Vs_30 (m/s)	Campbell Distance (km)	Joyner-Boore Distance (km)	Lowest Useable Freq. (Hz)	Horizontal Acceleration Time History Files	
21*	12101	752	6.9	1989	Loma Prieta	Strike-slip	Capitola	289	35.5	8.7	0.13	LOMAP/CAP000.at2	LOMAP/CAP090.at2
22*	12102	767	6.9	1989	Loma Prieta	Strike-slip	Gilroy Array #3	350	12.8	12.2	0.13	LOMAP/G03000.at2	LOMAP/G03090.at2
23	12103	783	6.9	1989	Loma Prieta	Strike-slip	Oakland - Outer Harbor	249	74.3	74.2	0.13	LOMAP/CH12000.at2	LOMAP/CH10270.at2
24	12104	776	6.9	1989	Loma Prieta	Strike-slip	Hollister - South & Pine	371	27.9	27.7	0.13	LOMAP/HSP000.at2	LOMAP/HSP090.at2
25	12105	777	6.9	1989	Loma Prieta	Strike-slip	Hollister City Hall	199	27.6	27.4	0.13	LOMAP/HCH090.at2	LOMAP/HCH180.at2
26	12106	778	6.9	1989	Loma Prieta	Strike-slip	Hollister Diff. Array	216	24.8	24.5	0.13	LOMAP/HDA165.at2	LOMAP/HDA255.at2
27*	12111	1633	7.4	1990	Manjil, Iran	Strike-slip	Abbar	724	13.0	12.6	0.13	MANJIL/ABBAR--L.at2	MANJIL/ABBAR--T.at2
28*	12121	721	6.5	1987	Superstition Hills	Strike-slip	El Centro Imp. Co. Cent	192	18.5	18.2	0.13	SUPERST/B-ICC000.at2	SUPERST/B-ICC090.at2
29*	12122	725	6.5	1987	Superstition Hills	Strike-slip	Poe Road (temp)	208	11.7	11.2	0.25	SUPERST/B-POE270.at2	SUPERST/B-POE360.at2
30	12123	728	6.5	1987	Superstition Hills	Strike-slip	Westmorland Fire Sta	194	13.5	13.0	0.13	SUPERST/B-WSM090.at2	SUPERST/B-WSM180.at2
31*	12132	829	7.0	1992	Cape Mendocino	Thrust	Rio Dell Overpass - FF	312	14.3	7.9	0.07	CAPEMEND/RIO270.at2	CAPEMEND/RIO360.at2
32*	12141	1244	7.6	1999	Chi-Chi, Taiwan	Thrust	CHY101	259	15.5	10.0	0.05	CHICHI/CHY101-E.at2	CHICHI/CHY101-N.at2
33*	12142	1485	7.6	1999	Chi-Chi, Taiwan	Thrust	TCU045	705	26.8	26.0	0.05	CHICHI/TCU045-E.at2	CHICHI/TCU045-N.at2
34	12143	1524	7.6	1999	Chi-Chi, Taiwan	Thrust	TCU095	447	45.3	45.2	0.05	CHICHI/TCU095-E.at2	CHICHI/TCU095-N.at2
35	12144	1506	7.6	1999	Chi-Chi, Taiwan	Thrust	TCU070	401	24.4	19.0	0.04	CHICHI/TCU070-E.at2	CHICHI/TCU070-N.at2
36	12145	1595	7.6	1999	Chi-Chi, Taiwan	Thrust	WGK	259	15.4	10.0	0.09	CHICHI/WGK-E.at2	CHICHI/WGK-N.at2
37	12146	1182	7.6	1999	Chi-Chi, Taiwan	Thrust	CHY006	438	13.2	9.8	0.04	CHICHI/CHY006-N.at2	CHICHI/CHY006-W.at2
38*	12151	68	6.6	1971	San Fernando	Thrust	LA - Hollywood Stor FF	316	25.9	22.8	0.25	SFERN/PEL090.at2	SFERN/PEL180.at2
39*	12171	125	6.5	1976	Friuli, Italy	Thrust (part blind)	Tolmezzo	425	15.8	15.0	0.13	FRIULI/A-TMZ000.at2	FRIULI/A-TMZ270.at2

* This marks the records that are included a smaller (22 record) far-field set (selected with a maximum of 2 records per event).
This smaller set was used in the Applied Technology Council Project 63.

Table C.2 Far-field ground motion set by Haselton and Deierlein (2007)- Cont'd.
(Ref: http://www.csuchico.edu/structural/researchdatabases/ground_motion_sets.shtml).

REFERENCES

Adam, C., Ibarra, L. F., and Krawinkler H. (2004). "Evaluation of P-Delta Effects in Non-deteriorating MDOF Structures from Equivalent SDOF Systems," *Proceedings of 13th World Conference on Earthquake Engineering,* Vancouver, B.C., Canada.

AISC (1992). Seismic Provisions for Structural Steel Buildings, Chicago.

Akiyama, H. (2002). "Collapse Modes of Structures under Strong Motions of Earthquake," *Annals of Geophysics,* 45(6), 791-798

Altoontash, A. (2004). *Simulation and Damage Models for Performance Assessment of Reinforced Concrete Beam-Column Joints,* Ph.D. Dissertation, Department of Civil and Environmental Engineering, Stanford University.

American Society of Civil Engineers. (2006). ASCE41-06: Seismic Rehabilitation of Existing Buildings, Reston, VA.

Ang, A.H.S., and Tang, W.H. (2007). *Probability Concepts In Engineering. Emphasis On Applications To Civil And Environmental Engineering*, 2nd Edition, John Wiley And Sons, Inc.

Applied Technology Council (2009). *Quantification of Building Seismic Performance Factors*, ATC-63 Project Report, FEMA.

Araki, Y., and Hjelmstad, K. D. (2000). "Criteria for Assessing Dynamic Collapse of Elastoplastic Structural Systems," *Earthquake Engineering and Structural Dynamics*, 29(8), 1177–1198.

Araya, R., and Saragoni, G. R. (1980). *Capacidad de los movimientos de producir daño estructral*, Publication SES I 7/80 (in Spanish), Division of Structural Engineering, Department of Engineering, University of Chile, Santiago.

Arias, A. (1970). "A Measure of Earthquake Intensity, in Seismic Design for Nuclear Power Plants," R. J. Hansen, Editor, M. I. T. Press, Cambridge, 438–483.

Ayoub, A., Mijo, C., and Chenouda, M. (2004). "Seismic Fragility Analysis of Degrading Structural Systems," *Proceedings of 13th World Conference on Earthquake Engineering,* Vancouver, B.C., Canada.

Baker J.W. (2007). "Probabilistic Structural Response Assessment Using Vector-Valued Intensity Measures," *Earthquake Engineering & Structural Dynamics,* 36 (13), 1861-1883.

Baker, J.W., and Cornell, C.A. (2005). "A Vector-Valued Ground Motion Intensity Measure Consisting of Spectral Acceleration and Epsilon," *Earthquake Engineering & Structural Dynamics,* 34 (10), 1193-1217.

Bernal, D. (1987). "Amplification Factors for Inelastic P-Δ Effects in Earthquake Analysis." *Earthquake Engineering & Structural Dynamics,* 15(5), 635–651.

Bernal, D. (1992). "Instability of Buildings Subjected to Earthquakes," *Journal of Structural Engineering,* 118(8), 2239–2260.

Bernal, D. (1998). "Instability of Buildings during Seismic Response," *Engineering Structures,* 20(4–6), 496–502.

Bertero, V. V., Anderson, J. C., and Krawinkler, H. (1994). *Performance of steel building structures during the Northridge Earthquake,* Rep. No. UCB/EERC-94/09, Earthquake Engineering Research Center, Univ. of California, Berkeley, Calif.

Bianchini, M., Diotallevi, P., and Baker, J.W. (2009). "Prediction of Inelastic Structural Response Using an Average of Spectral Accelerations," *10th International Conference On Structural Safety And Reliability (Icossar09),* Osaka, Japan.

Bradley, B. A., and Dhakal, R. P. (2008). "Error Estimation of Closed-Form Solution for Annual Rate of Structural Collapse," *Earthquake Engineering and Structural Dynamics*, 37(15), 1721-1737.

Castiglioni, C.A., and Pucinotti, R. (2009). "Review: Failure Criteria and Cumulative Damage Models for Steel Components under Cyclic Loading," *Journal of Constructional Steel Research*, 65, 751-765.

Challa, V. R. M., and Hall, J. F. **(**1994**)**. "Earthquake Collapse Analysis of Steel Frames," *Earthquake Engineering & Structural Dynamics,* 23**(**11**)**, 1199–1218.

Cornell, C.A, and Krawinkler, H. (2000). *Progress and challenges in seismic performance assessment*, PEER Center News, Spring 2000.

Cornell, C., Jalayer, F., Hamburger, R., and Foutch, D. (2002). "Probabilistic Basis for 2000 SAC/FEMA Steel Moment Frame Guidelines," *Journal of Structural Engineering*, 128(4), 526–533.

Deierlein, G.G., Krawinkler, H., and Cornell, C.A. (2003). "A Framework for Performance-Based Earthquake Engineering," *Pacific Conference On Earthquake Engineering*.

Deierlein, G. G., Liel, A. B., Haselton, C.B., and Kircher, C.A. (2007), "Assessing Building System Collapse Performance and Associated Requirements for Seismic Design," *SEAOC 2007 Convention Proceedings*, September 26 – 29.

Delgado, R., Costa, A., Arede, A., Pouca, N.V.,Guedes, J, Romao, X., Delgado, P., and Rocha, P. (2010). "Ongoing Research on Seismic Safety Assessment," *Bulletin of Earthquake Engineering*, 8,181–199

Elwood, K. J., and Moehle, J. P. **(**2003**)**. *Shake Table Tests and Analytical Studies on the Gravity Load Collapse of Reinforced Concrete Frames,* Rep. 2003/01, Pacific Earthquake Engineering Research Center, Univ. of California, Berkeley, California.

Engelhardt, M. D., (2001). "Ductile Detailing of Steel Moment Frames: Basic Concepts, Recent Developments and Unresolved Issues," *Proceedings, XIII Mexican Conference on Earthquake Engineering,* Guadalajara, Mexico, October 31 – November 2

Fajfar, P., Vidic, T., and Fischinger, M. (1990). "A Measure of Earthquake Motion Capacity to Damage Medium-Period Structures," Soil Dyn. *Earthquake Eng.*, 9 **(5)** 236–242.

FEMA **(**1997**)**. *NEHRP Guidelines for the Seismic Rehabilitation of Buildings,* Report No. FEMA-273, Applied Technology Council for the Building Seismic Safety Council, Washington, D.C.

FEMA (1998). *NEHRP Recommended Provisions for Seismic Regulations for New Buildings and Other Structures: Part I-Provisions,* Report No. FEMA-302, 1997 Ed., the Building Seismic Safety Council for the Federal Emergency Management Agency, Washington, D.C.

FEMA (2000). *Recommended Seismic Evaluation and Upgrade Criteria for Existing Welded Steel Moment-frame Buildings*, Report No. FEMA-351, SAC Joint Venture, Federal Emergency Management Agency, Washington, DC.

FEMA (2000). *State of the Art Report on Past Performance of Steel Moment-frame Buildings in Earthquakes,* Report No. FEMA-355E, SAC Joint Venture, Federal Emergency Management Agency, Washington, DC.

FEMA (2000a). *Recommended Seismic Design Criteria for New Steel Moment-frame Buildings*, Report No. FEMA-350, SAC Joint Venture, Federal Emergency Management Agency, Washington, DC.

FEMA (2000b). *Prestandard and Commentary for the Seismic Rehabilitation of Buildings*, Report No. FEMA-356, SAC Joint Venture, Federal Emergency Management Agency, Washington, DC.

Gardoni, P., Der Kiureghian, A., and Mosalam, K.M. (2002). "Probabilistic Capacity Models and Fragility Estimates for Reinforced Concrete Columns Based on Experimental Observations," *Journal of Engineering Mechanics, ASCE*, 128 (10), 1024-1038.

Ger, J.F., Cheng,, F. Y., and Lu, L. W. (1993). "Collapse Behavior of Pino Suarez Building during 1985 Mexico City Earthquake," *Journal of Structural Engineering, ASCE,* 119(3), 852–870.

Ghafory-Ashtiany, M., Mousavi, M., and Azarbakht, A. (2011). "Strong Ground Motion Record Selection for the Reliable Prediction of the Mean Seismic Collapse Capacity of a Structure Group*." Earthquake Engineering and Structural Dynamics*, 40(6), 691-708.

Gunay, S., and Mosalam, K.M. (2013). "PEER Performance-Based Earthquake Engineering Methodology, Revisited," *Journal of Earthquake Engineering*, 17(6), 829-858.

Haselton, C.B. (2006). *Assessing Seismic Collapse Safety of Modern Reinforced Concrete Moment Frame Buildings*. Phd Dissertation, Department of Civil and Environmental Engineering, Stanford University.

Haselton, C.B., and Deierlein, G.G. (2007). *Assessing Seismic Collapse Safety of Modern Reinforced Concrete Frame Buildings*, Report No. 156, The John A. Blume Earthquake Engineering Center, Stanford University, Stanford, CA.

Haselton, C.B, Liel, A.B., and Deierlein, G.G. (2009). "Simulating Structural Collapse due to Earthquakes: Model Idealization, Model Calibration, and Numerical Solution Algorithms," *COMPDYN 2009, 2nd International Conference on Computational Methods in Structural Dynamics and Earthquake Engineering*, Rhodes, Greece, June 22-24.

Haselton, C.H., Liel, A.B., Deierlein, G.G., Dean, B.S., and Chous, J.H. (2011). "Seismic Collapse Safety of Reinforced Concrete Buildings I: Assessment of Ductile Moment Frames," *Journal Of Structural Engineering*, 137(4), 481-491.

Housner, G.W. (1952). "Spectrum Intensities of Strong Motion Earthquakes," *Proceedings of Symposium on Earthquake and Blast Effects on Structures*, Earthquake Engineering Research Institute.

Housner, G.W. (1970). *Strong Ground Motion*, Ch. 4 In Earthquake Engineering, Edited By R. L. Wiegel, Prentice Hall Inc., Englewood Cliffs, NJ.

Housner, G.W. (1975). "Measures of Severity of Earthquake Ground Shaking," *Proceedings of U. S. National Conference on Earthquake Engineering*, Earthquake Engineering Research Institute, June 18-20, 1975, Ann Arbor, Michigan, 25–33.

Housner, G. W., and Jennings, P. C. (1964). "Generation of Artificial Earthquakes," *J. Eng. Mech. Div.* 90, Proceedings Paper 3806.

Ibarra, L. F., and Krawinkler, H. **(**2004**)**. "Global Collapse of Deteriorating MDOF Systems," *Proceedings of 13th World Conference on Earthquake Engineering,* Vancouver, B.C., Canada.

Ibarra, L.F., and Krawinkler, H. (2005). *Global Collapse of Frame Structures under Seismic Excitations,* PEER Report No. 2005/06, Pacific Earthquake Engineering Research Center, University Of California, Berkeley.

Ibarra, L., Medina, R., and Krawinkler, H. (2002). "Collapse Assessment of Deteriorating SDOF Systems," *Proceedings of The 12th European Conference on Earthquake Engineering*, September 9-13, London.

Ibarra, L. F., Medina, R. A., and Krawinkler, H. **(**2005**)**. "Hysteretic Models that Incorporate Strength and Stiffness Deterioration," *Earthquake Engineering and Structural Dynamics*, 34**(**12**)**, 1489–1511.

International Code Council (ICC). (2003). International Building Code, Falls Church, VA.

International Conference of Building Officials (ICBO). (1967). Uniform Building Code, Pasadena, CA.

Jalayer, F. and Cornell, C. A. (2003). *A Technical Framework For Probability-Based Demand and Capacity Factor Design (DCFD) Seismic Formats*, PEER Report 2003/08, Pacific Earthquake Engineering Center, University Of California Berkeley.

Jennings, P. C., and Husid, R. **(**1968**)**. "Collapse of Yielding Structures during Earthquakes," *Journal of Engineering Mechanics Division,* 94**(**5**)**, 1045–1065.

Kaewkulchai, G., and Williamson, E.B. (2004). "Beam Element Formulation and Solution Procedure for Dynamic Progressive Collapse Analysis," *Computers & Structures*, 82, 639-651.

Kanvinde, M (2003). "Methods to Evaluate the Dynamic Stability of Structures—Shake Table Tests and Nonlinear Dynamic Analyses," *EERI Annual Student Paper Competition*, Earthquake Engineering Research Institute, Oakland, Calif.

Kato, B., Akiyama, H., Suzuki, H., and Fukuzawa, Y. **(**1973**)**. "Dynamic Collapse Tests of Steel Structural Models," *Preprints of 5th World Conference on Earthquake Engineering*, Rome.

Khandelwal, K., and El-Tawil, S. (2007). "Collapse Behavior of Steel Special Moment Resisting Frame Connections," *Journal of Structural Engineering*, ASCE, 133(5), 646-655.

Kim, J., Lafave, J.M., and Song, J. (2007), "A New Statistical Approach for Joint Shear Strength Determination of RC Beam-Column Connections Subjected to Lateral Earthquake Loading", *Struct. Eng. Mech.*, 27 (4), 439-456.

Kratzig, W.B., Meyer, I.F., and Meskouris, K. (1989). "Damage Evolution in Reinforced Concrete Members under Cyclic Loading," *Proceedings of 5th International Conference on Structural Safety And Reliability, ASCE*, New York, USA. Vol (2). 795-802.

Krawinkler, H., and Zareian, F. (2007). "Prediction of Collapse – How Realistic and Practical Is It, and What Can We Learn from It?" *The Structural Design of Tall and Special Buildings*, 16, 633-653.

Krawinkler, H., Lignos, D., and Whittaker, A. (2008). "Sideways Collapse of Deteriorating Structural Systems, Project Website," http://nees.buffalo.edu/projects/ NEESCollapse/.

Krawinkler, H., Medina, R., and Alavi, B. **(**2003**)**. "Seismic Drift and Ductility Demands and their Dependence on Ground Motions," *Engineering Structures,* 25**(**5**)**, 637–653.

Krawinkler, H., Zareian, F., Lignos, D., and Ibarra, L. F. (2009). "Prediction of Collapse of Structures under Earthquake Excitations," *Proceedings of the 2nd International Conference on Computational Methods in Structural Dynamics and Earthquake Engineering (COMPDYN 2009)*, Rhodes, Greece, June 22–24.

Kurama, Y. and Farrow, K. (2003). "Ground Motion Scaling Methods for Different Site Conditions And Structure Characteristics," *Earthquake Engineering &Structural Dynamics* , 32(15), 2425-2450.

Lee. K., and Foutch, D.A. (2002) ."Seismic Performance Evaluation of Pre-Northridge Steel Frame Buildings with Brittle Connections," *Journal of Structural Engineering*, 128(4), 546-555.

Lee. K. and Foutch, D.A. (2004). "Performance Evaluation of Damaged Steel Frame Buildings Subjected to Seismic Loads," *Journal of Structural Engineering*, 130(4), 588-599.

Liel, A. B., Haselton, C.B., Deierlein, G. G. (2011). "Seismic Collapse Safety of Reinforced Concrete Buildings. II: Comparative Assessment of Nonductile and Ductile Moment Frames," *Journal of Structural Engineering,* ASCE, 137(4), 492-502.

Liel, A.B., Haselton, C.B., Deierlein, G.G., and Baker, J.W. (2009). "Incorporating Modeling Uncertainties in the Assessment of Seismic Collapse Risk of Buildings," *Structural Safety*, 31, 197-211.

Lignos, D.G. and Krawinkler, H. (2010). "A Steel Database for Component Deterioration of Tubular Hollow Square Steel Columns under Varying Axial Load for Collapse Assessment of Steel Structures under Earthquakes", *Proceedings 7th International Conference on Urban Earthquake Engineering (7CUEE)*, Tokyo, Japan, March 3rd - 5th, 2010.

Lignos, D.G. and Krawinkler, H. (2012). *Sidesway Collapse of Deteriorating Structural Systems under Seismic Excitations,* Report No. 177, The John A. Blume Earthquake Engineering Center, Department of Civil and Environmental Engineering, Stanford University.

Lignos, D.G., Krawinkler, H., and Whittaker, A.S. (2008). "Shaking Table Collapse Tests of Two Scale Models of a 4-Story Moment Resisting Steel Frame," *Proceedings of the 14th World Conference on Earthquake Engineering*, Beijing, China, October 12-17.

Lignos, D.G., Krawinkler, H., Whittaker, A., (2009). "Contributions to Collapse Prediction of Steel Moment Frames Through Recent Earthquake Simulator Collapse Tests", *Proceedings 3rd International Conference on Advances in Experimental Structural Engineering*, October 15-16, San Francisco, CA.

MacRae, G. A. **(**1994**)**. "P-Δ Effects on Single-Degree-of-Freedom Structures in Earthquakes," *Earthquake Spectra*, 10**(3)**, 539–568.

Mahin, S. (2008). "Sustainable Design Considerations In Earthquake Engineering," *The 14th World Conference on Earthquake Engineering,* October 12-17, 2008, Beijing, China.

Maison, B., Kasai, K., and Deierlein G. (2008). "Study of Building Collapse for Performance-Based Design Validation," *Proc. of Structures 2008: Crossing Borders*, April 24-26, Vancouver, Canada.

Maniatakis, Ch.A., Taflampas, I.M. and Spyrakos, C.C. (2008). "Identification of Near-Fault Earthquake Record Characteristics," *14th World Conference on Earthquake Engineering,* October 12-17, 2008, Beijing, China.

Martin, S. C., and Villaverde, R. **(**1996**)**. "Seismic Collapse of Steel Frame Structures," *Proceedings of 11th World Conference on Earthquake Engineering*, Acapulco, Mexico.

Medina, R. A., and Krawinkler, H. **(**2005**)**. "Strength Design Issues Relevant for the Seismic Design of Moment-Resisting Frames," *Earthquake Spectra,* 21**(**2**)**, 415–439.

Meguro, K., Tagel-Din, H. (2001). "Applied Element Simulation of RC Structures under Cyclic Loading," *ASCE Journal of Structural Engineering*, 127(11), 1295-1305.

Mehanny S.S., and Deierlein G.G. (2000). *Modeling and Assessment of Seismic Performance of Composite Frames with Reinforced Concrete Columns and Steel Beams*, Report No. 136, The John A. Blume Earthquake Engineering Center, Stanford University, Stanford, CA.

Mehanny, S. S. F., and Deierlein, G. G. **(**2001**)**. "Seismic Damage and Collapse Assessment of Composite Moment Frames," *Journal of Structural Engineering*, 127**(**9**)**, 1045–1053.

Menegotto, M., and Pinto, E. (1973). "Method of Analysis for Cyclically Loaded Reinforced Concrete Plane Frames Including Changes in Geometry and Non-Elastic Behavior of Elements under Combined Normal Force and Bending," *Proceedings of IABSE Symposium*, Lisbon, Portugal.

Miranda, E., and Akkar, D. **(**2003**)**. "Dynamic Instability of Simple Structural Systems," *Journal of Structural Engineering,* 129**(**12**)**, 1722–1726.

Nakashima, M., Roeder, C. W., and Maruoka, Y. (2000). "Steel Moment Frames for Earthquakes in United States and Japan," *Journal of Structural Engineering, ASCE,* 126(8), 861-868

National Geophysical Data Center (NGDC) /NOAA

National Information Service for Earthquake Engineering, University of California, Berkeley

Open System for Earthquake Engineering Simulation (2004). Pacific Earthquake Engineering Research Center, University of California, Berkeley, CA.

Park, Y.-J., and Ang, A.H.-S. (1985). "Mechanistic Seismic Damage Model for Reinforced Concrete,'' *Journal of Structural Engineering*, ASCE, 111(4), 722–739.

Park, Y.-J., Ang, A. H.-S., and Wen, Y. K. (1985). "Seismic Damage Analysis of Reinforced Concrete Buildings", *Journal of Structural Engineering,* 111, 740–757.

Riddell, R. (2007). "On Ground Motion Intensity Indices," *Earthquake Spectra,* 23, 147–173.

Riddell, R., and Garcia, J. E. (2001). "Hysteretic Energy Spectrum and Damage Control," *Earthquake Eng. Struct. Dyn.,* 30(12), 1791–1816.

Rodgers, J.E., and Mahin, S.A. (2004). *Effects of Connection Hysteretic Degradation on the Seismic Behavior of Steel Moment-Resisting Frame*, Pacfic Earthquake Engineering Research Center Report, PEER 2003/13.

Rodgers, J.E., and Mahin, S.A. (2006). "Effects of Connection Fractures on Global Behavior of Steel Moment Frames Subjected to Earthquakes," *Journal of Structural Engineering*, 132(1), 78-88.

Rodgers, J. E., and Mahin, S. A. (2008). "Local Fracture-Inducted Phenomena in Steel Moment Frames," *Earthquake Engineering & Structural Dynamics,* 38,135–155.

Rodgers, J.E., and Mahin, S.A. (2009). "Local Fracture-Induced Phenomena in Steel Moment Frames," *Earthquake Engineering and Structural Dynamics*, 38, 135-155.

Rodgers, J. E., and Mahin, S. A. (2011). "Effects of Connection Deformation Softening on Behavior of Steel Moment Frames Subjected to Earthquakes," *International Journal of Steel Structures*, 11(1), 29-37.

Song, C., Pujol, S., and Lepage, A. (2012). "The Collapse of the Alto Río Building during the 27 February 2010 Maule, Chile, Earthquake," Earthquake Spectra, 28(S1), S301-S334.

Song, J., Kang, W.-H., Kim, K.S., and Jung, S. (2010). "Probabilistic Shear Strength Models for Reinforced Concrete Beams Without Shear Reinforcement," *Structural Engineering and Mechanics*, 34(1), 15-38.

Suita, K., Yamada, S., Tada, M., Kasai, K. Matsuoka, Y., and Sato, E. (2008). "Results of Recent E-Defense Tests on Full-scale Steel Buildings: Part 1 – Collapse Experiments on 4-story Moment Frames," *Proceedings of 2008 Structural Congress*, Vancouver, Canada, April 24-26.

Sun, L., Zhou, C., Qin D., Fan, L. (2003) "Application of Extended Distinct Element Method with Lattice Model to Collapse Analysis of RC Bridges," *Earthquake Engineering and Structural Dynamics*, 32(8), 1217-1236.

Szyniszewski, S. (2009). "Dynamic Energy Based Method for Progressive Collapse Analysis," *Proceedings of 2009 Structures Congress, ASCE*, April 30-May 2, Austin, TX, 1259-1268.

Szyniszewski, S. and Krauthammer, T. (2012). "Energy Flow in Progressive Collapse of Steel Framed Buildings," *Engineering Structures*, 42, 142-153.

Takizawa, H., and Jennings, P. C. **(**1980**)**. "Collapse of a Model for Ductile Reinforced Concrete Frames under Extreme Earthquake Motions," *Earthquake Engineering & Structural Dynamics,* 8, 117–144.

Talaat, M., Mosalam, K. (2007). "Towards Modeling Progressive Collapse in Reinforced Concrete Buildings," *Proceedings of ASCE Structures Congress,* Long Beach, California.

Tipping, M.E. (2000). *The Relevance Vector Machine*, In S. A. Solla, T. K. Leen, and K.-R. Müller (Eds.), Advances In Neural Information Processing Systems, MIT Press, 12, 652–658.

Tothong, P., and Cornell, C. A. (2007). *Probabilistic Seismic Demand Analysis Using Advanced Ground Motion Intensity Measures, Attenuation Relationships, and Near-Fault Effects*, Pacific Earthquake Engineering Research Center, PEER Report 2006/11, University of

California, Berkeley.

Tothong, P., and Cornell, C. A. (2008). "Structural Performance Assessment under Near-Source Pulse-Like Ground Motions Using Advanced Ground Motion Intensity Measures," *Earthquake Engineering & Structural Dynamics,* 37(7), 1013-1037.

Trifunac, M.D. and Brady, A.G. (1975). "A Study on The Duration of Strong Earthquake Ground Motion," *Bulletin of The Seismological Society of America*, 65, 581-626.

Uang, C. M. and Bertero, V. V. (1990). "Evaluation of Seismic Energy in Structures," *Earthquake Engineering and Structural Dynamics,* 19,77–90.

Vamvatsikos, D., and Cornell, C.A. (2002). "Incremental Dynamic Analysis," *Earthquake Engineering and Structural Dynamics*, 31(3), 491-514.

Vamvatsikos, D., and Cornell, C.A. (2004). "Applied Incremental Dynamic Analysis," *Earthquake Spectra*, 20(2), 523-553.

Vamvatsikos, D., and Cornell, C. A. **(**2005**)**. "Direct Estimation of Seismic Demand and Capacity of Multidegree-of-Freedom Systems Through Incremental Dynamic Analysis of Single Degree of Freedom Approximation," *Journal of Structural Engineering,* 131**(**4**)**, 589–599.

Vamvatsikos, D., and Papadimitriou, C. (2005). "Optimal Multi-Objective Design of a Highway Bridge under Seismic Loading through Incremental Dynamic Analysis," *Proc. of ICOSSAR 2005*, June 20-23, Rome, Italy.

Vian, D., and Bruneau, M. **(**2003**)**. "Tests to Structural Collapse of Single Degree of Freedom Frames Subjected to Earthquake Excitations," *Journal of Structural Engineering,* 129**(**12**)**, 1676–1685.

Villaverde, R. (2007). "Methods to Assess the Seismic Collapse Capacity of Building Structures: State of the Art," *Journal of Structural Engineering*, 33(1), 57-66.

Williamson, E. B. **(**2003**)**. "Evaluation of Damage and P-Δ Effects for Systems under Earthquake

Excitation," *Journal of Structural Engineering,* 129**(**8**)**, 1036–1046.

Ye, L., Ma, Q., Miao, Z., Guan, H., and Zhuge, Y. (2013). "Numerical and Comparative Study of Earthquake Intensity Indices in Seismic Analysis," The Structural Design of Tall and Special Buildings, 22, 362–381.

Zareian, F. (2006). *Simplified Performance-Based Earthquake Engineering*, Ph.D. Dissertation, Department of Civil and Environmental Engineering, Stanford University.

Zareian, F., and Krawinkler, H. (2007). "Assessment of Probability of Collapse and Design for Collapse Safety," *Earthquake Engineering and Structural Dynamics*, 36(13), 1901-1914.

Zareian, F., Krawinkler, H., Ibarra, L., Lignos, D. (2010). "Basic Concepts and Performance Measures in Prediction of Collapse of Buildings under Earthquake Ground Motions," *The Structural Design Of Tall And Special Buildings,* 19 (1-2), 167-181.